

## Photoelectrocatalysis in water treatment

Bennani, Yasmina

**DOI**

[10.4233/uuid:5bf8b3c7-d069-4c64-90fd-3b2a5889f95d](https://doi.org/10.4233/uuid:5bf8b3c7-d069-4c64-90fd-3b2a5889f95d)

**Publication date**

2017

**Document Version**

Final published version

**Citation (APA)**

Bennani, Y. (2017). *Photoelectrocatalysis in water treatment*. [Dissertation (TU Delft), Delft University of Technology]. <https://doi.org/10.4233/uuid:5bf8b3c7-d069-4c64-90fd-3b2a5889f95d>

**Important note**

To cite this publication, please use the final published version (if applicable).  
Please check the document version above.

**Copyright**

Other than for strictly personal use, it is not permitted to download, forward or distribute the text or part of it, without the consent of the author(s) and/or copyright holder(s), unless the work is under an open content license such as Creative Commons.

**Takedown policy**

Please contact us and provide details if you believe this document breaches copyrights.  
We will remove access to the work immediately and investigate your claim.

# Photoelectrocatalysis in Water Treatment

# **Photoelectrocatalysis in Water Treatment**

## **Proefschrift**

ter verkrijging van de graad van doctor  
aan de Technische Universiteit Delft,  
op gezag van de Rector Magnificus prof. ir. K.C.A.M. Luyben,  
voorzitter van het College voor Promoties,  
in het openbaar te verdedigen op  
dinsdag 28 februari 2017 om 10:00 uur

door

Yasmina BENNANI  
Master of Chemical Engineering  
Faculty of Chemical Engineering and Technology, Kroatië  
geboren te Osijek, Kroatië

This dissertation has been approved by:  
promotor: Prof. dr. ir. L.C. Rietveld  
promotor: Prof. dr. ir. P.W. Appel

Composition of the doctoral committee:

Rector Magnificus	chairman
Prof. dr. ir. L.C. Rietveld	Technische Universiteit Delft
Prof. dr. ir. P.W. Appel	Technische Universiteit Delft

Independent members:	
Prof. dr. ir. J.P. van der Hoek	Technische Universiteit Delft
Prof. dr. M. D. Kennedy	UNESCO-IHE/Technische Universiteit Delft
Prof. dr. ir. J. A. M. H. Hofman	University of Bath, United Kingdom
Prof. dr. ir. A. R. D. Verliefde	Universiteit Gent, België
Dr. ir. K. Lekkerkerker-Teunissen	Dunea

This research was conducted within the framework of project LIGHTNING.

Proefschrift, Technische Universiteit Delft  
Met samenvatting in het Nederlands/With summary in Dutch

Copyright © 2017 by Yasmina Bennani

ISBN: 978-94-6186-792-6  
Printed by: AIO (Proefschrift all in one)  
Cover by: Mycona

An electronic version of this document is available free of charge in the TU Delft Repository



# CONTENTS

---

CONTENTS .....	v
SUMMARY .....	viii
SAMENVATTING.....	xii
ACKNOWLEDGEMENTS.....	xvii
INTRODUCTION .....	7
ENHANCED SOLAR LIGHT PHOTOELECTROCATALYTIC ACTIVITY IN WATER BY ANATASE-TO-RUTILE $\text{TiO}_2$ TRANSFORMATION.....	30
OPTIMISATION OF PARAMETERS IN A SOLAR LIGHT-INDUCED PHOTOELECTROCATALYTIC PROCESS WITH A $\text{TiO}_2/\text{Ti}$ COMPOSITE ELECTRODE PREPARED BY PAINT-THERMAL DECOMPOSITION .....	65
PHOTOELECTROCATALYTIC DEGRADATION OF CHLOROFORM IN AQUEOUS SOLUTION USING A $\text{TiO}_2/\text{Ti}$ COMPOSITE MESH ELECTRODE .....	100
HETEROGENEOUS PHOTOELECTROCATALYTIC DEGRADATION OF CHLOROFORM: FROM BATCH TO A FLOW-THROUGH SOLAR AND LPUV FLOW REACTOR.....	138
ELECTROCHEMICALLY ACTIVE BIOFILM AND PHOTOELECTROCATALYTIC REGENERATION OF THE TITANIUM DIOXIDE COMPOSITE ELECTRODE FOR ADVANCED OXIDATION IN WATER TREATMENT .....	158
PHOTOELECTROCATALYTIC OXIDATION OF PHENOL FOR WATER TREATMENT USING A $\text{BiVO}_4$ THIN-FILM PHOTOANODE .....	190
TREATMENT OF ORGANIC POLLUTANTS USING A SOLAR ENERGY DRIVEN PHOTO-OXIDATION DEVICE .....	225
CONCLUSIONS.....	227
LIST OF PUBLICATIONS.....	267
CURRICULUM VITAE .....	269







# SUMMARY

---

One of the most pervasive problems affecting people throughout the world is inadequate access to clean water and sanitation. Issues with polluted water are expected to grow worse in the coming years, with scarcity of drinking water occurring worldwide, even in areas considered as water-rich. Addressing these issues calls out for an intensive research to be done to identify robust new methods for water treatment at lower costs and with less energy consumption, while at the same time using less chemicals and having lower impact on the environment. Advances in drinking water and wastewater treatment have led to the development of advanced oxidation processes (AOPs) to oxidize organic (micro-)pollutants. These processes include chemical, photochemical, photocatalytic (PC) or electrochemical methods characterized by the generation of the hydroxyl radical species ( $\cdot\text{OH}$ ). Among the major problems encountered in the development of practical  $\text{TiO}_2$ /UV treatment systems, separation of titanium dioxide ( $\text{TiO}_2$ ) from aqueous phases and fast recombination rate of electron-hole pair could be listed. To avoid the filtering process and to increase catalyst durability,  $\text{TiO}_2$  catalyst is immobilized on solid supports as bound particles or thin films. Application of heterogeneous PC in combination with a small external electrical bias to  $\text{TiO}_2$ -coated anodes can decrease the recombination rate of electron-hole pairs and thus increase the photoactivity of  $\text{TiO}_2$ . The application of an external bias

leads most of the generated electrons away from the conduction band of  $\text{TiO}_2$ , wherefore lowering electron–hole recombination and promoting hole transfer to organic pollutants at the interface. Photoelectrocatalysis (PEC) is initiated via the illumination of light on a catalyst, e.g.  $\text{TiO}_2$ . The photocatalytic properties of  $\text{TiO}_2$  are obtained from the formed charge carriers (hole and electron) which are generated upon the absorption of ultraviolet (UV) light corresponding to the band gap of the catalyst. The generated holes in the catalyst valence band diffuse to the surface of the catalyst where they react with adsorbed water molecules, forming  $\cdot\text{OH}$ . The holes and the hydroxyl radicals oxidize organic molecules at the  $\text{TiO}_2$  surface. On the other hand, electrons in the conduction band take part in reduction processes, reacting with molecular oxygen in the water producing superoxide radical anions ( $\text{O}_2^{\cdot-}$ ).

Despite the fast development in the photocatalytic field, several uncertainties continue to exist. These can mainly be ascribed to the parameters, photon generation and catalyst efficiency. The basic concept of PEC has been demonstrated, but efficiency and the scale-up still remains a struggle.

Therefore, in this thesis, PEC is revisited from an experimental and engineering point of view.

Theory implies that by applying a small positive bias to a semiconductor photoanode the charge carrier (electron and hole) recombination, responsible for low photonic efficiency, can be minimized and efficiency improved. This predicted improvement has been demonstrated experimentally in the thesis. The enhanced photocatalytic activity was derived from the synergistic effect between the modified  $\text{TiO}_2/\text{Ti}$  composite electrode and an applied bias. The integration of the paint-thermal decomposition method with PEC technology with an applied bias of 1 V using solar light showed promising degradation efficiencies for phenol. Additionally, it was observed that mixed anatase/rutile systems show more favorable photocatalytic properties than any other

crystalline form. It was found that the modified  $\text{TiO}_2/\text{Ti}$  composite with an anatase-to-rutile ratio of 82/18 was optimal for both PC and PEC, which resulted in the highest efficiency when using solar light. The synergistic effect of the mixed systems has been attributed to a built-in driving force for separation of photogenerated charge carriers. That kind of driving force may have resulted from either a built-in electric field or from energy barriers blocking charge transfer at the interface between anatase and rutile.

The catalyst is considered to be the heart of the photocatalytic process and there are many factors which can influence on photocatalytic performance, including the size, specific surface area, pore volume, pore structure, crystalline phase, and the exposed surface facets. It has been found that the  $\text{TiO}_2$  film thickness was a factor with a strong influence on PEC degradation of phenol in water. The observations indicate that six layers might be an optimal number of layers of  $\text{TiO}_2$  film for an effective PEC reaction or in case of other catalyst,  $\text{BiVO}_4$ , 300 nm film thickness. Required organic pollutant removal efficiency of the system was further determined by the balance between reaction rate kinetics (retention time in the reactor) and energy consumption of the system. At the higher degradation percentages, lower UV intensities (30 and  $45 \text{ Wm}^2$ ) were much more energy efficient than the higher intensities.

In addition, research was performed on a new PEC application with electrochemically active biofilm electrodes.  $\text{TiO}_2/\text{Ti}$  composite electrodes were operated with variable biofilm coverage to study the effectiveness of biofilm formation in enhancing the electron transfer. An electrochemically active biofilm on the  $\text{TiO}_2/\text{Ti}$  composite electrode was even found to increase the kinetics of the reaction by 1.6 times. This increase was assisted by an increase in charge transfer (by lowering impedance) and was also observed by a higher phenol degradation efficiency.

To further improve the performance of PEC for water purification, a  $\text{TiO}_2/\text{Ti}$  mesh photoelectrode was successfully prepared. The  $\text{TiO}_2$  deposited on a Ti mesh showed an improvement in photocatalytic activity, compared to the  $\text{TiO}_2$  deposited on Ti plate. This can be demonstrated by about 17 % enhancement in the degradation efficiency after 90 min, when the  $\text{TiO}_2/\text{Ti}$  mesh electrode was used to photoelectrocatalyze chloroform. Moreover, the PEC process was operated on a larger scale, which included a self-designed PEC solar and LPUV reactor using mesh electrodes.

Onward with the development of photocatalysts, the efficient usage of solar energy becomes one of the main targets that will have a great effect on technological applications in the field of photocatalysis. The widespread technological application of  $\text{TiO}_2$  is, however, constricted by its wide band gap, which requires ultraviolet irradiation for photocatalytic activation. In this thesis advances have been made in the design and development of highly reactive and functional  $\text{BiVO}_4$  for utilization of visible or solar light for PEC.  $\text{BiVO}_4$  has been proposed as a viable option for PEC oxidation using solar light, as opposed to the used  $\text{TiO}_2$ . The material studies have shown that  $\text{BiVO}_4$ , with a band gap of 2.5 eV, is a better absorber for solar light compared to  $\text{TiO}_2$ .  $\text{BiVO}_4$  also showed a better phenol degradation performance compared to  $\text{TiO}_2$ , confirming that the enhanced light absorption, surface properties and electrical properties translates in an increase in phenol degradation.

Thus, in this thesis, the use of PEC was demonstrated as a potential technology for water treatment, and, more specifically, organics removal. However, it became also clear that there are many factors that can exert considerable influence on PEC performance, including the electron-hole recombination, inability to use visible light efficiently, specific surface area, pore volume, pore structure, crystalline phase, and the exposed surface facets. Therefore, the development of performance improvements by adjusting these factors remains the focus for future PEC research.

# SAMENVATTING

---

Een van de grootste wereldwijde, humanitaire problemen is onvoldoende toegang tot schoon water en sanitaire voorzieningen. Men verwacht dat de problemen met vervuild water de komende jaren alleen maar verder zullen toenemen, zelfs in gebieden die beschouwd worden als waterrijk. Om deze problemen aan te pakken zal er intensief onderzoek moeten worden gedaan naar het ontwikkelen van robuuste nieuwe methoden voor waterbehandeling, met aan de ene kant lagere kosten en aan de andere kant minder energie en chemicaliënverbruik, resulterend in een lagere impact op het milieu. Onderzoek naar drinkwater- en afvalwaterbehandeling heeft geleid tot de ontwikkeling van geavanceerde oxidatieprocessen die (micro-)verontreinigingen oxideren. Deze processen omvatten chemische-, fotochemische-, fotokatalytische- (PC) en elektrochemische methoden die gekenmerkt worden door het genereren van hydroxylradicalen ( $\cdot\text{OH}$ ). In de praktijk geeft de ontwikkeling van behandelingssystemen gebaseerd op  $\text{TiO}_2$ /UV een aantal problemen, waaronder de scheiding van titaniumdioxide ( $\text{TiO}_2$ ) uit water en de snelle recombinatie van het elektron-gat paar. Om een filtratie proces te vermijden en de katalysator duurzamer te maken, worden  $\text{TiO}_2$  katalysatoren geïmmobiliseerd op vaste dragers, als gebonden deeltjes of dunne films. Het gebruik van heterogene PC in combinatie met een kleine externe elektrische spanning op de  $\text{TiO}_2$  anoden kan recombinatie van elektron-gat paren verminderen en het verhoogt de fotoactiviteit van  $\text{TiO}_2$ .

Het toepassen van een externe spanning leidt het grootste deel van de gegenereerde elektronen weg van de  $\text{TiO}_2$  geleidingsband. Dit resulteert in het verlagen van elektron-gat recombinatie en bevordert de verplaatsing van het gat naar de organische verontreinigingen op de interface. Fotoelektrokatalyse (PEC) wordt gestart door het verlichten van een katalysator. De fotokatalytische eigenschappen van  $\text{TiO}_2$  worden verkregen uit de gevormde gaten en elektronen die worden gegenereerd na de absorptie van ultraviolet (UV) licht, dat overeenkomt met de bandafstand van de katalysator. De gegenereerde gaten in de valentieband van de katalysator komen naar het oppervlak van de katalysator waar ze reageren met geabsorbeerde watermoleculen en  $\cdot\text{OH}$  vormen. De gaten en de hydroxylradicalen oxideren organische moleculen aan het  $\text{TiO}_2$  oppervlak. De elektronen worden onderdeel van het reductieproces in de geleidingsband. Deze elektronen reageren met moleculaire zuurstof in het water en produceren superoxide radicaal-anionen ( $\text{O}_2^{\cdot-}$ ).

Ondanks de snelle ontwikkeling in het fotokatalytische veld, blijven een aantal onzekerheden bestaan. Deze worden voornamelijk toegeschreven aan parameters zoals fotongeneratie en katalysatorefficiëntie. Het basisconcept van PEC is aangetoond, maar de efficiëntie en de opschaling is nog steeds niet optimaal. Daarom wordt in dit proefschrift PEC uit een experimenteel en technisch oogpunt gezien.

De theorie impliceert dat door het toepassen van een kleine positieve spanning op een fotoanode, de recombinatie van elektronen en gaten (die voor de lage fotonische efficiëntie verantwoordelijk zijn) kan worden geminimaliseerd en de efficiency kan worden verbeterd. Deze verbetering is in het proefschrift experimenteel aangetoond. De verbeterde fotokatalytische

activiteit is de consequentie van het synergetische effect tussen de gemodificeerde  $\text{TiO}_2/\text{Ti}$  composietelektrode en een aangelegde spanning. De integratie van de verf-thermische ontledingsmethode met de PEC technologie (met een toegepaste spanning van 1 V en gebruikmakend van zonlicht), toonde een veelbelovende afbraak-efficiëntie voor fenol aan. Bovendien werd waargenomen dat gemengde anatase/rutiele systemen gunstigere fotokatalytische eigenschappen vertonen dan met andere kristalvormen. Het gemodificeerde  $\text{TiO}_2/\text{Ti}$  composiet met een anataas/rutiel verhouding van 82/18 was optimaal voor zowel PC als PEC, waardoor bij gebruik van zonlicht, het hoogste rendement wordt behaald. Het synergistische effect van de gemengde systemen wordt toegeschreven aan de drijvende kracht voor het scheiden van de elektronen en gaten. Deze drijvende kracht kan het gevolg zijn van een ingebouwd elektrisch veld van energiebarrières die de ladingsoverdracht op het snijvlak van anataas en rutiel blokkeren.

De katalysator wordt beschouwd als het hart van het fotokatalytische proces en er zijn vele factoren die fotokatalytische prestaties kunnen beïnvloeden, zoals de grootte, specifieke oppervlakte, poriënvolume, poriestructuur, kristalfases en blootgestelde oppervlaktefacetten. Gebleken is dat de  $\text{TiO}_2$  filmdikte een factor is met een sterke invloed op de afbraak van fenol in water met PEC. De waarnemingen geven aan dat zes lagen  $\text{TiO}_2$ -film een optimaal aantal is voor een effectieve PEC reactie. Bij een andere katalysator,  $\text{BiVO}_4$ , is een laag van 300 nm dikte optimaal. De gewenste afbraak van organische verontreinigingen door het systeem werd verder bepaald door het maken van een balans tussen reactiesnelheid (verblijftijd in de reactor) en het energieverbruik van het systeem. Bij hogere afbraak percentages, waren lagere UV-intensiteiten (30 en 45  $\text{Wm}^2$ ) veel (energie-)efficiënter dan bij hogere intensiteiten.

Hiernaast werd onderzoek uitgevoerd naar een nieuwe PEC applicatie met elektrochemisch actieve biofilmelektroden.  $\text{TiO}_2/\text{Ti}$  composietelektroden werden bewerkt met een biofilm om de doeltreffendheid van biofilmvorming te bestuderen bij het verbeteren van de elektronenoverdracht. Het bleek dat, met een elektrochemisch actieve biofilm op de  $\text{TiO}_2/\text{Ti}$  composietelektrode, de kinetiek van de reactie met 1,6 keer wordt verhoogd. Deze stijging werd ondersteund door een gemeten toename van de ladingsoverdracht (door het verlagen van de impedantie) en een waargenomen hogere fenol afbraak.

Om de prestaties van PEC voor waterzuivering verder te verbeteren is, met succes, een  $\text{TiO}_2/\text{Ti}$  mesh foto-elektrode gemaakt. De  $\text{TiO}_2$  op een Ti mesh vertoonde een verbetering van fotokatalytische activiteit ten opzichte van  $\text{TiO}_2$  afgezet op een Ti plaat. Aangetoond werd dat de afbraakcapaciteit van chloroform na 90 min met 17 % verbeterde. Daarnaast werd het PEC proces op grotere schaal uitgevoerd met een zelf ontworpen PEC zonne- en LPUV reactor, inclusief mesh elektroden.

Met het verder ontwikkelen van fotokatalysatoren, zal het efficiënter gebruik van zonne-energie een van de belangrijkste doelen worden. De wijdverspreide technologische toepassing van  $\text{TiO}_2$  is echter beperkt door de brede bandafstand die ultraviolette bestraling voor fotokatalytische activering vereist. In dit proefschrift is vooruitgang geboekt in het ontwerpen en ontwikkelen van een reactieve en functionele  $\text{BiVO}_4$  elektrode voor het gebruik van zichtbaar licht of zon-licht bij PEC. Studies hebben aangetoond dat  $\text{BiVO}_4$ , met een bandafstand van 2.5 eV, een betere absorptie van zonlicht geeft ten opzichte van  $\text{TiO}_2$ .  $\text{BiVO}_4$  gaf ook een betere fenol afbraak ten opzichte van  $\text{TiO}_2$ .



In dit proefschrift werd dus het gebruik van PEC gedemonstreerd als mogelijke techniek voor waterzuivering en, in het bijzonder, het verwijderen van organische stof. Het werd echter ook duidelijk dat er veel factoren zijn die een grote invloed kunnen uitoefenen op de PEC prestaties, waaronder de elektron-gat recombinatie, onvermogen om zichtbaar licht efficiënt te gebruiken, specifiek oppervlakte, poriënvolume, poriestructuur, kristalfases en blootgestelde oppervlak. De ontwikkeling van prestatieverbeteringen door aanpassing van deze factoren blijft de focus voor toekomstig PEC onderzoek.

# ACKNOWLEDGEMENTS

---

I would like to thank some people who contributed to the realization of this dissertation.

First and foremost, I thank my promotors, prof. Luuk C. Rietveld and prof. Peter Appel for providing me with the opportunity to complete my PhD thesis at Delft University of Technology. I appreciate all their contributions of time and ideas to make my PhD experience productive and stimulating. I especially want to thank my promotor, prof. Luuk C. Rievelde, whose support and guidance made my thesis work possible. He has been actively interested in my work and has always been available to advise me. I am very grateful for his patience, motivation, enthusiasm, and knowledge that, taken together, make him a great mentor.

It was a great pleasure and a big challenge to be the PhD student of Prof. Peter Appel! I want to thank him for all his valuable comments, advices and for his critical questions which often stimulated me to think “outside the box”.

Every result described in this thesis was accomplished with the help and support of fellow technical laborants and collaborators. I would like to thank Vidjay Brdja and Catarina Fernandez from Magneto Special Anodes for their hard work on TiO<sub>2</sub>/Ti anodes. Tonny Schuit and Armand Middeldorp from

Department of Sanitary Engineering, Civil Engineering as well as dr. ir. Volkert van Steijn and Wim van Oordt from Department of Product and Process Engineering, Chemical Engineering for their services in laboratories and their help with the equipment. They have been very kind and patient and always willing to help whenever I approached them and I acknowledge and appreciate them for all their efforts. I would like to thank Sander de Vree and Frank Kalkman, for their advice and help regarding laboratory conductive and insulating materials. Ruud Hendrikx from 3ME for XRD measurements. Special thanks to Ir. Ruben Abellon for showing me Photoluminescence Spectrometer and Veeco Dektak Profiler. Also, many thanks go to Zivko Momic and all the DEMO workshop members who provided me with the experimental setups. I am grateful to Dr. Amer El-Kalliny for his help and suggestions in the beginning of my PhD. I would also like to thank Duco Bosma and Marcel Bus from department of Chemical Engineering for introducing me to the Scanning electron microscope and Atomic force microscopy and showing me the subsequent analysis.

Next, it should be recognized that part of the success of this thesis was due to the cooperation and collaboration of the members from the Department of Electrical Sustainable Energy at TUD. It was a great pleasure to be part of such excellent team. First, I would like to express my sincerely thanks to prof. Arno Smets, Paula Perez Rodriguez and other members for their work, support and for their helpful and positive feedback on our research. Additionally, I would like to thank Dr. Marjolein Peters for our research collaboration which led to a publication of our mutual project.

I also had the opportunity to mentor students for their internship, bachelor or master studies, Albert Godoy Hernández, Tycho Nessen, Andrea Elshof and Mathew J. Alani, who tirelessly and with much enthusiasm tackled a difficult projects over the course of several months.

Finally, I would like to acknowledge friends and family who supported me during my time here. I would express a deep sense of gratitude to my parents, especially to my dearest mom, who has always stood by me like a pillar in times of need with her constant love, encouragement and moral support. Special thanks are to Justin who always strengthened my morale by standing by me in all situations.



# Part I

Description of thesis



# 1

## INTRODUCTION

---



Different organic compounds in rivers, most likely introduced through industrial and domestic effluents, present a serious threat for humans, as well as for flora and fauna in the water, due to their harmful nature. Considering the stress on the availability of clean and safe water world-wide it will come as no surprise that finding ways to purify more of the world's undrinkable water has become a global priority. Today the water industry is a 300 billion Euro market, which is dominated by a small number of large companies. However, these companies primarily use conventional, large-scale water treatment technologies that are sound but with limited applicability for small scale installation with un-skilled supervision (Nations, 2013).

Despite the huge economical and strategic potential of water treatment and purification technologies, there are few new technologies on the horizon that potentially could help to solve the wide range of water issues (Naajm & Trussell, 1999). Conventional treatment processes, including biotreatment, carbon adsorption, air stripping, and reverse osmosis, suffer from various limitations (Rittmann, et al., 1989; Cecen & Aktas, 2012; Kutzer, et al., 1995). They are not effective for all organic micro-pollutants and/or consume much energy, transfer the contaminants from one medium to another or generate waste that requires further treatment and disposal (Crittenden, et al., 1997; Topudurti, et al., 1993). Therefore, there is a need to develop alternative treatment processes for the degradation of organic pollutants, such as phenol, benzene, polychlorinated biphenyls, and disinfection by-products from groundwater, wastewater and drinking water, that are scalable, sustainable and more efficient.

### 1.1. Advanced oxidation technologies

Advanced oxidation processes (AOPs) for water treatment have received increasing attention in the last decades (Figure 1). These processes, e.g., Fenton's reaction (Brillas, 2014), ozonation (Lawrence & Cappelli, 1977), electrochemical (Chaplin, 2014) and photochemical technologies (Egerton, et al., 2006), have thrivingly been used for the removal or degradation of contaminants, or used as pre-treatment to transform pollutants into lower-chain compounds that can then be treated by conventional or biological processes.

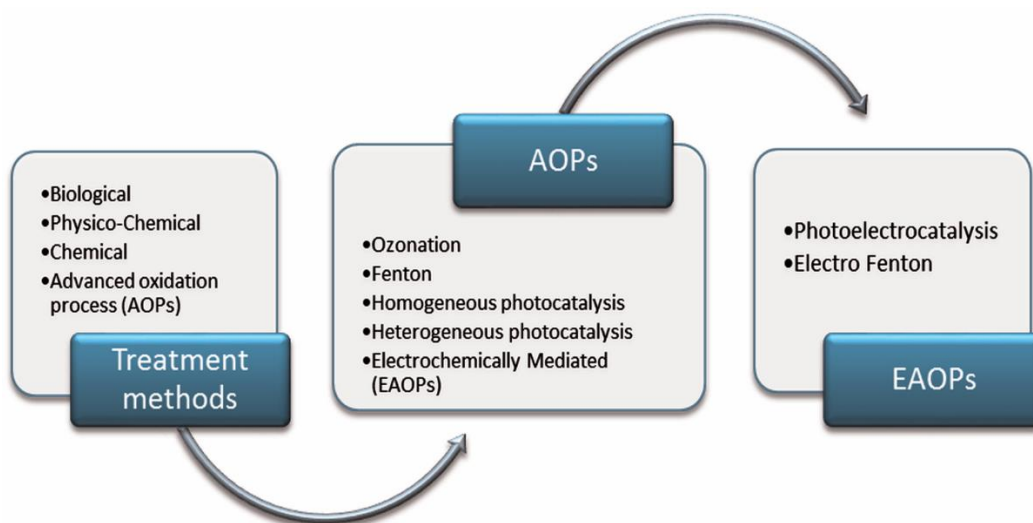


Figure 1.1. Treatment methods for degradation of organic pollutants, including conventional techniques and advanced oxidation processes

Electrochemical methods such as electrocoagulation, electrocatalysis oxidation and reduction, electro-Fenton, photoelectro-Fenton and photoelectrocatalysis (PEC) (Figure 1.1) have been pointed out as good alternatives to promote the degradation and mineralization of organic pollutants, since they combine the advantages of hydroxyl radicals formation and the efficiency of electrochemistry (Andreozzi, et al., 1999; Martinez-Huitle

& Brillas, 2009). PEC, as one of the AOPs, is a multidisciplinary field, involving surface science, electrochemistry, solid-state physics and optics. They involve two stages of oxidation: 1) the formation of strong oxidants (hydroxyl radicals ( $\cdot\text{OH}$ ), Table 1.1); 2) the reaction of these oxidants with organic contaminants in the water (Shan, et al., 2010).

Table 1.1. Oxidation potential and relative oxidizing power of chemical oxidants (Munter, 2001)

Compound	Oxidation potential, V	Relative oxidizing power
Hydroxyl radical	2.8	2.1
Sulfate radical	2.6	1.9
Ozone	2.1	1.5
Hydrogen peroxide	1.8	1.3
Permanganate	1.7	1.2
Chlorine dioxide	1.5	1.1
Chlorine	1.4	1.0
Oxygen	1.2	0.9
Bromine	1.1	0.8
Iodine	0.76	0.54

## 1.2. Photoelectrocatalysis: Basic concepts

PEC relies on a semiconductor (mostly  $\text{TiO}_2$ ) which is irradiated with light energy equal to or greater than its band-gap energy. Since 1972 it has been known that it is possible to promote photoelectrolysis of water (water splitting) under anodic bias potential (Fujishima & Honda, 1972). Since then, also photocatalysis (PC) has been explored to promote organics

oxidation (Bessegato, et al., 2013; Cardoso, et al., 2010; Brugnera, et al., 2010), inorganics reduction (Paschoal, et al., 2013; LaTempa, et al., 2012), disinfection of water containing biological materials (Brugnera, et al., 2012; Brugnera, et al., 2013) and production of electricity and hydrogen (Lianos, 2011; Paulauskas, et al., 2008; Abe, 2010). A semiconductor material is characterized by two energy bands separated by the band-gap energy, eg. a semiconductor at absolute zero is acting as insulator, because the valence band (lower energy level) is entirely occupied and the conduction band (higher energy level) entirely empty (Figure 1.2).

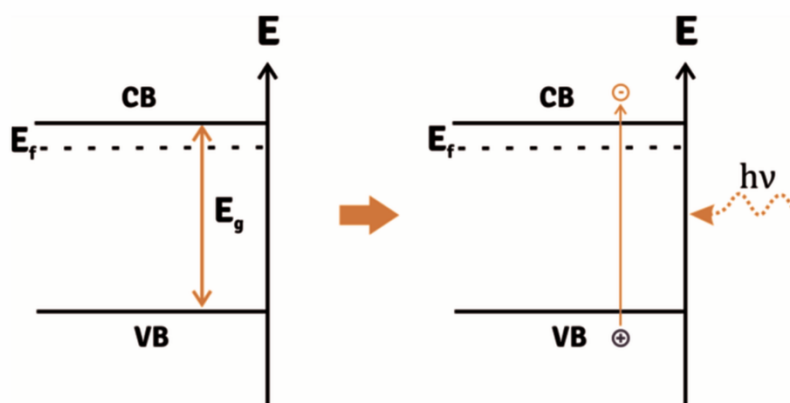
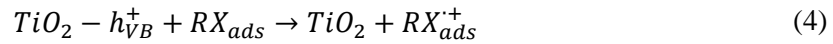
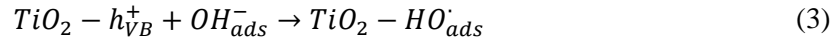
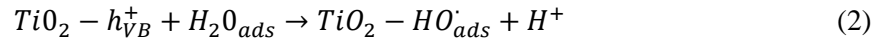
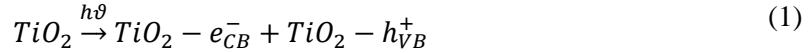


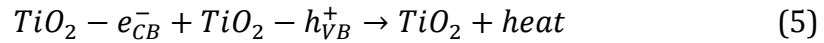
Figure 1.2. Schematic representation of energy band diagram in semiconductors and the mechanism of charge carrier generation of photoexcitation (Guijarro, et al., 2015)

In order to get conductive, charge carriers need to be created, usually by photoexcitation. The basic concept is that, when a semiconductor surface is irradiated by light ( $h\nu \geq E_g$ ), electron/hole pairs ( $e^-/h^+$ ) are generated by the promotion of electrons from the valence band (VB) to the conduction band (CB) (Equation 1) (Linsebigler, et al., 1995; Rajeshwar, 2007). The oxidizing nature of the holes ( $h^+$ ) in the valence band means they generate  $\cdot\text{OH}$  radicals,

by the oxidation of H<sub>2</sub>O molecules or OH<sup>-</sup> ions adsorbed on the semiconductor surface, that are able to oxidize organic molecules. The photoexcitation of TiO<sub>2</sub> and possible oxidation of an organic compound (RX) are represented in Equations 1–4 (Andreozzi, et al., 1999; Rajeshwar, et al., 2008).



In spite of the fact that heterogeneous photocatalysis is a well understood and investigated topic, and despite its promising results in water purification, its practical utilization has been restricted by its low photonic efficiency, which is mainly due to recombination of the e<sup>-</sup>/h<sup>+</sup> pair, as shown in Equation 5 (Egerton, et al., 2006; Rajeshwar, et al., 2008).



Since photodegradation by hydroxyl radicals occurs near the surface of the catalysts, also adsorption of organic pollutants plays an important role. It was reported that photocatalysts, especially the planar structured ones, have a limited adsorption capacity (Sun, et al., 2013; Kumar, et al., 2015). It is therefore desirable to design electrodes that are synergistically effective in both adsorption and photodegradation. The photo activity strongly depends on the presence and absence of an applied bias as well as on the material properties and configuration of the electrode. For efficient device applications, electrodes having a large specific surface area are the prime need of the present scenario, and semiconductors with porous morphology are a relevant component for system application. When the photocatalyst is deposited to a conductive substrate, there is an option to apply an anodic bias potential

to the semiconductor and to change the substrate/electrolyte interface. Introduction of bias in the system enhances the efficiency of charge separation by driving the generated electrons via the external circuit to the counter electrode (Andreozzi, et al., 1999; Fujishima & Honda, 1972). Figure 1.3 illustrates the mechanism of PEC. When a semiconductor is in contact with an electrolyte a junction semiconductor/electrolyte interface is created, which determines the carriers (electrons – holes) separation kinetics. A change in the electrochemical potential (Fermi level) is caused by the junction in a redox electrolyte due to differing potentials at the interface.

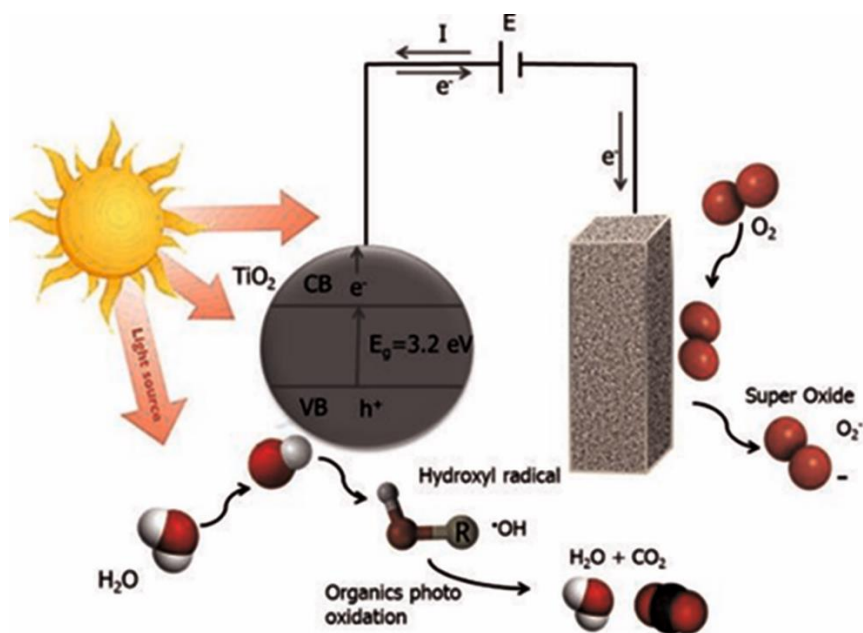


Figure 1.3. Schematic representation of the mechanism of separation and recombination of charges in the photocatalysis or PEC and mechanism of charge separation in a photoelectrochemical system, where a gradient of potential is created (Guijarro, et al., 2015; Zheng, et al., 2014)

Therefore, the equilibrium of this interface acquires the flow of charge from one phase to another, and a band-bending is created within the semiconductor

phase. The area where there is bending is called the space charge layer (SCL) and is characterized by the accumulation of electrons or holes at the surface (Chaplin, 2014; Linsebigler, et al., 1995; Paramasivam, et al., 2012; Finklea, 1988). Figure 1.4 shows the behavior of the electrons and holes in the semiconductor before and after equilibrium.

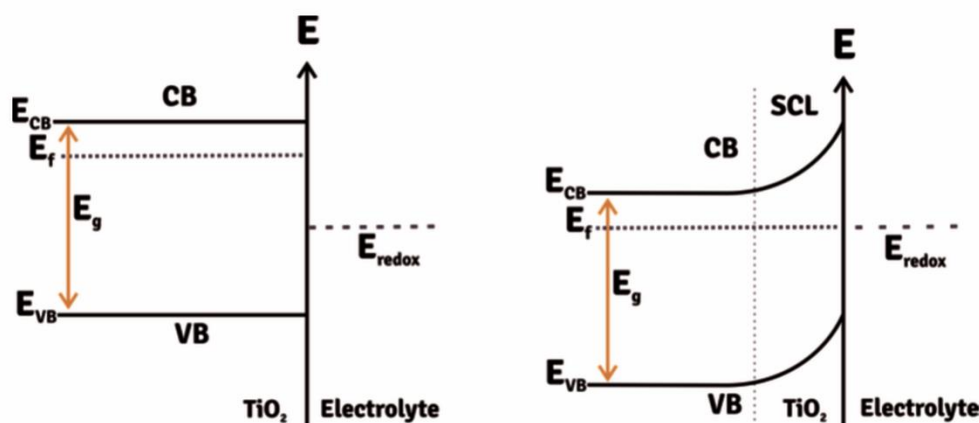


Figure 1.4. Energy band diagram for an n-type semiconductor before and after the equilibration of Fermi levels at the interface semiconductor/electrolyte, and the appearance of band-bending and the space charge layer (SCL) (Guijarro, et al., 2015; Zheng, et al., 2014)

Thus, to control the Fermi level (and therefore the band-bending) a bias potential is applied (Paramasivam, et al., 2012). For any given semiconductor and electrolyte, there is an exact potential, flat-band potential  $V_{fb}$ , for which there is no electrical charge in the semiconductor and therefore the potential drops between the surface and the bulk of the electrode is zero (Figure 1.5) (Memming, 2015). The application of any potential greater than the flatband potential will increase the band-bending at the n-type semiconductor electrode, such as TiO<sub>2</sub>. In this case electrons are consumed and holes enriched at surface, as we can see in Figure 1.5.

When  $\text{TiO}_2$  is irradiated, it is noticed that the generated holes have an oxidizing potential equivalent to the potential of the valence band edge, and are able to oxidize a molecule (formal potential is more negative than the valence band). In the case of  $\text{TiO}_2$  in water, the  $\text{H}_2\text{O}$  can be oxidized producing  $\cdot\text{OH}$  radicals. The electron from the conduction band further flows via an external circuit to the counter electrode, where undergoes the reduction reactions, such as the reduction of  $\text{H}^+$  ions to  $\text{H}_2$  (Figure 1.2). The greater the band-bending (and therefore the SCL) the faster the electron/hole separation occurs, and then the recombination of charges is minimized (Memming, 2015).

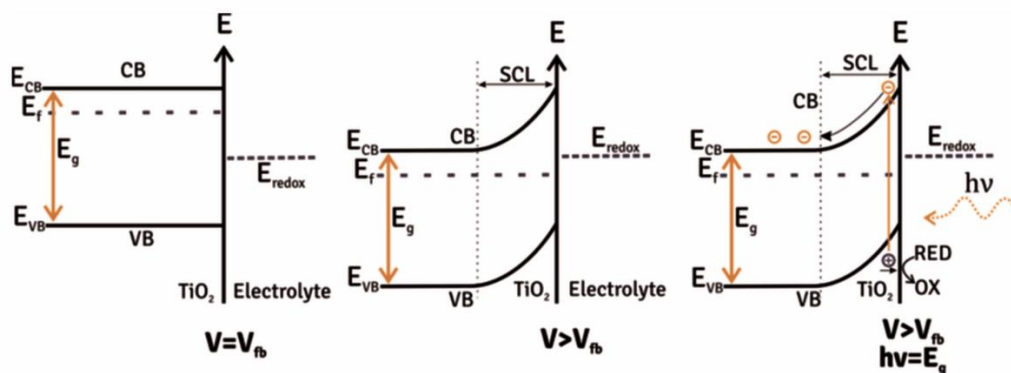


Figure 1.5. Energy band diagram for a n-type semiconductor when the applied potential ( $V$ ) is equal to flat-band potential ( $V_{fb}$ ) and when the applied potential ( $V$ ) is greater than  $V_{fb}$ . The last schematic shows the mechanism of charge separation when the electrode is submitted for a potential higher than the  $V_{fb}$  and irradiated with  $\lambda \geq E_g$  (Guijarro, et al., 2015; Memming, 2015)

### 1.3. Strategies to enhance the system efficiency and design of the PEC system

Several photocatalysts have been applied in PEC, among them  $\text{TiO}_2$ ,  $\text{WO}_3$ ,  $\text{ZnO}$ ,  $\text{CdS}$ ,  $\text{Fe}_2\text{O}_3$  and  $\text{SnO}_2$  (Sizilagyi, et al., 2012; Bai, et al., 2013; Wang, et al., 2014;



Mishra & Chun, 2015; Cun, et al., 2002). Over the years considerable efforts have been devoted to the improvement of the materials used in photo(electro)catalysis (P(E)C).  $\text{TiO}_2$  has become one of the most typical materials as it is environmentally friendly, long lasting and cheap; has a long lifetime of electron/hole pairs; presents a compatible energy position of VB and CB; and is chemically, thermally and mechanically stable (Egerton, et al., 2006; Pirkarami, et al., 2014). Among these features, the band edge positions relative to  $\text{H}_2\text{O}$  oxidation improves the applicability of  $\text{TiO}_2$  in P(E)C to create  $\cdot\text{OH}$  radicals (Paramasivam, et al., 2012). Heterogeneous PC started with the use of  $\text{TiO}_2$  semiconductors in a slurry system (suspension of fine powder). The most efficient powder reported in literature is the Degussa P25, which is a combination of rutile and anatase allotropic phases in the ratio 3:11 (Serrano, et al., 2007). There are some advantages of using this powder: it provides a large surface area showing a good photocatalytic activity, and it presents a good adsorptive affinity of organic compounds on the surface of the anatase (Gautam, et al., 2016). However, a post-treatment filtration step is required to separate it from the solution, which limits practical application. Moreover, the suspended particles tend to aggregate, especially at high concentrations, making the separation more complexed and limiting its application in continuous flow systems (Thiruvengkatachari, et al., 2008). In addition  $\text{TiO}_2$  particles in a slurry system behave as short-circuited microelectrodes under bandgap excitation. A high degree of recombination between photo-generated charge carriers loses the irradiation energy as heat. The immobilization of  $\text{TiO}_2$  on a substrate has offers an alternative way of using powder and a search for film deposition techniques started (Vergohl, et al., 2011). Several researchers have anchored photocatalysts onto a variety of surfaces, such as glass (ITO and FTO), silica gel, metal, ceramics, polymers, thin films, fibres, zeolites, alumina clays, activated carbons, cellulose, and reactor walls (Hanel, et al., 2010; Sopyan, et al., 2011; Kerkez & Boz, 2013; Sarno, et

al., 2015; Carneiro, et al., 2012). In order to support  $\text{TiO}_2$  three main points must be achieved: strong adherence, stability of the catalyst, high specific surface area to promote successful adsorption of the pollutant on the electrode surface (Ibhadon & Fitzpatrick, 2013). The electron transfer along the film is greatly influenced by the supporting material. It is reported by Ibhadon & Fitzpatrick that conducting glasses have a relatively poor connection within the film; while, metal substrates show a lower impedance since there is a reduction of charge transfer resistance resulting in better PEC activity (Ibhadon & Fitzpatrick, 2013).

Moreover, the P(E)C activity of a  $\text{TiO}_2$  system mainly depends on its intrinsic properties, such as particle size, surface area, film thickness, crystallinity and crystal phase (Ibhadon & Fitzpatrick, 2013; Shan, et al., 2010). The most reported preparation routes are sol-gel, chemical vapour deposition, electrodeposition, sol-spray, and hydrothermal methods (Zhu, et al., 2000; Byun, et al., 2000; Natarajan & Nogami, 1996). In addition to the preparation routes, the coating techniques also influence the resulting material properties. When compared to other methods, the advantages of the paint-thermal decomposition technique are easiness to control deposits, reliability and reproducibility, resulting in good-quality deposited films (Rincon, et al., 2001). Successful formation of the wanted crystal phase is directly connected to the used material, composition, deposition method and the annealing temperature. The crystal morphology is interconnected to the light absorption as incident light affects PEC efficiency. Layer thickness of the catalyst film can affect the light energy conversion efficiency and electron transfer. Thicker films can lower efficiency as these processes manifest a higher resistance (Linsebigler, et al., 1995; Rajeshwar, 2007; Finklea, 1988).

Although it is the mostly used material in PEC applications,  $\text{TiO}_2$  has some limitations that hinder its technological application. Existing challenge, when

working with  $\text{TiO}_2$ , is its deposition on the conductive substrate and consequently good properties of the formed film (Shan, et al., 2010).

The method of submission is very important to achieve a good adhesion of the  $\text{TiO}_2$  particles to the surface, with increased interest to enhance and investigate film properties for its relevant application in water treatment. In all cases, the properties of the electrode material have direct relevance to their good performance in practice (Finklea, 1988). The improvement in structural properties will also help to prevent  $\text{TiO}_2$  film from cracking and increase its durability and stability.

Choosing the deposition method and optimizing the film properties of the case specific deposition method, will decrease the gap in knowledge concerning the coating abilities and the structure of the  $\text{TiO}_2$  films used in PEC process. Moreover, it was observed that photo(electro)catalytic degradation of organic compounds are largely dependent on solution pH, light intensity, amount of catalyst deposited, pollutant concentration (Habibi, et al., 2005; Muruganandham & Swaminathan, 2006). Understanding the influence of these parameters on the photo(electro)catalytic degradation efficiency is of paramount importance for the electrode and system design.

Additional effort has been made to improve the optical absorption of catalysts for their photocatalytic activity, with metals, non-metals, or self-doping (Hameed & Rahman, 2008; Xiaoli, et al., 2003; Fakhouri, et al., 2014; Smith, et al., 2012; Smith, et al., 2012).

Instead of using only UV light, utilizing the entire solar spectrum is more attractive, as it increases the amount of energy that can be converted. Solar utilization in PEC technologies may thus improve the process effectiveness without substantially increasing the costs of the water treatment.

Working toward this goal, other photocatalysts based on metal oxides that are active under visible light must be considered.  $\text{BiVO}_4$ , which has previously been used for solar water splitting, is a suitable candidate due to its favorable

optical and electronic properties. It has also been used for photocatalytic degradation of contaminants in a spindle-like structure modified by polyaniline (PANI/BiVO<sub>4</sub>) and as a nanostructured electrode (Abdi, et al., 2013; Shang, et al., 2009; Hou, et al., 2012). Furthermore, BiVO<sub>4</sub> can be combined with solar cell, creating a bias-free device to directly use solar light for water purification.

Finally, the effect of PEC reactor design parameters on the treatment of water has received much attention in existing literature on the utilization of PEC technology (Xu, et al., 2008; Marugan, et al., 2013). Yet it seems that previous studies, due to different design and geometry of the reactors, have not combined all design parameters to achieve a high rate of removal efficiency in a cost-effective way.

The structures of substrate materials commonly used, do not allow an even light distribution in a reactor with the immobilized photocatalyst and therefore the recorded photocatalytic efficiency was much lower compared to that of slurry reactor (Silva, et al., 2012).

Therefore, the challenge of designing an efficient photocatalytic reactor is in using a suitable catalyst structure to optimize both the surface area covered by semiconductor particles and the light distribution. The design criteria of such a reactor should be continuous renewal of the catalyst-reactant interface, high surface area per unit reactor volume, and reduced light absorption and shadowing effect to the surface of the photocatalyst (Abhang, et al., 2011).

## **1.4. Objective and outline of the thesis**

### **1.4.1. Objective of the thesis**

Despite the fast development in the photocatalytic field, few uncertainties remain in the scientific world around the established area of interest such as

low quantum yield, reliable deposition method for higher surface areas and photocatalyst activation in the visible range.

Also in relation to the background given earlier, therefore, the objective that motivated this study is:

Development of a simple, solar energy based technology using photoelectrocatalysis, for the treatment of toxic and/or low biodegradable organic compounds.

To achieve this objective two pathways were sought:

- Improvement of the photoelectrocatalytic activity and its efficiency by reducing the charge carriers' recombination (by changing the crystal structure (annealing) and application of the bias) and optimising the process conditions (optimal light intensity, agitation, surface/volume ratio, optimal potential),
- Design and development of photoanodes and an optimised reactor that can work both under UV and visible or solar light irradiation.

In favour of a better utilization of the PEC, decreasing the recombination limitation of photogenerated charge carriers and higher responsiveness to the irradiated photons in PEC systems, different strategies have been developed and adopted in this research (Figure 1.6).

First, process optimization was studied by finding crystalline phase-optimised P(E)C performance, including the method by which the ratio of crystalline phases can be controlled. In addition, an outline of the effects of P(E)C operating parameters was included as second step in the process optimization strategy.

The second part of the study was summarized as PEC in water treatment, embracing work on photoanodes and their material, configuration and performance. Design and use of PEC UVC and solar TiO<sub>2</sub> flow reactors were incorporated in this part of the study.

The final part referred to application, including innovations in the field of PEC and broadening the scope into environmental and sustainable energy fields of research.

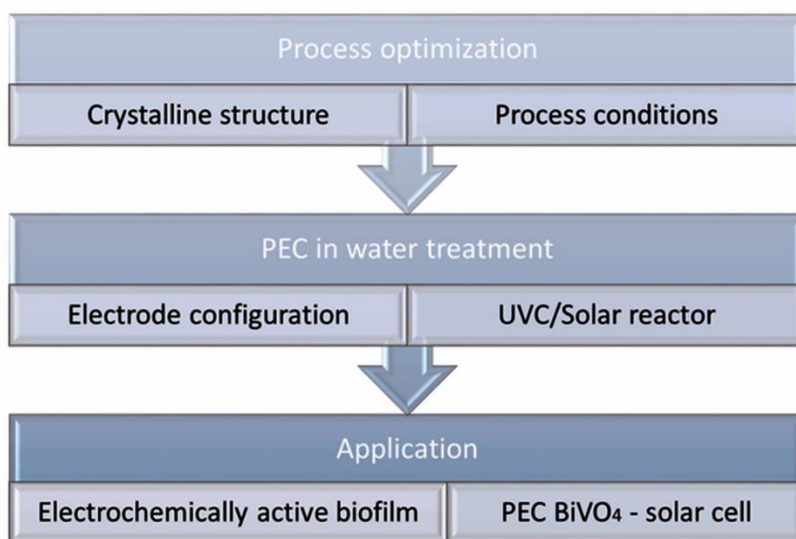


Figure 1.6. Strategies for enhancing PEC efficiency and scaling up of the technology

Thus, a bottom-up strategy was adopted to systematically investigate photo(electro)catalytic removal of organic contaminants and to finally propose practical application for potential commercialization of a photoelectrocatalytic system, of which the application of visible light might be a potential breakthrough.

## **1.5. Thesis outline**

Due to the large varieties of used photocatalysts and their deposition methods, it is a priori to apply an effective and quantitative catalyst screening under similar conditions.

The surface characteristics, and consequently the apparent photocatalytic activity, could be modified by various pre-treatment procedures. Chapter 2 describes the effect of TiO<sub>2</sub> thermal pretreatment and applied bias on the apparent photo(electro)catalytic activity. In this chapter it is described how a photocatalyst was assembled and verified for successful PEC application for phenol degradation in water.

The positive outcome of the photocatalyst screening provide a solid basis for further photocatalyst activity studies that show more insights into the complex interactions of reaction intrinsic kinetics, surface chemistry with reactant and photons, and the transportation characteristics of reactants/products.

In chapter 3 the effects of various experimental parameters (TiO<sub>2</sub> layer thickness, agitation, light intensity and initial concentration of phenol) on the PEC process performance of phenol degradation were discussed in order to determine which mechanism becomes dominant under varying conditions.

In PEC, a practical electrode configuration must combine the maximal capture of photons throughout the reactor with, minimal mass-transfer limitations to and from the electrodes, and minimal electrode resistance between the anode and cathode. Even with an optimal configuration of plate electrodes, the overall resistance of the oxidation process is at the anode. Therefore, this research, described in chapter 4, focuses on the configuration of the anode. A novel geometric arrangement of the electrodes with parallel mesh anodes exposed to the light source was, for the first time, used.

Moreover, the PEC process was operated on the larger scale, which included a self-designed PEC solar and UVC reactor that is reflected in chapter 5.

The research described in chapter 6 is an attempt to expand the gained knowledge of PEC on a new application in the field of electrochemically active biofilm electrodes. In such a system, a synergistic effect was expected to occur between the bio-electrochemical and photocatalytic oxidation processes.

TiO<sub>2</sub>/Ti composite electrodes were operated with variable biofilm coverage to study the effectiveness of biofilm formation in enhancing the electron transfer.

The last chapters (7 and 8) present the development, preparation, characterization and demonstration of an alternative visible light photoelectrode (BiVO<sub>4</sub>) in PEC systems for organic pollutant removal from water. The BiVO<sub>4</sub> anode was coupled to a solar cell.

In this way solar power could be used as a solution to reduce potential operational costs and increase energy self-reliance.

The final chapter of the thesis (chapter 9) summarises the outcomes of this study and future work.



## References

- Abdi, F. F., Han, L., Smets, A., Zeman, M., Dam, B. & R. v. d. Krol, 2013. Efficient solar water splitting by enhanced charge separation in a bismuth vanadate-silicon tandem photoelectrode. *Nat. commun.*, Volume 4.
- Abe, R., 2010. Recent progress on photocatalytic and photoelectrochemical water splitting under visible light irradiation. *J. Photochem. Photobiol., C*, Volume 11, pp. 179-209.
- Abhang, R. M., Kumar, D. & Taralkar, S. V., 2011. Design of Photocatalytic Reactor for Degradation of Phenol in Wastewater. *Int. J. Chem. Eng. Appl.*, Volume 2, pp. 337-341.
- Andreozzi, R., Caprio, V., Insola, A. & R. Marotta, 1999. Advanced oxidation processes (AOP) for water purification and recovery. *Catal. Today*, Volume 53, pp. 51-59.
- Bai, X., Wang, L., Zong, R., Lv, Y., Sun, Y. & Zhu, Y., 2013. Performance Enhancement of ZnO Photocatalyst via Synergic Effect of Surface Oxygen Defect and Graphene Hybridization. *Langmuir*, Volume 29, pp. 3097-3105.
- Bessegato, G. G., Cardoso, J. C., Silva, B. F. & Zanoni, M. V. B., 2013. Enhanced photoabsorption properties of composites of Ti/TiO<sub>2</sub> nanotubes decorated by Sb<sub>2</sub>S<sub>3</sub> and improvement of degradation of hair dye. *J. Photochem. Photobiol., A*, Volume 276, pp. 96-103.
- Brillas, E., 2014. A review on the degradation of organic pollutants in waters by UV photoelectro-Fenton and solar photoelectro-Fenton. *J. Braz. Chem. Soc.*, Volume 25, pp. 393-417.
- Brugnera, M. F., Miyata, M., Zocolo, J. T., Leite, C. Q. F. & Zanoni, M. V. B., 2012. Inactivation and disposal of by-products from *Mycobacterium smegmatis* by photoelectrocatalytic oxidation using Ti/TiO<sub>2</sub>-Ag nanotube electrodes. *Electrochim. Acta*, Volume 85, pp. 33-41.
- Brugnera, M. F., Miyata, M., Zocolo, J. T., Leite, C. Q. F. & Zanoni, M. V. B., 2013. A photoelectrocatalytic process that disinfects water contaminated with *Mycobacterium kansasii* and *Mycobacterium avium*. *Water Res.*, Volume 47, pp. 6596-6605.

- Brugnera, M. F., Rajeshwar, K., Cardoso, J. C. & Zanoni, M. V. B., 2010. Bisphenol A removal from wastewater using self-organized TiO<sub>2</sub> nanotubular array electrodes. *Chemosphere*, Volume 78, pp. 569-575.
- Byun, D., Jin, Y., Kim, B., Lee, J. K. & Park, D., 2000. Photocatalytic TiO<sub>2</sub> deposition by chemical vapor deposition. *J. Hazard. Mater.*, Volume 73, pp. 199-206.
- Cardoso, J. C., Lizier, T. M. & Zanoni, M. V. B., 2010. Highly ordered TiO<sub>2</sub> nanotube arrays and photoelectrocatalytic oxidation of aromatic amine. *Appl. Catal., B*, Volume 99, pp. 96-102.
- Carneiro, J. O., Teixeira, V., Azevedo, S., Fernandes, F. & Neves, J., 2012. Development of photocatalytic ceramic materials through the deposition of TiO<sub>2</sub> nanoparticles layers. *J. Nano Res. Vols.*, Volume 18, pp. 165-176.
- Cecen, F. & Aktas, O., 2012. *Activated Carbon for Water and Wastewater Treatment*. Weinheim: Wiley-VCH Verlag & Co. KGaA.
- Chaplin, B. P., 2014. Critical review of electrochemical advanced oxidation processes for water treatment applications. *Environ. Sci.: Processes Impacts*, Volume 16, pp. 1182-1203.
- Chopra, A. K., Sharma, A. K. & Vinod, K., 2011. Overview if electrolytic treatment: an alternative technology for purification of wastewater. *Appl. Sci. Res.*, Volume 3, pp. 191-206.
- Crittenden, J. C., Liu, J., Hand, D. W. & Perram, D. L., 1997. Photocatalytic oxidation of chlorinated hydrocarbons in water. *Water Res.*, Volume 31, pp. 429-438.
- Cun, W., Jincai, Z., Xinming, W., Bixian, M., Guoying, S., Pingan, P. & Jiamo, F., 2002. Preparation, characterization and photocatalytic activity of nano-sized ZnO/SnO<sub>2</sub> coupled photocatalyst. *Appl. Catal., B*, Volume 39, pp. 269-279.
- Egerton, T. A., Christensen, P. A., Kosa, S. A. M., Onoka, B., Harper, J. C. & Tinlin, J. R., 2006. Photoelectrocatalysis by titanium dioxide for water treatment. *Int. J. Environ. Pollut.*, Volume 27, pp. 2-19.
- Fakhouri, H., Smith, W., Pulpytel, J., Zolfaghari, A., Mortaheb, H., Meshikini, F., Jafari, R. & Arefi-Khonsari, F., 2014. Visible Light Water Splitting and Enhanced UV Photocatalysis from Nitrogen Doped TiO<sub>2</sub> Thin Films. *Appl. Catal., B*, Volume 144, pp. 12-21.

- Finklea, H. O., 1988. Semiconductor electrodes. New York: Elsevier.
- Fujishima, A. & Honda, K., 1972. Electrochemical photolysis of Water at a Semiconductor Electrode. *Nature*, Volume 238, pp. 37-38.
- Gautam, A., Kshirsagar, A., Biswas, R., Banerjee, S. & Khanna, P. K., 2016. Photodegradation of organic dyes based on anatase and rutile TiO<sub>2</sub> particles. *RSC Adv.*, Volume 6, pp. 2746-2759.
- Guijarro, N., Prevot, M. S. & Sivula, K., 2015. Surface modification of semiconductor electrodes. *Phys. Chem. Chem. Phys.*, Volume 17, pp. 15655-15674.
- Habibi, M. H., Hassanzadeh, A. & Mahdavi, S., 2005. The effect of operational parameters on the photocatalytic degradation of three textile azo dyes in aqueous TiO<sub>2</sub> suspensions. *J. Photochem. Photobiol., A*, Volume 172, pp. 89-96.
- Hameed, B. H. & Rahman, A. A., 2008. Removal of phenol from aqueous solutions by adsorption on activated carbon prepared from biomass material. *J. Hazard. Mater.*, Volume 160, pp. 576-581.
- Hanel, A., Moren, P., Zaleska, A. & Hupka, J., 2010. Photocatalytic activity of TiO<sub>2</sub> immobilized on glass beads. *Physicochem. Probl. Miner. Process.*, Volume 45, pp. 49-56.
- Hou, L., Yang, L., Li, J., Tan, J. & Yuan, C., 2012. Efficient Sunlight-induced Methylene Blue Removal over One-Dimensional Mesoporous Monoclinic BiVO<sub>4</sub> nanorods. *J. Anal. Methods Chem.*, Volume 2012.
- Ibhadon, A. O. & Fitzpatrick, P., 2013. Heterogeneous Photocatalysis: Recent Advances and Applications. *Catalysts*, Volume 3, pp. 189-218.
- Kerkez, O. & Boz, I., 2013. Efficient removal of methylene blue by photocatalytic degradation with TiO<sub>2</sub> nanorod array thin films. *React. Kinet. Mech. Catal.*, Volume 110, pp. 543-557.
- Kumar, R., Rashid, J. & Barakat, M. A., 2015. Zero valent Ag deposited TiO<sub>2</sub> for the efficient photocatalysis of methylene blue under UV-C light irradiation. *Colloids and Interface Science Communications*, Volume 5, pp. 1-4.
- Kutzer, S., Wintrich, H. & Mersmann, A., 1995. Air stripping- a method for treatment of wastewater. *Chem. Eng. Technol.*, 18(3), pp. 149-155.

- LaTempa, T. J., Rani, S., Bao, N. & Grimes, C. A., 2012. Generation of fuel from CO<sub>2</sub> saturated liquids using a pi-Si nanowire parallel to n-TiO<sub>2</sub> nanotube array photoelectrochemical cell. *Nanoscale*, Volume 4, pp. 2245-2250.
- Lawrence, J. & Cappelli, F. P., 1977. Ozone in drinking water treatment: A review. *Sci. Total Environ.*, Volume 7.
- Lianos, P., 2011. Production of electricity and hydrogen by photocatalytic degradation of organic wastes in a photoelectrochemical cell: The concept of the Photofuelcell: A review of a re-emerging research field. *J. Hazard. Mater.*, Volume 185, pp. 575-590.
- Linsebigler, A. L., Lu, G. Q. & Yates, J. T., 1995. Photocatalysis on TiO<sub>2</sub> surfaces-Principles, Mechanism, and Selected Results. *Chem. Rev.*, Volume 95, pp. 735-758.
- Martinez-Huitle, C. A. & Brillas, E., 2009. Decontamination of wastewaters containing synthetic organic dyes by electrochemical methods: A general review. *Appl. Catal., B*, Volume 87, pp. 105-145.
- Marugan, J., v. Grieken, R., Pablos, C., Adan, C. & Timmers, R., 2013. Determination of Photochemical, Electrochemical and Photoelectrochemical Efficiencies in a Photoelectrocatalytic reactor. *Int. J. Chem. React. Eng.*, Volume 11, pp. 787-797.
- Memming, R., 2015. *Semiconductor Electrochemistry*. Weinheim: Wiley-VCH.
- Mishra, M. & Chun, D. M., 2015.  $\alpha$ -Fe<sub>2</sub>O<sub>3</sub> as a photocatalytic material: A review. *Appl. Catal., A*, Volume 498, pp. 126-141.
- Munter, R., 2001. Advanced oxidation processes-current status and prospects. *Proc. Estonian Acad. Sci. Chem.*, Volume 50, pp. 59-80.
- Muruganandham, M. & Swaminathan, M., 2006. TiO<sub>2</sub>-UV photocatalytic oxidation of Reactive Yellow 14: Effect of operational parameters. *J. Hazard. Mater.*, Volume 135, pp. 78-86.
- Naajm, I. & Trussell, R. R., 1999. New and Emerging Drinking Water Treatment Technologies. In: *Identifying Future Drinking Water Contaminants*. Washington D. C.: National Academy Press, pp. 220-243.
- Natarajan, C. & Nogami, G., 1996. Cathodic Electrodeposition of Nanocrystalline Titanium Dioxide Thin Films. *J. Electrochem. Soc.*, Volume 143, pp. 1547-1550.

United Nations, 2013. Sustainable Development Challenges, New York: United Nations Publication.

Paramasivam, I., Jha, H., Liu, N. & Schmuki, P., 2012. Review of Photocatalysis using Self-organized TiO<sub>2</sub> Nanotubes and Other Ordered Oxide Nanostructures. *Small*, Volume 8, pp. 3073-3103.

Paschoal, F. M. M., Nunez, L., Lanza, M. R. d. V. & Zanoni, M. V. B., 2013. Nitrate removal on a Cu/Cu<sub>2</sub>O Photocathode under UV irradiation and bias potential. *J. Adv. Oxid. Technol.*, Volume 16, pp. 63-70.

Paulauskas, I. E., Katz, J. E., Jellison, G. E., Lewis, N. S. & Boatner, L. A., 2008. Photoelectrochemical studies on semiconducting photoanodes for hydrogen production via water dissociation. *Thin Solid Films*, Volume 516, pp. 8175-8178.

Pirkarami, A., Olya, M. E. & Farshid, S. R., 2014. UV/Ni-TiO<sub>2</sub> nanocatalyst for electrochemical removal of dyes considering operating costs. *Water Resources and Industry*, Volume 5, pp. 9-20.

Rajeshwar, K., 2007. Fundamentals of Semiconductor Electrochemistry and Photoelectrochemistry. Weinheim: Wiley.

Rajeshwar, K., Osugi, M. E., Chanmanee, W., Chenthamarakshan, C. R., Zanoni, M. V. B., Kajitvichyanukul, P. & Krishnan-Ayer, R., 2008. Heterogeneous photocatalytic treatment of organic dyes in air and aqueous media. *J. Photochem. Photobiol., C*, Volume 9, pp. 171-192.

Rincon, M. E., Gomez-Daza, O., Corripio, C. & Orihuela, A., 2001. Sensitization of screen-printed and spray-painted TiO<sub>2</sub> coatings by chemically deposited CdSe thin Films. *Thin Solid Films*, Volume 389, pp. 91-98.

Rittmann, B. E., Huck, P. M. & Bouwer, E. J., 1989. Biological treatment of public water supplies. Taylor&Francis, pp. 119-184.

Sarno, G., Vaiano, V., Sannino, D. & Ciambelli, P., 2015. Photocatalytic applications with TiO<sub>2</sub>-Zeolites Composites Anchored on Ceramic Tiles. *Chemical Engineering Transactions*, Volume 43, pp. 2283-9216.

Serrano, D. P., Calleja, G., Sanz, R. & Pizarro, P., 2007. Development of crystallinity and photocatalytic properties in porous TiO<sub>2</sub> by mild acid treatment. *J. Mater. Chem.*, Volume 17, pp. 1178-1187.

Shan, A. Y., Ghazi, T. I. M. & Rashid, S. A., 2010. Immobilisation of titanium dioxide onto supporting materials in heterogeneous photocatalysis: A review. *Appl. Catal., A*, Volume 389, pp. 1-8.

Shan, A. Y., Ghazi, T. I. M. & Rashid, S. A., 2010. Immobilisation of titanium dioxide onto supporting materials in heterogeneous photocatalysis: A review. *Appl. Catal., A*, Volume 389, pp. 1-8.

Shang, M., Wang, W., Sun, S., Ren, J., Zhou, L. & Zhang, L., 2009. Efficient Visible Light-Induced Photocatalytic Degradation of Contaminant by Sprondle-like PANI/BiVO<sub>4</sub>. *J. Phys. Chem.*, Volume 113, pp. 20228-20233.

Silva, F. V., Lansarin, M. A. & Moro, C. C., 2012. A comparison of slurry and immobilized TiO<sub>2</sub> in the photocatalytic degradation of phenol. *Lat. Am. Appl. Res.*, Volume 42, pp. 275-280.

Sizilagyi, I. M., Forizs, B., Rosseler, O., Szegedi, A., Nemeth, P., Kiraly, P., Tarkanyi, K., Vajna, B., Varga-Josepovits, K., Laszlo, K., Toth, A. L., Baranyai, P. & Leskela, M., 2012. WO<sub>3</sub> photocatalyst: Influence of structure and composition. *J. Catal.*, Volume 294, pp. 119-127.

Smith, W., Fakhouri, H., Mori, S., Pulpytel, J. & Arefi-Khonsari, F., 2012. Oxidation Kinetics of Tin Films Deposited by RF Reacting Sputtering at High and Low Pressure. *J. Phys. Chem. C*, Volume 116, pp. 15855-15866.

Smith, W., Fakhouri, H., Pulpytel, J. & Arefi-Khansari, F., 2012. Control of the Optical and Crystalline Properties of TiO<sub>2</sub> in Photoactive TiO<sub>2</sub>/TiN Bi-Layer Thin Film Stacks. *J. Appl. Phys.*, Volume 111, p. 024301.

Sopyan, I., Hafizah, N. & Jamal, P., 2011. Immobilization of TiO<sub>2</sub> with cement: Photocatalytic degradation of phenol and its kinetic studies. *Indian J. Chem. Technol.*, Volume 18, pp. 263-270.

Sun, J., Fu, Y., Xiong, P., Sun, X., Xu, B. & Wang, X., 2013. A magnetically separable P25/CoFe<sub>2</sub>O<sub>4</sub>/graphene catalyst with enhanced adsorption capacity and visible-light-driven photocatalytic activity. *RSC Advances*, Volume 3, pp. 22490-22497.

Thiruvengkatachari, R., Vigneswaran, S. & Moon, I. S., 2008. A review on UV/TiO<sub>2</sub> photocatalytic oxidation process. *Korean J. Chem. Eng.*, Volume 25, pp. 64-72.

- Topudurti, K. V., Lewis, N. M. & Hirs, S. H., 1993. The applicability of UV/oxidation technologies treat contaminated groundwater. *Environ. Prog.*, Volume 12, pp. 54-60.
- Vergohl, M., Althues, H., Frach, P., Gloss, D., Graumann, T., Hubner, C., Neumann, F., Neubert, T., Schottner, G. & Song, D. K., 2011. Photocatalytic TiO<sub>2</sub> films deposited by different methods. *Vakuum in Forschung und Praxis*, Volume 23, pp. 17-21.
- Wang, Q., Li, j., Bai, Y., Lian, J., Huang, H., Li, Z., Lei, Z. & Shangguan, W., 2014. Photochemical preparation of Cd/CdS photocatalyst and their efficient photocatalytic hydrogen production under visible light irradiation. *Green Chem.*, Volume 16, pp. 2728-2735.
- Xiaoli, Y., Huixiang, S. & Dahui, W., 2003. Photoelectrocatalytic Degaradtion of Phenol using a TiO<sub>2</sub>/Ni Thin-Fulm Electrode. *Korean J. Chem. Eng.*, Volume 20, pp. 679-684.
- Xu, Y., He, Y., Cao, X., Zhong, D. & Jia, J., 2008. TiO<sub>2</sub>/Ti Rotating Disk Photoelectrocatalytic Reactor (PEC): A Combination of Highly Effective Thin-Film PEC and Conventional PEC Process on a Single Electrode. *Environ. Sci. Technol.*, Volume 42, pp. 2612-2617.
- Zheng, X., Li, D., Li, X., Yu, L., Wang, P., Zhang, X., Fang, J., Shao, Y. & Zheng, Y., 2014. Photoelectrocatalytic degradation of rhodamine B on TiO<sub>2</sub> photonic crystals. *Phys. Chem. Chem. Phys.*, Volume 16, pp. 15299-15306.
- Zhu, Y., Zhang, L., Gao, C. & Cao, L., 2000. The syntehsis of nanosized TiO<sub>2</sub> powder using a sol-gel method with TiCl<sub>4</sub> as a precursor. *J. Mater. Sci.*, Volume 35, pp. 4049-4054.





# Part II

Chapters of thesis



# 2

## ENHANCED SOLAR LIGHT PHOTOELECTROCATALYTIC ACTIVITY IN WATER BY ANATASE-TO-RUTILE $\text{TiO}_2$ TRANSFORMATION

---

$\text{TiO}_2/\text{Ti}$  composites were synthesized by the paint-thermal decomposition method, in which a titanium (Ti) substrate was used due to low impedance between the  $\text{TiO}_2$  film and Ti plate, providing a strong adhesion. Photoactive  $\text{TiO}_2/\text{Ti}$  composites were further modified by an annealing treatment (500-750 °C). The structural evolution during annealing of the films was studied by XRD analysis. Morphology and microstructure characteristics were obtained by SEM and AFM measurements, respectively. The effects of photocatalytic (PC) activity and photoelectrocatalytic (PEC) activity were evaluated on the degradation of phenol in an aqueous solution and by the formation of hydroxyl radicals through a photoluminescence technique using terephthalic acid. It was found that the modified  $\text{TiO}_2/\text{Ti}$  composite with an anatase-to-rutile ratio of 82/18 was optimal for both PC and PEC, which resulted in the highest efficiency when using solar light. The PEC degradation was 2.8 times higher than that of PC with the optimal mixture of anatase and rutile. The enhanced photocatalytic activity was derived from the synergistic effect between the modified  $\text{TiO}_2/\text{Ti}$  composite electrode and an applied bias.

## 2.1. Introduction

Titanium dioxide has been extensively investigated due to its wide range of functional properties such as very strong oxidation power, biological and chemical stability, non-toxic properties as well as long-term stability against optical and chemical corrosion. This semiconductor has attracted much interest in recent years due to many breakthroughs that have continually been made (Ollis & Al-Ekabi, 1993; Hoffmann, et al., 1995). Nevertheless, difficulties of separation and recovery are encountered when powder catalysts are used. When the catalyst is immobilized, there is an inherent decrease in the surface area available for reaction, the quantum efficiency may also decrease, and the catalytic efficiency is too low to be used for the efficient oxidation of pollutants (Ollis & Al-Ekabi, 1993; Hoffmann, et al., 1995; Zacharakis, et al., 2013; Vinodgopal, et al., 1993). Thus, a technique that neither involves filtration of the photocatalyst used nor decreases the photo oxidation rate is desirable. Different strategies have been developed for improving the photocatalytic efficiency of immobilized  $\text{TiO}_2$ , although most researchers in this field have focussed on morphological (increasing the surface area and porosity) and chemical (incorporation of additional components in the  $\text{TiO}_2$  structure) modifications (Pelaez, et al., 2012; Egerton, et al., 2006; Datye, et al., 1995; Xu & Yu, 2011). However, increasing the surface area of the immobilised photocatalyst faces the problem of increasing the shadowing effect. In addition, a higher porosity will not give a much higher efficiency in the immobilised systems (Fan, et al., 2000). On the other hand, chemical modifications will increase the number of steps in the preparation of the films, making design procedures for the photoactive catalyst more complicated, less practical and costly. This study, therefore, focuses on the

recombination of photo-generated charge carriers as the major limitation of photocatalytic efficiency.

In order to decrease the recombination limitation of photo-generated charge carriers and to enhance the quantum efficiency of the immobilised photocatalyst, two approaches were adopted: first, the optimisation of the anatase-to-rutile ratio and, secondly, the application of a bias to the TiO<sub>2</sub> film. TiO<sub>2</sub> crystallizes in three natural phases: brookite (orthorhombic), anatase (tetragonal), and rutile (tetragonal). The photocatalytic performance of anatase is generally considered superior to that of the more stable rutile. This is due to a higher density of localised states and, as a consequence, surface-adsorbed hydroxyl radicals and a slower charge carrier recombination in anatase relative to rutile (Emilio, et al., 2006; Scalafani & Herrmann, 1996; Fox & Dulay, 1992; Hadjiivanov & Klissurski, 1996; Hwang, et al., 2006; Setiawati, et al., 2008; Hanaor & Sorrell, 2011). The higher rate of electron-hole recombination in rutile is attributed to the typically larger grain size of the crystal phase (Zhang, et al., 2000; Zhang, et al., 1998) and its resultant lower capacity to adsorb dissolved compounds (Fox & Dulay, 1992; Kesselman, et al., 1994; Lewis & Rosenbluth, 1989).

In contrast to the widely reported photocatalytic superiority of anatase, several publications have suggested that electron transfer between anatase and a residual quantity of rutile (Ohno, et al., 2003) may facilitate improved photo-oxidative reactions, as in mixed-phase titanium catalysts. Therefore, in light of the importance of understanding the titanium phases, their transformation and the method by which their ratio can be controlled are likely to be critical to achieving phase-optimised photocatalytic performance. Photocatalysis (PC) is based on the generation of hydroxyl radicals ( $\cdot\text{HO}$ ) which are the principal agents responsible for the oxidation of numerous aqueous organic contaminants (Legrini, et al., 1993; Huang, et al., 1993). This radical is a powerful oxidant; however, due to its high reactivity, it is unstable

and must be continuously produced *in situ* by means of chemical or photochemical reactions. Among the different ways to generate the hydroxyl radicals on the basis of immobilized TiO<sub>2</sub> photocatalytic oxidation, researchers have developed photoelectrocatalytic (PEC) oxidation by applying an anodic bias to the TiO<sub>2</sub>/Ti composite (Vinodgopal, et al., 1993; Wang, et al., 2001; Candal, et al., 1998; Li, et al., 2002).

By applying a bias larger than the flat band potential of a semiconductor electrode, the separation of photo-generated charge carriers can be enhanced with the electrons moving toward the bulk of the crystal and the holes migrating toward the surface under the influence of the electric field across the depletion layer (Hung, et al., 2012; Liu, et al., 2009; Lin, et al., 2013; Centi & Santen, 2007; Fravventura, et al., 2013; Marugan, et al., 2009). Electrons and holes generated beyond the depletion layer also diffuse, and become separated, as a result of the electric field. The quantum efficiency is, therefore, increased.

However, Marugán et al. (Marugan, et al., 2009) showed that the efficiency of the photoelectrocatalytic process strongly depends on the characteristics of the photoelectrode, not only on the TiO<sub>2</sub> surface but also on the conductive support. In recent years, many techniques have been proposed for the immobilization of TiO<sub>2</sub> on solid supports such as glass (Deki, et al., 1997), quartz (Herrmann, et al., 1997), silica (Vohra & Tanaka, 2003), stainless steel (Matos, et al., 2001), fiberglass cloth (Horikoshi, et al., 2002), zeolites (Anandan & Yoon, 2003) and optical fibre (Peill & Hoffmann, 1998; Peill & Hoffmann, 1997). However, it was found that the electron mass transfer between the TiO<sub>2</sub> film and the supporting substrates was not very efficient due to a poor connection between some of the materials (Li, et al., 2002). Oxidizing titanium to create TiO<sub>2</sub> films provides a strong adhesion of the oxide to the substrate, overcoming adherence problems (Anpo, et al., 2005; Schvezov, et al., 2010). Therefore, it improves substrate stability of the electrodes in

solution and reduces the resistance to electron transfer and the recombination of photo-generated charge carriers. Furthermore, since the vapour pressure of titanium is very low ( $10^{-3}$  Torr at 1577 °C) and titanium has a high melting point (1668 °C), direct oxidation of  $\text{TiO}_2$  using an organic precursor was obtained on the bare Ti plates, which cannot be applied using other conductive substrate materials (Chen & Mao, 2007). In this study, a photoactive  $\text{TiO}_2/\text{Ti}$  film electrode with high durability was studied. The paint-thermal decomposition method was used for the preparation of the photoactive  $\text{TiO}_2/\text{Ti}$  plates (Beer, 1969).

Films obtained by this method were additionally modified in order to improve performance of already existing  $\text{TiO}_2/\text{Ti}$  composite electrodes. The modification was performed by additional annealing treatments and by changing the anatase to rutile (A/R) ratio. The preparation method was integrated with the PEC process in order to achieve the highest photocatalytic efficiency in the presence of solar light ( $\text{UV}_{300-400}$ , 60  $\text{W}/\text{m}^2$ ).

## **2.2. Experimental methods**

### **2.2.1. Preparation of $\text{TiO}_2/\text{Ti}$ composite electrodes**

Photocatalytic plates were manufactured and prepared by the company Magneto special anodes B.V. (Schiedam, The Netherlands) according to the paint-thermal decomposition method (Beer, 1969). Using this method, the electrodes were prepared by applying a layer of a solution containing an organic, solvent-based titanium oxide precursor to a titanium substrate. After an air drying period, the support with paint was transferred to an air circulated oven to obtain a heat treatment of 400°C up to 600°C. Heat treatment decomposes and oxidises the salt giving an oxide layer.

Several layers of paint were applied which were subsequently dried and heated. For the manufacturing of this type of electrode, patent GB1, 147, 442, was incorporated as a reference.

### **2.2.2. Experimental approach**

Using an organic precursor as the oxidant in the paint-thermal decomposition method, the  $\text{TiO}_2$  was produced directly on a metal Ti substrate. Films obtained by this decomposition method were additionally modified by changing the A/R ratio.

The effect of the annealing treatment in the temperature range from 500-750°C on prepared photoactive  $\text{TiO}_2/\text{Ti}$  films was studied. Additionally, the roughness, adhesion, and the scanning electron microscopic (SEM) images of the  $\text{TiO}_2$  films were investigated. A photoluminescence technique was used in order to evaluate the photocatalytic activity of the films. Furthermore, the comparison between the PC degradation of phenol using the PC process and the PEC process was also investigated.

### **2.2.3. Modification of $\text{TiO}_2/\text{Ti}$ composite electrodes and characterization**

After being synthesized, the  $\text{TiO}_2/\text{Ti}$  composite electrodes were further treated by the annealing treatment. The annealing treatments of the  $\text{TiO}_2$  film were carried out in a furnace (NeyTech Vulcan Benchtop Muffle Furnace 3-550). The  $\text{TiO}_2$  film was annealed for five hours in ambient atmosphere at different temperatures from 500 to 750°C; and the temperature was raised 8°C/min from room temperature. The thickness of the  $\text{TiO}_2$  layer was measured by Veeco Dektak 8 Stylus Profiler fitted with a 12.5  $\mu\text{m}$  tip.



Quantification of the phase proportions was carried out by X-ray diffraction (XRD) (Datye, et al., 1995; Candal, et al., 1998; Li, et al., 2002; Hung, et al., 2012). The analyses were made using the method described by Spurr and Myers (25, 27), which utilises the ratio of the rutile (110) peak at  $27.355\ 2\theta$  to the anatase (101) peak at  $25.176\ 2\theta$ . The X-ray film diffraction patterns were obtained using the Bruker D8 Discover with Eulerian cradle, goniometer radius 300 mm. The scanning range was  $10-90^\circ\ (2\theta)$  with a step size of  $0.02^\circ$  and a step time of 2.0 s. The surface homogeneity and particle size of the annealed  $\text{TiO}_2$  films were investigated using an SEM (Jeol JSM-6010LA). Surface roughness and root mean square roughness (RMS) were measured by atomic force microscopy (AFM) (NTMDT Ntegra).

Commercially available tips (Digital Instruments standard tips) were used and the surface was imaged in tapping mode. The  $\text{TiO}_2$  films were investigated, then the roughness of the film surface was quantified by means of a statistical data analysis of AFM images. Amplitude parameters are the principal parameters in characterizing surface topography. The most used amplitude parameters are the average roughness (Ra) and the root mean square roughness (RMS). The RMS roughness of a surface is similar to the roughness average, with the only difference being that it takes the mean squared absolute values of the surface roughness profile, making it more sensitive to peaks and valleys than the average roughness. Particularly, RMS is used to study temporal changes in the creation of a new surface as well as spatial differences when studying the surface feature using different scales (Raposo, et al., 2007). The reason for this is that this parameter is more sensitive to large deviations with respect to the mean line. But, in order to make our corresponding data comparable to other research, we included both data in Table 1. A tape-casting method P-A-T (Paint Adhesion Test Kit), produced by Gardco which meets the ASTM Test Method D 3359, ISO 2409, Method B & DIN Standard No. 53151, was used.

The cross-hatch in the TiO<sub>2</sub> film was cut with a razor blade (PA-2054, 11 tooth, 1,5 mm cutter), followed by applying the tape (3M Scotch Tape) to the cross-hatch area and then removing the tape. According to ASTM 3359, the results of the adhesion test are qualitatively divided into 6 grades, from 5 to 0, where grade 5 represents the highest level of adhesion and 0 the lowest level.

#### **2.2.4. Evaluation of photocatalytic and photoelectrocatalytic activity**

To evaluate the PC and PEC activity of the TiO<sub>2</sub>/Ti plates, the degradation of phenol ( $\geq 99\%$ , Sigma Aldrich) as a model compound and the formation of hydroxyl radicals through a photoluminescence technique were investigated. The PC and PEC oxidation experiments were carried out in the batch-scale single-compartment cell reactor system as shown in Figure 2.1. This system consists of a cylindrical quartz glass reactor with an effective vessel volume of 200 ml, an external solar light source and a three-electrode configuration. The reaction solution was 175 ml phenol with a concentration of 2 mg/L, or  $5 \times 10^{-4}$  M terephthalic acid (TA) solution and 0.1 M Na<sub>2</sub>SO<sub>4</sub> supporting electrolyte which was used in both the PC and PEC experiments. The samples were collected from the reaction solution at regular time intervals to determine the concentration of phenol or 2-hydroxyterephthalic acid (2-OHTA). The concentration of 2-OHTA was measured in order to evaluate the concentration of the formed  $\cdot\text{OH}$  radicals. For each experiment, 175 mL of this phenol solution was stirred for three hours with the TiO<sub>2</sub>/Ti catalyst in the dark to take the water bath temperature and to ensure adsorption equilibrium. Demineralized water (RiOs 5 Reverse Osmosis System) was used throughout the experiments. All other chemicals were of analytical grade and used without further purification. The pH of the solution, 7.2, was measured before the experiment. The single-compartment cell reactor system, consisting of 3

Xenon lamps irradiating solar light (UV<sub>300-400</sub>) with an intensity of 60 W/m<sup>2</sup>, was placed inside the chamber of the SUNTEST XXL+ (Atlas). The solar spectrum of these Xenon lamps was measured by a Black C-50 spectrometer, a product of StellarNet. The temperature was controlled for 25 ± 1°C by letting the water flow in a water bath through a recirculation cooler (Julabo, FL300). During the experiments the reactor was closed with custom made quartz lids to prevent evaporation of the phenol and at the same time to be permeable to UV light. As a photoanode, the TiO<sub>2</sub>/Ti plate with a surface area of 16 cm<sup>2</sup> was placed on the quartz glass stand, incorporated in the reactor to receive solar light irradiation. The TiO<sub>2</sub> thin film supported on the Ti plate was used as the photocatalyst. A graphite cylinder was used as a cathode.

An electrode Ag/AgCl was used as a reference. The electrode potential and working current were controlled with a potentiostat-galvanostat system (Autolab PGSTAT128N with a BOOSTER10A). The photoelectrocatalytic experiments were performed with constant potentials. To evaluate the reactivity of the electrochemical and photochemical oxidation reaction in the three-electrode system, several sets of degradation experiments were carried out in an undivided cell with the stirred solution kept at a constant temperature.

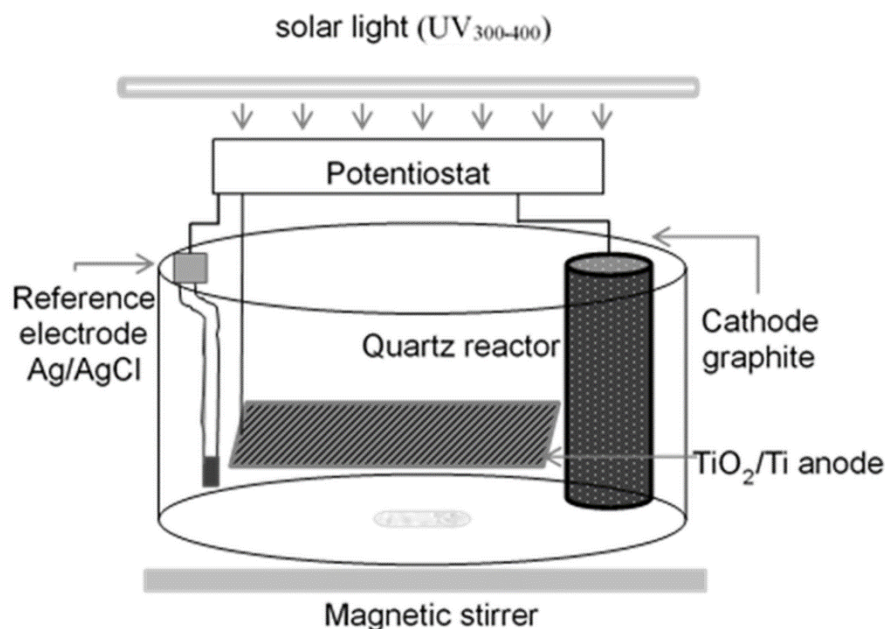


Figure 2.1. Schematic view of the batch-scale single-compartment cell reactor system

### 2.2.5. Analytical methods

The phenol concentration was monitored with a Hach Lange DR 5000 spectrophotometer by using Hach Lange cuvette tests (LCK 345 with a measuring range 0.05-5.00 mg/L). Phenol reacts with 4-nitroaniline to form a yellow-coloured complex which is then measured by photometry. The rate constants,  $k$  for phenol degradation, were calculated through the linear relationship between  $\ln([C_6H_5OH]/[C_6H_5OH]_0)$  and time. The hydroxyl radical concentration ( $\cdot OH$ ) was detected by photoluminescence (PL) using TA (Sigma Aldrich, 98%) as a probe molecule. TA readily reacts with  $\cdot OH$  radicals to produce a highly fluorescent product: 2-hydroxyterephthalic acid (Yu & Wang, 2010). The PL signal intensity of 2-OHTA acid at 425 nm is proportional to the amount of  $\cdot OH$  produced at the catalyst/solution interface. A stock solution of TA ( $5 \times 10^{-2}$  M) was prepared in a potassium dihydrogen phosphate buffer (pH 6.5). This stock solution was diluted with distilled water into a

concentration  $5 \times 10^{-4}$  M to be used for the assessment of the photocatalytic activity. The PL spectra of the generated 2-OHTA were measured on the PL Spectrophotometer PIT Quanta Master Model QM-1. After irradiation for three hours in the batch quartz reactor, an aliquot of the reaction solution was used to measure the PL intensity at 425 nm with excitation at 315 nm.

## **2.3. Results and discussion**

### **2.3.1. Characterization of the TiO<sub>2</sub> films**

X-ray diffraction (XRD) analyses were carried out on TiO<sub>2</sub> films annealed at temperatures in the range from 500-750°C. Table 2.1 shows an overview of the percentages of anatase and rutile as measured by XRD. The brookite and anatase crystalline phases, which are stable at low temperatures, transform into rutile when the sample is annealed at higher temperatures (Wang, et al., 2001; Lim, et al., 2013).

The XRD analyses show that all the films consisted of both anatase and rutile phases and, with an increase in annealing temperatures above 600°C, an increase in the relative content of rutile TiO<sub>2</sub> was observed. Dachille et al. (Dachille, et al., 1968) reported pressure-temperature diagrams approximating equilibrium for TiO<sub>2</sub>. The key observation in their study was the apparent A/R phase transformation conditions of 605°C at 1 atm pressure, as measured by XRD. Although it is difficult to ascertain the behaviour of titanium, this is accepted as the region of the onset temperature of the A/R transformation in bulk pure anatase in air (Jamieson & Olinger, 1968; Kumar, 1995; Zhang, et al., 2000). This finding was confirmed by XRD of the annealed samples. Transformation from anatase to rutile, phase conversion and micro-structural modification after annealing at high temperatures occurred (Kim, et al., 2007).

The A/R transformation mechanisms can be explained as: the A/R phase transformation is a nucleation and growth process at the boundary of the anatase phase (Li, et al., 2004; Gouma & Mills, 2001) and, with increasing annealing temperature, rutile nucleates within the anatase phase grow in size consuming the surrounding anatase (Zhang, et al., 2000; Zhang, et al., 2006).

Table 2.1. Values of surface roughness of TiO<sub>2</sub> films after the annealing process (500-750°C) with varying weight percentages of anatase and rutile phases

Annealing temperature °C	Weight % anatase	Weight % rutile	Average surface roughness $\mu\text{m}$	RMS roughness $\mu\text{m}$
500	95	5	0.550	0.683
600	85	15	0.838	1.048
650	82	18	0.735	0.936
700	74	26	0.718	0.883
750	50	50	0.836	1.052

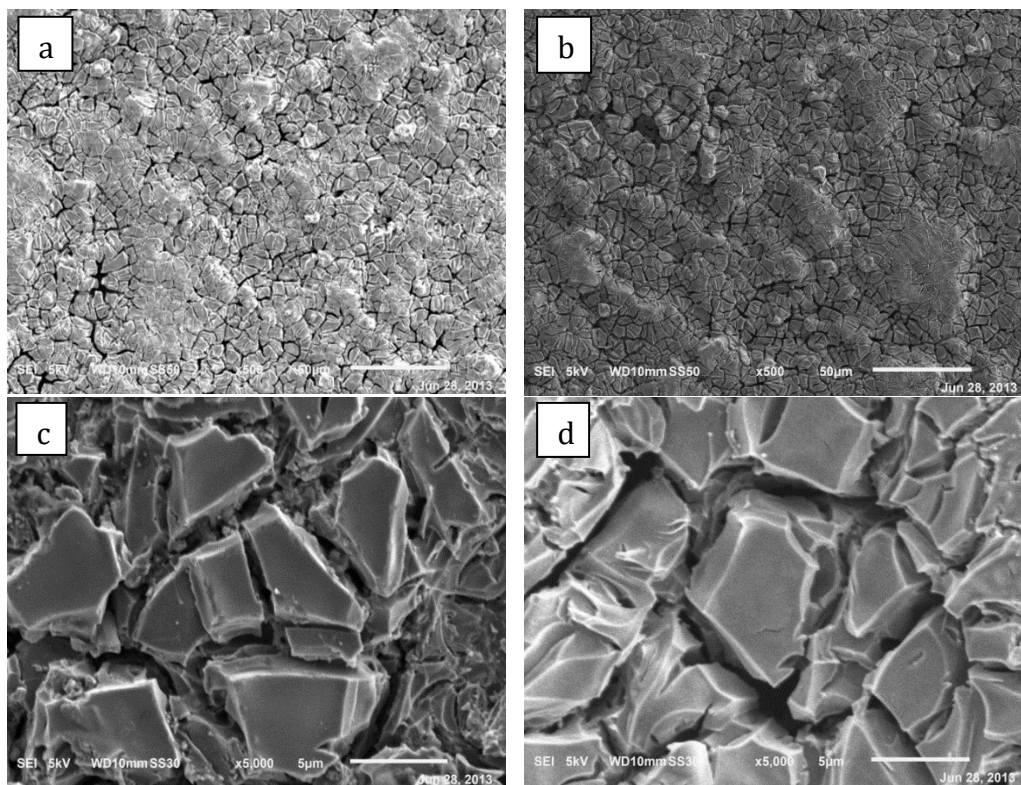


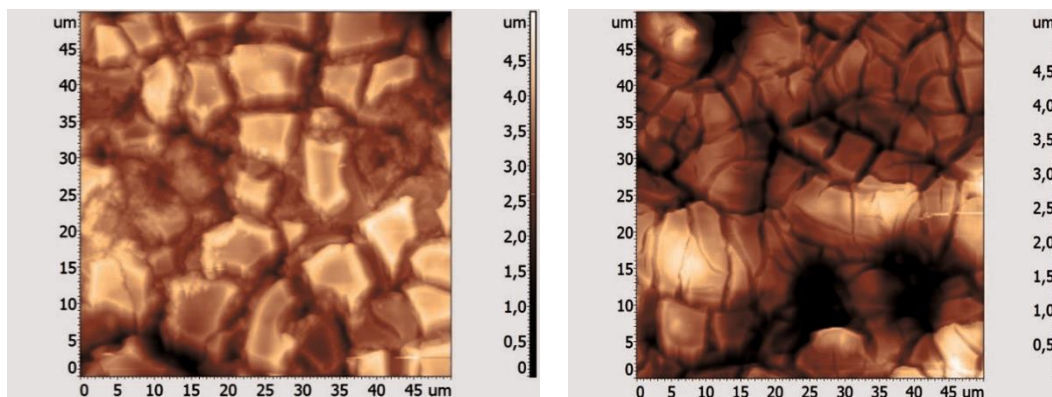
Figure 2.2. SEM images of  $\text{TiO}_2$ , surface of the deposited films and size of the particles a)  $\text{TiO}_2$  film annealed at  $500^\circ\text{C}$ , low magnification; b)  $\text{TiO}_2$  film annealed at  $750^\circ\text{C}$ , low magnification; c)  $\text{TiO}_2$  film annealed at  $500^\circ\text{C}$ , high magnification; d)  $\text{TiO}_2$  film annealed at  $750^\circ\text{C}$ , high magnification

Figure 2.2 shows SEM micrographs of the  $\text{TiO}_2$  films after thermal treatment for the minimum ( $500^\circ\text{C}$ ) and maximum ( $750^\circ\text{C}$ ) annealing temperature. The low magnification images (5 kV, WD10 mm SS50, x50,  $50\text{ }\mu\text{m}$ ) of  $\text{TiO}_2$  films show a good homogeneity while high magnification images (5 kV, WD10 mm SS30, x5000,  $5\text{ }\mu\text{m}$ ) show globular and uniform particles and the existence of micro cracks. Even though micro cracks were formed at the surface of the  $\text{TiO}_2$  films, no  $\text{TiO}_2$  particles detached during the washing step that would lead to a decrease in hydroxyl radical formation.

We hypothesise that the formation of cracks was due to two reasons: first, stress induced during the film shrinkage, a mismatch of the thermal expansion between the titanium substrate and the TiO<sub>2</sub> film; second, a decrease in TiO<sub>2</sub> particle bonding strength as the film thickened, which was also found in the literature (Bockmeyer & Lobmann, 2007). Nevertheless, the crack formations did not increase with the increase in the annealing temperature, and the formation of the cracks did not influence the adhesion of the films. This observation indicates that the surface of the samples was rough, which might be beneficial for enhancing the adsorption of the model compound due to its relatively high surface area. However, no difference in the surface homogeneity or change in the particle size of the photoactive TiO<sub>2</sub> films that were annealed in temperature range from 500-750°C was observed. The average diameter of the particles, calculated from the micrograph, gave a value close to 4 µm. From the SEM results, it can be confirmed that the TiO<sub>2</sub> films were well-coated and TiO<sub>2</sub> particles were well spread on the conductive substrate during the paint-thermal decomposition process.

Figure 2.3 shows the AFM images of the TiO<sub>2</sub>/Ti films annealed at 500 and 750°C. The surface diversification and topography of the examined thin films was examined by the AFM measurements. The surface roughness increases with an increase in annealing temperature, followed by particle growth (Sabyrov, et al., 2013). However, from the RMS values it can be observed that the annealing process slightly increased the surface roughness, which is in agreement with the AFM images of the TiO<sub>2</sub> films. The RMS roughness varied according to the densities and sizes of the hillocks and grains on the surfaces. Table 2.1 summarizes the average surface roughness and RMS roughness as a function of the percentages of anatase and rutile.





a)

b)

Figure 2.3. AFM images of  $\text{TiO}_2$  films with a) 95/5 A/R ratio (annealed at  $500^\circ\text{C}$ ) and b) 50/50 A/R ratio (annealed at  $750^\circ\text{C}$ )

Since adhesion for immobilized  $\text{TiO}_2$  films is an important property in water treatment, a tape-casting method (P-A-T) was performed on the photoactive  $\text{TiO}_2/\text{Ti}$  composites to evaluate the strength of  $\text{TiO}_2$  film adhesion. The results revealed that on the plates annealed at temperatures below  $700^\circ\text{C}$  there was no delamination or disturbance of the  $\text{TiO}_2$  films (Figure 2.4). Therefore, the percentage of the rutile that gave the highest adhesion was considered to be a film annealed at  $650^\circ\text{C}$  with an A/R ratio of 82/18. The squares of the lattice were not detached after pulling off the tape, corresponding to ASTM Class 5B. Samples annealed at 700 and  $750^\circ\text{C}$  showed slight delamination. The results also indicate that the adhesion of the film on the etched titanium substrate was strong enough to withstand mild to moderate forces.

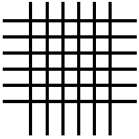
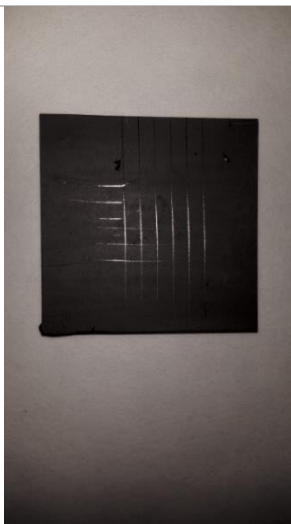
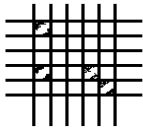
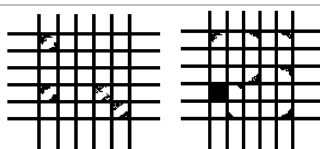
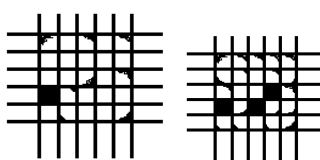
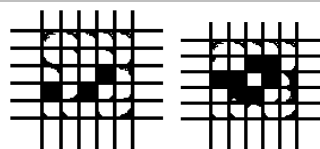
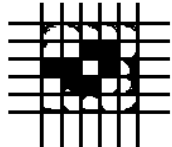
	Classification	Percent Area Removed	Surface of Cross-Cut Area from which Flaking has Occurred for Six Parallel Cuts and Adhesion Range by Percent
	5B	0 % None	
	4B	Less than 5 %	
	3B	5-15 %	
	2B	15-35 %	
	1B	35-65 %	
	0B	Greater than 65 %	

Figure 2.4. Adhesion results for photoactive  $\text{TiO}_2$  film on the  $\text{TiO}_2/\text{Ti}$  composite prepared by the paint-thermal decomposition method, annealed at  $650^\circ\text{C}$  with an A/R ratio 82/18, together with a classification scale using the-tape casting method, P-A-T, and the surface of the cross-cut area from which flaking has occurred for six parallel cuts and adhesion arranged by %

### 2.3.2. Photocatalytic and photoelectrocatalytic degradation

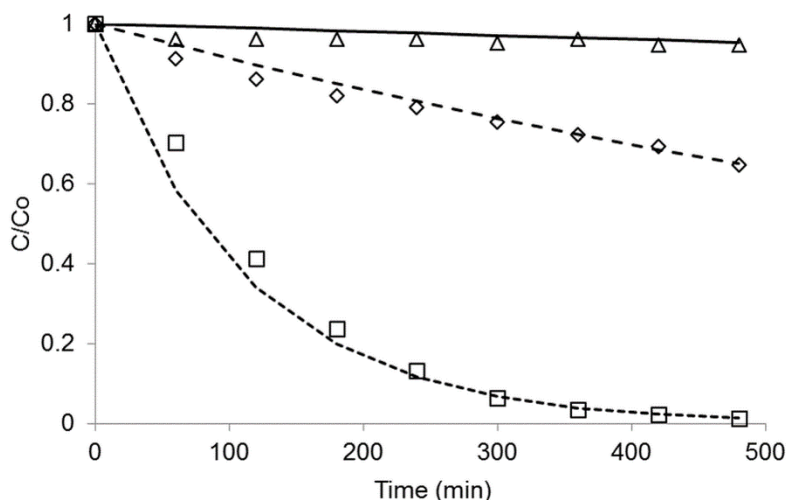


Figure 2.5. Degradation of phenol with photolysis ( $\Delta$ ), PC ( $\diamond$ ) and PEC ( $\square$ ) at 1 V for the  $\text{TiO}_2$  sample annealed at  $650^\circ\text{C}$  (A/R ratio 82/18); (solid line) 1st order kinetics of photolysis; (dashed line) 1st order kinetics of PC; and, (square dot) 1st order kinetics of PEC

The PC and PEC activity of the samples was expressed by a first-order rate constant. Figure 2.5 shows the impact of the synergistic effect between the A/R ratio on the PC and PEC process. It was demonstrated that the removal rate of phenol in PEC oxidation was more than that in the PC oxidation and direct photolysis. During the measurements, overall photocurrent and the photocurrent in the dark conditions were recorded. The limiting photocurrent that was obtained by subtracting the photocurrent obtained in the dark conditions from overall photocurrent was used in the calculations. The  $\text{TiO}_2/\text{Ti}$  composite electrodes exhibited a very low dark current density of  $1.84 \times 10^{-5} \text{ mA/cm}^2$ , excluding the effect of electrolysis of phenol.

When no external potential was applied, irradiation with solar light resulted in the 35.3 % phenol degradation after eight hours and with a first-order rate constant  $k$  of  $0.93 \times 10^{-3} \text{ min}^{-1}$ . The rate constants for phenol degradation were calculated through the linear relationship between  $\ln([C_6H_5OH]/[C_6H_5OH]_0)$  and time. This relationship revealed first-order kinetics as it yielded a straight line up to a six-hour exposure time for the PC and PEC processes. When applying 1 V to the  $TiO_2/Ti$  composite electrode, however, about 90 % of the phenol degraded after eight hours of solar irradiation and a substantially higher rate constant of  $9.0 \times 10^{-3} \text{ min}^{-1}$  was calculated. It was found that the A/R ratio (82/18) was optimal for both the PC and PEC processes. The overall oxidation efficiency of the PEC process was better than the PC process by an enhancement ratio-PEC/PC of 2.5.

### **2.3.3. Effect of potential on PEC efficiency**

The purpose of this section is to optimize the PEC process by choosing the appropriate bias. To select an appropriate bias potential, we determined the photocurrent yielded by using different external potentials.

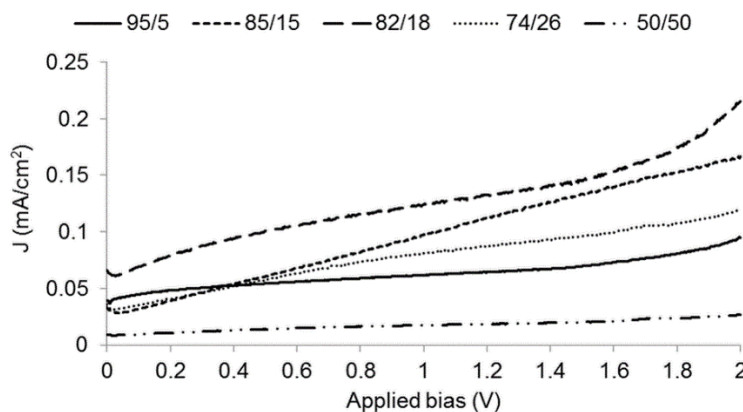


Figure 2.6. Photocurrent density after 30 min of solar irradiation ( $UV_{300-400}$ ,  $60 \text{ W/m}^2$ ) of different A/R ratios by using an external bias in the range of 0-2 volts. Measurements were obtained at pH 7.2 in a phenol solution ( $2 \text{ mg/L}$ ) with supporting electrolyte ( $0.1 \text{ M Na}_2\text{SO}_4$ )

Figure 2.6 shows the effect of the applied potential on the photocurrent density in the phenol solution using films with different A/R ratios (95/5; 85/15; 82/18; 74/26; 50/50). The PEC reactions were performed with a different electrical bias in the range of 0-2 volts, each with a duration of 30 minutes. At low potentials, the current density increased with increasing potential bias, which implies that the electron-hole recombination in the film determined the overall photocatalytic process. Since for a given compound at a given concentration the rate of electron injection or photo hole capture is constant, the photocurrent will saturate with respect to potential bias (Hung, et al., 2012; Liu, et al., 2009; Lin, et al., 2013; Neumann-Spallart, 2007). When the current is saturated the system achieves its maximum photoelectron collection efficiency and there is no influence of the electron transport across the film. Further observation indicates that the A/R ratio had an effect on the size of the photocurrent density.

The TiO<sub>2</sub> film with an A/R ratio of 95/5 (500°C) had a lower photocurrent density due to its reduced transformation of anatase into rutile: only 5 % from the original pure anatase sample, resulting in more defects in the film. At an A/R ratio of 82/18 (650°C), the film showed the highest photocurrent density due to its biphasic structure and increased transformation of anatase into rutile: 18% of the pure anatase. By further increasing the annealing temperature to 700°C (A/R ratio 74/26), the photocurrent density decreased due to a decrease in anatase content and an increase in the electron-hole recombination rate. At 750°C, a low photocurrent density was observed as a result of the formation of a dense rutile film. Photocatalytic activity of TiO<sub>2</sub> usually depends on competition between the following two processes (Yu & Wang, 2010; Yu, et al., 2013): first, the ratio of the transfer rate of surface charge carriers from the interior to the surface and, secondly, the recombination rate of photo-generated electrons and holes. If the recombination of photo-generated electrons and holes occurs too fast (<0.1 ns), then there is not enough time for any other chemical reaction to occur. Compared to other semiconductors, the surface charge carriers of TiO<sub>2</sub> have a relatively long life (around 250 ns), allowing the electrons or holes to travel to the crystallite surface (Yu & Wang, 2010). This implies that the rutile phase in the TiO<sub>2</sub> mixture has a higher recombination rate of photo-generated electrons and holes than the anatase phase and charge carriers cannot transfer to the surface from the interior. Therefore, it is not surprising that rutile exhibited a negligible photocurrent and photo(electro)catalytic activity (Yu, et al., 2013; Ovenstone, 2001; Einaga, et al., 2004; Dai, et al., 2011).

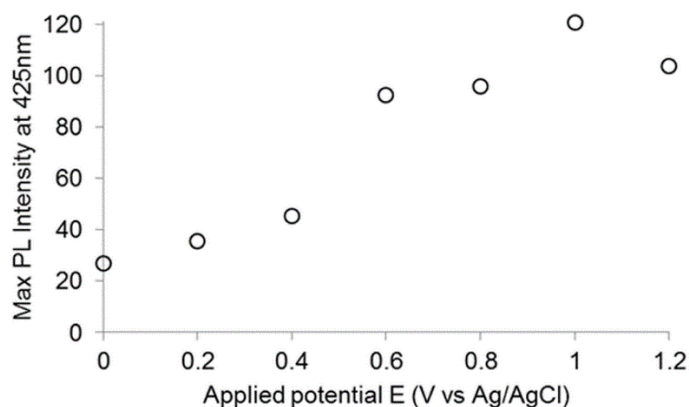


Figure 2.7. Maximum PL intensity of 2-OHTA at 425 nm as a function of the applied potential  $E$  for the  $\text{TiO}_2$  sample with A/R ratio 82/18

Figure 2.7 shows the effect of the applied potential  $E$  on the Max PL intensity of 2-OHTA at 425 nm formed by the reaction of TA with  $\cdot\text{OH}$  after solar irradiation ( $\text{UV}_{300-400}$ ,  $60 \text{ W/m}^2$ ) for three hours. The experiments were conducted by applying electrical biases of 0, 0.2, 0.4, 0.6, 0.8, 1 and 1.2 V. Utilization of the potential causes an increase in the separation of electron-hole pair; excited electrons drive to the counter electrode, and holes remain at the surface of the working electrode. Therefore, the recombination rate declines (Ovenstone, 2001; Einaga, et al., 2004). Results showed that, indeed, at the potential of 1 V, the highest PL intensity of 2-OHTA at 425 nm was obtained. This observation is in accordance with the experiments of phenol photodegradation. Figure 2.8 shows the effect of the applied potential on the first-order degradation rate constant  $k$  of phenol using the  $\text{TiO}_2/\text{Ti}$  composite (A/R ratio 82/18). The rate constants for the phenol degradation  $k$  for the PEC process with different constant potentials were calculated through the linear relationship between  $\ln([\text{C}_6\text{H}_6\text{O}]/[\text{C}_6\text{H}_6\text{O}]_0)$  and time.

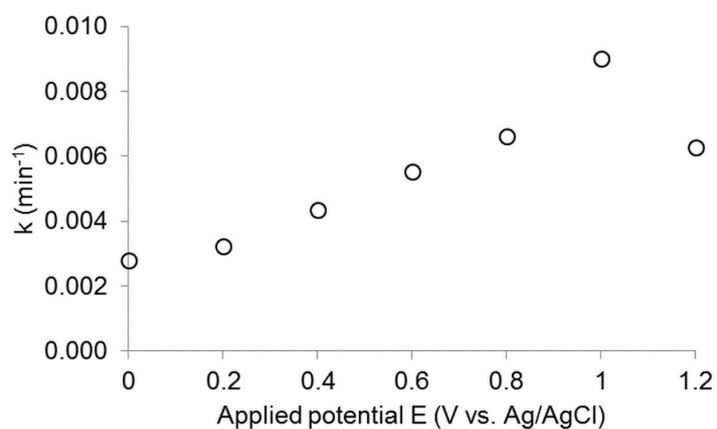


Figure 2.8. First-order degradation rate constant  $k$  of phenol for the  $\text{TiO}_2/\text{Ti}$  composite (with A/R ratio 82/18) vs applied potential

Table 2.2. The first-order rate constants and current density values obtained for the degradation experiments of (2 mg/L) phenol with  $\text{TiO}_2$  film (A/R ratio 82/18) in PEC system under different applied potential E/V

Applied potential E/V	Rate constant $k$ $\text{min}^{-1} \cdot 10^{-3}$	$R^2$	J $\text{mA}/\text{cm}^2$ $\cdot 10^{-3}$
0	2.80	0.989	0.0736
0.2	3.24	0.999	8.5571
0.4	4.36	0.999	8.6153
0.6	5.52	0.986	9.6344
0.8	6.60	0.986	9.8921
1	9.00	0.988	10.0686
1.2	6.26	0.982	10.3945

It can be observed that when the applied bias potential was low ( $<1.0$  V), the degradation rate constant was increased along with an increase in potential. However, when the potential was higher than 1.0 V, the degradation rate decreased again.



Further increase in the applied potential beyond 1 V led to a decrease in both the Max PL intensity of 2-OHTA at 425 nm and the first-order degradation rate constant. This phenomenon is in agreement with previous study (Ovenstone, 2001) and can be explained by the electrolysis of water by photo-generated holes (Hoffmann, et al., 1995; Egerton, et al., 2006). The highest obtained first-order rate constant was equal to  $9.0 \times 10^{-3} \text{ min}^{-1}$ . Further, PEC of the phenol solution using a higher constant potential of 1.2 V yielded a linear relationship between  $[\text{C}_6\text{H}_6\text{O}]$  and time. The rate constant was  $6.26 \times 10^{-3} \text{ min}^{-1}$ . Thus, the constant degradation rate of phenol photo(electro) degradation decreased from  $9.0 \times 10^{-3} \text{ min}^{-1}$  to  $6.26 \times 10^{-3} \text{ min}^{-1}$ . The results indicated that, at the higher potential, other chemical reactions were occurring at the surface of  $\text{TiO}_2$ . The values are shown in Table 2.2. In order to perform a valid test that represents the optimal performance of the photocatalyst without the influence of the electron transport across the film and potential water electrolysis, a potential bias of 1 V was subsequently adopted for the experiments.

#### **2.3.4. Effect of A/R ratio on PEC efficiency**

The purpose of this section is to optimise the A/R ratio in the PEC system by focusing on the  $\cdot\text{OH}$  radical formation and photo degradation of phenol. The performance and efficiency of the modified photoactive films were evaluated by the detection of  $\cdot\text{OH}$  in the PEC process and PEC degradation of phenol in an aqueous solution with 0.1 M  $\text{Na}_2\text{SO}_4$  as supporting electrolyte under solar irradiation ( $\text{UV}_{300-400}$ ,  $60 \text{ W/m}^2$ ). Figure 2.9 shows the comparison of the Max PL intensity of 2-OHTA at 425 nm, that was formed by the reaction of TA with  $\cdot\text{OH}$  radicals after solar irradiation of the  $\text{TiO}_2$  samples for three hours, for different A/R ratios.

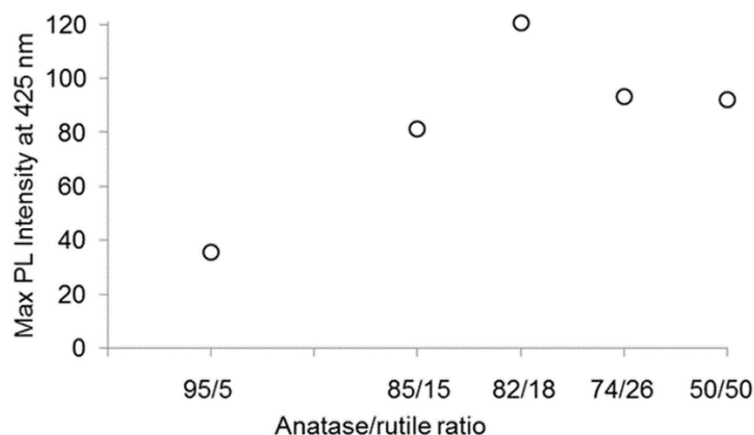


Figure 2.9. Maximum PL intensity at 425 nm of 2-OHTA at 425 nm as a function of the A/R ratio for PEC with an anodic bias of 1 V

It can be observed that the A/R ratio had a large influence on the  $\cdot\text{OH}$  formation. A gradual increase in Max PL intensity was observed with a decrease in the A/R ratio of  $\text{TiO}_2$  films. At a fixed time (three hours), the amount of  $\cdot\text{OH}$  detected on the  $\text{TiO}_2$  sample with an A/R ratio of 82/18 was the largest, which could be caused by a better separation of free charge carriers and an enhanced yield of reaction between photo-generated holes and adsorbed water molecules on the photocatalyst surface (Marugan, et al., 2009). This also suggests that the  $\text{TiO}_2$  film with an A/R ratio of 82/28 had the highest photo(electro)catalytic activity. The hydroxyl radical experiments further confirm that the detection rate of  $\cdot\text{OH}$  had a positive relation with the photo(electro)catalytic activity, which can be observed from Figure 10. Some electrons in the anatase particles that were excited from the valance band to the conduction band transfer to the rutile particles because the energy level of the conduction band in the anatase particles is higher than in the rutile particles.

The correlation that was found in this study between anatase and rutile ratio and catalyst performance agrees with the findings of H. Nakajima et al. (Ramamurthy & Schanze, 2003; Lin, et al., 2009; Nakajima, et al., 2005).

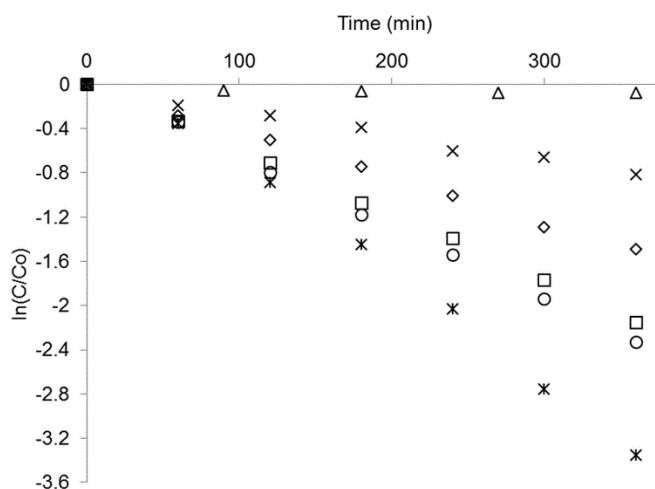


Figure 2.10. Effects of A/R ratio on degradation of phenol (2 mg/L, 0.1 M Na<sub>2</sub>SO<sub>4</sub> supporting electrolyte), photolysis (Δ); A/R ratio (95/5) (◇); A/R ratio 85/15 (□); A/R ratio 82/18 (⋈); A/R ratio 74/26 (○); A/R ratio 50/50 (x)

Figure 2.10 provides an overview of the effect of the A/R ratio of the photoactive TiO<sub>2</sub> films on the phenol degradation. The relationship between  $\ln([C_6H_6O]/[C_6H_6O]_0)$  and the time for phenol degradation resulted in a straight line, which suggests that the PEC behaviour obeys first-order kinetics. Table 2.3 shows the values of the first-order rate constants  $k$  (min<sup>-1</sup>) for phenol with different A/R ratios. From the adsorption experiments it was concluded that the TiO<sub>2</sub> films showed a very small adsorptive capacity for phenol, and the adsorbed concentration of phenol was under the detection limit (data not shown in the figure). This observation was confirmed by other studies (Tian, et al., 2012; Hidaka, et al., 2003).

Current density-voltage (J-V) curves were recorded during the phenol oxidation experiments with different TiO<sub>2</sub> mixtures.

Corresponding parameters and characteristics are summarized in Table 3. It was found that the sample of TiO<sub>2</sub>/Ti annealed at 650°C with a mixture of anatase (82 %) and rutile (18 %), exhibited the highest photoelectrocatalytic efficiency on the degradation of phenol of all the tested TiO<sub>2</sub> samples, and its  $k$  reached 0.009 min<sup>-1</sup>. The  $k$  was determined to be 0.0042 min<sup>-1</sup> for the 500°C annealed sample with an A/R ratio of 95/5. This shows, the photoelectrocatalytic activity of the 650°C annealed sample exceeded that of the 500°C annealed sample by a factor of 2.14.

Table 2.3. The first-order rate constants and current density values, obtained for the degradation experiments of (2 mg/L) phenol with TiO<sub>2</sub> films with different A/R ratios in the PEC system biased at 1 V

Annealing temperature °C	Weight % anatase	Weight % rutile	Rate constant $k$ min <sup>-1</sup> *10 <sup>-3</sup>	R <sup>2</sup>	j mA/cm <sup>2</sup> *10 <sup>-2</sup>
500	95	5	4.21	0.999	6.3306
600	85	15	5.91	0.999	7.0807
650	82	18	9.00	0.999	10.0686
700	74	26	6.46	0.986	7.5404
750	50	50	2.29	0.986	1.9045

When further increasing the annealing temperature to 750°C, at an A/R ratio of 50/50, the photoelectrocatalytic activity decreased. This is ascribed to the following cause: most of the anatase phase changed into a rutile phase (50 %), which has the lowest photocatalytic activity among three different crystalline phases of TiO<sub>2</sub> (anatase, brookite and rutile) (Yu, et al., 2002; Yu, et al., 2009; Yu, et al., 2009; Yu, et al., 2007). This observation is in the accordance with the ·OH radical formation, shown in Figure 2.9.

## 2.4. Conclusions

The phase transformation of  $\text{TiO}_2$  was studied with the objective to improve photoelectrocatalytic efficiency on the degradation of organic pollutants.

The conclusions drawn from this study can be summarized as follows:

- Modification of thermal-paint decomposition synthesized films by annealing treatment in the range of 500–600°C showed that the anatase phase appeared to be dominant, while at higher temperatures (650-750°C) the rutile phase became present in higher percentages;
- The deposited films were well -coated and  $\text{TiO}_2$  particles were well spread on the conductive substrate during the deposition process;
- The mechanical strength and durability of the annealed  $\text{TiO}_2$  films was high, presenting a significant advantage for the use of these  $\text{TiO}_2$  films in practice;
- It was found that the A/R ratio (82/18) was optimal for both PC and PEC process.
- The  $\text{TiO}_2/\text{Ti}$  modified electrode had two times greater performance than the initial  $\text{TiO}_2/\text{Ti}$  electrode in the PEC process. The overall oxidation efficiency of the PEC process was better than the PC process by the enhancement ratio PEC/PC of 2.8;
- The improved photocatalytic activity was derived from the synergistic effect between a modified  $\text{TiO}_2/\text{Ti}$  composite electrode and an applied bias.

## References

- Anandan, S. & Yoon, M., 2003. Photocatalytic activities of the nano-sized TiO<sub>2</sub> supported Y zeolites. *J. Photochem. Photobiol., C*, Volume 4, pp. 5-18.
- Anpo, M., Dohshi, S., Kitano, M., Hu, Y., Takeuchi, M. & Matsuoka, M., 2005. The preparation and characterization of highly efficient titanium oxide-based photofunctional materials. *Annu. Rev. Mater. Res.*, Volume 35, pp. 1-27.
- Beer, H., 1969. Improvements in or relating to electrodes for electrolysis. s. l. Patent No. GB1, 147, 442.
- Bockmeyer, M. & Lobmann, P., 2007. Crack formation in TiO<sub>2</sub> films prepared by sol-gel processing: quantification and characterization. *Thin solid films*, Volume 515, pp. 5212-5219.
- Candal, R. J., Zeltner, W. A. & Anderson, M. A., 1998. TiO<sub>2</sub>-Mediated Photoelectrocatalytic purification of water. *J. Adv. Oxid. Technol.*, Volume 3, pp. 270-276.
- Centi, G. & Santen, R. A. v., 2007. Catalysis for renewables: From feedstock to energy production. Weinheim: Wiley-VCH Verlag GmbH & Co.
- Chen, X. & Mao, S. S., 2007. Titanium dioxide nanomaterials: synthesis, properties, modifications, and applications. *Chem. Rev.*, Volume 107, pp. 2891-2959.
- Dai, G., Yu, J. & Liu, G., 2011. Synthesis and enhanced visible-light photoelectrocatalytic activity of p-n junction BiOI/TiO<sub>2</sub> nanotube arrays. *J. Phys. Chem. C*, Volume 115, pp. 7339-7346.
- Datye, A. K., Riegel, G., Bolton, J.R., Huang, M. & Prairie, M.R., 1995. Microstructural characterization of a fumed titanium dioxide photocatalyst. *J. Solid State Chem.*, Volume 115, pp. 236-239.
- Deki, S., Aoi, Y., Miyake, Y., Gotoh, A. & Kajinamiet, A., 1997. Novel wet processes for preparation of vanadium dioxide thin film. *J. Mater. Sci.*, Volume 32, pp. 4269-4273.
- Egerton, T. A., Christensen, P. A., Kosa, S. A. M. & Onoka, B., 2006. Photoelectrocatalysis by titanium dioxide for water treatment. *Int. J. Environ. Pollut.*, Volume 27.

- Einaga, H., Ibusuki, T. & Futamura, S., 2004. Improvement of catalyst durability by deposition of Rh on TiO<sub>2</sub> in photooxidation of aromatic compounds. *Environ. Sci. Technol.*, Volume 38, pp. 286-289.
- Emilio, C. A., Litter, M. I., Kunst, M., Bouchard, M. & Colbeau-Justin, C., 2006. Phenol Photodegradation on Platinized-TiO<sub>2</sub> Photocatalysts Related to Charge-Carrier Dynamics. *Langmuir*, Volume 22, pp. 3606-3613.
- Fan, Q., McQuillin, B., Ray, A. K., Turner, M. L. & Seddon, A. B., 2000. High density, non-porous anatase titania thin films for device application. *J. Phys. D: Appl. Phys.*, Volume 33, pp. 2683-2686.
- F, D., Simons, P. Y. & Roy, R., 1968. Pressure-temperature studies of anatase, brookite, and rutile and TiO<sub>2</sub> (II): A discussion. *The American Mineralogist*, Volume 53, pp. 1929-1939.
- Fox, M. A. & Dulay, M. T., 1992. Heterogeneous Photocatalysis. *Chem. Rev.*, Volume 93, pp. 341-357.
- Fravventura, M., Deligiannis, C. D., Schins, J. M., Siebbeles, L. D. A. & Savenije, T. J., 2013. What limits photoconductance in anatase TiO<sub>2</sub> nanostructures? A real and imaginary microwave conductance study. *J. Phy. Chem. C*, Volume 117, pp. 8032-8040.
- Gouma, P. & Mills, M. J., 2001. Anatase to rutile transformation in titania powders. *J. Am. Ceram. Soc.*, Volume 84, pp. 619-622.
- Hadjiivanov, K. & Klissurski, D. G., 1996. Surface chemistry of titania and titania-supported catalysts. *Chem. Soc. Rev.*, Volume 25, pp. 61-69.
- Hanaor, D. A. H. & Sorrell, C. C., 2011. Review of the anatase to rutile phase transformation. *J. Mater. Sci.*, Volume 46, pp. 855-874.
- Herrmann, J. M., Tahiri, H., Ait-Ichou, Y., Lassaletta, G., Gonzalez-Elipe, A. R. & Fernandez, A., 1997. Characterization and photocatalytic activity in aqueous medium of TiO<sub>2</sub> and Ag-TiO<sub>2</sub> coatings on quartz. *Appl. Catal., B*, Volume 13, pp. 219-228.
- Hidaka, H., Honjo, H., Horikoshi, S. & Serpone, N., 2003. Photocatalyzed degradations on a TiO<sub>2</sub>-cpated quartz crystal microbalance. I. Adsorption/desorption processes in the degradation of phenol and catechol. *New J. Chem.*, Volume 27, pp. 1371-1376.

- Hoffmann, M. R., Martin, S. T., Choi, W. & Bahnemann, D. W., 1995. Environmental Applications of Semiconductor Photocatalysis. *Chem. Rev.*, Volume 95, pp. 69-96.
- Horikoshi, S., Watanabe, N., Onishi, H., Hidaka, H. & Serpone, N., 2002. Photodecomposition of a nonylphenol polyethoxylate surfactant in a cylindrical photoreactor with TiO<sub>2</sub> immobilized fiberglass cloth. *Appl. Catal., B*, Volume 37, pp. 117-129.
- Huang, C. P., Dong, C. & Tang, Z., 1993. Advanced chemical oxidation: its present role and potential future in hazardous waste treatment. *Waste management*, Volume 13, pp. 361-377.
- Hung, C. H., Kao, C. L. & Wu, K. R., 2012. Surface characteristics and photoelectrocatalytic capabilities of nanoporous titanium dioxide/tin indium oxide composite thin film electrodes. *Electrochim. Acta*, Volume 86, pp. 3-9.
- Hwang, D. S., Lee, N. H., Lee, D. Y., Song, J. S., Shin, S. H. & Kim, S. J., 2006. Phase transition control of nanostructured TiO<sub>2</sub> powders with additions of various metal chlorides. *Smart Mater. Struct.*, Volume 15, p. S74.
- Jamieson, J. C. & Olinger, B., 1968. High-pressure polymorphism of titanium dioxide. *Science*, Volume 161, pp. 893-895.
- Kesselman, J. M., Shreve, G. A., Hoffmann, M. R. & Lewis, N. S., 1994. Flux-matching condition at TiO<sub>2</sub> photoelectrodes: Is interfacial electron transfer to O<sub>2</sub> rate-limiting in the TiO<sub>2</sub>-catalyzed degradation of organics? *J. Phys. Chem.*, Volume 98, p. 13385-13395.
- Kim, C. S., Kwon, I. M., Moon, B. K., Jeong, J. H., Choi, B. C., Kim, J. H., Choi, H., Yi, S. S., Yoo, D. H., Hong, K. S., Park, J. H. & Lee, H. S., 2007. Synthesis and particle size effect on the phase transformation of nanocrystalline TiO<sub>2</sub>. *Mater. Sci. Eng.*, Volume C27, pp. 1343-1346.
- Kumar, K. N. P., 1995. Growth of rutile crystalites during the initial stage of anatase-to-rutile transformation in pure titania and in titania-alumina nanocomposites. *Scripta Metallurgica et Materialia*, Volume 32, pp. 873-877.
- Legrini, O., Oliveros, E. & Braun, A. M., 1993. Photochemical process for water treatment. *Chem. Rev.*, Volume 93, pp. 671-698.
- Lewis, N. S. & Rosenbluth, M. L., 1989. Preparation and characterization of Semiconductors. New York: John Wiley.



- Lim, Y. C., Zainal, Z., Hussein, M. Z. & Tan, W. T., 2013. The effect of heat treatment on phase transformation, morphology and photoelectrochemical response of short TiO<sub>2</sub> nanotubes. *Digest journal of nanomaterials and biostructures*, Volume 8, pp. 167-176.
- Lin, J., Zong, R. L., Zhou, M. & Zhu, Y. F., 2009. Photoelectric catalytic degradation of methylene blue by C60-modified TiO<sub>2</sub> nanotube array. *Appl. Catal., B*, Volume 89, pp. 425-431.
- Lin, W. C., Chen, C. H., Tang, H. Y., Hsiao, Y. C., Pan, J. R., Hu, C. C. & Huang, C., 2013. Electrochemical photocatalytic degradation of dye solution with a TiO<sub>2</sub>-coated stainless steel electrode prepared by electrophoretic deposition. *Appl. Catal., B*, Volume 141, pp. 32-41.
- Liu, S., Yang, L., Xu, S., Luo, S. & Cai, Q., 2009. Photocatalytic activities of C-N-doped TiO<sub>2</sub> nanotube array/carbon nanorod composite. *Electrochem. Commun.*, Volume 11, pp. 1748-1751.
- Li, W., Ni, C., Lin, H., Huang, C. P. & Shah, S. I., 2004. Size dependence of thermal stability of TiO<sub>2</sub> nanoparticles. *J. Appl. Phys.*, Volume 96, p. 6663.
- Li, X. Z., Li, F. B., Fan, C. M. & Sun, Y. P., 2002. Photoelectrocatalytic degradation of humic acid in aqueous solution using a Ti/TiO<sub>2</sub> Mesh photoelectrode. *Water Res.*, Volume 36, pp. 2215-2224.
- Li, X. Z., Liu, H. L., Li, F. B. & Mak, C. L., 2002. Photoelectrocatalytic oxidation of rhodamine B in aqueous solution using Ti/TiO<sub>2</sub> mesh photoelectrodes. *J. Environ. Sci. Health A Tox Hazard. Subst. Environ. Eng.*, Volume 37, pp. 55-69.
- Marugan, J., Christensen, P., Egerton, T. & Purnama, H., 2009. Synthesis, characterization and activity of photocatalytic sol-gel TiO<sub>2</sub> powders and electrodes. *Appl. Catal., B*, Volume 89, pp. 273-283.
- Matos, J., Laine, J. & Herrmann, J. M., 2001. Effect of the type of activated carbons on the photocatalytic degradation of aqueous organic pollutants by UV-irradiated titania. *J. Catal.*, Volume 200, pp. 10-20.
- Nakajima, H., Mori, T., Shen, Q. & Toyoda, T., 2005. Photoluminescence study of mixtures of anatase and rutile TiO<sub>2</sub> nanoparticles: Influence of charge transfer between the nanoparticles on their photo luminescence excitation bands. *Chem. Phys. Lett.*, Volume 409, pp. 81-84.

- Neumann-Spallart, M., 2007. Aspects of photocatalysis on semiconductors: Photoelectrocatalysis. *Chimia*, Volume 61, pp. 806-809.
- Ohno, T., Tokieda, K., Higashida, S. & Matsumura, M., 2003. Synergism between rutile and anatase TiO<sub>2</sub> particles in photocatalytic oxidation of naphthalene. *Appl. Catal., A*, Volume 244, pp. 383-391.
- Ollis, D. & Al-Ekabi, H., 1993. Photocatalytic purification and treatment of water and air. Amsterdam: Elsevier.
- Ovenstone, J., 2001. Preparation of novel titania. Photocatalysts with high activity. *J. Mater. Sci.*, Volume 36, pp. 1325-1329.
- Peill, N. J. & Hoffmann, M. R., 1997. Solar-powered photocatalytic fiber-optic cable reactor for waste stream remediation. *J. Sol. Energy. Trans.*, Volume 119, pp. 229-236.
- Peill, N. J. & Hoffmann, M. R., 1998. Mathematical model of a photocatalytic fiber optic cable reactor for heterogeneous photocatalysis. *Environ. Sci. Technol.*, Volume 32, pp. 398-404.
- Pelaez, M., Nolan, N. T., Pillai, S. C., Seery, M. K., Falaras, P., Kontos, A. G., Dunlope, P. S. M., Hamilton, J. W. J., Byrne, J. A., O'Shea, K., Entezari, M. H. & Dionysiou, D. D., 2012. A review on the visible light active titanium dioxide photocatalysts for environmental applications. *Appl. Catal., B*, Volume 125, pp. 331-349.
- Ramamurthy, V. & Schanze, K. S., 2003. Semiconductor photochemistry and photophysics. New York: Marcel Dekker.
- Raposo, M., Ferreira, Q. & Ribeiro, P. A., 2007. A guide for atomic force microscopy analysis of soft-condensed matter. *Modern Research and Educational Topics in Microscopy*.
- Sabyrov, K., Burrows, N. D. & Penn, R. L., 2013. Size-dependent anatase to rutile phase transformation and particle growth. *Chem. Mater.*, Volume 25, pp. 1408-1415.
- Scalafani, A. & Herrmann, J. M., 1996. Comparison of the photoelectronic and photocatalytic activities of various anatase and rutile forms of titania in pure liquid organic phases and in aqueous solutions. *J. Phys. Chem.*, pp. 13655-13661.

- Schvezov, C. E., Alterach, M. A., Vera, M. L., Rosenberger, M. R. & Ares, A. E., 2010. Characteristics of hemocompatible TiO<sub>2</sub> nanofilms produced by the sol-gel and anodic oxidation techniques. *JOM*, Volume 62, pp. 84-87.
- Setiawati, E., Kawano, K., Tsuboi, T. & Seo, H. J., 2008. Studies on thermal migration of Eu ion doped into TiO<sub>2</sub> nanoparticles. *Jpn. J. Appl. Phys.*, Volume 47, pp. 4651-4657.
- Tian, L., Liu, H. & Gao, Y., 2012. Degradation and adsorption of rhodamine B and phenol on a TiO<sub>2</sub>/MCM-41. *Kinet. Catal.*, Volume 53, pp. 554-559.
- Vinodgopal, K., Hotchandani, S. & Kamat, P. V., 1993. Electrochemically assisted photocatalysis: titania particulate film electrodes for photocatalytic degradation of 4-chlorophenol. *J. Phys. Chem.*, Volume 97, pp. 9040-9044.
- Vohra, M. S. & Tanaka, K., 2003. Photocatalytic degradation of aqueous pollutants using silica-modified TiO<sub>2</sub>. *Water Res.*, Volume 37, pp. 3992-3996.
- Wang, J., Limas-Ballesteros, A. R., Lopez, T., Moreno, A., Gomez, R., Navaro, O. & Bokhimi, X., 2001. Quantative determination of titanium lattice defects and solid-state reaction mechanism in iron-doped TiO<sub>2</sub> photocatalysts. *J. Phys. Chem. B*, Volume 105, pp. 9692-9698.
- Xu, Z. & Yu, J., 2011. Visible light induced photoelectrochemical behaviours of Fe modified TiO<sub>2</sub> nanotube arrays. *Nanoscale*, Volume 3, pp. 3138-3144.
- Yu, J. C., Yu, J. G., Ho, W. K., Jiang, Z. T. & Zhang, L. Z., 2002. Effects of F-doping on the photocatalytic activity and microstructures of nanocrystalline TiO<sub>2</sub> powders. *Chem. Mater.*, Volume 14, pp. 3808-3816.
- Yu, J. G., Wang, W. G., Cheng, B. & Su, B. L., 2009. Effects of hydrothermal temperature and time on photocatalytic activity and microstructures of bimodal mesoporous TiO<sub>2</sub> powders. *J. Phys. Chem. C*, Volume 113, p. 6743.
- Yu, J. G., Xiang, Q. J. & Zhou, M. H., 2009. Preparation, characterization and visible-light driven photocatalytic activity of Fe-doped titania nanorods and first-principles study for electronic structures. *Appl. Catal., B*, Volume 90, pp. 595-602.
- Yu, J. G., Zhang, L. J., Cheng, B. & Su, Y. R., 2007. Hydrothermal preparation and photocatalytic activity of hierarchically sponge-like macro-/mesoporous titania. *J. Phys. Chem. C*, Volume 111, p. 10582.

Yu, J. & Wang, B., 2010. Effect of calcination temperature on morphology and photoelectrochemical properties of anodized titanium dioxide nanotube arrays. *Appl. Catal., B*, Volume 94, pp. 295-302.

Yu, J., Wang, Y. & Xiao, W., 2013. Enhanced photoelectrocatalytic performance of SnO<sub>2</sub>/TiO<sub>2</sub> rutile composite films. *J. Mater. Chem. A*, Volume 1, pp. 10727-10735.

Zacharakis, A., Chatzisyneon, E., Binas, V., Frontistis, Z., Venieri, D. & Mantzavinos, D., 2013. Solar photocatalytic degradation of bisphenol A on immobilized ZnO or TiO<sub>2</sub>. *Int. J. Photoenergy*, Volume 2013.

Zhang, J., Li, M., Feng, Z., Chen, J. & Li, C., 2006. UV Raman Spectroscopic study on TiO<sub>2</sub>. I. Phase transformation at the surface and in the bulk. *J. Phys. Chem. B*, Volume 110, pp. 927-935.

Zhang, Q., Gao, L. & Guo, J., 2000. Effects of calcination on the photocatalytic properties of nanosized TiO<sub>2</sub> powders prepared by TiCl<sub>4</sub> hydrolysis. *Appl. Catal., B*, Volume 26, pp. 207-215.

Zhang, W. F., He, Y. L., Zhang, M. S., Yin, Z. & Chem, Q., 2000. Raman scattering study on anatase TiO<sub>2</sub> nanocrystals. *J. Phys. D: Appl. Phys.*, Volume 33, p. 912.

Zhang, Z., Wang, C., Zakaria, R. & Ying, J., 1998. Role of particle size in nanocrystalline TiO<sub>2</sub>-based photocatalysts. *J. Phys. Chem. B*, Volume 102, p. 10871-10878.



# 3

## OPTIMISATION OF PARAMETERS IN A SOLAR LIGHT-INDUCED PHOTOELECTROCATALYTIC PROCESS WITH A $\text{TiO}_2/\text{Ti}$ COMPOSITE ELECTRODE PREPARED BY PAINT-THERMAL DECOMPOSITION

---

This chapter presents an outline of the effects of photoelectrocatalytic operating parameters in a batch reactor on the kinetics of photo(electro) catalytic (PEC) oxidation, using phenol as a model compound. Process parameters and electrode configuration were varied to examine which mechanism becomes dominant under which conditions. The parameters studied were: the effect of the  $\text{TiO}_2$  layer thickness, agitation, different light intensities ( $\text{UV}_{300-400}$ ), and the initial concentration of phenol in an aqueous solution as encountered in practice. The findings show that there is an optimal catalyst-layer thickness for oxidation efficiency, which is six layers. A higher initial concentration of phenol led to a higher overall degradation percentage of phenol as well, highlighting the importance of the surface area of the catalyst. Increasing the solar light intensity increased the kinetics of phenol oxidation due to the increasing concentration of reactive  $\cdot\text{OH}$ . However, the energy efficiency for the lower intensities was in the range of  $0.1\text{--}2.7 \text{ kWh/m}^3$  and was up to 1.3 times more energy efficient than the system using higher intensities. A trade-off exists between the energy efficiency of the system and the desired level of degradation of the chosen pollutant to obtain the desired rate of the reaction with an optimal energy consumption.

### 3.1. Introduction

Different organic compounds in rivers, mostly introduced through industrial effluents, present a serious threat for humans and aquatic life due to their toxic nature. Conventional methods for their removal, including biotreatment, carbon adsorption, air stripping, reverse osmosis and chlorine treatment, suffer from various limitations (Sincero & Sincero, 2003; Droste, 1997; Parson, 2004; Grega, et al., 1994).

These conventional methods transfer contaminants from one medium to another or generate waste that requires further treatment and disposal (Crittenden, et al., 1999; Topudurti, et al., 1993). Therefore, there is a need to develop efficient and cost-effective technologies for the degradation of organic pollutants, such as phenol, benzene, polychlorinated biphenyls (from groundwater and wastewater) to less harmful compounds or to their complete mineralization (Matthews, 1991). Methods such as Fenton's reaction (Szpyrkowicz, et al., 2001), ozonation (Chu & Ma, 2000), electrochemical (Alinsafi, et al., 2005) and photochemical technologies (Dai, et al., 2007; Khataee & Kasiri, 2010) have been developed to decompose these pollutants. However, the efficiency of the photocatalytic (PC) process is limited by the high percentage of electron-hole recombination (Yu, et al., 1997; Li, et al., 2009; Long, et al., 2014; Babu, et al., 2014).

Two approaches that reduce the effect of recombination have been described in a previous publication (Bennani, et al., 2014): (1) TiO<sub>2</sub> structural optimisation and (2) the application of a suitable positive electric potential on the TiO<sub>2</sub> film electrode. Under the application of a positive potential, the electron is directed more effectively to the counter electrode where it reacts with an electron acceptor in the solution, while the holes may react with H<sub>2</sub>O/OH<sup>-</sup> to generate hydroxyl radicals ( $\cdot$ OH) with a high oxidizing power

(Carneiro, et al., 2005). For a given system, the rate of the photocatalytic reaction at the surface of the catalyst is determined by the concentrations of both the photoholes in the anode and the scavengers at the cathode surface.

The former is determined by the intensity of the incident radiation and layer thickness, and the latter by the bulk concentration of the scavenger.

Various deposition methods, including: plasma beam deposition, ion-assisted deposition, chemical vapour deposition, sol-gel, dip-coating, and sputtering techniques, have been used to prepare TiO<sub>2</sub> films (Vergohl, et al., 2011). The more simple paint-thermal decomposition method has also proven to be effective in controlling the desired layer thickness, the roughness, and the crystalline structure of the TiO<sub>2</sub> films to increase photo-catalytic efficiency (Bennani, et al., 2014). Furthermore, the path length of incident radiation and therefore adsorption can be increased by light scattering in the composite electrode with an admixture of large and small particles in the layers and by increasing the number of layers (Jeng, et al., 2013). The light scattering layer on the top of the other layers confines the incident light within an electrode or diffracts it backward. Additionally, according to Pareek et al., it is difficult to get uniform light intensity distribution in the system (Pareek, et al., 2008). Due to this, it is important to determine the optimal light intensity to minimize energy consumption and to increase the rate of pollutant degradation.

For application in practice, the use of UV irradiation emitted by solar instead of UV light can reduce treatment costs. In addition, the use of solar light with a non-doped simple, TiO<sub>2</sub>/Ti composite electrode, e.g. prepared with the paint-thermal method, would avoid drawbacks such as thermal instability (metal centres acting as electron traps), which reduces the photocatalytic efficiency, and would be less expensive (Zhang, et al., 2014). Furthermore, the paint-thermal decomposition method can be adapted to large-area coatings, providing a large area available for charge transfer reactions, while the mechanical strength and durability of the annealed TiO<sub>2</sub> films is high, which



could present an advantage during the use of TiO<sub>2</sub> films in practice (Bennani, et al., 2014).

When enhancing degradation kinetics of organic compounds (Mogyorosi, et al., 2002; Beltran, et al., 2005), it is important to remember that working conditions are case-specific and need to be carefully optimized.

Although the effects of various operating parameters such as catalyst suspension concentration, pH, and UV light intensity have been widely investigated (Puma & Yue, 2002; Bayarri, et al., 2005; Pablos, et al., 2014), there are some questions still remain about the mechanisms becoming dominant under certain operating conditions. Other studies on design and optimisation of the systems, e.g., infer the existence of mass transfer limitations, but did not include them in the research. Mass transfer limitations that need to be minimized are mainly affected by accessible surface area. However, to date, very few of the PEC studies were done using realistic and proportional surface area/volume ratio, necessary for representative efficiency, adsorption and diffusion of the components (Oliveira, et al., 2007). Laboratory-scaled systems have the advantage of a controlled environment and, hence, they allow the study of various near electrode phenomena. However, their shortfall is related to boundary conditions which may not be satisfactorily scaled up to full-scale systems without impacting current and potential distributions. Therefore a thorough optimisation of PEC systems needs to be provided. In order to obtain knowledge about the influence of different reactor designs effecting the process parameters, suitable for upscaling to the use in practice, and providing data for future standardised solar simulator measurements, the experiments in this work were conducted using solar light (UV<sub>300-400</sub>) and simple TiO<sub>2</sub>/Ti composite electrodes demonstrating that targeted degradation efficiency could be achieved under these conditions, which is, to the authors' knowledge, investigated for the first time.

Analysis of the energy usage of the PEC system could show PEC as an efficient and cost-effective technology to replace and compete with already established advanced oxidation technologies.

## **3.2. Material and methods**

### **3.2.1. Experimental approach**

TiO<sub>2</sub> film electrodes were manufactured and prepared by Magneto special anodes B.V. (Schiedam, The Netherlands) according to the paint-thermal decomposition method (Beer, 1969). Films obtained with this decomposition method were additionally modified by an annealing process. To determine experimentally the optimal conditions for the selected process parameters, the initial phenol concentration, TiO<sub>2</sub> layer thickness and solar light intensity, were varied. A photoluminescence technique was used in order to evaluate the photocatalytic activity of the TiO<sub>2</sub> films with different thicknesses, while the other parameters were monitored by measuring the phenol degradation in an aqueous solution.

### **3.2.2. Modification of TiO<sub>2</sub>/Ti composite electrodes and characterization**

Electrodes coated with TiO<sub>2</sub> were prepared by applying a layer of a solution containing an organic, solvent-based titanium oxide precursor on a titanium substrate. After air drying for a few hours, the support with paint was transferred to an air-circulating oven for its first heat treatment at temperatures between 400°C and 600°C for 2 hours. This heat treatment decomposes and oxidises the salt, giving an oxide layer. Up to six layers of paint were applied first, followed by drying and heat treatment for all the applied layers (Beer, 1969).

The TiO<sub>2</sub> film electrodes were further treated by a second heat treatment, an annealing treatment, in order to gain the optimal ratio of anatase to rutile crystals in a TiO<sub>2</sub> structure (Bennani, et al., 2014). The annealing treatment of the TiO<sub>2</sub> film was carried out in a furnace (NeyTech Vulcan Benchtop Muffle Furnace 3-550). The second heat treatment was carried out according to the procedures already used in a previous study (Bennani, et al., 2014). The TiO<sub>2</sub> film was annealed for five hours at ambient pressure at 650°C, and the temperature was raised 8°Cmin<sup>-1</sup> from room temperature. The thickness of the TiO<sub>2</sub> layer was measured by an Atomic Force Microscopy type Veeco Dektak 8 Stylus Profiler fitted with a 12.5 µm tip. The thickness of the TiO<sub>2</sub> film can be varied through the number of TiO<sub>2</sub> paint layers onto the substrate. The thicknesses of the films were 0.83 µm, 1.22 µm, 2.04 µm, 3.8 µm and 4.33 µm.

### **3.2.3. Photoelectrochemical measurements and analysis of hydroxyl radicals (·OH) and phenol in an aqueous solution**

Photoelectrochemical measurements were carried out with a set-up consisting of a cylindrical quartz glass reactor with an effective vessel volume of 200 ml, an external solar light source (UV<sub>300-400</sub>) and a three-electrode configuration. The initial volume of the working solution was 175 ml phenol (≥99%, Sigma Aldrich) with different initial concentrations (from 2 to 150 mgL<sup>-1</sup>). Demineralized water (RiOs 5 Reverse Osmosis System) was used throughout the experiments for dilution. To eliminate the influence of solution resistance, 0.1 M Na<sub>2</sub>SO<sub>4</sub> was chosen as the supporting electrolyte. The samples were collected from the reaction solution at regular time intervals to determine the residual concentration of phenol or 2-hydroxyterephthalic acid (2-OHTA) for detection of ·OH.

At the start of each experiment, the phenol solution was stirred for three hours with the  $\text{TiO}_2/\text{Ti}$  catalyst in the dark conditions, sufficient for adsorption to reach equilibrium. The pH of the solution was kept constant at 7.2 and was measured before the experiment, using a Sentix 81 pH meter. The cylindrical quartz glass reactor system was placed inside the chamber of the Atlas solar simulator type SUNTEST XXL+, consisting of three Xenon lamps emitting solar light ( $\text{UV}_{300-400}$ ). The emitted spectrum of the Xenon lamps was measured by a StellarNet spectrometer, type Black C-50. The spectrum of the light between 200-850 nm is shown in Figure 3.1. The absorption spectrum of the  $\text{TiO}_2$  layer was also measured with an integrated sphere of UV/VIS/NIR spectrophotometer, model Lambda 90, Perkin Elmer, also shown in Figure 3.1. Confirming that sufficient light is emitted in the region where photons are adsorbed by  $\text{TiO}_2$  whereby hydroxyl radicals are being generated.

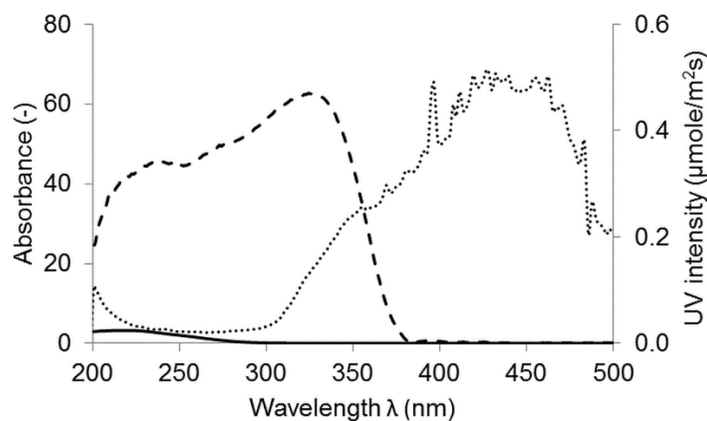


Figure 3.1. The efficiency of light absorption by  $\text{TiO}_2$  for UV emitted by the lamps in the solar simulator. Emission spectra of the Xenon lamps inside the chamber of the SUNTEST XXL+ (···), absorbance spectrum at 2 ppm concentration of phenol (---) and  $\text{TiO}_2$  (6 layers) (—)

The temperature was controlled at  $25 \pm 1^\circ\text{C}$  by recirculating the cooling water in a water bath equipped with a cooler (Julabo, FL300). During the experiments the reactor was closed by UV permeable quartz lids to prevent evaporation of the phenol. A photo-anode consisting of a  $\text{TiO}_2/\text{Ti}$  plate with a surface area of  $16\text{ cm}^2$  was incorporated in the reactor to receive solar light irradiation. The  $\text{TiO}_2$  film supported on the Ti plate was used as the photocatalyst. A graphite plate of  $20\text{ cm}^2$  was used as a cathode and placed at a distance of 1 cm from the anode. An  $\text{Ag}/\text{AgCl}$  electrode was used as a reference electrode. The electrode potential and working current were controlled with a potentiostat-galvanostat system (Autolab PGSTAT128N with a BOOSTER10A). Bias voltages between -0.2 and 0.3 V were employed at a scan rate of  $0.01\text{ Vs}^{-1}$  while dark current and photocurrent under solar light irradiation were recorded. Voltage during each experiment was sufficiently high that the limiting current was reached. The net current was calculated by subtracting dark current from photocurrent in order to determine the photoactivity of the films. The phenol photo degradation experiments were performed with constant potential. The optimal potential of 1 V was taken from the previous study with the same  $\text{TiO}_2/\text{Ti}$  composite electrodes (Bennani, et al., 2014). In order to investigate whether the oxidation of phenol was due to oxidation by hydroxyl radicals rather than electrochemical oxidation, degradation kinetics experiments of phenol as well as the reaction between  $\cdot\text{OH}$  and terephthalic acid (TA) were carried out in an undivided cell, with the stirred solution kept at a constant temperature. All chemicals used in the experiments were of analytical grade and used without further purification.

The absorption spectrum of phenol is shown in Figure 3.1. It shows that the absorption spectrum of phenol does not overlap with the emission spectrum of the solar light ( $\text{UV}_{300-400}$ ) used in the experiments. Therefore, the

breakdown of phenol by photolysis is expected to play an insignificant role in the experiments.

Photosensitivity of the  $\text{TiO}_2/\text{Ti}$  composite electrode was analysed by linear sweep voltammetry (LSV) combined with illumination under solar light ( $\text{UV}_{300-400}$ ) with an intensity from 25 to  $60 \text{ Wm}^{-2}$ . The qualitative determination of  $\cdot\text{OH}$  generated during the experiments was achieved by photoluminescence (PL), using TA (Sigma Aldrich, 98 %) (Yu & Wang, 2010).

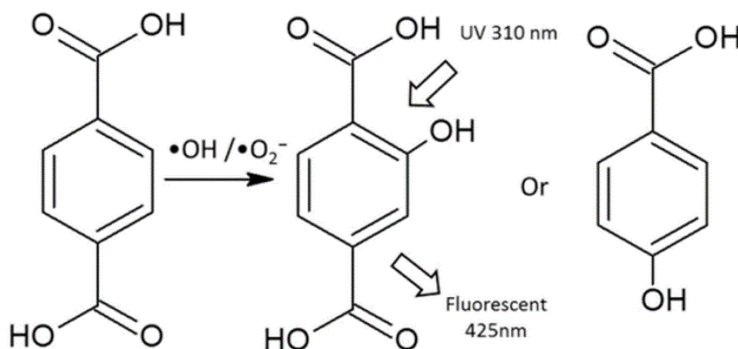


Figure 3.2. Formation of 2-OHTA or 4-HBA through the reaction of TA with  $\cdot\text{OH}$  and  $\text{O}_2^{\cdot-}$  (Yu & Wang, 2010)

The method used relies on the PL signal at 425 nm of 2-OHTA. The PL intensity of 2-OHTA (Figure 3.2) is proportional to the amount of  $\cdot\text{OH}$  produced in water. A stock solution of TA ( $5 \cdot 10^{-2} \text{ M}$ ) was prepared in a potassium dihydrogen phosphate buffer (pH 6.5). This stock solution was diluted with distilled water into a concentration of  $5 \cdot 10^{-4} \text{ M}$  to be used to assess photocatalytic activity. Terephthalic acid as the fluorescent probe can readily react with hydroxyl radicals ( $\cdot\text{OH}$ ) and superoxide anion radical ( $\text{O}_2^{\cdot-}$ ) to produce fluorescent products (Bubacz, et al., 2013). As shown in Figure 3.2, the main products of terephthalic acid are 2-hydroxyterephthalic acid (2-HTA)

or hydroxybenzoic acid (4-HBA), and only 2-HTA is highly fluorescent and thus can be easily determined by fluorescence spectroscopy (Mogyorosi, et al., 2002; Beltran, et al., 2005).

It has been proven that under these experimental conditions (low concentration of terephthalic acid, less than  $10^{-3}$  M, room temperature), the hydroxylation reaction of terephthalic acid proceeds mainly by  $\cdot\text{OH}$  radicals (Ishibashi, et al., 2000). PL spectra of the generated 2-OHTA were measured on the PL Spectrophotometer PIT Quanta Master Model QM-1. After irradiation for three hours in the batch quartz reactor, an aliquot of the reaction solution was used to measure the PL intensity at 425 nm with excitation at 315 nm. A series of anodes with a different number of  $\text{TiO}_2$  layers (2, 4, 6, 8 and 10) were studied in order to analyse the  $\text{TiO}_2$  layer effect on the  $\cdot\text{OH}$  formation and the total transport resistance  $R$  of the  $\text{TiO}_2/\text{Ti}$  composite electrode with  $R$  linked to the transport of charged species (Jiao, et al., 2012). For a given light intensity, the total resistance  $R$  varied with the number of  $\text{TiO}_2$  layers, which in turn determined the maximum reaction rate.

A stirrer was placed at the bottom of the cell to agitate the reactants. Agitation experiments were carried out at various speeds of agitation (0-1100 rpm) to determine at what speed the resistance caused by concentration polarization due to mass transfer limitations was no longer contributing to the voltage-current measurements. This determination was established by measuring the change in phenol concentration over time, keeping all other conditions constant. The phenol concentration was monitored with a Hach Lange DR 5000 spectrophotometer by using Hach Lange cuvette tests (LCK 345 with a measuring range of  $0.05\text{-}5.00\text{ mgL}^{-1}$ ,  $5\text{-}50\text{ mgL}^{-1}$  and  $20\text{-}200\text{ mgL}^{-1}$ ). Phenol reacts with 4 -nitroaniline to form a yellow-coloured complex which is then measured by photometry.

### 3.2.4. Kinetic studies on phenol photodegradation

The photocatalytic oxidation kinetics of many organic compounds are often modelled by the Langmuir-Hinshelwood (L-H) equation. L-H kinetics combines adsorption and desorption with a surface reaction. In the L-H model, the rate reaction ( $r$ ) is proportional to the fraction of surface covered by the substrate, ( $\theta$ ) that is (Barka, et al., 2008)

$$r = -\frac{dC}{dt} = k_r \theta \quad (1)$$

and

$$\theta = \frac{K_{LH} C}{(1 + K_{LH} C)} \quad (2)$$

where

$$k'_r = \frac{V}{A} k_r \quad (3)$$

thus

$$\begin{aligned} r &= -\frac{dC}{dt} = \frac{A}{V} k'_r \theta \\ &= \frac{A}{V} k'_r \left[ \frac{K_{LH} C}{(1 + K_{LH} C)} \right] \end{aligned} \quad (4)$$

where  $k_r$  ( $\text{min}^{-1}$ ) is the reaction rate constant,  $k'_r$  is normalized constant rate by specific surface area ( $\text{min}^{-1}\text{m}^{-2}\text{L}$ ),  $K_{LH}$  ( $\text{Lmol}^{-1}\text{m}^{-2}$ ) is the constant of adsorption equilibrium of the L-H isotherm, and  $C$  (mol) is the concentration of the phenol in the bulk at any time. The equation can be integrated to be:

$$\ln\left(\frac{C_o}{C}\right) + K_{LH}(C_o - C) = \frac{A}{V} k'_r K_{LH} t \quad (5)$$



where  $C_0$  (mol) is initial concentration of the phenol in the bulk and  $t$  (min) is the irradiation time. When  $C_0$  is very small, the reaction is assumed a first-order reaction, resulting in the following equation:

$$r = -\frac{dC}{dt} = \frac{A}{V} k'_r K_{LH} C = kC \quad (6)$$

where  $k$  ( $\text{min}^{-1}\text{m}^{-2}\text{L}$ ) is the rate constant of a first order reaction. Thus, equation (5) can be simplified:

$$\ln \frac{[C_6H_6O]}{[C_6H_6O]_0} = kt \quad (7)$$

By plotting  $\ln[C_6H_6O]/[C_6H_6O]_0$  versus  $t$ , the rate constant  $k$  can be determined from the slope of the curve obtained.

Values of  $k'_r$  and  $K_{LH}$  for phenol photo(electro)catalytic degradation can be obtained by using the following equation:

$$r_o = -\frac{dC}{dt} = \frac{A}{V} k'_r K_{LH} C + K_{LH} C_0 \quad (8)$$

Hence,

$$\frac{1}{r_o} = \frac{1}{\frac{A}{V} k'_r K_{LH} C_0} + \frac{1}{\frac{A}{V} k'_r} \quad (9)$$

where  $k'_r$  ( $\text{molm}^2\text{L}^{-1}\text{min}^{-1}$ ) is often interpreted in the literature as a first-order Langmuir Hinshelwood rate coefficient,  $K_{LH}$  ( $\text{Lmol}^{-1}\text{m}^{-2}$ ) as an equilibrium constant and  $r_o$  ( $\text{molm}^2\text{L}^{-1}\text{min}^{-1}$ ) as the initial degradation rate. The Langmuir–Hinshelwood kinetic parameters were determined from the slope and intercept of the linear fit of  $1/r_o$  vs  $1/C_0$ .

### 3.2.5. Incident photocurrent efficiency, quantum yield, faradaic efficiency and energy efficiency

Optimisation of the applied current variation was based on the incident photon to current efficiency (IPCE) of TiO<sub>2</sub>/Ti (Wang, et al., 2009). The IPCE measurement was carried out in the 260–850 nm wavelength range of the light source. The TiO<sub>2</sub>/Ti composite electrode with a 2 µm TiO<sub>2</sub> layer thickness was immersed into the phenol aqueous solution with 0.1 M Na<sub>2</sub>SO<sub>4</sub> electrolyte, and connected to a potentiostat, with Ag/AgCl as the reference electrode. The samples were illuminated with solar light (UV<sub>300-400</sub>) with intensities varying from 25-60 Wm<sup>-2</sup>. Current efficiency was calculated according to the following equation

$$IPCE = \frac{j}{\left(\frac{F}{P}\right)} \quad (9)$$

where  $j$  (Am<sup>-2</sup>) is the measured current density,  $P$  (Einsteins<sup>-1</sup>m<sup>-2</sup>) is the incident light intensity, and  $F$  (96485.33 sAmol<sup>-1</sup>) is the Faraday constant (Xie, et al., 2010).

Faradaic efficiency is given by the ratio:

$$f = \frac{-\frac{dc}{dt}V}{\left(\frac{j}{F}\right)} \quad (10)$$

The quantum yield for the generation of ·OH radicals plays a very important role in the efficiency of photodegradation of pollutants. Quantum yields are calculated by the following equation:

$$\emptyset = f \cdot IPCE \quad (11)$$

The mechanism of phenol oxidation proposed by Devlin and Harris (Devlin & Harris, 1984) includes an initial conversion of phenol into catechol and hydroquinone. Although many reaction paths for phenol  $\cdot\text{OH}$  radicals are possible, previous experimental evidence by the authors revealed only traces of other products; almost negligible compared to the two OH-addition reactions mentioned. Moreover, the work of Kilic et al. (Kilic, et al., 2007) has shown a low quantum yield for reactions other than the ones considered. Therefore, for practical purposes, in the present work only these two OH-addition reactions were considered when calculating the quantum yield.

The energy efficiency for processes in which light is an input can be calculated easily using electrical energy per order (EE/O) (Zhang, et al., 2004). This value is defined as the electrical energy (kWh) required to mineralize the pollutant in 1 m<sup>3</sup> of contaminated water by one order of magnitude. The EE/O is given by:

$$\frac{EE}{O} = \frac{P_t}{V \log\left(\frac{C_0}{C}\right)} \quad (12)$$

where  $P_t$  is input energy in kWh,  $V$  is volume in m<sup>3</sup> and  $C_0$  and  $C$  are initial concentration and concentration at time  $t$ , mg/L.

### 3.3. Results and discussion

#### 3.3.1. The effect of TiO<sub>2</sub> film electrode thickness on the performance of the electrode system

TiO<sub>2</sub>/Ti performance is affected by the number of TiO<sub>2</sub> layers, as seen in Figure 3.3. The effect of the number of TiO<sub>2</sub> layers is shown on the maximum photoluminescence (Max PL) intensity of 2-OHTA at 425 nm formed by the reaction of TA with  $\cdot\text{OH}$  after solar irradiation for three hours.

The results show that the highest PL intensity of 2-OHTA at 425 nm was obtained with a TiO<sub>2</sub> film electrode that consists of six layers.

A. Saranya et al. with UV-Visible study confirmed the existence of an optimal number of layers and that the optical transmittance reduces as the number of layers and corresponding thickness of the film increases (Saranya, et al., 2014). What those authors additionally observed was that the energy gap value decreases with an increase in both the number of coatings and the post-annealing temperature. Considering Figure 3.3, the lower PL intensity at 425 nm with the lower number of TiO<sub>2</sub> layers could be attributed to back-scattering light, resulting in lower solar efficiency. Flocculated or agglomerated TiO<sub>2</sub> particles in the TiO<sub>2</sub>/Ti composite electrode (Bennani, et al., 2014) could have significantly reduced the light-scattering performance and require the use of more TiO<sub>2</sub> to achieve a desirable opacity. This observation was confirmed by C. Pablos, who showed that the increase in thickness of the TiO<sub>2</sub> layer led to a higher UVA absorption as the number of TiO<sub>2</sub> coating cycles increased (Pablos, et al., 2014). On the other hand, thicker TiO<sub>2</sub> layers resulted in low PL intensity due to the increased resistance of electron transport through the TiO<sub>2</sub> layer to the current collector. Increased resistance of electron transport is likely due to the increased path length of the generated electrons to be collected by conductive substrate, causing an increase in electron-hole recombinations and a decrease in current efficiency (Jeng, et al., 2013).

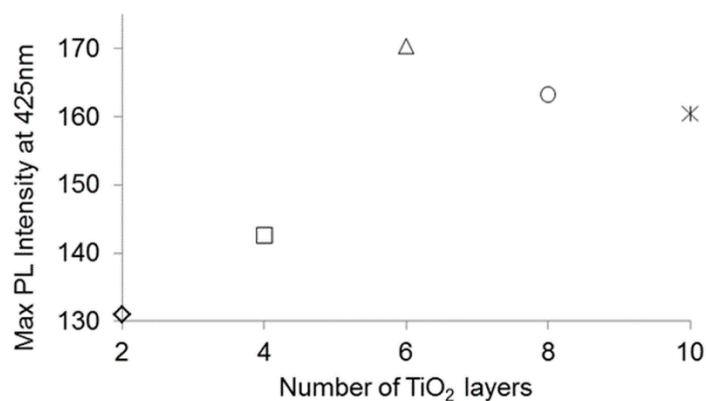


Figure 3.3. Maximum PL intensity of 2-OHTA at 425 nm as a function of the number of TiO<sub>2</sub> layers, at applied potential of 1 V

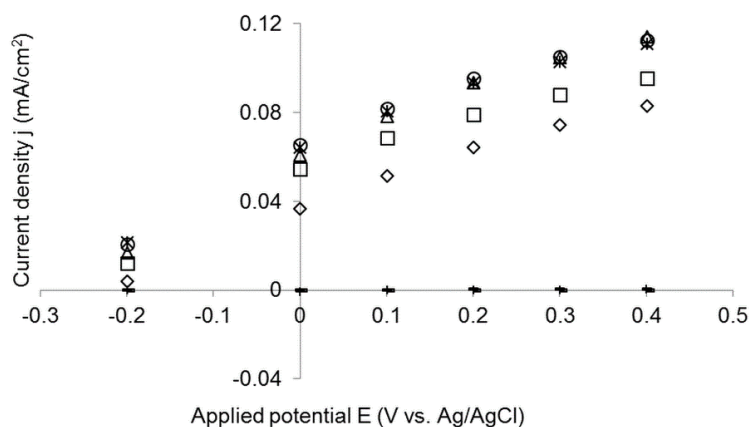


Figure 3.4. LSV Voltammograms of the TiO<sub>2</sub> photo-anodes (scan rate 0.01 V/s) under solar light (UV<sub>300-400</sub>) intensity in a TA solution with 0.1 M Na<sub>2</sub>SO<sub>4</sub> as the supporting electrolyte. 2 layers (◇); 4 layers (□); 6 layers (Δ); 8 layers (⋈) and 10 layers (o) and corresponding dark currents

Furthermore, to analyse the effect of film thickness on electron transport and the degradation kinetics, the transport resistance values for each layer thickness in Figure 3.4 were defined (according to Ohm's law) by dividing the potential difference by the corresponding photocurrent difference of layer thickness.

$R$  values obtained from the interception of the linear regression equations for all thicknesses are shown in the Figure 3.5 and plotted against the number of applied  $\text{TiO}_2$  layers. Figure 3.5 shows that the electron transport resistance values have a minimum at six layers.

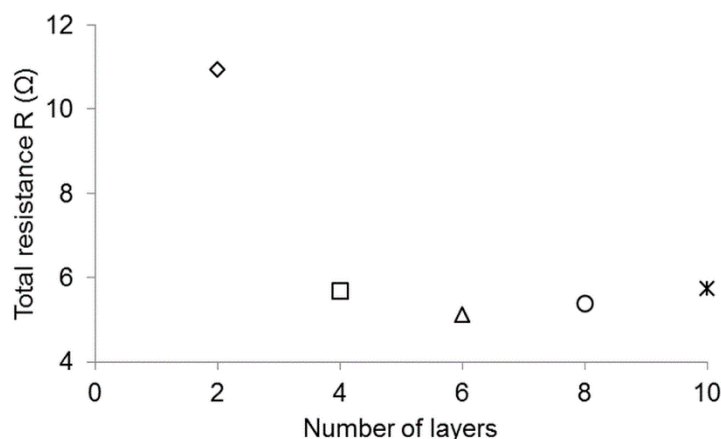


Figure 3.5. Calculated total transport resistance and the effect of the number of the  $\text{TiO}_2$  layers on the resistance, 2 layers (o); 4 layers ( $\Delta$ ); 6 layers ( $\square$ ); 8 layers ( $\diamond$ ); 10 layers ( $\times$ ); (solar light intensity  $60 \text{ Wm}^{-2}$ , TA solution with  $0.1 \text{ M Na}_2\text{SO}_4$  as the supporting electrolyte)

As shown in Figure 3.5, the resistance related to the electron transport decreases as the  $\text{TiO}_2$  thickness is increased up to an optimal six layers of  $\text{TiO}_2$ . This reduction in the total resistance induces the improvement of the system efficiency as can be seen in the Figure 3.3.

C. Pablos et al. (Pablos, et al., 2014) showed that electron generation increases with an increasing thickness of the  $\text{TiO}_2$  layer because of the higher light absorption. This increase can be explained by assuming that more TA molecules will react with more  $\cdot\text{OH}$  radicals formed due to the larger surface area of the  $\text{TiO}_2$ , leading to more electron-hole pairs being generated, fewer electron-hole recombinations and, consequently, a higher limiting current. Although a larger film thickness (beyond the optimal thickness) tended to increase the amount of TA adsorption, it also caused a higher electron transport resistance and increased the recombination of electrons with holes in the  $\text{TiO}_2$  layer, resulting in a decrease in  $\cdot\text{OH}$  formation. Even though Ming Jer-Yeng et al. observed an increase in charge transfer resistance by increasing the number of layers, they do point out the importance of an optimal number of layers as a way to achieve maximum efficiency (Jeng, et al., 2013). As seen in Figure 3.5, resistance  $R$  was found to be lowest for the  $\text{TiO}_2$  film with six layers. From Figures 3.3 and 3.5 it can be concluded that the performance of the  $\text{TiO}_2/\text{Ti}$  composite electrode improves when this total resistance is small. Yet, Ming Jer-Jeng et al. also showed that the optimal  $\text{TiO}_2$  thickness for achieving the maximum efficiency does not depend only on the thickness and number of the layers and light absorbance but also on the particle size distribution in the layers (Jeng, et al., 2013). The choice of particle size in the bottom layer is more important than it is in the top layer to achieve better solar efficiency.

Table 3.1. First-order rate constants  $k$  of phenol in an aqueous solution for different stirring rates under the same conditions

Light intensity $\text{Wm}^{-2}$	$C_0$ mg/L	$k$ $\text{min}^{-1}$	$R^2$	Rate of stirring (RPM)
60	2	0.0036	0.9976	0
60	2	0.0059	0.9995	220 (2)
60	2	0.0063	0.9998	440 (4)
60	2	0.0068	0.9990	660 (6)
60	2	0.0090	0.9998	880 (8)
60	2	0.0080	0.9979	1100 (10)

Optimisation of the photoelectrocatalytic system can be further investigated. Additionally, the effect of stirring on the first-order degradation rate constant was determined and results are reported in Table 3.1. The rate of photo degradation is affected not only by the electrode reaction itself but also by the transport of species to and from a bulk solution. This transport can occur by diffusion, convection and migration. The contribution of migration in this case can be neglected due to the presence of supporting electrolytes (0.1 M  $\text{Na}_2\text{SO}_4$ ) which transport almost all the current in the bulk solution in the cell. Mass transport due to diffusion and convection of the phenol molecules to the interface, therefore, determines the overall efficiency. The values are presented in Table 3.1. Due to the homogeneous distribution of phenol molecules in the solution, no concentration gradient therein should be present. However, a concentration gradient exists at the electrode surface during the photo electrochemical degradation experiment. Phenol molecules react at the electrode surface with the formed  $\cdot\text{OH}$  radicals leading to a decrease in the phenol concentration in that region. Table 3.1 displays a slight increase in photocurrent when higher stirring rates were applied.



When the mass transfer is rate-limiting, the current response is proportional to the concentration gradient  $dC/dX$ , where  $C$  represents concentration and  $X$  the thickness of the boundary layer (Jeng, et al., 2013). When the system is operating at the potential of limiting current (1 V), the phenol concentration on the electrode surface is zero. With conventional electrolysis, since the phenol concentration in the bulk would have been kept constant, an increase in stirring rate results in the thickness of the boundary layer being lowered. As a result, the concentration gradient over the boundary layer increases, the mass transfer rate increases, and the current response increases, as well. With PEC and with very high agitation rates, it is also possible that the limiting current is determined by the availability (concentration) of hydroxyl radicals at the surface to draw electrons from the reactant present at the solution/TiO<sub>2</sub> surface, rather than the concentration of the reactant at this surface. It is also possible that the phenol concentration at the surface is rate-limiting even when there is no boundary layer in which the phenol concentration decreases. This rate limitation is possible when the bulk concentration of phenol is very low, so the surface concentration will be low without assuming a concentration gradient in the hydrodynamic boundary layer. It was shown experimentally that the rate of degradation of phenol in solution is higher in the stirred solutions as compared to the unstirred one. From Table 3.1, we observe that the phenol degradation rate  $k$  shifts to slightly higher values, indicating faster degradation when agitated. The minimum speed of stirring that provided good mixing was 880 rpm. Also, the hydroxyl radicals produced at the surface can react more quickly, thereby decreasing the chance for electron-hole recombination. At this agitation speed, experiments were carried out in which the rate of degradation was not limited by mass transfer rates.

### 3.3.2. Effect of solar light intensity on phenol degradation and the performance of the system

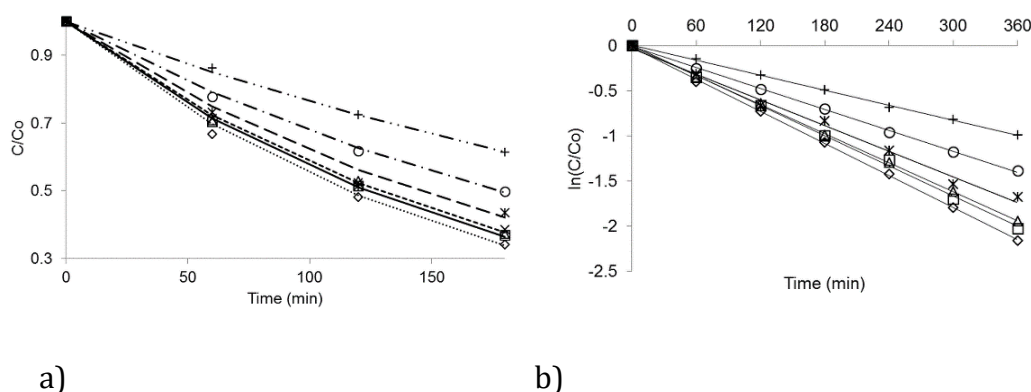


Figure 3.6. Degradation of phenol with PEC at 1V for the  $\text{TiO}_2$  sample under different solar light intensities: 60  $\text{Wm}^{-2}$  ( $\diamond$ ); 55  $\text{Wm}^{-2}$  ( $\square$ ); 50  $\text{Wm}^{-2}$  ( $\Delta$ ); 45  $\text{Wm}^{-2}$  ( $\times$ ); 40  $\text{Wm}^{-2}$  ( $\bowtie$ ); 30  $\text{Wm}^{-2}$  ( $\circ$ ) and 25  $\text{Wm}^{-2}$  ( $+$ ). (round dotted line) 1<sup>st</sup> order kinetics of 60  $\text{Wm}^{-2}$ ; (solid line) 1<sup>st</sup> order kinetics of 55  $\text{Wm}^{-2}$ ; (square dotted line) 1<sup>st</sup> order kinetics of 45  $\text{Wm}^{-2}$ ; (dashed line) 1<sup>st</sup> order kinetics of 40  $\text{Wm}^{-2}$ ; (long dash dotted line) 1<sup>st</sup> order kinetics of 30  $\text{Wm}^{-2}$  and (long dash dot dot) 1<sup>st</sup> order kinetics of 25  $\text{Wm}^{-2}$

According to Wang et al. (Wang, et al., 2009; Wang, et al., 2010), light intensity influences the extent of the photo-generated electron-hole pairs and consequently the kinetics of the photocatalytic reaction. The plot in Figure 6 represents the effect of solar light intensity on phenol degradation in the PEC system. The relationship between  $\ln([C_6H_5OH]/[C_6H_5OH]_0)$  and the degradation time for phenol in the PEC system resulted is linear, which suggests that PEC degradation obeys first-order kinetics. Table 1 shows the values of the first-order PEC rate constants  $k$  ( $\text{min}^{-1}$ ) for phenol. As a result, the experimental data are fitted according to first-order kinetics as shown in Figure 3.6.

As the solar light intensity increased from 25 to 60  $\text{Wm}^{-2}$ , the rate constant  $k$  of the first-order reaction of phenol degradation also increased (see the Table 3.2). The phenol conversion at 60  $\text{Wm}^{-2}$  reached 76 % after four hours, whereas the conversion at 25  $\text{Wm}^{-2}$  was less than 50 % after a four-hour irradiation time. These results can be explained based on the flux of photons in the reaction system at low and high solar light intensities (Sohrabi & Ghavami, 2010; Moon, et al., 2012). These findings are in good agreement with the results observed by A. F. Alkaim et al. who described the effects of light intensity on the kinetics of the photocatalytic process and stated that (1) at low light intensities, the rate increases linearly with increasing light intensity (first-order regime), (2) at intermediate light intensities beyond a certain value, the rate increases with the square root of the light intensity (half-order regime), and (3) at high light intensities, the rate is independent of the light intensity (diffusion limit) (Alkaim, et al., 2013).

Table 3.2. PEC kinetic rate constants and correlation coefficients of  $\text{TiO}_2/\text{Ti}$  composite electrode (with 6  $\text{TiO}_2$  layers) under different solar light ( $\text{UV}_{300-400}$ ) intensities and bias of 1 V

Solar intensity $\text{Wm}^{-2}$	First-order rate constant, $k \text{ min}^{-1}$	Correlation coefficient, $R^2$	% phenol degraded
25	0.0027	0.9989	62.86
30	0.0039	0.9989	74.89
40	0.0048	0.9912	81.28
45	0.0054	0.9989	86.02
50	0.0054	0.9997	85.64
55	0.0056	0.9981	86.76
60	0.0060	0.9993	88.47

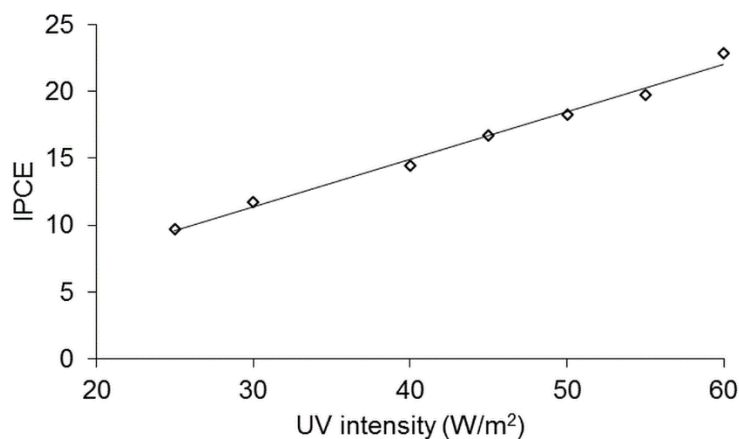


Figure 3.7. IPCE for phenol degradation on TiO<sub>2</sub> film electrode under different UV intensities

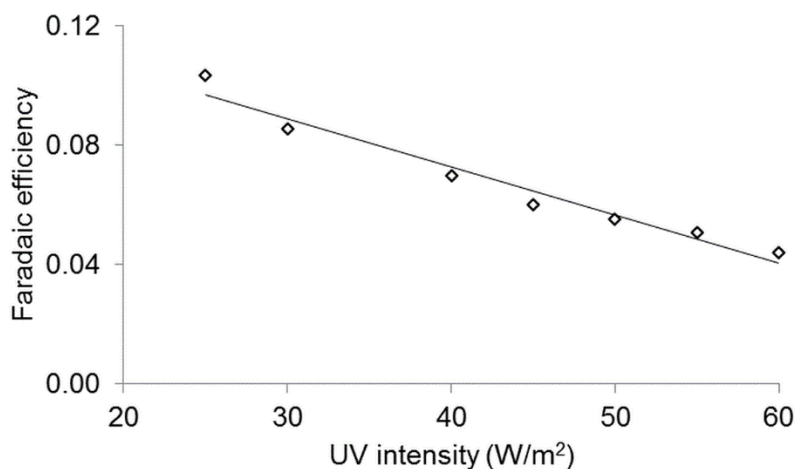


Figure 3.8. Faradaic efficiencies of phenol degradation on TiO<sub>2</sub> film electrode under different UV intensities

IPCEs and Faradaic efficiencies of the degradation experiments mentioned in Section 3.2.3. are shown in Figures 3.7 and 3.8, for different UV intensities, respectively. For higher UV intensities, the IPCE increases while the Faradaic efficiency decreases. Although the Faradaic efficiency decreases with higher intensities, the slope is smaller than the slope of calculated IPCE.

Therefore, it seems possible to achieve acceptable degradation levels over a wider range of intensities.

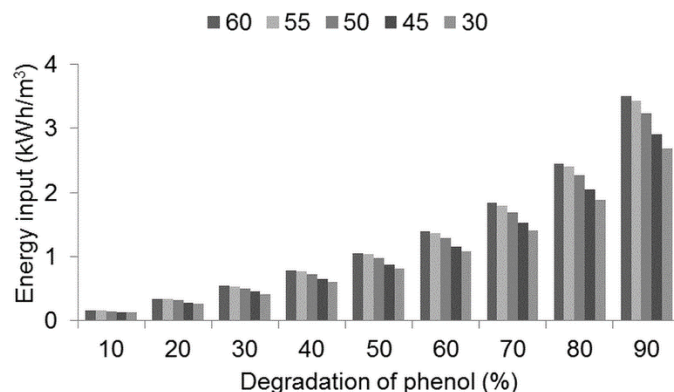


Figure 3.9. Electrical energy per order using different solar light ( $UV_{300-400}$ ,  $Wm^{-2}$ ) intensities for different degradation percentages of phenol

The calculated energy efficiency for the five different intensities at the same reaction conditions is shown in Figure 3.9. From the results obtained, the intensities shown have similar energy efficiencies up to 50 % phenol degradation. At the higher degradation percentages, 30 and 45  $Wm^{-2}$  are much more energy efficient than the higher intensities. For example, the energy efficiency of 30  $Wm^{-2}$  is up to 1.3 times lower than that of 60  $Wm^{-2}$ . Degradation of phenol at a UV intensity of 30  $Wm^{-2}$  with an electric energy of 1  $kWhm^{-3}$  reached 60 % after 235 min. With the same electrical energy of 1  $kWhm^{-3}$  and 50 % degradation, the required reaction time was decreased to the desired 115 min by increasing the intensity up to 60  $Wm^{-2}$ . According to Crittenden et al., an energy input of less than 0.265  $kWhm^{-3}$  is both cost and energy 'efficient' and could be reasonably scaled to full scale treatment (Crittenden, 2012). The implementation of PEC and a determination of its

effectiveness by comparing it to other advanced oxidation processes (AOPs) is difficult.

As with all treatment technologies, the effectiveness of any AOP will be largely determined by the water matrix of the treated water. However, in this case, it can be shown that the values of the required energy input in the PEC system are at the same order of magnitude as in the UV/H<sub>2</sub>O<sub>2</sub> (Martijn, et al., 2010). Higher radiation intensities are accompanied by excess carriers being generated. Electron-hole recombination is at that point able to compete with charge carrier transfer, thereby causing a lower effect on oxidation kinetics and quantum yield. A trade-off between energy efficiency of the system and the desired level of degradation of the chosen pollutant exists. For each pollutant, a balance needs to be established between the acceptable energy demand and the desired rate of the reaction kinetics.

### **3.3.3. Effect of the initial phenol concentration on phenol degradation and the performance of the system**

The effect of the initial phenol concentration on its degradation by the PEC process was investigated as well as the  $\cdot\text{OH}$  generation on the TiO<sub>2</sub> surface. The results are shown in Figure 3.10 and Table 3.2. From Figure 3.10 it can be seen that between 90 % and 15 % of the phenol in solution was removed by PEC for initial phenol concentrations ranging from 2 to 150 mg/L, at a pH of 7.2, and a solar light (UV<sub>300-400</sub>) intensity of 60 Wm<sup>-2</sup>. The fact that phenol adsorption on the TiO<sub>2</sub> surface was under detection limits (data not shown) indicates that the phenol was not physically adsorbed but chemically reacted on the TiO<sub>2</sub>/Ti composite electrode surface. This condition was also reported by Santos et al. (Santos, et al., 1999). Figure 3.10 clearly shows the transition from availability of the PEC system by means of the available TiO<sub>2</sub> surface area to  $\cdot\text{OH}$  radical formation limitations.

From this figure it can be concluded that the capacity of any photo(electro)chemical reactor for removal of a desired pollutant depends on the ratio between available pollutant molecules and formed  $\cdot\text{OH}$  radicals.

Table 3 lists the rate constant  $k$  ( $\text{min}^{-1}$ ) values with the corresponding calculated Langmuir-Hinshelwood parameters (Figure 3.11). It can be seen that  $k$  ( $\text{min}^{-1}$ ) decreases with an increasing initial phenol concentration.

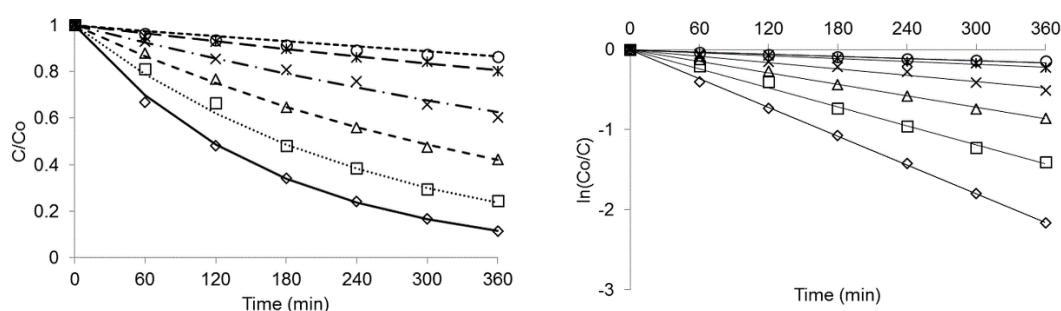


Figure 3.10. Effect of initial concentration of phenol on the PEC degradation at 1 Volt bias under solar light illumination ( $\text{UV}_{300-400}$ ), ( $60 \text{ Wm}^{-2}$ ,  $\text{TiO}_2/\text{Ti}$  electrode with 6  $\text{TiO}_2$  layers);  $2 \text{ mgL}^{-1}$  ( $\diamond$ );  $10 \text{ mgL}^{-1}$  ( $\square$ );  $20 \text{ mgL}^{-1}$  ( $\Delta$ );  $50 \text{ mgL}^{-1}$  ( $\times$ ),  $100 \text{ mgL}^{-1}$  ( $\text{ж}$ );  $150 \text{ mgL}^{-1}$  ( $\circ$ )

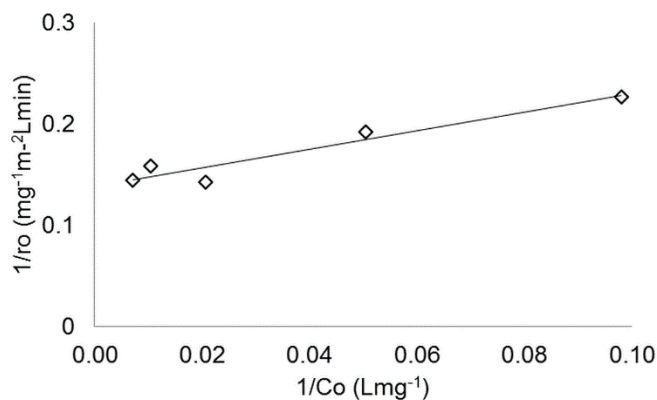


Figure 3.11. Langmuir isotherm plot of phenol adsorption onto  $\text{TiO}_2$  using different initial concentrations of phenol, normalized by specific surface area

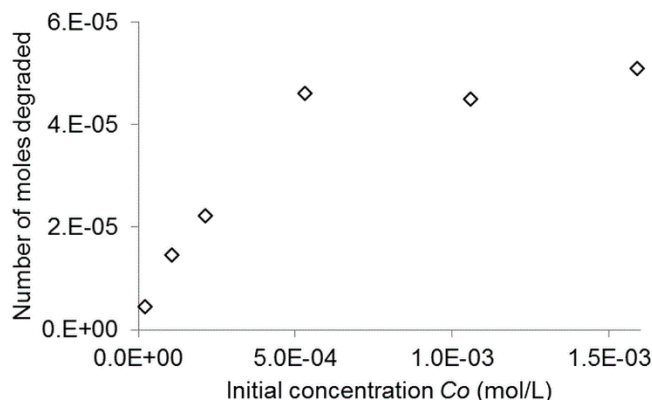


Figure 3.12. Number of moles of phenol degraded when different initial concentrations are applied

To determine the efficiency of the PEC system when using different concentrations, the number of moles of phenol degraded per each initial phenol concentration consumed is plotted against the initial concentration of phenol (Figure 3.12). The figure shows that the number of moles degraded increases notably in the range of initial concentration from  $2.13 \cdot 10^{-5}$ – $5.31 \cdot 10^{-4}$  molL<sup>-1</sup>, and is not significantly further enhanced at higher initial concentrations ( $1.06 \cdot 10^{-3}$  and  $1.59 \cdot 10^{-3}$  molL<sup>-1</sup>). Therefore, it can be concluded that at concentrations higher than  $1.06 \cdot 10^{-3}$  molL<sup>-1</sup> the catalytic surface area becomes rate-limiting for the generation of hydroxyl radicals to oxidize phenol. This is in contrast to an explanation reported in the literature [48] that upon increasing the initial concentration of phenol, a larger amount of phenol is present on the surface of the TiO<sub>2</sub>, causing a reduction in the generation of hydroxyl radicals since there are fewer active sites available for the adsorption of hydroxyl ions and the generation of  $\cdot\text{OH}$  (Santos, et al., 1999; Lam, et al., 2010).

Quantum yields of the degradation experiments were calculated according to Equations 9, 10 and 11, as mentioned in Section 3.2.5.



The quantum yield  $\phi$  for  $\cdot\text{OH}$  radical formation, using phenol at different initial concentrations as a degrading compound, was determined at a UV intensity of  $60 \text{ Wm}^{-2}$ .

This is shown in Table 3.3. It can be concluded that  $\phi$  increases with an increase in the initial concentration of phenol.

Table 3.3. First-order rate constants  $k$ , quantum yield and conversions for different initial concentrations of phenol in an aqueous solution

Light intensity $\text{Wm}^{-2}$	$C_0$ mg /L	$k$ $\text{min}^{-1}\text{m}^{-2}\text{L}$	$R^2$	% phenol degraded	$\phi$	$r_o$ $\text{mgm}^2\text{L}^{-1}\text{min}^{-1}$	$k_r$ $\text{mgm}^2\text{L}^{-1}\text{min}^{-1}$	$K_{LH}$ $\text{Lmg}^{-1}\text{m}^{-2}$
60	2	0.6551	0.9993	88.47	0.0886	0.0118	0.1515	1.0085
60	10	0.4331	0.9952	75.49	0.2238	0.0408		
60	20	0.2635	0.9979	57.63	0.3487	0.0475		
60	50	0.1443	0.9811	39.71	0.7626	0.0632		
60	100	0.0656	0.9909	19.65	0.8799	0.0577		
60	150	0.0492	0.9643	13.48	0.8799	0.0564		

### 3.4. Conclusions

The conclusions drawn from this study can be summarized as follows:

- The film thickness is a key parameter in controlling the electron transfer as well as the light-harvesting efficiency. The observations indicate that six layers might be an optimal number of layers of  $\text{TiO}_2$  film for an effective PEC reaction.

- According to Ming-Jer Jeng proper dispersion and size of the  $\text{TiO}_2$  particles in the layers are the keys to achieving optimum optical performance [20].
- An increase in the initial concentration of phenol increased the probability of phenol molecules reacting with  $\cdot\text{OH}$ . However, at higher initial phenol concentrations, the available surface area for  $\cdot\text{OH}$  formation becomes the rate-limiting factor, as there is an excess of phenol molecules at the surface.
- Elimination of mass transfer limitations and ensuring that any other possible influencing parameters (cathode/anode ratio, limiting current) are constant is essential for optimisation of other PEC system parameters (energy demand, layer thickness).
- Electrical energy per order was proposed to assess the relative performance of the PEC system. Energy use of the same order of magnitude as reported in AOPs (Lam, et al., 2010), suggests that PEC is a promising technology.
- Required organic pollutant removal efficiency of the system is determined by the balance between reaction rate kinetics (retention time in the reactor) and energy consumption of the system.

## References

- Alinsafi, A., Khemis, M., Pons, M. N., Leclerc, J., Yaacoubi, A., Benhammou, A. & Nejmeddine, A., 2005. Electro-coagulation of reactive textile dyes and textile wastewater. *Chem. Eng. Process.*, Volume 44, pp. 461-470.
- Alkaim, A. F., Kandiel, T. A., Hussein, F. H., Dillert, R., Bahnemann, D. W., 2013. Enhancing the photocatalytic activity of TiO<sub>2</sub> by pH control: a case study for the degradation of EDTA. *Catal. Sci. Technol.*, Volume 3, pp. 3216-3222.
- Babu, V. J., Vempati, S. & Ramakrishna, S., 2014. Reduced recombination and enhanced UV-assisted photocatalysis by highly anisotropic titanates from electrospun TiO<sub>2</sub>-SiO<sub>2</sub> nanostructures. *R. Soc. Chem.*, Volume 4, pp. 27979-27987.
- Barka, N., Qourzal, S., Assabbane, A., Nounahb, A. & Ait-Ichou, Y., 2008. Factors influencing the photocatalytic degradation of Rhodamine B by TiO<sub>2</sub>-coated non-woven paper. *J. Photochem. Photobiol., A*, Volume 195, pp. 346-351.
- Bayarri, B., Gimenez, J., Curco, D. & Esplugas, S., 2005. Photocatalytic degradation of 2,4-dichlorophenol by TiO<sub>2</sub>/UV: kinetics, actinometries and models. *Catal. Today*, Volume 101, pp. 227-236.
- Beer, H., 1969. Improvements in or relating to electrodes for electrolysis. s.l. Patent No. GB1, 147, 442.
- Beltran, F. J., Rivas, F. J. & Gimeno, O., 2005. Comparison between photocatalytic ozonation and other oxidation processes for the removal of phenols from water. *J. Chem. Technol. Biotechnol.*, Volume 80, pp. 973-984.
- Bennani, Y., El-Kalliny, A. S., Appel, P. & Rietveld, L. C., 2014. Enhanced solar light photoelectrocatalytic activity in water by anatase-to-rutile TiO<sub>2</sub> transformation. *J. Adv. Oxid. Technol.*, Volume 17, pp. 286-296.
- Borji, S. H., Nasser, S., Mahvi, A. H., Nabizadeh, R. & Javadi, A. H., 2014. Investigation of photocatalytic degradation of phenol by Fe(III)-doped TiO<sub>2</sub> and TiO<sub>2</sub> nanoparticles. *J. Environ. Health Sci. Eng.*, Volume 12, pp. 101-111.

- Bubacz, K., Kusiak-Nejman, E., Tryba, B. & Morawski, A. W., 2013. Investigation of  $\cdot\text{OH}$  radicals formation on the surface of  $\text{TiO}_2/\text{N}$  photocatalyst at the presence of therephthalic acid solution. Estimation of optimal conditions. *J. Photochem. Photobiol., A*, Volume 261, pp. 7-11.
- Carneiro, P. A., Osugi, M. E., Fugivara, C. S., Boralle, N., Furlan, M., Zanoni, M. V. B., 2005. Evaluation of different electrochemical methods on the oxidation and degradation of reactive blue 4 in aqueous solution. *Chemosphere*, Volume 431-439, p. 59.
- Chu, W. & Ma, C. W., 2000. Quantitative prediction of direct and indirect dye ozonation kinetics. *Water Res.*, Volume 35, pp. 3153-3160.
- Crittenden, J. C., 2012. *MWH's water treatment principles and design*. Hoboken: John Wiley & Sons.
- Crittenden, J. C., Hu, S., Hand, D. W. & Green, S. A., 1999. A kinetic model for  $\text{H}_2\text{O}_2/\text{UV}$  process in a completely mixed batch reactor. *Water Res.*, Volume 33, pp. 2315-2328.
- Dai, K., Chen, H., Peng, T., Ke, D. & Yi, H., 2007. Photocatalytic degradation of methyl orange in aqueous suspension of mesoporous titania nanoparticles. *Chemosphere*, Volume 69, pp. 1361-1367.
- Devlin, H. R. & Harris, I. J., 1984. Mechanism of the oxidation of aqueous phenol with dissolved oxygen. *Ind. Eng. Chem. Fundam.*, Volume 23, pp. 387-392.
- Droste, R., 1997. *Theory and practice of water and wastewater treatment*. New York: John Wiley and Sons.
- Grega, M. S. L., Buckingham, P. L. & Evans, J. C., 1994. *Hazardous waste management*. New York: McGraw-Hill.
- Ishibashi, K., Fujishima, A., Watanabe, T. & Hashimoto, K., 2000. Detection of active oxidative species in  $\text{TiO}_2$  photocatalysis using the fluorescence technique. *Electrochem. Commun.*, Volume 2, pp. 207-210.
- Jeng, M. J., Wung, Y. L., Chang, L. B. & Chow, L., 2013. Particle size effects of  $\text{TiO}_2$  layers on the solar efficiency of dye-sensitized solar cells. *Int. J. Photoenergy*, Volume 563897, p. 9.

Jiao, X., Wang, X., Li, X., Chen, H., Wang, G., Li, J., & Lin, H., 2012. Electron transport in dye-sensitized solar cells based on TiO<sub>2</sub> nanowires. *Sci. China-Phys. Mech. Astron.*, Volume 57, pp. 892-897.

Khataee, A. R. & Kasiri, M. B., 2010. Photocatalytic degradation of organic dyes in the presence of nanostructured titanium dioxide: influence of the chemical structure of dyes. *J. Mol. Catal. A: Chem.*, Volume 328, pp. 8-26.

Kiliç, M., Koçtürk, G., San, N. & Çinar, Z., 2007. A model for prediction of product distributions for the reactions of phenol derivatives with hydroxyl radicals. *Chemosphere*, Volume 69, pp. 1396-1408.

Lam, S. M., Sin, J. C. & Mohamed, A. R., 2010. Parameter effect on photocatalytic degradation of phenol using TiO<sub>2</sub>-P25/activated carbon (AC). *Korean J. Chem. Eng.* Volume 27, pp. 1109-1116.

Li, S., Ye, G. & Chen, G., 2009. Low-temperature preparation and characterization of nanocrystalline anatase TiO<sub>2</sub>. *J. Phys. Chem. C*, Volume 113, pp. 4031-4037.

Long, R., English, N. J. & Prezhdoo, O. V., 2014. Minimizing electron-hole recombination on TiO<sub>2</sub> sensitized with PbSe quantum dots: time-domain Ab initio analysis. *J. Phys. Chem. Lett.*, Volume 5, pp. 2941-2946.

Martijn, B. J., Fuller, A. L., Malley, J. P. & Kruithof, J. C., 2010. Impact of IX-UF pretreatment on the feasibility of UV/H<sub>2</sub>O<sub>2</sub> treatment for degradation of NDMA and 1,4-Dioxane, *Ozone: Science, Engineering & The journal of the international ozone association*, Volume 32, pp. 383-390.

Matthews, R. W., 1991. Photooxidative degradation of coloured organics in water using supported catalysts TiO<sub>2</sub> on sand. *Water Res.*, Volume 25, pp. 1169-1176.

Mogyorosi, M., Farkas, A. & Dekany, I., 2002. TiO<sub>2</sub>-based photocatalytic degradation of 2-chlorophenol adsorbed on hydrophobic clay. *Environ. Sci. Technol.*, Volume 36, pp. 3618-3624.

Moon, B., Kwak, D. & Sung, Y., 2012. Optical and electrochemical characteristics of nanostructural TiO<sub>2</sub>/Ti/Glass electrode. *Int. J. Theor. Appl. Nanotechnol.*, Volume 1, pp. 1929-1248.

- Oliveira, H. G., Nery, D. C., Paschoalino, M. P., Jardim, W. F. & Longo, C., 2007. Photoelectrochemical and photocatalytic properties of nanocrystalline TiO<sub>2</sub> electrodes. *Solar hydrogen and nanotechnology II*, Volume 6650, pp. 277-786.
- Pablos, C., Marugán, J., Grieken, R. v. & Adán, C., 2014. Correlation between photoelectrochemical behaviour and photoelectrocatalytic activity and scaling-up of P25-TiO<sub>2</sub> electrodes. *Electrochim. Acta*, Volume 130, pp. 261-270.
- Pareek, V., Chong, S., Tadé, M. & Adesina, A. A., 2008. Light intensity distribution in heterogeneous photocatalytic reactors. *Asia-Pac. J. Chem. Eng.*, Volume 3, pp. 171-201.
- Parson, S., 2004. *Advanced oxidation processes for water and wastewater treatment*. London: IWA Publishing.
- Puma, G. L. & Yue, P. L., 2002. Effect of radiation wavelength on the rate of photocatalytic oxidation of organic pollutants. *Ind. Eng. Chem. Res.*, Volume 41, pp. 5594-5600.
- Santos, A., Barroso, E. & García-Ochoa, F., 1999. Overall rate of aqueous-phase catalytic oxidation of phenol: pH and catalyst loading influences. *Catal. Today*, Volume 48, pp. 109-117.
- Saranya, A., Pandiarajan, J., Jeyakumuran, N. & Prithivikumuran, N., 2014. Influence of annealing temperature and number of layers on the properties of nanocrystalline TiO<sub>2</sub> thin films: Structural and optical investigations. *Int. J. ChemTech Res.*, Volume 6, pp. 2237-2239.
- Sincero, A. P. & Sincero, G. A., 2003. *Physical-Chemical Treatment of water and wastewater*. New York: IWA Publishing.
- Sohrabi, M. R. & Ghavami, M., 2010. Comparison of direct yellow 12 dye degradation efficiency using UV/semiconductor and UV/H<sub>2</sub>O<sub>2</sub>/semiconductor systems. *Desalination*, Volume 252, pp. 157-162.
- Szpyrkowicz, L., Juzzolino, C. & Kaul, S. N., 2001. A comparative study on oxidation of disperse dyes by electrochemical process, ozone, hypochlorite and Fenton reagent. *Water Res.*, Volume 35, pp. 2129-2136.

Topudurti, K. V., Lewis, N. M. & Hirsh, S. R., 1993. The applicability of UV/oxidation technologies to treat contaminated groundwater. *Environ. Prog.*, Volume 12, pp. 54-60.

Vergöhl, M., Althues, H., Frach, P., Glöß, D., Graumann, T., Hübner, C., Neumann, F., Neubert, T., Schottner, G. & Song, D. K., 2011. Photocatalytic TiO<sub>2</sub> films deposited by different methods. Weinheim: Wiley-VCH Verlag GmbH & Co..

Wang, N., Li, X., Wang, Y., Quan, X. & Chen, G., 2009. Evaluation of bias potential enhanced photocatalytic degradation of 4-chlorophenol with TiO<sub>2</sub> nanotube fabricated by anodic oxidation method. *Chem. Eng. J.*, Volume 146, pp. 30-35.

Wang, W. Y., Yang, M. L. & Ku, Y., 2010. Photoelectrocatalytic decomposition of dye in aqueous solution using Nafion as an electrolyte. *Chem. Eng. J.*, Volume 165, pp. 273-280.

Xie, K., Sun, L., Wang, C., Lai, Y., Wang, M., Chen, H. & Lin, C., 2010. Photoelectrocatalytic properties of Ag nanoparticles loaded TiO<sub>2</sub> nanotube arrays prepared by pulse current deposition. *Electrochim. Acta*, Volume 55, pp. 7211-7218.

Yu, J. C., Lin, J. & Kwok, R. W. M., 1997. Enhanced photocatalytic activity of Ti<sub>1-x</sub>V<sub>x</sub>O<sub>2</sub> solid solution on the degradation of acetone. *J. Photochem. Photobiol., A*, Volume 111, pp. 199-203.

Yu, J. & Wang, B., 2010. Effect of calcination temperature on morphology and photoelectrochemical properties of anodized titanium dioxide nanotube arrays. *Appl. Catal., B*, Volume 94, pp. 295-302.

Zhang, W., Zou, L., Lewis, R. & Dionysio, D., 2014. A review of visible-light sensitive TiO<sub>2</sub> synthesis via sol-gel N-doping for the degradation of dissolved organic compounds in wastewater treatment. *J. Mater. Sci. Chem. Eng.*, Volume 2, pp. 28-40.

Zhang, Z., Anderson, W. A. & Moo-Young, M., 2004. Experimental analysis of a corrugated plate photocatalytic reactor. *Chem. Eng. J.*, Volume 99, pp. 145-152.





# 4

## PHOTOELECTROCATALYTIC DEGRADATION OF CHLOROFORM IN AQUEOUS SOLUTION USING A $\text{TiO}_2/\text{Ti}$ COMPOSITE MESH ELECTRODE

---

Photoelectrocatalysis provides a promising way to enhance the degradation of toxic chlorinated pollutants, such as chloroform, that are difficult to degrade and that are present in chlorinated drinking water. However, the development of an efficient electrode system for photoelectrocatalysis remains a challenge. A practical electrode configuration must combine the maximal capture of photons throughout the reactor, minimal mass-transfer limitations to and from the electrodes, and minimal electrode resistance between the anode and cathode. Even with an optimal configuration of plate electrodes, the overall resistance of the oxidation process is at the anode. It is, therefore, logical to focus this research on the configuration of the anode. A novel geometric arrangement of the electrodes with parallel mesh anodes exposed to the light source was, for the first time, used for the photoelectrocatalytic degradation of chloroform.

With an initial concentration of 500  $\mu\text{g/L}$  - the level of chloroform concentration normally found in chlorinated water, this electrode system reduced the chloroform concentration by 60% within about two hours, reaching the maximum acceptable concentration of chloroform in drinking water set by the World Health Organization (200  $\mu\text{g/L}$ ). Current distribution, light harvesting efficiency and photo-to-current efficiency were analysed to optimize the

electrode efficiency and the number of meshes. Experimental analysis showed that meshes could have up to six times the active surface area of a flat plate, enhancing the degradation kinetics up to two times. Further increase in surface area had no additional benefit.

#### **4.1. Introduction**

Halomethanes, in particular trihalomethanes (THMs), are frequently detected in both groundwater and surface water sources (WHO, 1996). They have half-lives of months or years, even in bodies of water exposed to the sun, and pose significant environmental concerns (Pavelic, et al., 2006; Agency, 1980; Agency, 1980). THMs can be released into the environment from direct processes, including water chlorination, or as a result of its formation from other substances (Bouwer & McCarty, 1983). Important anthropogenic chloroform sources are pulp and paper mills, water treatment plants, chemical manufacturing plants, and waste incinerators (McCulloch, 2003). Organic compounds such as fulvic and humic acids, if present, contribute to THM formation in chlorinated drinking water (Peters, et al., 1980). THMs are also produced by natural sources such as volcanic emissions and marine algae (Laternus, et al., 2002). A median concentration of total THMs in drinking water of 28 µg/L and concentrations as high as 500 µg/L have been reported, especially in countries where chlorine is used as a disinfectant (Symons, et al., 1975; WHO, 1996). The presence of these substances even in small amounts is a potential health risk and, consequently, they have been the subject of many studies over the years (Innocenzi, et al., 2008). Several routes have been developed to remove chloroform from drinking water:

- Reduce concentrations of humic acid and other organic precursors before chlorination.
- Use alternative disinfectants such as UV light or ozone (Glaze, 1986).
- Remove the THMs after the chlorination step.

Since chlorination of drinking water is predominantly preferred because it is a cost effective and efficient disinfection method, any method for the physical or chemical removal (or avoidance of formation) of THMs must be cost efficient as well.

In this study chloroform, which is the major constituent of THMs, has been chosen as a model contaminant for studying heterogeneous photo(electro)catalysis. The advantage of heterogeneous photocatalysis over homogeneous photocatalysis is that no chemical precursors are required. Chloroform has been reported to be completely mineralized using  $\text{TiO}_2$  suspensions with UV irradiation under specific laboratory conditions (Hsiao, et al., 1983; Pruden & Ollis, 1983; Kormann, et al., 1991; Murabayashi, et al., 1989; Choi & Hoffmann, 1996). While many advancements in photo(electro)catalytical performance have been made, developing a cost-effective, scalable design is the most critical challenge for the process to become commercialized. For example, the difficult separation of  $\text{TiO}_2$  powder and a low efficiency of immobilized  $\text{TiO}_2$  on a titanium plate limit the application of this approach. Compared to photocatalysis (PC), in photoelectrocatalysis (PEC) the electrons, generated at the catalyst/water interface, are drawn to the cathode under a positive bias potential. To complete the electrical circuit, these electrons generate dissolved ionic species at the cathode. This bias minimizes the recombination of electron-hole pairs, thus enhancing the degradation efficiency of the chosen pollutant (Liao, et al., 2012). However, the photo activity strongly depends on the material properties and configuration of the electrode as well as on the presence and absence of an applied potential. A new PEC system, studied and detailed in this paper, is based on a  $\text{TiO}_2/\text{Ti}$  composite mesh electrode. Compared to a plate electrode, a mesh configuration has a larger surface area, faster transport of electrons and reactants to and from the surfaces, and lower recombination rate, enabling it to potentially achieve higher PEC activity and efficiency (Zhao,

et al., 2014). Radicals formed on either plates or meshes have been assumed to be the dominant oxidizing agents in PEC systems, with a preference for attacking organic compounds adsorbed on or transported near to the  $\text{TiO}_2$  surfaces for quick quenching (Zhao, et al., 2014).

Since surface adsorption is important for interactions between the organic molecules and the photo-excited electrons or holes, differences in adsorption capacities could therefore affect PC and PEC degradation.

Thus, for the first time  $\text{TiO}_2/\text{Ti}$  composite mesh electrodes prepared by the paint-thermal decomposition were used for the removal of chloroform from an aqueous solution as a representative of THMs under the solar light, with a focus on the parameters that influence the PEC process. Power losses caused by non-homogeneous current distribution, a voltage drop in the bulk solution between the electrodes, and side reactions should be minimized by optimizing the electrode structure and cell design. Therefore, the performance of plate and mesh electrodes was analysed in terms of current efficiency, light absorbance, efficiency of adsorption, and degradation of chloroform. The electrode interface was also analysed by electrochemical impedance and discussed through double layer capacitance.

## **4.2. Material and methods**

### **4.2.1. Experimental approach**

$\text{TiO}_2$  film electrodes (plates and meshes) were manufactured and prepared by Magneto special anodes B.V. (Schiedam, the Netherlands), according to the paint-thermal decomposition method (Beer, 1969). Films obtained with this decomposition method were additionally modified by an annealing process. The mesh electrodes were characterized in terms of mesh number (number of lines of mesh per inch), with different wire diameters and pore sizes.

Electrochemical Impedance Spectroscopy (EIS) was used to study the impedance and capacitance of the TiO<sub>2</sub> electrodes in the dark and under UV illumination. The results of the EIS were examined with the photocurrent measurements along with P(E)C degradation of chloroform.

The combined results led to a better understanding of the effect of the adsorbed chloroform molecules on the electrode double layer capacitance and electron transfer between the TiO<sub>2</sub> electrode and the solution. In addition, kinetics for chloroform degradation were determined to investigate the possible scale-up to a plug flow reactor (PFR) system.

#### **4.2.2. Sampling and measurements**

PEC measurements were carried out with a set-up consisting of a cylindrical quartz glass reactor with an effective vessel volume of 300 mL and a three-electrode configuration. The TiO<sub>2</sub>/Ti composite photoanode, with different configurations, had a surface area of 0.0016 m<sup>2</sup> for a plate and 0.0024 m<sup>2</sup> for one mesh. The photoanode was placed on the stand incorporated in the reactor to receive solar light irradiation. The TiO<sub>2</sub> film supported on the Ti plate/mesh was used as the photocatalyst. X-ray diffraction (XRD) and scanning electron microscope (SEM) measurements can be found in a previous publication (Bennani, et al., 2014). A graphite plate was used as the cathode and an Ag/AgCl electrode was used as the reference electrode. The initial volume of the working solution was a 250 mL chloroform solution (containing 0.75 % ethanol as stabiliser) with an initial concentration of 500 ppb. Demineralized water (RiOs 5 Reverse Osmosis System) was used throughout the experiments for dilution. To eliminate the influence of solution resistance, 0.1 M Na<sub>2</sub>SO<sub>4</sub> was chosen as the supporting electrolyte. Nevertheless, potentially up-scaled systems would have to rely more on the optimal distance between electrodes other than the use of electrolytes. At

regular time intervals (i.e. every hour), 25 mL samples were collected from the reaction solution, added to an extraction flask and measured with gas chromatography (GC) to determine the residual concentration of chloroform. At the start of each experiment, the chloroform solution, was stirred in the dark for 15 hours with the TiO<sub>2</sub>/Ti composite electrode. This was sufficient for adsorption to reach equilibrium. The pH of the solution was kept constant at 7.2 and was measured before the experiment using a Sentix 81 pH meter. The cylindrical quartz glass reactor system was placed inside the chamber of an Atlas solar simulator type SUNTEST XXL+, consisting of three Xenon lamps emitting light in the solar spectrum (UV<sub>300-400</sub>). The absorption spectrum of the chloroform was measured with a UV/Vis spectrophotometer (Hach Lange DR5000).

The temperature was controlled at  $25 \pm 1$  °C by recirculating cooling water in a water bath equipped with a cooler (Julabo, FL300). During the experiments the reactor was closed by UV permeable quartz lids to prevent evaporation of the chloroform. The electrode potential and working current were controlled with a potentiostat-galvanostat system (Autolab PGSTAT128N with a BOOSTER10A). Software from the same producer (Nova Software) was used to run the electrochemistry routines, which included chronoamperometry (CA) and electrochemical impedance spectroscopy (EIS). Impedance is expressed as a complex number, where the reactance is the imaginary part and the resistance is the real part. The real part is plotted on the x-axis and the imaginary part is plotted on the y-axis (Bennani, et al., 2014; Bisquert, et al., 2014). Some characteristics of coatings, such as porosity, solution adsorption and/or film delamination, can be determined by EIS (Park, et al., 2001; Rabaey, et al., 2004). The EIS was conducted while maintaining a direct current voltage between the working electrode and the reference electrode. The adsorption of chloroform and degradation was also monitored by EIS.

The efficiency of a PEC process is largely dependent on the charge transfer between  $\text{TiO}_2$  and chloroform molecules and the level of electron-hole recombination of the used catalyst (Bisquert, et al., 2014).

Electrochemical impedance was used to analyse the electron transfer and recombination processes at photocatalyst/electrolyte interfaces (Park, et al., 2001; Rabaey, et al., 2004; Dumas, et al., 2008).

The measurements were taken at different time intervals. EIS was performed at a potential of 1 V versus Ag/AgCl, with a perturbation amplitude of 0.1 V and in the range of frequencies from 0.01 to  $10^5$  Hz. The values were measured during both dark and illuminated conditions.

To interpret the EIS data, the electrochemical system can be simplified to an equivalent electrical circuit model. This model represents the electrode behaviour as a combination of resistances (solution and polarization) and capacitances, which have a clear physical meaning, related to the response of the electrochemical system (Park, et al., 2001). In this work the simple equivalent circuit model was used, as presented in Figure 1. The circuit consists of a series resistor ( $R_s$ ) connected to a resistor ( $R_p$ ) and capacitor ( $C_p$ ) in parallel (Figure 4.1).

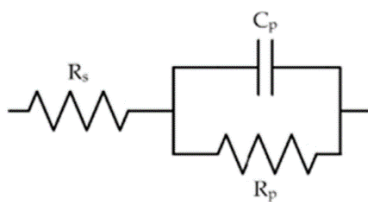


Figure 4.1. The equivalent circuit model representing the EIS response of the films (Park, et al., 2001)

The impedance is expressed in an Nquist plot graph (later shown in Figures 4.11 and 4.12). The left intersection with the x-axis is the electrolyte resistance and the diameter of the semicircle is the charge-transfer resistance.



The double-layer capacitance is equal to (Park, et al., 2001):

$$C_{dl} = \frac{1}{\omega \cdot R_{ct}} \quad (1)$$

where  $\omega=2\pi f$  is the angular frequency and  $f$  is the frequency at the top of the semicircle.

The chloroform photo degradation experiments were performed with constant potential and were done in triplicates. The optimal anode potential of 1 V versus the reference electrode was taken from a previous study, using the same TiO<sub>2</sub>/Ti composite electrodes (Bennani, et al., 2014). The dark current and photocurrent were recorded during the degradation experiments. The applied potential difference between the electrodes during each experiment was chosen sufficiently high so that the limiting current for the system was reached. The net current was calculated by subtracting the dark current from the photocurrent.

To evaluate the performance of the mesh-electrode system, incident photon-to-current-efficiency (IPCE) measurements were conducted. IPCE is a measure of the effectiveness of the conversion of photons incident on the anode to the photocurrent between anode and cathode. An anode bias of 1 V versus a normal hydrogen electrode reference electrode (NHE) was applied during the measurement of the IPCE values as a function of the wavelength. The IPCE spectra were measured in 500 ppb chloroform solution and 0.1 M Na<sub>2</sub>SO<sub>4</sub> as a supporting electrolyte and as regenerator, respectively. The IPCE was calculated from the photocurrent and the photon flux, using an Oriel Cornerstone 130 1/8M Monochromator supplied by an Oriel Apex Illuminator (Newport model numbers 74001 and 70612). The measurement range of the monochromator was between 300 and 1000 nm, obtained by 150 Watt Xenon arc lamp.

Diffuse transmittance and reflectance measurements, both for TiO<sub>2</sub> on the plate and mesh substrate and for the substrate without coating, were carried out with a UV/Vis/NIR spectrophotometer (Lambda 90, PerkinElmer) equipped with an integrating sphere, as presented in Figure 4.6.

The absorption spectrum of the chloroform solution was measured in the Hach Lange DR 5000 spectrophotometer and it is shown in Figure 4.5.

#### **4.2.3. Analytical methods**

Following method 551 used by the EPA (Environmental Protection Agency) to determine the chloroform concentration, the chloroform concentration was analysed using micro liquid-liquid extraction (Hodgeson & Cohen, 1990). Twenty-five mL of the sample were added to 5 g of sodium chloride (used to promote phase separation) already present in the extraction flask equipped with a polytetrafluoroethylene (PTFE)-faced silicone septum. Samples were taken every 2 h; 5 mL of methyltertbutylether (MTBE) was added to the extraction flasks and the solution was shaken vigorously for 2 min. After allowing the solution to settle for 2 min, 1 mL of the organic phase was added to a GC vial using a pipette. For actual analysis of the chloroform concentration the Agilent Technologies 7890A GC system equipped with an electron capture detector (ECD) was used.

Specific surface area of TiO<sub>2</sub>/Ti composite plate sample

Brunauer, Emmett and Teller (BET) is the most common method used to describe specific surface area (Figueiredo, et al., 2008). An adsorption isotherm is obtained by measuring the amount of gas adsorbed across a wide range of relative pressures at a constant temperature. This can be plotted as relative pressure ( $P/P_o$ ) vs. adsorbed volume ( $V_{ads}$ ), ccg<sup>-1</sup>.

At least three measurements of  $V_{ads}$  each at different values of  $P/P_o$  are required for the determination of specific surface area by volumetric gas adsorption. Further on, for the calculations of specific surface area, a linearized form of the presented BET equation was used (Figueiredo, et al., 2008):

$$\frac{V_{ads}}{V_m} = \frac{C(P/P_o)}{(1-P/P_o)(1-P/P_o+C(P/P_o))} \quad (2)$$

where  $(C - 1)/VmC$  is slope and  $1/VmC$  intercept. Specific surface area ( $m^2/g$ ) is equal to  $S = \frac{V_m Na}{m \cdot 22400}$ , where  $V_m$  is volume of gas adsorbed at STP to produce the apparent monolayer on the surface mL,  $N$  is Avogadro constant,  $a$  effective cross-sectional area of one adsorbate molecule ( $m^2$ ) and  $m$  mass (g) of the tested powder. For a sample with a low specific surface area, the use of krypton (Kr) or argon rather than nitrogen improves the accuracy of the measurements (Lowell, et al., 2004).

Kr adsorption measurements were made on  $TiO_2/Ti$  plate samples (Delft Solids Solutions B.V.) in order to measure the available specific surface area of the  $TiO_2/Ti$  composite sample by determining the adsorption isotherm at 77 K on a Quantachrome Autosorb 1C analyzer. Prior to the adsorption measurements, the samples were degassed in a vacuum for 16 h at 300°C. The dry sample weight obtained after the pre-treatment was used in the calculations.

The extent of the surface coverage with adsorbed molecules is expressed as<sup>28</sup>:

$$\theta = (\#sites\ occupied)/(\#sites\ available)$$

In order to obtain the efficiency of the electrode surface coverage with chloroform molecules and determine the layer formation, the following approach was followed.

The area occupied by the molecules can be calculated by using the equation  $\sigma = 1.091 \left( \frac{M_r}{\rho_L N_A} \right)^{2/3}$ , where  $\sigma$  is the area occupied by one molecule of chloroform,  $M_r$  is the molecular weight of chloroform (g/mol),  $\rho_L$  is the density of the chloroform (g/m<sup>3</sup>),  $N_A$  is the Avogadro constant (6.023·10<sup>23</sup> molecules/mol) and 1.091 is the coefficient ascribed to a spherical shape and the hexagonal close packing of molecules (Aligizaki, 2006).

The homogeneity of the coating layer was investigated by the optical stereo microscope “Stereo-Discovery V8” from Carl Zeiss, shown in Figure 4.2 a).

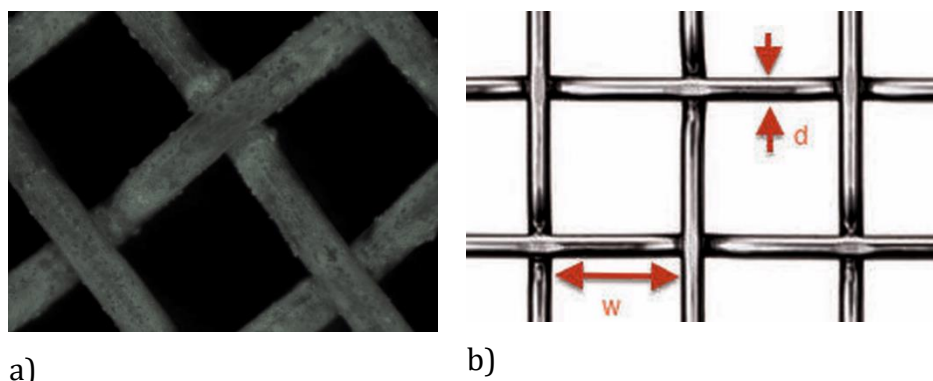


Figure 4.2. a) Microscope image of coated Ti mesh with TiO<sub>2</sub> at high magnification (400 μm); b) schematic plan view of a woven wire mesh, d – diameter; W – aperture width

### 4.3. Results

The results obtained from Kr adsorption on the plate sample are shown in Figure 3 and described below.

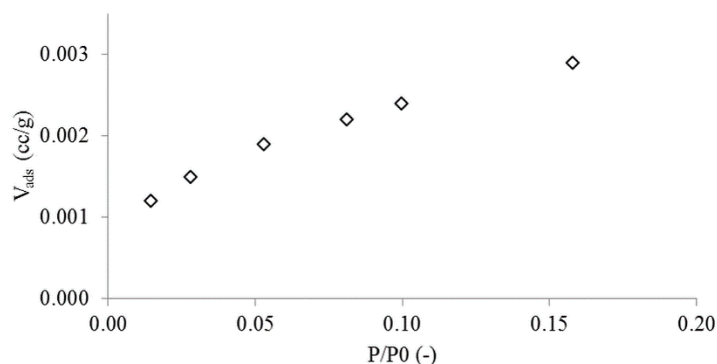


Figure 4.3. Kr adsorption isotherm (adsorbed volume vs. relative pressure at 77 K over  $\text{TiO}_2/\text{Ti}$  plate sample

From Figure 4.3 it can be seen that the  $\text{TiO}_2$  sample exhibits an uptake (volume of Kr adsorbed per g of  $\text{TiO}_2$  at standard temperature and pressure) over the whole investigated relative pressure range ( $P/P_0$ ). The BET surface area of the  $\text{TiO}_2$  film deposited at the plate substrate, determined by Kr adsorption experiments, was  $0.015 \text{ m}^2/\text{g}$ .

The area occupied by one molecule of chloroform was calculated to be  $2.84 \cdot 10^{-19} \text{ m}^2$  and the total surface areas of the  $\text{TiO}_2$  are  $3.12 \cdot 10^{-5} \text{ m}^2$  for the plate and  $1.84 \cdot 10^{-4} \text{ m}^2$  for the 4 – mesh electrode.

Figure 4 shows the adsorption percentage for chloroform versus adsorption time in the dark on the surface of  $\text{TiO}_2$ .

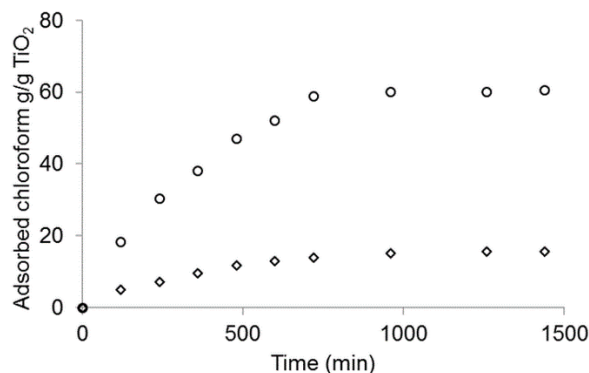


Figure 4.4. Adsorption of chloroform (g chloroform/g TiO<sub>2</sub>) in dark by plate (o) and 4-mesh (◇) TiO<sub>2</sub>/Ti composite electrode configuration in the presence of the 0.1 M Na<sub>2</sub>SO<sub>4</sub> electrolyte

From Figure 4.4, it can be seen that adsorption reached equilibrium after about 10 hours and the plate adsorbed more chloroform per g TiO<sub>2</sub> than the mesh electrode.

The UV absorption spectra for chloroform, as seen in Figure 4.5, shows the highest absorbance between 200-300 nm, a lower region than for TiO<sub>2</sub>, which has highest absorbance at around 330 nm (Figure 4.6), assuming that the light absorption of the solution did not have an influence on the light absorption of TiO<sub>2</sub> and consequently on the reactions on the TiO<sub>2</sub> surface (Bennani, et al., 2014).

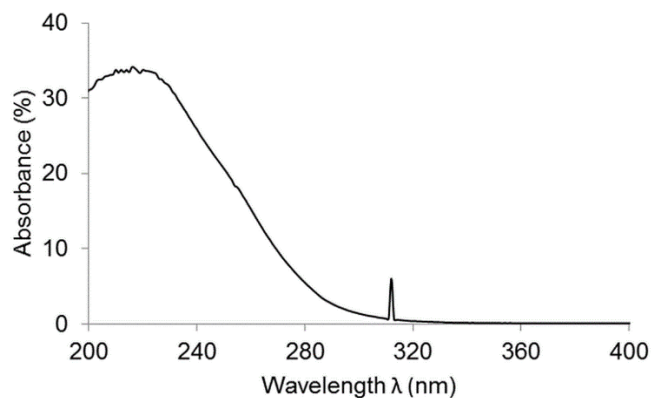


Figure 4.5. UV light absorbance of chloroform

The influence of the mesh configuration on the PEC degradation of chloroform was examined by varying the number of meshes and, consequently, varying the amount of adsorbed chloroform (g) per g of deposited  $\text{TiO}_2$  and current densities (Table 4.1). In this analysis, the values of the current densities for different surface areas increased with an increasing surface area.

The light absorption by mesh and plate electrodes and corresponding IPCE spectra are shown in Figures 4.6 and 4.7.

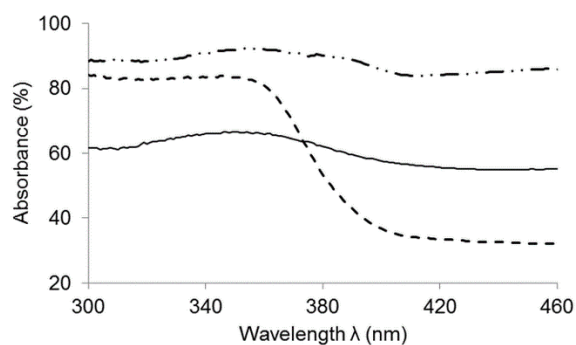


Figure 4.6. Light absorbance spectra of pure Ti substrate (—line) and of  $\text{TiO}_2$  films: on a plate (---line); on mesh (—•— line)

The magnitude of the IPCE spectrum depends on how much light is absorbed by the  $\text{TiO}_2$  (shown in Figure 4.7) and what percentage of the absorbed photons is converted into electrons. In Figures 4.6 and 4.7, the spectra are seen to be slightly different in shape, although the same electrodes were used. Figure 7 also shows that the  $\text{TiO}_2$  film coated on the Ti plate achieved efficient sensitivity over the whole measured range (300-460 nm), yielding an IPCE of about 4 %, while an IPCE of 7 % was achieved with the mesh configuration in the PEC system.

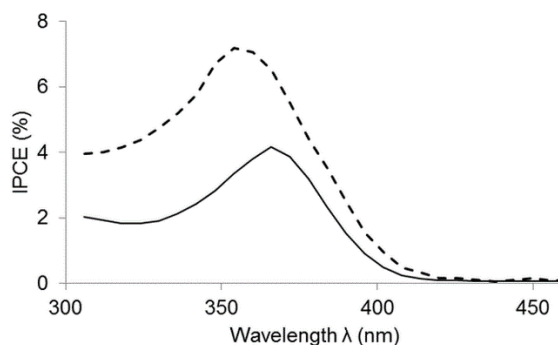


Figure 4.7. The IPCE spectra for  $\text{TiO}_2/\text{Ti}$  composite electrodes, with different sample configurations, plate (—line) and mesh (--- line)

Figure 4.8 shows the degradation kinetics of chloroform by PEC, using different numbers of meshes. The error bars were obtained from three replicate measurements. From Figure 4.9 it can be seen that, even though the total amount of adsorbed chloroform increased with the fifth mesh, the reaction rate constant  $k$  had roughly the same value as did the fourth and third mesh.



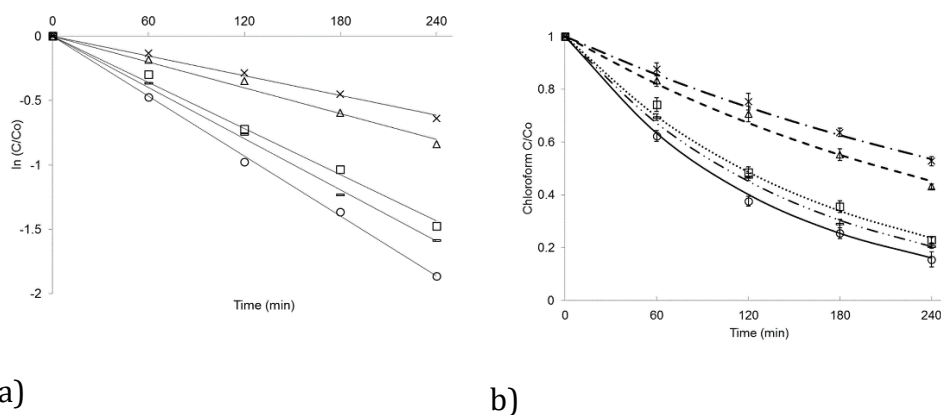


Figure 4.8. PEC degradation of chloroform with a  $\text{TiO}_2/\text{Ti}$  composite mesh electrode configuration by applying different numbers of meshes; a) single mesh (x), 2 meshes ( $\Delta$ ), 3 meshes ( $\square$ ), 4 meshes (o), and 5 meshes (—); b) (—•— line) 1<sup>st</sup> order kinetics of PEC using 1 mesh, (— — line) 1<sup>st</sup> order kinetics of PEC using 2 meshes, (round dot line) 1<sup>st</sup> order kinetics of PEC using 3 meshes, (—•— line) 1<sup>st</sup> order kinetics of PEC using 4 meshes, (—•— line) 1<sup>st</sup> order kinetics of PEC using 5 meshes. The error bars were obtained from three replicate measurements.

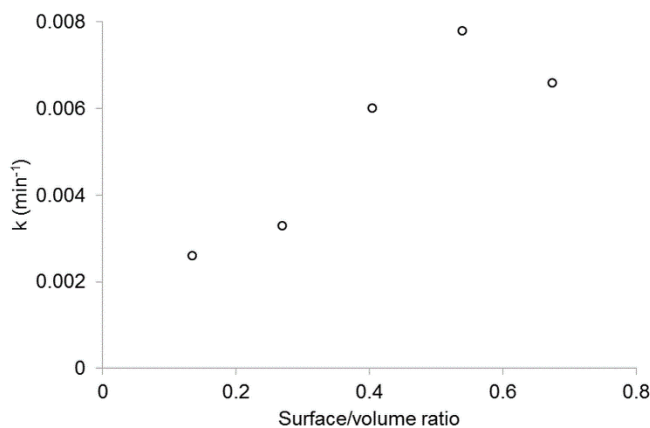


Figure 4.9. Effect of surface area/volume ratio on the constant rate of the reaction  $k$  ( $\text{min}^{-1}$ )

Even though the reaction rate constant with higher numbers of meshes remained at similar values, the current density had higher values. It can be noted from Table 4.1 that increasing the current density above 0.0108 mA/cm<sup>2</sup> did not show improvement in the percentage of chloroform removal.

Table 4.1. Dependence of TiO<sub>2</sub>/Ti composite electrode properties on the number of meshes used.

Number of meshes	Calculated specific surface area cm <sup>2</sup>	Chloroform adsorbed % after 10 h	Current density j mA/cm <sup>2</sup>
1	23.6	23.2	0.0109
2	47.2	42.2	0.0108
3	70.8	73.0	0.0115
4	94.4	88.2	0.0137
5	118.0	85.6	0.0157

Knowing the optimal number of meshes for the electrode used, the P(E)C activities of the different configurations (plate and 4 - mesh) and settings (PC and PEC) were evaluated by comparing the first order reaction rate constants ( $k$ ) and efficiency to convert incident photons at a given wavelength into extracted electrons.

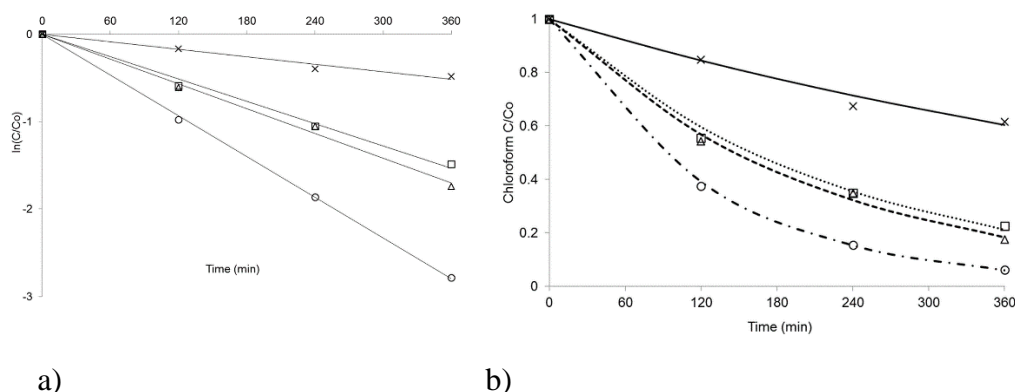


Figure 4.10. Degradation of chloroform under UV<sub>300-400</sub>, with different TiO<sub>2</sub>/Ti composite electrode configurations and under different conditions: a) PC plate electrode (x); PEC at 1 V, plate electrode ( $\square$ ), PC 4 - mesh electrode ( $\Delta$ ), and PEC at 1 V with 4 - mesh electrode (o); b) (— line) 1<sup>st</sup> order kinetics of PC plate electrode, (•• line) 1<sup>st</sup> order kinetics of PEC plate electrode; (— line) 1<sup>st</sup> order kinetics PC 4 - mesh electrode and (—• line) 1<sup>st</sup> order kinetics of PEC 4 - mesh electrode

The rate constants  $k$  for chloroform degradation were calculated through the linear relationship between  $\ln([CHCl_3]/[CHCl_3]_0)$  and time (Figures 4.9 and 4.10). This relationship showed first-order kinetics for the PC and PEC processes as it yielded straight lines up to 6 hours of exposure time. Direct comparison of the rate constants between the TiO<sub>2</sub>/Ti composite electrode configurations, presented in Figure 4.10, showed that PEC performed considerably better than PC and that the mesh configuration was more efficient than the plate configuration.

The rate constant exhibited a maximum of  $0.0078 \text{ min}^{-1}$  when using the 4-mesh configuration in PEC, a value that is 1.7 times higher than that of the plate configuration under the same conditions.

The mesh electrode with a greater surface area (94.4 cm<sup>2</sup>) achieved 50 % conversion within about 1.5 h, whereas the plate electrode with a low surface area only reached 33 % conversion (Figure 4.10).

Table 4.2. Comparison of process characteristics for plate vs 4-mesh TiO<sub>2</sub>/Ti composite electrode configurations

Treatment method	Electrode configuration	Rate constant $k \text{ min}^{-1}$	Calculated specific surface area cm <sup>2</sup>	Chloroform adsorbed %	Current density mA/cm <sup>2</sup>
PC	plate	0.0014	16.0	60.1	0
PC	4 - mesh	0.0043	94.4	72.3	0
PEC	plate	0.0047	16.0	68.4	0.0693
PEC	4 - mesh	0.0078	94.4	88.2	0.0109

In order to characterize the interfacial reaction between the photocatalyst and chloroform and analyse the adsorption characteristics, EIS was performed under irradiation. The data are presented as Nyquist plots (Figures 4.11 and 4.12) which, in turn, were used to calculate the corresponding values in the components in the model (Figure 4.1) used for describing electrode behaviour. These values are listed in Table 4.3.

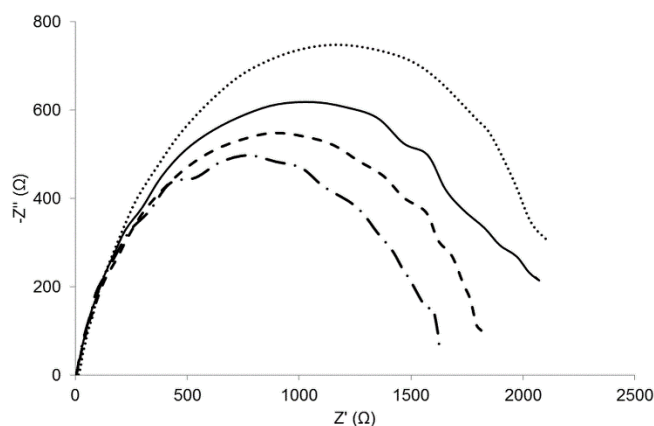


Figure 4.11. Nyquist plots for plate after adsorption and during PEC removal of chloroform at 1V for  $\text{TiO}_2/\text{Ti}$  composite plate electrode configuration; after adsorption equilibrium was reached ( $\bullet\bullet$  line), clean plate (—line), after 2 h of degradation (— line) and after 4 h of degradation (—•— line)

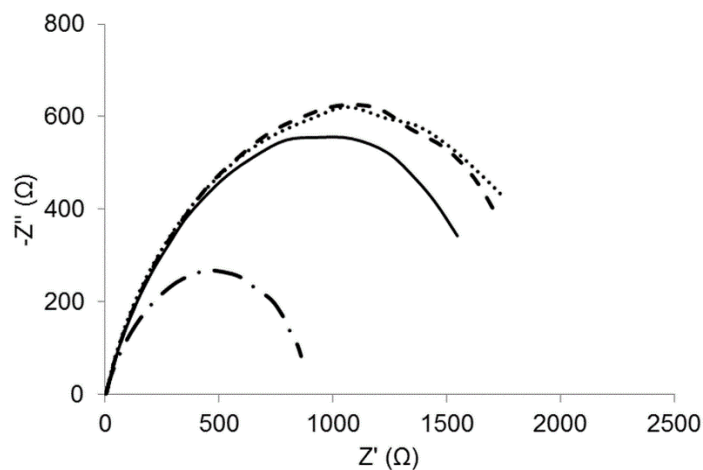


Figure 4.12. Nyquist plots for plate after adsorption and during PEC removal of chloroform at 1 V for  $\text{TiO}_2/\text{Ti}$  composite 4 - mesh electrode configuration, after adsorption equilibrium was reached ( $\bullet\bullet$  line), clean mesh (—line), after 2 h of degradation (— line) and after 4 h of degradation (—•— line)

Table 4.3. Results of EIS spectra (Figure 4.11 and 4.12) for TiO<sub>2</sub>/ Ti plate and 4 – mesh configuration

Process	Electrode configuration	Charge transfer resistance $R_{ct}/\Omega$	Double layer capacitance $C_{dl}/\text{mF}$
Before adsorption	Plate	2055.5	0.4865
	4 – mesh	1547.4	0.6463
Adsorption	Plate	2124.9	0.4706
	4 – mesh	1751.4	0.5710
2 h degradation	Plate	1812.6	0.5516
	4 – mesh	1727.1	0.5790
4 h degradation	Plate	1624.9	0.6154
	4 – mesh	862.17	1.1600

The real axis value at the low frequency intercept (the intercept furthest from the origin) represents the sum of the polarization resistance (charge transfer resistance) and the solution resistance. The semicircle's diameter is then equal to the polarization resistance. Referring to Figures 4.11 and 4.12 (see the real axis value at the high frequency intercept, the intercept near the origin of the plot), it can be seen that the conductivity of the solution was high enough for the solution resistance during the experiments to be considered negligible. As a consequence, for all experiments it can be assumed that the potential drop between the cathode and anode can be determined by both the surface and concentration over potentials at the anode only, as intended. The calculated charge transfer resistances, capacitance and current densities are shown in the Table 4.3.

The initial radius of the semicircles for both mesh and plate electrodes before adsorption were much smaller than that measured after adsorption. The lowest resistance was obtained for the 4-mesh configuration after four hours of degradation.

#### **4.4. Discussion**

As mentioned in the introduction, numerous studies have demonstrated that PEC achieves higher efficiency than PC. However, it was found that the conversion of photons to generated electrons when using a  $\text{TiO}_2$  plate electrode was not very efficient, due to the low available surface area. A  $\text{TiO}_2/\text{Ti}$  mesh photoelectrode was used in order to increase the photocatalytic activity. This electrode had a large surface area and its surface structure was able to provide a higher adsorption of chloroform. The study was tailored to determine the photo-oxidation efficiency of this  $\text{TiO}_2/\text{Ti}$  mesh photoelectrode for the degradation of chloroform at different reaction conditions. The adsorption-degradation effect was studied in terms of the influence of the surface and geometry of the electrodes as well as the effect of light in the process with different electrodes. The scope was to describe the effects of the main geometrical and operating parameters in order to optimise the conditions for a full-scale process.

##### **4.4.1. Adsorption-degradation synergistic effect of removal chloroform**

Specific surface area measurements of the  $\text{TiO}_2$  films deposited, both on the plate and mesh Ti substrate using Kr as an adsorbate, showed the available specific surface area of the samples, seen calculated in Section 3, to be quite

small compared to the BET surface area found in the literature (Raj & Viswanathan, 2009; Liu, et al., 2012).

The reason is the low fraction of small pores, as these are known to substantially enhance the specific surface area (Liu, et al., 2012; Bennani, et al., 2015). The low specific surface area could be explained by pores becoming less accessible, because the annealing process at high temperatures leads to a reduction in the BET surface, pore volume and pore size (Behnajady, et al., 2013; Bartholomew & Farrauto, 2006). Since the TiO<sub>2</sub> film with the same properties was deposited at the mesh and plate surfaces, the adsorption capacity of the chloroform increased due to a higher available surface area of the mesh (Figure 4.4). Furthermore, it was calculated that, if the surface were fully occupied by adsorbed chloroform molecules, the TiO<sub>2</sub> surface of the plate electrode and the 4-mesh electrode could theoretically be covered by approximately  $1.097 \cdot 10^{14}$  and  $6.47 \cdot 10^{14}$  chloroform molecules, respectively. However, using Figure 4.4 it was calculated that the number of adsorbed molecules for the plate and meshes was  $2.12 \cdot 10^{18}$  and  $2.96 \cdot 10^{18}$  respectively. Hence, the area occupied by adsorbed molecules is greater than available, as measured by Krypton adsorption. This can be explained by Brunauer's model of multi-layer adsorption (Figueiredo, et al., 2008). For an efficient catalyst, the adsorption sites must be both numerous and available to the reactant molecules. Adsorption sites located only at the surface are insufficient to ensure optimum performance. However, potential adsorption sites located deeper within a micropore that is too narrow for the molecule to enter or for the reaction product to exit cannot be an active participant in adsorption and reaction processes (Xue, et al., 2011).



#### 4.4.2. Degradation of the chloroform in the aqueous solution

Higher overall adsorption, due to a higher available surface area, led to a higher constant degradation rate for the chloroform  $k$  (Figure 4.9 and Table 4.2).

This observation confirmed the synergy between adsorption and photo-degradation which was previously studied by Gang Xue et al. on the TiO<sub>2</sub>/activated carbon composites (Krivec, et al., 2014).

However, from Figure 4.4 it can also be observed that at the mesh electrode surface less chloroform (g) was adsorbed relative to the total grams of TiO<sub>2</sub> deposited on the mesh surface. This observation might be explained by the lower adsorption rate due to the low driving force and reduced accessible surface area. Due to the higher surface area of the mesh, a higher adsorption rate was possible. The higher adsorption rate led to a lower concentration in the bulk of the solution and thus a lower concentration gradient. Furthermore, fewer molecules of neutral chloroform in the solution were present; also present were more ions from the applied electrolyte (Wang & Wang, 2002). This could have led to an increased number of ions at the surface of the electrode, thereby blocking the available sites for the adsorption of the wanted pollutant. This is further confirmed by Figures 4.11 and 4.12 and Table 4.3, where it is shown that double layer capacitance after adsorption for the mesh is higher (0.6463 mF) than for the plate electrode (0.4865 mF). The initial radius of the semicircles for both mesh and plate electrodes before adsorption were much smaller than that measured after adsorption. This net decrease in capacitance agrees with Wang et al. and Contu et al. who observed a decrease in capacitance when Ti electrodes were immersed in a solution of simulated body fluid and fetal bovine serum (Wang & Wang, 2002; Contu, et al., 2002; Bakar, et al., 2010). The decrease in capacitance (Figures 11 and 12) has been

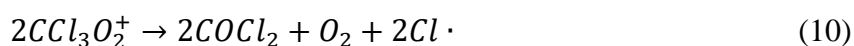
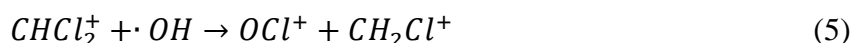
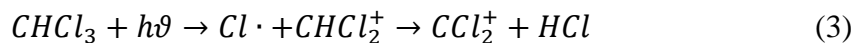
attributed to the adsorption of neutral molecules of chloroform on the surface of TiO<sub>2</sub>. The extent of the capacitance decrease agrees with the amount of adsorbed chloroform; the greater the adsorbed amount, the greater the capacitance decrease. It is assumed that the adsorption process involves the displacement of adsorbed ions from the surface which causes a decrease in the double layer capacitance.

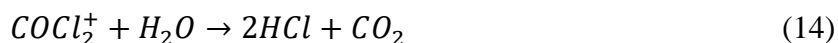
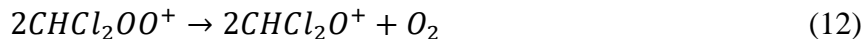
The lowest resistance was obtained for the 4-mesh configuration after four hours of degradation. This observation can be explained by the high adsorption (low initial concentration at beginning of the degradation step) and consequent degradation.

The low concentration of the chloroform in the solution after adsorption and thus the low amount of chloroform at the surface led to more available ions and their readsorption on the surface electrode as a double layer.

Resistance in both cases decreased with increased degradation time. Due to the high adsorption in the system with mesh electrodes, even after 2 hours of the PEC process, neutral molecules of chloroform blocked electrode sites and capacitance remained low. The TiO<sub>2</sub>/Ti composite electrode with four meshes was found to be the most effective in chloroform degradation.

Furthermore, a possible reaction pathway for the photo(electro)catalytic degradation of chloroform is as follows (Lin, et al., 2012):





The optimal number of meshes was selected by selecting the highest constant degradation rate of chloroform and the highest current density.

A decrease in the first-order reaction constant rate of the degradation with an increase in the number of meshes above four meshes (Figure 4.9) could be due to the poor activation of the last mesh by light (low light intensity), leading to a low number of photo-generated electron/holes. This result is also reflected in the produced photocurrent shown in Table 1. Increasing the current density above 0.0108 mA/cm<sup>2</sup> did not show improvement in the percentage of chloroform removal. This could be because of unwanted side reactions (oxygen evolution through water oxidation) occurring as the pollutant concentration decreases, as well as by a higher contribution of side reactions on meshes that receive less light (El-Kalliny, et al., 2014).

Additionally, in PEC processes, the photocurrent also depends on the concentration of negatively charged ions in the solution. Sulphate (SO<sub>4</sub><sup>2-</sup>) anions can be adsorbed on the positively charged photoanode surface in the PEC process. Under illumination and at lower chloroform concentrations, these species react with photo-generated holes and electrons, yielding sulphate radicals. These reactions also decrease the recombination of the electron-hole pairs. As a result, the photocurrent increases accordingly, as observed in Table 1 (Xue, et al., 2011). This observation was confirmed by El-Kalliny et al. who showed that for efficient light capture three to four meshes were sufficient to absorb 96 % of irradiated solar light (El-Kalliny, et al., 2014).

In addition, the effect of charge recombination was excluded by application of the positive potential bias. In a PEC system with the plate anode, the first-order reaction constant of  $0.0043 \text{ min}^{-1}$  shown in Figure 4.10 and Table 4.2 was not too different from the value of the reaction rate for the four-mesh in PC, even when the bias was applied. However, the applied bias had a higher influence on the reaction rate constant when using a plate over a mesh electrode (Table 4.2 and Figure 4.10).

This observation could be due to the high adsorption of the mesh electrode leading to the low initial concentration.

The initial concentration, after adsorption and at the beginning of the reaction for the mesh electrode, was lower than for the plate electrode, affecting the mass transfer of chloroform in the system and consequently the rate of the reaction. For the removal of the chloroform for mesh and plate in a PC system, electron transfer to the cathode was considered the limiting process; in the PEC mass transfer limitation was considered a critical factor for the reaction rate enhancement. Moreover, interstitial fissures between the mesh wires allowed chloroform molecules to access the photocatalyst surface more easily, which could have additionally contributed to the total photo(electro)catalytic removal of chloroform (Figure 4.10).

For the possible geometry of a reactor, the kinetics of the chemical reactions being carried out are of particular importance. Experiments in the batch reactor were carried out under well-controlled conditions in order to obtain the experimental data required for predicting reactor performance. This assembly could be further likened to a plug-flow reactor (PFR). In a catalytic reaction, the reaction during some resident time in a PFR is assumed to be equal to that during a specified reaction time in a batch system. In addition to the reactor type, the irradiated area is also an important factor influencing photocatalytic activity.

Accordingly, to convert batch data to flow data, it is necessary to correct the differences in the irradiated area and the length of the reactor between these two systems. In order to prevent the products diffusing back and little or no back mixing, a flow pattern could be created with mesh structure being used as the electrodes in the PEC system.

#### **4.4.3. Electrical impedance and double layer charge**

The electrode impedance brings insight in the electrical double layer that exists at the interface between the electrode and the surrounding electrolyte.

This double layer is formed if either positively or negatively charged species from the solution preferentially adsorb onto the electrode surface. This charge is then counterbalanced by the diffuse part of the double layer by species with an opposite charge, driven towards the electrode surface by the potential gradient near its surface. In the impedance measurements, this is represented in the model by the double layer capacitor. From the Figures 4.11 and 4.12 and Table 4.3, it can be seen that the high adsorption of chloroform, non-charged species on the surface of the electrode decreased the double – layer capacitance. A decrease in capacitance corresponds to an increase in impedance, resulting in a reduction of the current. However, it was found that the charge-transfer resistance  $R_{ct}$  of the plate after adsorption decreased with time, diminishing the adsorbed amount of chloroform. Further, concentration changes in the solution reduced the driving force of the chloroform molecules to the surface of the catalyst. This led to a decrease in the chloroform degradation efficiency (Figure 4.9), making it the rate-determining step of the degradation process. On the other hand, impedance of the  $\text{TiO}_2/\text{Ti}$  four mesh electrode configuration even after two hours of PEC degradation remained the same, as a result of a higher adsorption capacity. Availability of the chloroform

molecules at the interface of the catalyst seemed to be of high importance for the further removal. Moreover, higher surface area allowed more charge to pass by and thus reduced impedance to lower values than that of the plate configuration after four hours of degradation (Figure 4.12). Additionally, electrons prefer to travel along edges rather than flat surfaces (Butson & McIntyre, 2005; Wei & Grill, 2005).

Thus, this could have significantly reduced the probability of charge recombination and increased the process efficiency as seen in the Figure 9.

#### **4.4.4. Influence of surface area on incident to photon current efficiency**

For the four meshes (as four is proven to be the optimum number of meshes for degradation), light absorbance and harvesting of the light by the meshes and their effect on produced photocurrent and efficiency of the degradation process were investigated. The light absorbance (Figure 4.6) and expected enhanced light scattering were more efficient using the TiO<sub>2</sub> films coated on the mesh rather than on the plate. Unlike the planar Ti plate, the loss of photons at the mesh electrode was minimized since the coated films on the meshes could absorb reflected and/or refracted light, which resulted in a higher IPCE. The low IPCE values in the semiconductor photoanode can be attributed to reflection losses, improper absorption of the incident photons and recombination of the charge carriers within the bulk (Lu & Pichat, 2013). Reviewing Figures 4.6 and 4.7, the spectra can be seen as slightly different in shape, although the same electrodes were used. This difference can be explained by water absorption. Between 300 and 500 nm, water absorbs strongly causing a filtering effect at these wavelengths for the electrode and, therefore, decreasing the IPCE (Tilley, et al., 2010). Observations from the absorbance spectrum of the electrodes, and the subsequent IPCE spectra, led to the conclusion that the light consumption/scattering and photon

conversion to the electron and holes is a process enhancing factor, and not the limiting one.

#### **4.5. Conclusions**

We have successfully developed a TiO<sub>2</sub>/Ti mesh photoelectrode by paint-thermal deposition. Compared with the TiO<sub>2</sub>/Ti plate electrode, the mesh electrode possesses a greater surface area with high efficiency in degrading chloroform.

- TiO<sub>2</sub> coating on the four-mesh configuration yielded a 1.7 times faster constant removal rate of chloroform than plate configuration in PEC; 5.6 times faster constant rate than than plate configuration in PC.
- The mesh electrode with the higher surface area (94.4 cm<sup>2</sup>) achieved 50 % conversion within 1.5 h, whereas the plate electrode, with a low surface area only reached 33 % conversion
- By introducing a four-mesh configuration into the PEC system, an IPCE of 7 % was achieved, meaning more electrons were produced by incident photons than by the plate electrode at the same number of incident photons.
- Adsorption of chloroform caused a decrease in double-layer capacitance, as demonstrated by an increased impedance and fouling of the electrode. Despite this effect, PEC enhanced overall degradation.
- Correlation between EIS and photo-degradation indicated that the adsorption and surface concentration of molecules on the catalyst were the limiting factor for the degradation of chloroform.

## Appendix A

The meshes that were used in the experiment were cut 4x4 cm<sup>2</sup>. To calculate the specific surface area of these meshes the following known properties were used (see figure 2 b)):

- Wire diameter  $d = 0.118 \text{ inch} = 0.02997 \text{ cm}$
- Open surface area  $A_o = 58 \%$

The aperture width was calculated with the following equation (Zhao, et al., 2013; Selcuk, et al., 2003):

$$A_o = \frac{w^2}{(w+d)^2} \cdot 100 \% \quad (\text{A.1})$$

$$w = 0.09573 \text{ cm}$$

The mesh number is the number of openings in 2.54 cm:

$$N_r = \frac{2.54}{w+d} = 20 \quad (\text{A.2})$$

The mesh size ( $n$ ) is the number of openings in 4 cm:

$$n = \frac{20}{2.54} \cdot 4 = 32 \quad (\text{A.3})$$

The total specific surface area of one mesh was calculated to be:

$$S = \pi d w \cdot 2n(n+1) + \frac{3}{2} \pi d^2 + (n+1)^2 = 23.6 \text{ cm}^2 \quad (\text{A.4})$$



## References

- Agency, E. P., 1980. Ambient Water Quality Criteria for Chloroform, Washington: EPA Document 440/5-80-033.
- Agency, E. P., 1980. Ambient Water Quality Criteria for Halomethanes, Washington: EPA Document 440/5-80-051.
- Aligizaki, K. K., 2006. Pore structure of cement-based materials. Testing, interpretation and requirements. Oxon: Taylor&Francis.
- Bakar, W. A., Ali, R. & Othman, M., 2010. Manganeses oxide doped noble metals supported catalyst for carbon dioxide methanation reaction. Chemistry and Chem. Eng., Volume 17, pp. 1-14.
- Bartholomew, C. H. & Farrauto, R. J., 2006. Fundamentals of industrial catalytic processes. New Jersey: John Wiley and Sons.
- Beer, H., 1969. Improvements in or relating to electrodes for electrolysis. s.l. Patent No. GB1, 147, 442.
- Behnajady, M. A., Alamdari, M. E. & Modirshahla, N., 2013. Investigation of the effect of heta treatment process on characteristics and photocatalytic activity of TiO<sub>2</sub>-UV100 nanoparticles. Environ. Prot. Eng., Volume 39, p. 33.
- Bennani, Y., Appel, P. & Rietveld, L. C., 2015. Optimisation of parameters in a solar-light induced photoelectrocatalytic process with a TiO<sub>2</sub>/Ti composite electrode prepared by paint-thermal decomposition. J. Photochem. Photobiol. A, Volume 305, pp. 83-92.
- Bennani, Y., El-Kalliny, A. S., Appel, P. W. & Rietveld, L. C., 2014. Enhanced solar light photoelectrocatalytic activity in water by anatase-to-rutile TiO<sub>2</sub> transformation. J. Adv. Oxid. Technol., Volume 17, pp. 285-296.
- Bisquert, J., Bertoluzzi, L., Mora-Sero, I. & Garcia-Belmonte, G., 2014. Theory of impedance and capacitance spectroscopy of solar cells with dielectric relaxation, drift-difussion transport, and recombination. J. Phys. Chem. C, Volume 118, pp. 18983-18991.

- Bouwer, E. J. & McCarty, P. L., 1983. Transformation of 1- and 2- carbon halogenated aliphatic organic compounds under methanogenic conditions. *Appl. Environ. Microbiol.*, Volume 45, pp. 1286-1294.
- Butson, C. R. & McIntyre, C., 2005. Tissue and electrode capacitance reduce neural activation volumes during deep brain stimulation. *Clin. Neurophysiol.*, Volume 116, pp. 2490-2500.
- Choi, W. & Hoffmann, M. R., 1996. Novel photocatalytic mechanism for  $\text{CHCl}_3$ ,  $\text{CHBr}_3$ , and  $\text{CCl}_3\text{CO}_2^-$  degradation and the fate of photogenerated radicals on  $\text{TiO}_2$ . *Environ. Sci. Technol.*, Volume 31, pp. 89-95.
- Contu, F., Elsener, B. & Böhni, H., 2002. Characterization of implant materials in fetal bovine serum and sodium sulfate by electrochemical impedance spectroscopy. *J. Biomed. Mater. Res.*, Volume 62, pp. 412-421.
- Dumas, C., Basseguy, R. & Bergel, A., 2008. Electrochemical activity of *Geobacter sulfurreducens* biofilms on stainless steel anodes. *Electrochim. Acta*, Volume 53, pp. 5235-5241.
- El-Kalliny, A. S., Ahmed, S. F., Rietveld, L. C. & Appel, P. W., 2014. Immobilized photocatalyst on stainless steel woven meshes assuring efficient light distribution in a solar reactor. *Drink. Water. Eng. Sci.*, Volume 7, pp. 41-52.
- Figueiredo, J. L., Pereira, M. M. & Faria, J., 2008. *Catalysis from theory to application*, Coimbra: Coimbra University Press.
- Glaze, W. H., 1986. Reaction products of ozone: a review. *Environ. Health Perspect.*, Volume 69, pp. 151-157.
- Hodgeson, J. W. & Cohen, A. L., 1990. Determination of chlorination disinfection byproducts and chlorinated solvents in drinking water by liquid-liquid extraction and gas chromatography with electron-capture detector, Method 551: US Environ Protection Agency.
- Hsiao, C. Y., Lee, C. L. & Ollis, D. F., 1983. Heterogeneous photocatalysis: degradation of dilute solutions of dichloromethane ( $\text{CH}_2\text{Cl}_2$ ), chloroform ( $\text{CHCl}_3$ ), and carbon tetrachloride ( $\text{CCl}_4$ ) with illuminated  $\text{TiO}_2$  photocatalyst. *J. Catal.*, Volume 82, pp. 418-423.
- Innocenzi, P., Zub, Y. L. & Kessler, V. G., 2008. *Sol-Gel Methods for Materials Processing*. Kiev: Springer.

- Kormann, C., Bahnemann, D. W. & Hofmann, M. R., 1991. Photolysis of chloroform and other organic molecules in aqueous TiO<sub>2</sub> suspensions. *Environ. Sci. Technol.*, Volume 25, pp. 494-500.
- Krivec, M., Dillert, R., Bahnemann, D. W., Mehle, A., Štrancar, J. & Dražić, G., 2014. The nature of chlorine-inhibition of photocatalytic degradation of dichloroacetic acid in a TiO<sub>2</sub>-based microreactor. *Phys. Chem. Chem. Phys.*, Volume 16, pp. 14867-14873.
- Laternus, F., Haselmann, K. F., Borch, T. & Grøn, C., 2002. Terrestrial natural sources of trihalomethane (chloroform, CHCl<sub>3</sub>)-an overview. *Biogeochemistry*, Volume 60, pp. 121-139.
- Liao, J., Lin, S., Zhang, L., Pan, N., Cao, X. & Li, J., 2012. Photocatalytic degradation of methyl orange using a TiO<sub>2</sub>/Ti mesh electrode with 3D nanotube arrays. *Appl. Mater. Interfaces*, Volume 4, pp. 171-177.
- Lin, Y., Li, D., Hu, J., Xiao, G., Wang, J., Li, W. & Fu, X., 2012. Highly efficient photocatalytic degradation of organic pollutants by PANI-modified TiO<sub>2</sub> composite. *J. Phys. Chem. C*, Volume 116, pp. 5764-5772.
- Liu, B., Nakata, K., Sakai, M., Saito, H., Ochiai, T., Murakami, T., Takaqi, T. & Fujishima, A., 2012. Hierarchical TiO<sub>2</sub> spherical nanostructures with tunable pore size, pore volume, and specific surface area: facile preparation and high-photocatalytic performance. *Catal. Sci. Technol.*, Volume 2, pp. 1933-1939.
- Lowell, S., Shields, J. E., Thomas, M. A. & Thommes, M., 2004. Characterization of porous solids and powders: surface area, pore size and density. Netherlands: Springer.
- Lu, M. & Pichat, P., 2013. Photocatalysis and water purification. From fundamentals to recent applications. Weinheim: Wiley-VCH.
- McCulloch, A., 2003. Chloroform in the environment: occurrence, sources, sinks and effects. *Chemosphere*, Volume 50, pp. 1291-1308.
- Murabayashi, M., Itoh, K., Ohta, Y. & Kamata, K., 1989. Photocatalytic degradation of chloroform on platinized titanium dioxide powder. *Denki Kagaku*, Volume 57, pp. 1221-1222.

- Park, H. S., Kim, B. H., Kim, H. S., Kim, H. J., Kim, G. T., Chang, I. S., Park, Y. K. & Chang, H. I., 2001. A novel electrochemically active and Fe(III) reducing bacterium phylogenetically related to *Clostridium butyricum* isolated from a microbial fuel cell. *Anaerobe*, Volume 7, pp. 297-306.
- Pavelic, P., Dillon, P. J. & Nicholson, B. C., 2006. Comparative evaluation of the fate of disinfection byproducts at eight aquifer storage and recovery sites. *Environ. Sci. Technol.*, Volume 40, pp. 501-508.
- Peters, C. J., Young, R. J. & Perry, R., 1980. Factors influencing the formation of haloforms in the chlorination of humic materials. *Environ. Sci. Technol.*, Volume 14, pp. 1391-1395.
- Pruden, A. L. & Ollis, D. F., 1983. Degradation of chloroform by photoassisted heterogeneous catalysis in dilute aqueous suspension of titanium-dioxide. *Environ. Sci. Technol.*, Volume 17, pp. 628-631.
- Rabaey, K., Boon, N., Siciliano, S. D., Verhaege, M. & Verstraete, W., 2004. Biofuel cells select for microbial consortia that self-mediate electron transfer. *Appl. Environ. Microbiol.*, Volume 70, pp. 5373-5382.
- Raj, K. J. A. & Viswanathan, B., 2009. Effect of surface area, pore volume and particle size of P25 titania on the phase transformation of anatase to rutile. *Indian J. Chem.*, Volume 48A, pp. 1378-1382.
- Selcuk, H., Sene, J. J. & Anderson, M. A., 2003. Photoelectrocatalytic humic acid degradation kinetics and effect of pH, applied potential and inorganic ions. *J. Chem. Technol. Biotechnol.*, Volume 78, pp. 979-984.
- Symons, J. M., Bellar, T. A., Carswell, J. K., DeMarco, J., Kropp, K. L., Robeck, G. G., Seeger, D. R., Slocum, C. J., Smith, B. L. & Stevens, A. A., 1975. National organics reconnaissance survey for halogenated organics. *J. Am. Water Works Assoc.*, Volume 67, pp. 634-647.
- Tilley, S. D., Cornuz, M., Sivula, K. & Grätzel, M., 2010. Light-induced water splitting with hematite: improved nanostructure and iridium oxide catalysis. *Angew. Chem.*, Volume 49, pp. 6405-6552.
- Wang, C. X. & Wang, M., 2002. Electrochemical Impedance Spectroscopy study of the nucleation and growth of apatite on chemically treated titanium. *Mater. Lett.*, Volume 54, pp. 30-36.

Wei, X. F. & Grill, W. M., 2005. Current density distributions and impedance analysis of segmented deep brain stimulation electrodes. *J. Neural. Eng.*, Volume 2, pp. 139-147.

WHO, 1996. Guidelines for drinking-water quality, Trihalomethanes in drinking-water, Geneva: World Health Organization.

Xue, G., Liu, H., Chen, Q., Hills, C., Tyrer, M. & Innocent, F., 2011. Synergy between surface adsorption and photocatalysis during degradation of humic acid on  $\text{TiO}_2$ /activated carbon composites. *J. Hazard. Mater.*, Volume 186, pp. 765-772.

Zhao, Y., Hu, C., Song, L., Wang, L., Shi, G., Dai, L. & Qu, L., 2014. Functional graphene nanomesh foam. *Energy environ Sci.*, Volume 7, pp. 1913-1918.

Zhao, Z., Peles, Y. & Jensen, M. K., 2013. Properties of plain weave metallic wire mesh screens. *Int. J. Heat Mass Transfer*, Volume 57, pp. 690-697.



# 5

## HETEROGENEOUS PHOTOELECTROCATALYTIC DEGRADATION OF CHLOROFORM: FROM BATCH TO A FLOW-THROUGH SOLAR AND LPUV FLOW REACTOR

---

TiO<sub>2</sub> photocatalyst was successfully immobilized on mesh electrodes using the paint – thermal decomposition method. Two photocatalytic reactors with different light sources were tested: a) rectangular photocatalytic reactor with re-circulation mode and solar irradiation and b) a cylindrical LPUV photocatalytic reactor with re-circulation mode. Results from corresponding batch experiments were included as well. The reactors were used for degradation of chloroform from water. The effects of various factors as flow rate, anode cathode distance and surface to volume ratio were studied. The experimental results indicated that the half-life time,  $t_{1/2}$ , of the photocatalytic degradation of chloroform at an initial chloroform concentration of 500 ppb, was 216 and 13 min for the solar and UVC reactor, respectively. The increase of recirculating in the solar reactor leads to decrease of the degradation rate due to the reduction of the residence time and redirection of the flow over the meshes rather than through the meshes. Scaling up of the anode showed that surface to volume ratio should be sized accordingly since has a high influence on the kinetics of the chloroform degradation.

### 5.1. Introduction

Advanced oxidation processes (AOPs) have been studied for the removal of chemical compounds present in water. Among them, photoelectrocatalysis using  $\text{TiO}_2$ , based on the activation of the photocatalyst upon UV irradiation to produce oxidant species such as hydroxyl radicals, seems to be efficient for the oxidation of several organic compounds (Pan, et al., 2015). The main advantages of  $\text{TiO}_2$  photocatalysis over other AOPs are that it operates under ambient temperature and pressure and that it has the possibility of using solar light as renewable and decentralised radiation source (Hashimoto, et al., 2005). However, commercial applications of photocatalytic processes have usually been hindered by the low quantum yield (4 – 5 %), because of high electron-hole recombination followed by the loss of energy as heat and the low available surface area, while with homogeneous catalysis the adsorbed light is utilized efficiently and high quantum yields can be achieved (Yang, et al., 2016). One of the proposed solutions for the first listed problem is the application of a small potential bias between a photocatalytic electrode ( $\text{TiO}_2$  immobilized onto a conductive support) and a counter electrode (CE). Under illumination, the holes migrate to the semiconductor-electrolyte interface where the water oxidation occurs, producing hydroxyl radicals, and the electrons are directed to the back of the conductive substrate by the positive potential towards the cathode where the oxygen reduction takes place (Lewerenz, et al., 2010). This flow of electrons is recorded as a photocurrent measurement, which has often been suggested to correlate with the photocatalytic electrode activity for the oxidation of chemical compounds. Thus, the spatial separation of both reactions would reduce the charge-carrier recombination, leading to an increase in photocatalytic efficiency.



Since the early work of Vinodgopal et al. and Kim et al., reporting this electric field enhancement (EFE) to be able to improve photocatalytic efficiency for degradation of organic pollutants, further investigations have been carried out for oxidation of organic compounds in water (Vinodgopal, et al., 1996; Kim & Anderson, 1996; Egerton, 2011). Moreover, the efficiency of this photoelectrocatalytic (PEC) process strongly depends on the available surface area of the photoelectrode (Li, et al., 2002). This problem could be solved by using mesh electrodes instead of plates, immediately increasing the available surface area for adsorption of organic compounds and light absorption. However, some bottlenecks in the development of  $\text{TiO}_2$  PEC reactors like immobilization of  $\text{TiO}_2$  on the meshes, the recombination of the electron-hole pairs, mass transfer, and irradiation light absorption by solution still exist (Byrne, et al., 1998; R. A. Damodar, 2008; Shan, et al., 2010; Yates, 2009; Hua, et al., 2009; Dionysiou, et al., 2002).

A practical electrode configuration must combine the maximal capture of photons throughout the reactor, minimal mass-transfer limitations to and from the electrodes, and minimal electrode resistance between the anode and cathode (Shan, et al., 2010). Therefore, the aim of this work is to study the efficiency of newly developed  $\text{TiO}_2/\text{Ti}$  composite mesh electrodes in a photoelectrocatalytic batch reactor, and the scaling up of the investigated electrode to be used in two different photoelectrocatalytic flow-through reactors.

## **5.2. Materials and methods**

### **5.2.1. Experimental set-up**

In this study one batch reactor and two flow-through systems, with solar and UVC irradiation respectively, were investigated for a contaminant removal by changing the distance between anode and cathode, and reactor volume to surface area. Halomethanes, in particular trihalomethanes (THMs), are frequently detected in both groundwater and surface water sources.

In this study chloroform, which is the major constituent of THMs, has been chosen as a model contaminant for studying heterogeneous photo(electro)catalysis.

### **5.2.2. Batch reactor**

Kinetic experiments of photoelectrocatalytic removal of chloroform from water in a batch reactor were carried out with a set-up consisting of a cylindrical quartz glass reactor with an effective vessel volume of 0.3 L and a three-electrode configuration, as presented by Bennani et. al. (Bennani, et al., 2015). The initial volume of the chloroform solution in the batch experiments was 250 mL (Baker analysed, containing 0.75 % ethanol as stabiliser) with an initial chloroform concentration of 500 ppb.

A TiO<sub>2</sub>/Ti composite 4-mesh photoanode was used in the batch reactor with a surface area of 0.0096 m<sup>2</sup>. The number of meshes was adopted from previous research (see chapter 4). The photoanode in the batch reactor was placed on a stand, incorporated in the reactor, to receive solar light irradiation.

### 5.2.3. Photoelectrocatalytic reactor

The flow rate through the reactor affects the photocatalytic reaction by changing the convective mass transfer and residence time in the reactor. In addition, increased turbulence can stimulate mass transfer. Therefore, information gained from the batch reactor was further used for comparison with the larger-scale application in photoelectrocatalytic flow-through reactors. Other option to a batch process is to feed the reactants continuously into the reactor allowing the reaction to take place and observe the influence of the flow on the kinetics in the reactor.

In a reactor with recirculation a homogeneous distribution of the reactants and products should be present to get reliable kinetic results (Meng, et al., 2015).

Flow-mode photoelectrocatalytic oxidation of chloroform was performed with both solar and UVC systems under the same conditions (0.1 M  $\text{Na}_2\text{SO}_4$  electrolyte, pH 7, 500 ppb of the initial concentration of chloroform solution). The experimental setup, represented in Figure 5.1 a), consists of a solar flow-through reactor with two possible sizes: 30 cm long, 4 cm deep (2.2 L); and 19 or 11 cm wide (1.3 L) respectively, operated in a closed recirculating circuit driven by a pump (Cole Parmer 12 Volt DC Miniature Gear Pump). The solar reactor had surface to a volume ratio of 0.2 and 0.12 respectively. Figure 5.1 b) shows the low pressure UV lamp (LPUV) – cylindrical type reactor with a diameter of 10 cm, a height of 21 cm and a volume of 1.2 L. The chloroform solution was kept and stirred in a glass container connected to the reactor. A gear pump (PQ-12 DC, Cole Parmer) was applied to circulate the solution between the reactors and the solution container by a polytetrafluoroethylene (PTFE) tubing. The flow velocity was controlled by a flow meter (Khrone, glass tube flow meter DK 800). The residence times in the irradiated photoreactors were 5, 15 and 30 min respectively.

The surface area of the TiO<sub>2</sub>/Ti composite 4-mesh photoanode in the solar and UVC flow-through reactors were 0.0260 m<sup>2</sup> and 0.3276 m<sup>2</sup> respectively. The TiO<sub>2</sub> film was supported on the Ti mesh, deposited by the paint-thermal decomposition method and used as the photocatalyst both in the solar and UV reactor (Bennani, et al., 2014).

A graphite plate was used as a cathode and an Ag/AgCl (0.5 M KCl) electrode was used as a reference electrode. The effects of varying the anode-cathode distance (ACD) were tested in the solar simulator by varying the distances (0.3, 0.9 and 1.4 cm).

#### **5.2.4. Analytical procedures**

Demineralized water (RiOs 5 Reverse Osmosis System) was used throughout the experiments for dilution. To eliminate the influence of solution resistance, 0.1 M Na<sub>2</sub>SO<sub>4</sub> was chosen as supporting electrolyte. At regular time intervals (i.e. every hour) 25 mL samples were collected from the reaction solution, added to an extraction flask and measured with gas chromatography (GC, Agilent Technologies 7890A GC system equipped with an electron capture detector (ECD)) to determine the residual concentration of chloroform, following method 551 of EPA (Environmental Protection Agency) (Hodgeson, 1990). 25 mL of the sample were added to 5 g of sodium chloride (used to promote phase separation) already present in the extraction flask equipped with a polytetrafluoroethylene (PTFE)-faced silicone septum. Samples were taken every 2 h; 5 mL of methyltertbutylether (MTBE) was added to the extraction flasks and the solution was shaken vigorously for 2 min. After allowing the solution to settle for 2 min, 1 mL of the organic phase was added to a GC vial using a pipette.

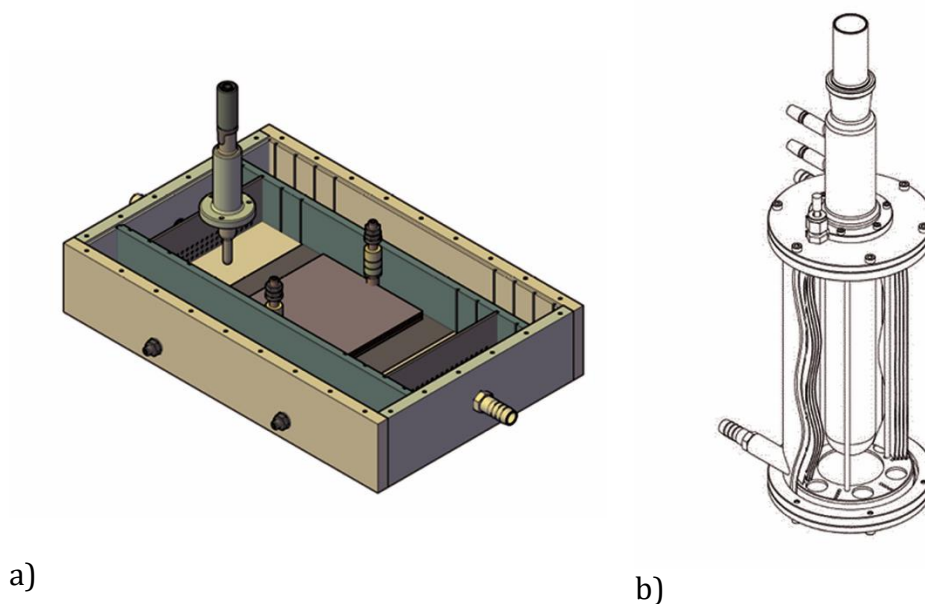


Figure 5.1. Schematic representation of experimental reactor setup (see text for details), a) solar rectangular flow reactor; b) LPUV circular type flow reactor

### 5.2.5. Experimental approach

At the start of each experiment, the chloroform solution, was stirred for 15 hours with the  $\text{TiO}_2/\text{Ti}$  composite electrode in the dark. This turned to be sufficient for adsorption, to reach equilibrium. The experiment was performed with 250 mL beakers closed with special quartz glass lids. The stirrer was positioned inside beakers.

A stock solution of 500 ppb chloroform was prepared in water. All prepared beakers were placed in the water bath inside the solar simulator chamber. The water bath was held at a constant temperature of 25 °C using the Julabo FL300 cooling system. The samples were stirred for 15 hours inside the solar simulator chamber in the dark. Samples of 30 mL were taken every 1 hour, 25 mL was added to an extraction flask

The pH of the solution was kept constant at 7.2 and was measured before the experiment, using a Sentix 81 pH meter.

The cylindrical quartz glass batch reactor system was placed inside the chamber of an Atlas solar simulator type SUNTEST XXL+, consisting of three Xenon lamps emitting solar light (UV300–400). The same solar simulator was used for the experiments conducted in the solar reactor. For the cylindrical UVC reactor, a low pressure ozone free lamp (GPH212T5L/4, input power 10 W) was used. The LPUV lamp was immersed centrally in a quartz glass sleeve and was connected to the quartz cooling water jacket. Classified as being in the same group as fluorescent or germicidal lamps, the main light emission is a 254 nm line comprising an 185nm line of far shorter wavelength. The emission spectrum of the LPUV can be found in research done by Amer El-Kalliny (El-Kalliny, 2013).

The electrode potential and working current throughout all the experiments in the batch and flow reactors were controlled with a potentiostat-galvanostat system (Autolab PGSTAT128N with a BOOSTER10A). The chloroform photo degradation experiments were performed with a constant potential. The optimal potential of 1 V was taken from a previous study with the same TiO<sub>2</sub>/Ti composite electrodes (Bennani, et al., 2014). Dark current and photocurrent were recorded. The voltage during each experiment was sufficiently high so that the limiting current was reached. The net current was calculated by subtracting dark current from photocurrent in order to determine the photoactivity of the films.

### 5.2.6. Evaluation of the results

The Langmuir-Hinshelwood model was used to describe the relationship between the rates of the photocatalytic degradation of chloroform as a function of irradiation time (Houas, et al., 2001).

The rate equation is used in the form (Sun, et al., 2002):

$$\frac{-dC}{dt} = \frac{k_{L-H}K_{ad}C}{1+K_{ad}C}, \quad (1)$$

where  $K_{ad}$  is the adsorption coefficient of the reactant on  $TiO_2$ ,  $k_{L-H}$  is the reaction rate constant and  $C$  is the concentration at any time  $t$ . By integration of equation 1:

$$\ln\left(\frac{C_0}{C}\right) = K(C - C_0) + k_{L-H}K_{ad}t, \quad (2)$$

Where  $C_0$  is the initial concentration.

For first-order reaction  $K_{ad}$  is usually much smaller than 1, so Equation 1 can be simplified and integrated to be:

$$\ln\left(\frac{C_0}{C}\right) = k_{L-H}K_{ad}t = kt, \quad (3)$$

Where  $k$  is the first-order reaction rate constant, and the half-life time  $t_{1/2}$  can be calculated using the following expression.

$$t_{1/2} = (1/k)\ln 2 \quad (4)$$

Plotting the natural logarithm of the ratio between the initial concentration of chloroform and the concentration after photocatalytic degradation ( $\ln(C/C_0)$ ) versus the corresponding irradiation time (min) yields a linear relationship as shown in Figure 2 (first order reaction).

### 5.3. Results

#### 5.3.1. Performance of the batch reactor

Figure 5.2 shows the change in the concentration of chloroform removed from the solution with the reaction time in the batch reactor under solar ( $UV_{300-400}$ ) irradiation.

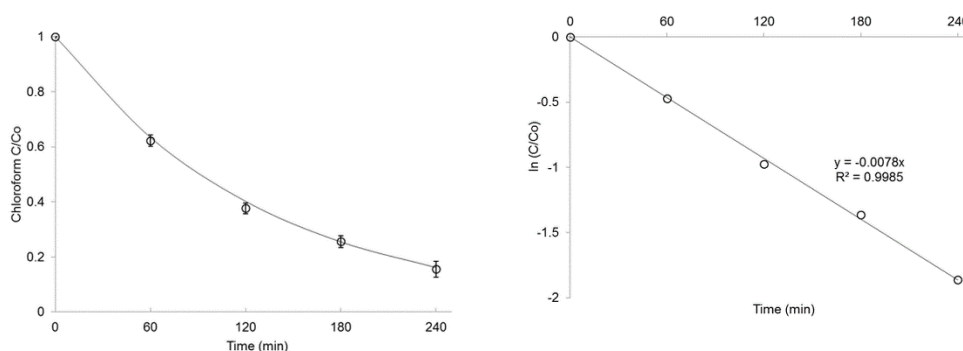


Figure 5.2. The change in the concentration of chloroform ( $C_0 = 500$  ppb) removed from the solution as a function of reaction time in a batch reactor under solar ( $UV_{300-400}$ ) irradiation with corresponding fit for the first order reactions. The error bars were obtained from three replicate measurements.

The first order reaction rate constant under solar irradiation was estimated to be  $7.6 \times 10^{-3} \text{ min}^{-1}$  and the half-life time of photoelectrocatalytic degradation of chloroform was calculated to be 91 min.

#### 5.3.2. Optimisation of anode-cathode distance of the solar flow-through reactor

A chloroform solution, with initial concentration of 500 ppb, was treated by the solar flow-through PEC reactor with single side illumination. The results



of the removal rate were optimized by varying the ACD. The effects of varying the ACD can be observed from Figure 3, which shows the obtained first-order reaction rate constants for chloroform degradation against ACD at a constant potential. Changes in current density by varying ACD were also observed and are shown in the Table 5.1.

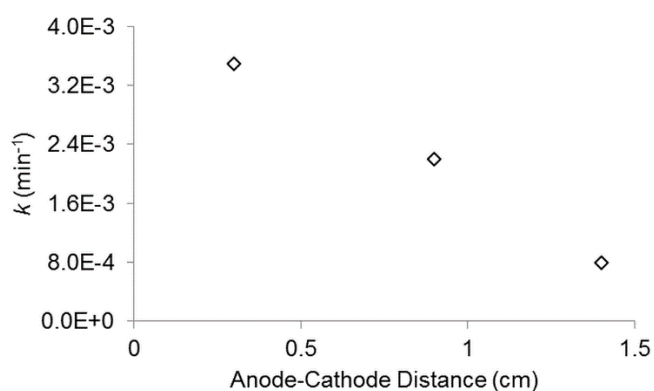


Figure 5.3. First-order reaction constant  $k$  ( $\text{min}^{-1}$ ) extracted from chloroform degradation in three-mesh flow-through reactor (30 min residence time) under solar irradiation ( $\text{UV}_{300-400}$ )

Table 5.1. Current density values during experiments with varying ACD

ACD (cm)	j mA/cm <sup>2</sup>
0.3	0.00375
0.9	0.00358
1.4	0.00275

### 5.3.3. Influence of flow rate on the performance of the solar flow-through reactor

The influent flow rate was varied to examine the effect of residence time (5, 15 and 30 min) on chloroform oxidation performance and possible mass transfer limitations (Turchi & Ollis, 1988).

As seen in the Figure 5.4, the concentration of chloroform decreased with increasing residence time up to a value of 30 min and the performance decreased with increasing flow. The highest chloroform photooxidation reaction, with a residence time of 30 min, had a constant rate of reaction of  $3.75 \cdot 10^{-3} \text{ min}^{-1}$  and a chloroform degradation half-life time of 216 min, classified as a moderate rate (Wright, 2006).

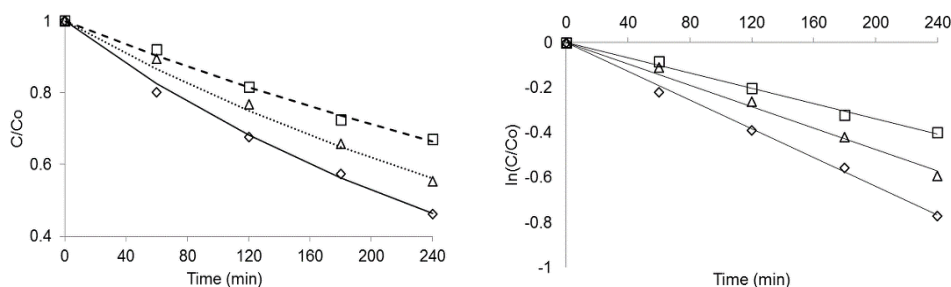


Figure 5.4. Chloroform degradation as a function of average reactor residence time, 5 min ( $\square$ ); 15 min ( $\Delta$ ) and 30 min ( $\diamond$ ). Model results fitted to the residence time; 1<sup>st</sup> order kinetics of chloroform degradation with residence time of 5 min (dashed line); 1<sup>st</sup> order kinetics of chloroform degradation with residence time of 15 min (dotted line) and 1<sup>st</sup> order kinetics of chloroform degradation with residence time of 30 min (solid line)

### 5.3.4. Performance of the LPUV flow reactor

Three sets of experiments were performed to verify the feasibility of the PEC LPUV reactor. In the LPUV flow-through reactor, the chloroform was also removed from the aqueous solution. The first set of experiments was to circulate the solution to evaluate the photo-degradation of the chloroform under different flow conditions.

Figure 5.5 shows the photo-degradation efficiency of chloroform in a reaction over the  $\text{TiO}_2/\text{Ti}$  4-mesh electrode irradiated with LPUV light.

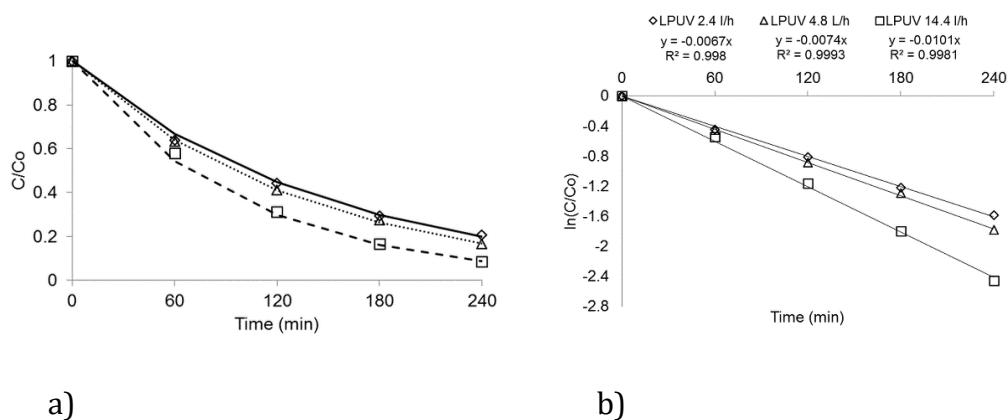


Figure 5.5. Chloroform degradation a) as a function of average reactor residence time, 5 min ( $\square$ ); 15 min ( $\Delta$ ) and 30 min ( $\diamond$ ). Model results fitted to the residence time; 1st order kinetics of chloroform degradation with residence time of 5 min (dash line); b) 1<sup>st</sup> order kinetics of chloroform degradation with residence time of 15 min (dot line) and 1<sup>st</sup> order kinetics of chloroform degradation with residence time of 30 min (solid line)

Corresponding current densities are shown in the Table 5.2 together with according half-life time of chloroform degradation.

Table 5.2. Current density and half-life time for chloroform degradation values during experiments with varying flow

Flow l/h	j mA/cm <sup>2</sup>	t <sub>1/2</sub> min
2.4	0.0380	18,24
4.8	0.0423	16,39
14.4	0.0522	13,28

#### 5.4. Discussion

From the degradation results from the batch reactor, shown in Figure 2, it can be observed that under optimal conditions, determined in previous research (constant potential of 1 V, optimized agitation, UV intensity, layer thickness and constant cooling).

Based upon preliminary test measurements of the immobilized catalyst activity under batch conditions, the residence time for the reactor experiments was selected in order to achieve between 50-90 % degradation of the target micropollutant. In addition, continuous-flow experimental setups at varying scales and light sources were studied.

The removal of the chloroform in the PEC system in the solar reactor can be highly affected by experimental parameters such as temperature, ACD and flow rate (Brahmi, et al., 2015). Therefore, the ACD was varied to find the best distance resulting in the highest removal rate of the chloroform and minimizing energy consumption (Zhang, 2011). The best ACD of the tested ones was 0.3 cm, determined by the (highest) current density. Within the same degradation time of four hours, decreasing the ACD from 1.4 cm to 0.3 cm resulted in an increase in chloroform removal rate of up to 4.3 times. This observation can be explained by the ohmic potential drop in relation to the

anode and cathode (decrease in electrolyte conductivity and current) and increase in the resistance to mass transfer; leading to a slow-down of the kinetics of both charge transfer and chloroform oxidation (Zhang, 2011). Hence, an ACD of 0.3 cm was adopted for further experiments.

Compared to the batch reactor from Figure 5.2 it can be observed that the constant rate of chloroform removal in the solar reactor decreased by a factor 2, from  $7.6 \times 10^{-3}$  to  $3.75 \times 10^{-3} \text{ min}^{-1}$ . This decrease was probably a result of the difference in surface area/volume ratio which is considered to be an important reactor design parameter in PEC (Belhouta, et al., 2010).

The surface area/volume ratio in the solar flow-through reactor was 0.2, which is 1.5 times smaller than in the batch reactor, adsorbing less chloroform per volume and producing less hydroxyl radicals per volume, and resulting in more current density consumption (Belhouta, et al., 2010).

Furthermore, an increase in the degradation rate with increase in retention time in the solar simulator (Figure 5.4) could be attributed to its reactor design, leading to short circuit flows at smaller retention times.

In the LPUV reactor (Figure 5.5) the removal efficiency of chloroform increased from 68 to 74 % as the flow increased from 2.4 l/h to 14.4 l/h, respectively. In this study chloroform, which is the major constituent of THMs, has been chosen as a model contaminant for studying heterogeneous photo(electro)catalysis. Indicating possible mass transfer limitations. A removal efficiency of 60 % at highest flow rates was reached after 1.6 hours.

When comparing the kinetics obtained from the solar flow-through and LPUV lamp photoelectrocatalytic reactors (Figures 5.4 and 5.5), it can be concluded that the latter removal rate of chloroform was three times higher. However, the PEC reactors used in this study were not standardized according to their operational procedures, mostly due to the light penetration and design differences, making the relative comparison between the experiments performed in different reactors challenging and not feasible.

In order to activate  $\text{TiO}_2$  with a band gap of 3.0 eV, wavelengths lower than 400 nm are required which is only 5 % of the solar spectrum. In the circular reactor with the low pressure UV lamp, the anode was situated around the immersed sleeve containing the lamp and was only few centimetres away from the light source, resulting in a higher light intensity coming into contact with the surface of the catalyst.

Additionally, comparing to the design of the solar flow through reactor, flow in the LPUV reactor is circular along the reactor height and through the meshes, ensuring good contact with the catalyst and homogeneous solution, ensuring faster kinetics and better removal of the micropollutant.

## **5.5. Conclusions**

A solar flow-through reactor was developed using a stable and active  $\text{TiO}_2$  film supported on a Ti mesh substrate. The removal of the chloroform showed a dependence on distance between anode and cathode in the reactor. From the three distances between anode and cathode, the best performance was found with an ACD of 0.3 cm. Reactor performance with different flow rates of chloroform solution suggested that no mass transfer limitations occurred. As a consequence, higher degradation was observed at the largest residence (the lowest flow rate) time of 30 min. However, the performance was much lower when compared to the corresponding batch tests. Probably the flow-through system is restricted to low surface to volume ratio of the reactor. The second tested reactor was a LPUV reactor with a 4 mesh electrode, which showed high removal percentages of chloroform in a short period of time. In addition, the removal efficiencies of chloroform in the LPUV reactor could be increased with increasing flow velocities (2.4 l/h to 14.4 l/h) up to a residence time of 5 min, which indicates possible mass transfer limitations.

## References

- Belhouta, D., Ghernaouta, D., Djezzar-Douakhb, S. & Kellila, A., 2010. Electrocoagulation of a raw water of Ghrib Dam (Algeria) in batch using aluminium and iron electrodes. *Desalin. Water Treat.*, Volume 16, pp. 1-9.
- Bennani, Y., Appel, P. & Rietveld, L. C., 2015. Optimisation of parameters in a solar light-induced photoelectrocatalytic process with a TiO<sub>2</sub>/Ti composite electrode prepared by paint-thermal decomposition. *J. Photochem. Photobiol., A*, Volume 305, pp. 83-92.
- Bennani, Y., El-Kalliny, A. S., Appel, P. W. & Rietveld, L., 2014. Enhanced Solar Light Photoelectrocatalytic Activity in Water by Anatase-to-rutile TiO<sub>2</sub> Transformation. *J. Adv. Oxid. Technol.*, Volume 17, pp. 285-296.
- Brahmi, K., Bouguerra, W., Hamrouni, B., Elaloui, E., Loungou, M. & Tlili, Z., 2015. Investigation of electrocoagulation reactor design parameters effect on the removal of cadmium from synthetic and phosphate industrial wastewater. *Arabian J. Chem.*.
- Byrne, J. A., Eggins, B. R., Brown, N. M. D., McKinney, B. & Rouse, M., 1998. Immobilisation of TiO<sub>2</sub> powder for the treatment of polluted water. *Appl. Catal. B*, Volume 17, pp. 25-36.
- Dionysiou, D. D., Suidan, M. T., Baudin, I. & Laine, J., 2002. Oxidation of organic contaminants in a rotating disk photocatalytic reactor: reaction kinetics in the liquid phase and the role of mass transfer based on the dimensionless Damkohler number. *Appl. Catal. B*, Volume 38, pp. 1-16.
- Egerton, T. A., 2011. Does photoelectrocatalysis by TiO<sub>2</sub> work? *J. Chem. Technol. Biotechnol.*, Volume 86, pp. 1024-1031.
- El-Kalliny, A., 2013. Photocatalytic Oxidation in Drinking Water Treatment Using Hypochlorite and Titanium Dioxide. Delft: TU Delft.
- Hashimoto, K., Irie, H. & Fujishima, A., 2005. TiO<sub>2</sub> Photocatalysis: A Historical Overview and Future Prospects. *Jpn. J. Appl. Phys.*, Volume 44, pp. 8269-8285.
- Hodgeson, A. C. J., 1990. Determination of chlorination disinfection byproducts and chlorinated solvents in drinking water by liquid-liquid extraction and gas chromatography with electron capture detection, Cincinnati: US Environment protection Agency.

Houas, A., Lachheb, H., Ksibi, M., Elaloui, E., Guillard, C. & Herrmann, J., 2001. Photocatalytic degradation pathway of methylene blue in water. *Appl. Catal. B*, Volume 31, pp. 145-157.

Hua, X. S., Zhang, Y. J., Ma, N. H., Li, X. F. & Wang, H. W., 2009. A new coral structure  $\text{TiO}_2/\text{Ti}$  film electrode applied to photoelectrocatalytic degradation of reactive brilliant red. *J. Hazard. Mater.*, Volume 172, pp. 256-261.

Kim, D. H. & Anderson, M. A., 1996. Solution factors affecting the photocatalytic and photoelectrocatalytic degradation of formic acid using supported  $\text{TiO}_2$  thin films. *J. Photochem. Photobiol., A*, Volume 94, pp. 221-229.

Lewerenz, H. J., Heine, C., Skorupska, K., Szabo, N., Hannappel, T., Vo-Dinh, T., Campbell, S. A., Klemm, H. W. & Munoz, A. G., 2010. Photoelectrocatalysis: principles, nanoemitter applications and routes to bio-inspired systems. *Energy Environ. Sci.*, Volume 3, pp. 748-760.

Li, X. Z., Li, F. B., Fan, C. M. & Sun, Y. P., 2002. Photoelectrocatalytic degradation of humic acid in aqueous solution using a  $\text{TiO}_2/\text{Ti}$  mesh photoelectrode. *Water Res.*, Volume 36, pp. 2215-2224.

Mathews, R. W. & McEvoy, S. R., 1992. Destruction of phenol in water with sun, sand and photocatalysis. *Solar Energy*, Volume 49, pp. 507-513.

Matthews, R. W., 1991. Photooxidative degradation of coloured organics in water using supported catalyst. *Water Res.*, Volume 25, pp. 1169-1176.

Meng, X., Zhang, Z. & Li, X., 2015. Synergetic photoelectrocatalytic reactors for environmental remediation: A review. *J. Photochem. Photobiol., C*, Volume 24, pp. 83-101.

Navarro, S., Fenoll, J., Vela, N., Ruiz, E. & Navarro, G., 2009. Photocatalytic degradation of eight pesticides in leaching water by use of  $\text{ZnO}$  under natural sunlight. *J. Hazard. Mater.*, Volume 172, pp. 1303-1310.

Pablos, C., Grieken, R. v., Marugan, J., Adan, C., Osuna, M. & Palma, J., 2013. Photoelectrocatalytic study and scaling up of titanium dioxide electrodes for wastewater treatment. *Water Sci. Technol.*, Volume 68, pp. 999-1003.

Pan, J., Li, X., Zhao, Q., Li, T., Tade, M. & Liu, S., 2015. Construction of  $\text{Mn}_{0.5}\text{Zn}_{0.5}\text{Fe}_2\text{O}_4$  modified  $\text{TiO}_2$  nanotube array nanocomposite electrodes and their photoelectrocatalytic performance in the degradation of 2,4-DCP. *J. Mater. Chem. C*, Volume 3, pp. 6025-6034.



- R. A. Damodar, T. S., 2008. Performance evaluation of a continuous flow immobilized rotating tube photocatalytic reactor (IRTPR) immobilized with  $\text{TiO}_2$  catalyst for azo dye degradation. *Chem. Eng. J.*, Volume 144, pp. 59-66.
- Shan, A. Y., Ghazi, T. I. M. & Rashid, S. A., 2010. Immobilisation of titanium dioxide onto supporting materials in heterogeneous photocatalysis: a review. *Appl. Catal. A*, Volume 389, pp. 1-8.
- Sun, Z., Chen, Y., Ke, Q., Yang, Y. & Yuan, J., 2002. Photocatalytic degradation of a cationic azo dye by  $\text{TiO}_2$ /bentonite nanocomposite. *J. Photochem. Photobiol. A*, Volume 149, pp. 169-174.
- Turchi, C. & Ollis, D. F., 1988. Photocatalytic reactor design: an example of mass-transfer limitations with an immobilised catalyst. *J. Phys. Chem.*, Volume 92, pp. 6852-6853.
- Vinodgopal, K., Bedja, I. & Kamat, P. V., 1996. Nanostructured Semiconductor Films for Photocatalysis. Photoelectrochemical Behavior of  $\text{SnO}_2/\text{TiO}_2$  Composite Systems and Its Role in Photocatalytic Degradation of a Textile Azo Dye. *Chem. Mater.*, Volume 8, pp. 2180-2187.
- Wright, M. R., 2006. *An Introduction to Chemical Kinetics*. Chichester: John Wiley & Sons Ltd.
- Xu, Y. L., He, Y., Cao, X. D., Zhong, D. J. & Jia, J. P., 2008.  $\text{TiO}_2/\text{Ti}$  rotating disk photoelectrocatalytic (PEC) reactor: a combination of highly effective thin-film PEC and conventional PEC processes on a single electrode. *Environ. Sci. Technol.*, Volume 42, pp. 2612-2617.
- Yang, L., Chu, D., Chen, Y., Wang, W., Zhang, Q., Yang, J., Zhang, M., Cheng, Y., Zhu, K., Lv, J., He, G. & Sun, Z., 2016. Photoelectrochemical Properties of  $\text{Ag}/\text{TiO}_2$  Electrodes Constructed Using Vertically Oriented Two-Dimensional  $\text{TiO}_2$  Nanosheet Array Films. *J. Electrochem. Soc.*, Volume 163, pp. 180-185.
- Yates, J. T., 2009. Photochemistry on  $\text{TiO}_2$ : mechanism behind the surface chemistry. *Surf. Sci.*, Volume 603, pp. 1605-1612.
- Zhang, X. G., 2011. Galvanic Corrosion. In: *Uhlig's Corrosion Handbook*. Hoboken: John Wiley & Sons, pp. 123-143.



# 6

## ELECTROCHEMICALLY ACTIVE BIOFILM AND PHOTOELECTROCATALYTIC REGENERATION OF THE TITANIUM DIOXIDE COMPOSITE ELECTRODE FOR ADVANCED OXIDATION IN WATER TREATMENT

---

A novel bio-photoelectrocatalytic system was used to effectively reduce phenol as a model organic pollutant through the utilization of energy derived from bacteria and the use of solar energy for activation of  $\text{TiO}_2$ . In such a system, a synergistic effect occurs between the bio-electrochemical and photocatalytic oxidation processes.  $\text{TiO}_2/\text{Ti}$  composite electrodes were operated with variable biofilm coverage (partially developed biofilm after 6 days and fully developed biofilms after 12, 20 and 40 days at room temperature and pH 7). The study depicted the effectiveness of biofilm formation in enhancing the electron transfer. Kinetic analysis showed that the system exhibited a more rapid phenol degradation at a rate two times higher than rates by individual photo(electro)catalytic and biodegradable methods. Higher current density ( $8.4 \times 10^{-2} \text{ mAcm}^{-2}$ ) and phenol removal efficiency of 62 % after four hours of irradiation were observed especially with electrochemically active biofilm developed after 20 days.  $\text{TiO}_2/\text{Ti}$  composite electrode. After the additional application of cleaning process, the  $\text{TiO}_2/\text{Ti}$  composite electrode could be used several times with nearly the same efficiency, leading to decrease in the final cost of the treatment process.

## 6.1. Introduction

Microorganisms as bio-catalysts are used in bio-electrochemical systems (BESs). The base of the biofilm is water, extracellular polymeric substances (EPS) and bacteria, and is characterised by surface attachment, structural heterogeneity, genetic diversity and complex community interactions (O'Toole, et al., 2000). Biofilm formation is a dynamic process involving initial attachment, aggregation, maturation and dissolution (O'Toole, et al., 2000). The major role of microorganisms is to generate electrons through substrate metabolism and to help mediate the electron transfer to the anode, functioning as a catalyst (Erable, et al., 2010). Electrically-catalytic microorganisms transfer electrons to electrode as a final electron acceptor (Picioreanu, et al., 2007). Four mechanisms are known for the transfer of electrons from bacteria to the conductive substrate: oxidation of bacterial metabolism products, electron transfer by artificial electrochemical mediators, bacteria that produce their own mediators, and direct electron transfer (Lovley, 2006). An anode plays an important role in transferring electrons within the electrochemical system, and it serves as a medium on which the electrically-catalytic microorganisms are attached. It has been shown that some electrogenic bacteria form layers of biofilm on the anode surface (Picioreanu, et al., 2007). The role of biofilm formation on the anode and anode material may be critical to increase current production (Khan, et al., 2014).

Different electrode materials and electrode modifications have been used in order to improve the performance of the similar systems (Khan, et al., 2014; Benetton, et al., 2010). Conductive polymer-based electrodes, such as polyaniline (PAni) over Pt, fluorinated PAni over graphite, and 1, 4-naphthoquinone derivatives over carbon cloth, have been evaluated as potential anode materials (Kalathil, et al., 2013). However these materials

exhibit poor bacterial adhesion and low electron-transfer efficiency (Zhao, et al., 2014).

On the other hand,  $\text{TiO}_2$  coated on the Ti offers rich abundance, low cost, nontoxicity, chemical stability and good electron transfer (Bessegato, et al., 2014; Kalathil, et al., 2013). In addition, the use of solar light with a non-doped simple,  $\text{TiO}_2/\text{Ti}$  composite electrode, e.g., prepared with the paint-thermal method, would avoid drawbacks such as thermal instability (metal centres acting as electron traps), which reduces the photocatalytic efficiency, and would be less expensive (Kalathil, et al., 2013). In nature, biofilms can be found as part of the synthesis and degradation of organic matter; the degradation of various pollutants; and the cycling of nitrogen, sulphur, and metals (Kougo, et al., 2012). Biofilms are ubiquitous in water bodies and are also used to treat waste-water in engineered systems. Nowadays, anthropogenic organic compounds are extensively produced as pesticides, herbicides, pharmaceuticals, etc., and they, together with their by-products, can be found back in the environment (Chasib, 2013). They have recently also been found in groundwater and other drinking water sources (Chasib, 2013).

Many of these compounds are recalcitrant constituents that challenge conventional biological treatment systems and also pose severe health risks to humans and the environment. Therefore, the development of new methods and systems (Exon, 1984; Balasubramanian & Venkatesan, 2012) for the removal of the mentioned compounds from wastewater and drinking water has attracted significant interest. Different advanced oxidation processes such as ozone, Fenton's reagent and photo(electro)catalysis have been applied for the treatment of wastewater or drinking water containing phenols as a model organic compound (Nickehslat, et al., 2013; Kusic, et al., 2006).

However, sometimes these processes may be limited by economics, oxidative potential, effluent characteristics or a tendency to form harmful by-products. In order to succeed in the treatment of a particular water, given these limitations, the situation may require a combination of available processes in such a way as to exploit their individual strengths and thus attain the desired water characteristics (Liu, et al., 2014). With these methods, phenol can be mineralized or degraded into simpler and/or less harmful compounds that can be further processed by microorganisms (Scott & Ollis, 1995; Reddy, et al., 2004; Wataru & Mitsumasa, 2003; Pant, et al., 2011).

A promising approach for water treatment and the removal of toxic organics is thus to combine characteristics from AOP with biodegradation. Even though the germicidal effect of UV light has been known for many years (Gayan, et al., 2013), microorganisms in the biofilm show different properties from those in planktonic life.

The microbial communities are much more resistant to congenital methods of deactivation of bacteria (such as antibiotics, sterilization by heat or chemical process and UV radiation) (Costerton, et al., 1995) which makes them suitable for use in a photoelectrocatalytic (PEC) system. Additionally, A. M. Lasso showed that the presence of organics that had different interactions with TiO<sub>2</sub> surfaces provoked a negative effect on the photocatalytic inactivation of bacteria cells, suggesting that the possible bacteria-TiO<sub>2</sub> interaction might play a key role in its inactivation (Moncayo-Lasso, et al., 2012). The AOP can break the complex structures by hydroxyl attacks, generating products that are readily biodegradable (Shen, et al., 2014). Marsolek successfully demonstrated the concept of coupling photocatalysis and biodegradation for 2, 4, 5-TCP (Marsolek, et al., 2007; Marsolek, et al., 2007).

In this study we propose a novel, extended alternative, combining biodegradation with photoelectrocatalysis, creating bio-photoelectrocatalysis for water treatment.

The aim of this research was to bring insight into the coupled system, bio-photoelectrocatalysis, as well as to assess and demonstrate the efficiency for degrading environmental pollutants. The role of biofilm growth (6, 12, 20 and 40 days) and the extent of its coverage on the anode surface was studied, in relation to enhanced degradation kinetics of phenol in a batch-scale photoelectrocatalytic reactor.

An anode with a fully developed biofilm (FDB) was compared with an electrode without biofilm coverage in separate systems. This article also includes spectroscopic, electrochemical and microscopic techniques for analysing and defining the development of the biofilm at different growth stages. The morphology of the bacteria that formed a biofilm on the anode surface and coverage of the biofilm were examined by scanning electron microscopy (SEM). Pyrosequencing was used to analyse the bacterial communities of the biofilm formed at the surface of the catalyst.

## **6.2. Experimental**

### **6.2.1. Electrode preparation and biofilm development**

TiO<sub>2</sub>/Ti composite electrodes (Magneto B.V., Schiedam, the Netherlands) with a surface of 0.0016 m<sup>2</sup> were used as the anode. The electrode surfaces were washed twice with acetone and deionized water to remove organic substances. Cleaned electrodes were immersed into a body fluid analog medium and left for 6, 12, 20 and 40 days in order to grow biofilm on the surface of the electrode. The medium was made with non-chlorinated Dutch tap water. In addition, 20 mg urea, 0.5 mg sodium citrate, 2 mg creatine and 0.1 mg potassium phosphate were added per litre of solution.

Ingredient selection for biofilm formation was made on the basis of previous biofilm characterisation, whereas bacteria genera in samples of biofilm were found as well, either in surface water or ground water (Bartram, et al., 2003). After the addition of the salts, the medium was placed in a PVC cup in which one electrode was installed. The cup was placed in a climate room where the air temperature was controlled at 32°C. After each experiment, the electrode surfaces were cleaned with a 1 molL<sup>-1</sup> NaOH treatment.

### **6.2.2. Experimental setup assembly**

Impact on phenol degradation of progressing biofilm growth on the anode was studied. This was done by first evaluating the degradation by the individual processes: biodegradation, photolysis and photo(electro)catalysis. Subsequently, various combinations of these processes were investigated with respect to the mineralization of phenol. Every mentioned process was evaluated by the rate of phenol degradation and the extent of enhancement driven by either applied potential, *E* or attached bacteria in biofilm. However, experimental studies suggest that bacterial death is an important process in biofilm growth: at low nutrient conditions cell death is accelerated and the accumulation of damaged cells can lead to disintegration of the biofilm (Fagerlind, et al., 2012).

Additionally, Bond (Bond, et al., 2012) showed that thicker and more mature biofilms become less effective at producing current. Taking into account previously mentioned studies, regeneration of the electrode was studied. In order to remove disintegrated biofilm formed on the surface of the catalyst and restore the adsorptive capacity and current density, cleaning of the anode was performed. Regeneration experiments included removal of the biofilm by



activation of the  $\text{TiO}_2/\text{Ti}$  composite electrode in the demineralized water. The formed biofilms were also analysed and the information was used for its characterisation.

The  $\text{TiO}_2/\text{Ti}$  composite electrodes were inserted in a custom-made batch reactor that was closed with a quartz glass lid, with an effective vessel volume of 200 ml. The electrochemical batch reactor had previously been washed in  $3 \text{ molL}^{-1} \text{ HNO}_3$ . After the addition of a small magnetic stir bar, the cell was autoclaved for 15 min. The setup consists of a three-electrode configuration. An  $\text{Ag}/\text{AgCl}$  (0.230 V vs. standard hydrogen electrode (SHE)) was used as the reference electrode (Metrohm Autolab B. V., the Netherlands) and a graphite plate as the cathode. The reactor was placed in a water bath to maintain the water temperature at  $25^\circ\text{C}$ . The initial volume of the working solution was 175 ml phenol solution ( $\geq 99\%$ , Sigma Aldrich) with an initial concentration of  $20 \text{ mgL}^{-1}$ .

Phenol has been so far extensively used as a model compound in electrochemical systems since it is a simple organic compound, easily soluble in water at different condition of acidity and in addition phenol constitutes one of the main pollutants to be removed from wastewater (Song, et al., 2014). In this study phenol was used as well used as a model compound for the degree of conversion, therefore the degradation mechanism was not studied. Demineralized water (RiOs 5 Reverse Osmosis System) was used throughout the experiments for dilution. To eliminate the influence of solution resistance,  $0.1 \text{ molL}^{-1} \text{ Na}_2\text{SO}_4$  was chosen as supporting electrolyte throughout the experiments. Nevertheless, potentially up-scaled systems would have to rely more on the optimal distance between electrodes other than the use of electrolytes. The samples were collected from the reaction solution at regular

time intervals to determine the residual concentration of phenol. The cylindrical quartz glass reactor system was placed inside the chamber of the SUNTEST XXL+ (Atlas), consisting of 3 Xenon lamps irradiating solar light, having a wavelength spectral distribution with about 0.5 % of emitted photons <300 nm (UV-C range) and about 7% between 300 and 400 nm (UV-B, A range). The emission spectrum between 400 and 800 nm follows the solar spectrum. The solar spectrum of these Xenon lamps was measured by a Black C-50 spectrometer, a product of StellarNet.

### **6.2.3. Electrochemical instrumentation**

A 4-channel potentiostat (PGSTAT128N, Metrohm Autolab B.V., the Netherlands) was connected to the three-electrode cell using Ag/AgCl (saturated with KCl) as reference electrode, carbon as a counter electrode and electrochemically active biofilm on TiO<sub>2</sub>/Ti as the working electrode in 175 mL phenol solution (pH 7, 20 mgL<sup>-1</sup>) with 0.1 molL<sup>-1</sup> Na<sub>2</sub>SO<sub>4</sub> as a supporting electrolyte. Software from the same producer (Nova Software) was used to run the electrochemistry routines, which included chronoamperometry (CA) and electrochemical impedance spectroscopy (EIS). The parameters for CA were as follows: *E* applied (*E*) 1 V versus Ag/AgCl (saturated with KCl).

The photoelectrochemical performance is largely dependent on charge transfer and the level of recombination of the used catalyst (Balaji, et al., 2011). Electrochemical impedance was used to analyse the charge carriers' transfer and recombination processes at photocatalyst/electrolyte interfaces (Park, et al., 2001; Rabaey, et al., 2004; Dumas, et al., 2008). EIS was conducted while maintaining a direct applied potential of 1 V between the working electrode (electrochemically active biofilm on TiO<sub>2</sub>/Ti) and the reference electrode Ag/AgCl (KCl saturated). The growth of the biofilm on the TiO<sub>2</sub>/Ti

composite electrode was monitored with EIS. The measurements were taken at different biofilm growth periods (6, 12, 20 and 40 days).

EIS was performed at a potential of 1 V versus Ag/AgCl (KCl saturated), with a perturbation amplitude of 0.1 V. The values were measured for both dark and light periods. Most biological charge transfer phenomena were found in the frequency range from  $10^5$  to 0.01 Hz, where the measurements frequencies were set during the experiments (Khan, et al., 2014; Barsoukov & Macdonald, 2005). EIS was measured as independent bioelectrochemical analysis in triplicates.

The impedance is expressed in a graph as a real part  $Z'$  (X-axis) and imaginary part  $Z''$  (Y-axis) as a semi-circle. Each point on the plot represents the impedance at a certain frequency. The impedance at the high frequency limit is the ohmic resistance ( $R_s$ ), and the diameter of the semi-circle is the polarization resistance ( $R_p$ ).  $R_p$  is also known as charge transfer resistance or interfacial resistance, occurring at the surface of the electrode, which is affected by the kinetics of the electrode reactions. A smaller arc radius suggests a higher charge transfer efficiency (Randviir & Banks, 2013). The capacitance  $C$  (F) is commonly obtained from EIS data using the real part of impedance  $Z(\text{re})$  ( $\Omega$ ) for a given frequency  $\omega$  (Hz) by means of the following equation (Randviir & Banks, 2013):

$$Z = \frac{1}{\omega C} \quad (1)$$

#### **6.2.4. Analytical methods and scanning electron microscope analyses**

To be able to determine biofilm growth, the biofilm was removed from the electrode by applying three times High-Energy-Sonification (20 % amplitude,

120 s) with 0.040 L of demineralized water. Bacterial growth was assessed by measuring total cells and intact cells with flow cytometry (FCM), live/dead staining according to Prest (Prest, et al., 2013), where it was assumed that the intact cells were living (Wang, et al., 2010).

Urea measurements were attained with a test kit (Merck, Darmstadt, Germany). After the addition of urease, urea was converted to carbon dioxide and ammonia. The urea concentration was therefore measured as  $\text{mg NH}_4\text{-NL}^{-1}$  with a spectrophotometer (Spectroquant Nova 60, Merck, Darmstadt, Germany). The samples were measured in triplicate.

The phenol concentration was monitored with a Hach Lange DR 5000 spectrophotometer by using Hach Lange cuvette tests (LCK 345 with a measuring range of  $0.05\text{-}5.00\text{ mgL}^{-1}$ ,  $5\text{-}50\text{ mgL}^{-1}$  and  $20\text{-}200\text{ mgL}^{-1}$ ). Phenol reacts with 4 -nitroaniline to form a yellow-coloured complex which is then measured by photometry.

A scanning electron microscope (SEM) (Jeol, JSM-6010LA) was used to image  $\text{TiO}_2/\text{Ti}$  electrodes containing biofilms with different growth periods. After being cleaned with deionized water, the electrodes were air dried. It is recognised that air-drying may reduce the biofilm volume (Fish, et al., 2015), however, air-drying was minimal so the position of the components was preserved.

All the samples were treated identically, therefore results remained comparable. The electrodes were placed directly into the SEM vacuum compartment and examined at an accelerating potential of 5 kV. Images were analysed and taken at low vacuum mode, 30 Pa with a backscatter detector. The images were analysed as well with a secondary electron detector. Energy dispersive spectroscopy (EDS) was used for identification of particular elements and their relative proportions (mass % and atom %).

### **6.2.5. Pyrosequencing**

To be able to characterise the bacterial population in the biofilm, DNA isolation was performed using the UltraClean Microbial DNA Isolation Kit of MO BIO laboratories.

Next, the samples were further analysed at the Regional Laboratory for Public Health, Haarlem, the Netherlands. 16S quantification by qPCR was performed according to Yang (Yang, et al., 2002). Thereafter, 16S deep sequencing was done essentially as described by Schloss (Schloss, et al., 2011) using the V3-V5 primers and the Mothur software package.

## **6.3. Results and Discussion**

Bio-photoelectrocatalytic systems is envisaged to be a promising water treatment technology. This kind of technology offers a sustainable power source with advantages of low maintenance, environmentally friendliness, high conversion efficiency, ambient, and thus low, operating temperatures (Khan, et al., 2014; Kalathil, et al., 2013). Bio-photoelectrocatalytic systems can also directly convert chemical energy in organic compounds to electricity via microbial metabolism. Here a mixed culture biofilm was chosen above a single culture, since in field conditions these will predominate (Khan, et al., 2014).

### 6.3.1. Surface characteristics of titanium dioxide composite electrodes with and without biofilm

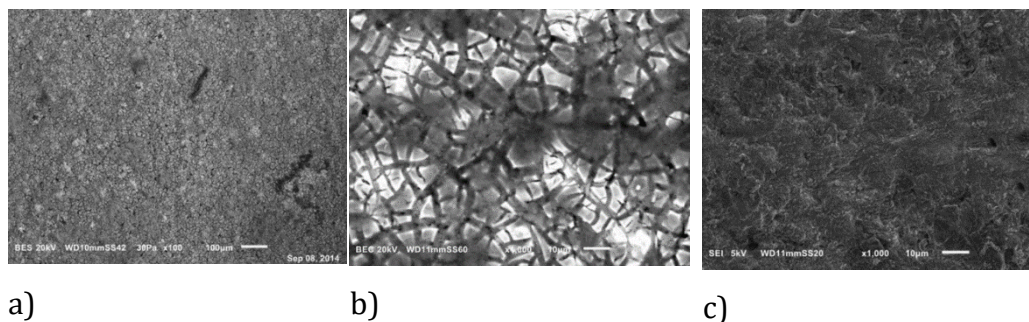


Figure 6.1. a) SEM image of the surface of  $\text{TiO}_2/\text{Ti}$  composite electrode with biofilm developed after 6 days (20 kV, 100  $\mu\text{m}$ , x 100) back scatter detector; b) SEM image (20 kV, 10  $\mu\text{m}$ , x 1000) backscatter detector; c) SEM image (5 kV, 10  $\mu\text{m}$ , x 1000) with secondary detector

Figures 6.1, 6.2, 6.3 and 6.4 show the surface features of the  $\text{TiO}_2/\text{Ti}$  electrodes covered with biofilm in different growth stadia. Figures 6.1 a) and b) reveal that after 6 days of biofilm growth, the biofilm coverage was poor. From Figure 6.1 c), after applying a secondary detector in the SEM analysis at the same place on the sample as in Figure 6.1 b), it can be seen that the surface of the electrode is covered with a thin crystalline layer. The formation of the crystalline foundation layer allows bacteria to attach and colonize. The formed microcrystalline foundation layer from the EDS results contained carbon and nitrogen which were expected because of the nutrients that were added in the medium to encourage bacterial growth. Stickler (Stickler & Morgan, 2008) had similar findings in the early stages of biofilm formation on a range of Foley catheters in a laboratory model of the catheterized bladder. In their research, under the alkaline conditions, crystals of calcium and magnesium phosphates were formed in urine and a crystalline biofilm developed on the catheter.

Figures 6.2 a) and b) show SEM images of the electrode with a biofilm developed after 12 days. On these electrodes bacteria have attached and created biofilm clusters rather than uniform biofilm monolayers. The electrode with a biofilm developed after 20 days showed uniformity of this biofilm (Figures 6.3 a) and b)). Figure 6.3 b) shows a low magnification SEM image of a developed biofilm. Figure 6.4 a) shows an SEM image (20 kV, 10  $\mu$ m, x 1000) of the surface of the TiO<sub>2</sub>/Ti composite electrode with biofilm developed after 20 days. This surface area was additionally analysed with EDS and it was found that clusters with bacteria contained calcium and phosphate.

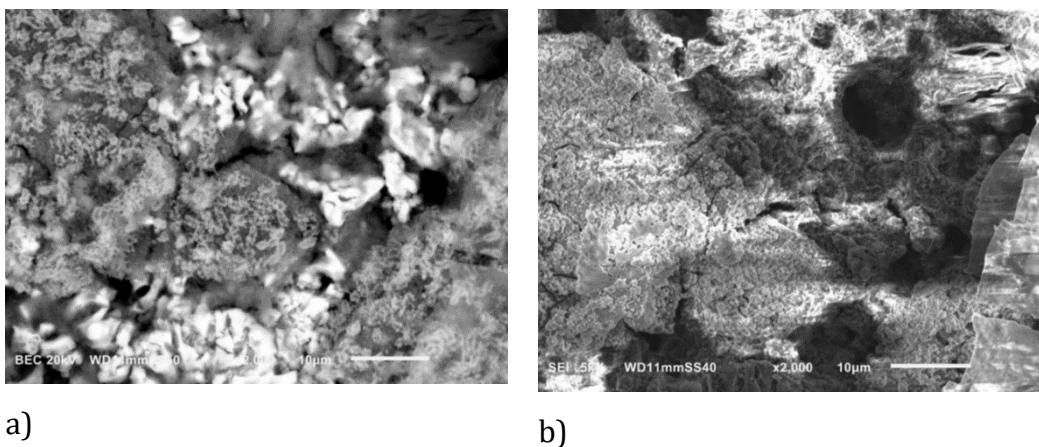
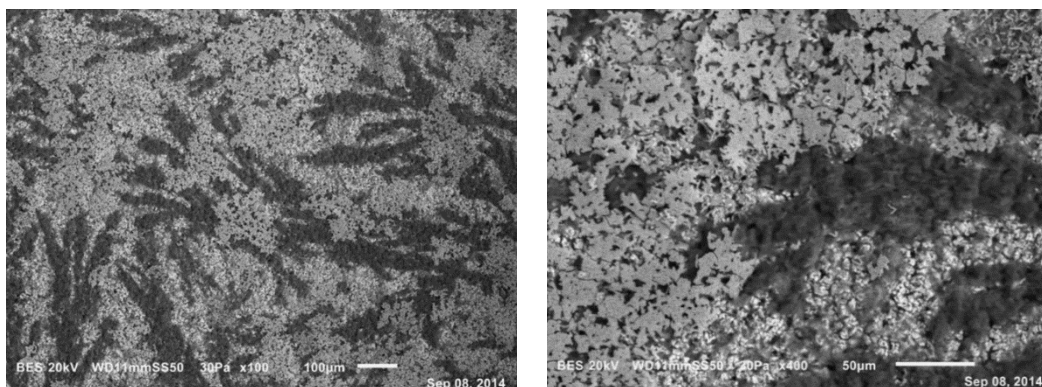
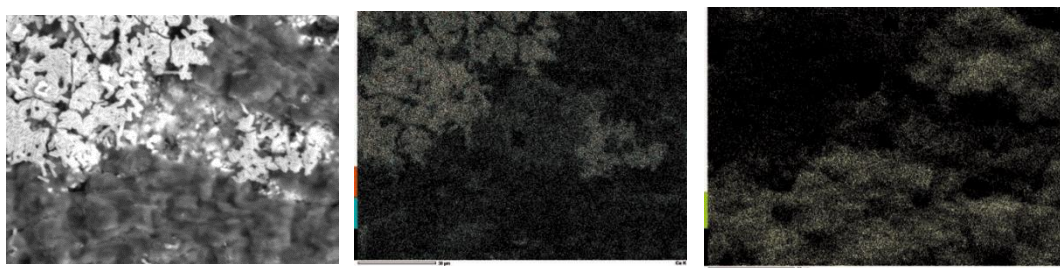


Figure 6.2. a) SEM images of the surface spot on the sample surface of a TiO<sub>2</sub>/Ti composite electrode with biofilm developed after 12 days (20 kV, 10  $\mu$ m, x 2000) back scatter detector; b) SEM image (5 kV, 10  $\mu$ m, x 2000) secondary detector



a) b)

Figure 6.3. a) SEM image (20 kV, 100  $\mu\text{m}$ , x 100) of the surface of a TiO<sub>2</sub>/Ti composite electrode with biofilm developed after 20 days; b) SEM image (20 kV, 50  $\mu\text{m}$ , x 400) mixed culture of bacteria cells



a) b) c)

Figure 6.4. a) SEM image (20 kV, 10  $\mu\text{m}$ , x 1000) of the surface of a TiO<sub>2</sub>/Ti composite electrode with biofilm developed after 20 days; b) EDS image for Ca and P analysis; c) EDS image for N and C analysis

### 6.3.2. Characterisation of the biofilm

To better understand the SEM analyses and why calcium and phosphate were found, the biofilm population was characterised with pyrosequencing. To simulate an average biofilm population, the microorganisms from the biofilms



of days 6, 12, 20 and 40 were combined as was done for the water population. The main bacteria family present was *Pseudomonadaceae* (66 %), characterised as the genus *Pseudomonas*. Within the *Pseudomonas* genus there are about 140 species (Stickler & Morgan, 2008; Ravichandran, et al., 2009) of which *P. aeruginosa* is the best known since it causes infections and is antibiotic resistant. *Pseudomonas* species are present in insects, humans, soil, plants and water (Nikel & E. Martinez-Garcia, 2014) and is therefore wide spread. Other bacteria that were present for more than 5 % were *Caulobacteraceae* (7 %) and *Xanthomonadaceae* (6 %).

The microbial population in the water around the biofilm also had the family *Pseudomonadaceae* as its main population (61%). Others that were present for more than 5 % were *Caulobacteraceae* (14 %), *Comamonadaceae* (6 %) and *Xanthomonadaceae* (5 %). Comparing the biofilm population with the water population, it turns out that the percentage of *Caulobacteraceae* in the water phase is higher than for the attached biofilm phase, where the other bacteria were present in similar percentages.

Combining these pyrosequencing results with the corresponding cell counts (shown in Table 6.1), the actual concentration of each family could be calculated. Overall, a total concentration of  $13.45 \times 10^8$  cells  $\text{cm}^{-2}$  was found in the biofilm, summing up the cell concentration on day 6, 12, 20 and 40. The water around the biofilm contained  $5.69 \times 10^8$  cells  $\text{cm}^{-3}$ . Therefore, in general, 2.5 times more bacteria were found in the water phase than in the biofilm.

The main presence of *Pseudomonas* on the titanium electrode and in the water around it, can be used to explain the high calcium and phosphate precipitation on the electrode. Firstly, the medium mainly consisted of urea which was dissolved in Dutch tap water. Different microorganisms are able to convert urea into ammonia. This enzymatic hydrolysis produces an alkaline environment (Morris, et al., 1999) caused by proton consumption. Chemically, this creates an environment in which calcium and phosphate are no longer

soluble. One of the microorganisms which is able to make this conversion is *P. aeruginosa*, (Broomfield, et al., 2009).

It was observed that the urea concentration decreased from an initial 25.4 to 17.6 mgNH<sub>4</sub>-NL<sup>-1</sup> after 20 days. Thereafter, the urea concentration increased again until 25.4 mgNH<sub>4</sub>-NL<sup>-1</sup> after 40 days. Furthermore, regarding proton reduction, the pH of the water was 8, creating an alkaline environment with fewer protons available. Together with the phosphate inside the medium, the calcium present in the tap water (total hardness 0.0015 molL<sup>-1</sup>) (Rijswick & Havekes, 2012) precipitated (VON-Commission, 2004). Citrate could decrease the formation of these precipitates (Broomfield, et al., 2009), however the concentration of citrate in this medium was low and probably not sufficient to decrease the formation.

### 6.3.3. Photo(electro)catalytic and bio-degradation of phenol

In order to see the effect of biofilm formation on the reaction kinetics of phenol degradation and efficiency of the process, photo(electro)catalytic experiments using an anode with and without the biofilm were conducted. Figure 6.5 shows the removal of phenol in the process of the photolysis, biodegradation, photo(electro)catalysis, and bio-photo(electro)catalysis with a constant initial concentration of 20 mgL<sup>-1</sup> of phenol. Phenol removal by photolysis and biodegradation was low while constant removal rates by heterogenic photocatalysis and bio-photocatalysis were 5 to 12 times greater. The biofilm on the TiO<sub>2</sub>/Ti composite plate showed a lower rate of phenol removal during photocatalysis compared to the removal rate of photocatalysis without the presence of the biofilm. The lower removal rate could be due to the retardation of the interfacial electron transfer by the biofilm, followed by the increase in the electron-transfer resistance and thus the electron-hole recombination.

Lower light adsorption onto the electrode is additionally contributing to the inefficiency.

Phenol was more efficiently removed by the photoelectrocatalytic process. The removal of phenol was additionally enhanced when the  $\text{TiO}_2/\text{Ti}$  composite electrode with the biofilm was used in the bio-photoelectrocatalytic system. This observation suggests that the bacteria attached to the  $\text{TiO}_2$  electrode acted as an electrochemically active biofilm where it oxidized the phenol into end- and by-products. The electrons produced by the electrochemically active biofilm were probably injected into the conduction band (CB) of the  $\text{TiO}_2$  (Kalathil, et al., 2012). The removal percentage of phenol with the biofilm- $\text{TiO}_2/\text{Ti}$  composite electrode in a 3-electrode cell was, after 6 h of irradiation, 1.6 times higher than that of photoelectrocatalysis.

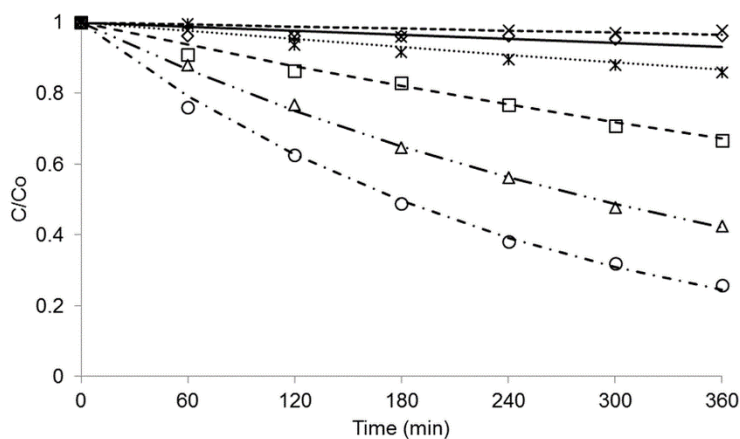


Figure 6.5. Phenol degradation by photolysis (◇); biodegradation (x); photocatalysis (□); photoelectrocatalysis (Δ); bio-photocatalysis with a biofilm developed after 20 days (⋈) and bio-photoelectrocatalysis with a biofilm developed after 20 days (o)

Figure 6.6 shows the influence of the inoculation time of the biofilm (6, 12, 20 and 40 days) on the  $\text{TiO}_2/\text{Ti}$  composite electrode on the removal enhancement of the phenol (showing a constant first-order reaction rate).

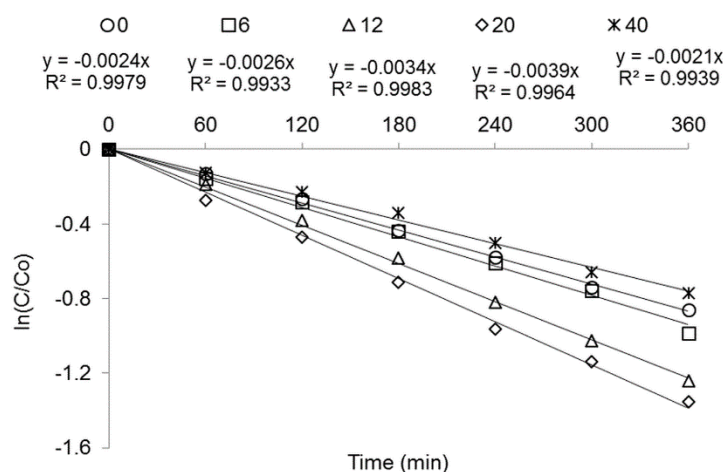


Figure 6.6. Phenol degradation using  $\text{TiO}_2/\text{Ti}$  composite electrodes without and with biofilm with different inoculation times; no biofilm (○); 6 days (□); 12 days (△); 20 days (◇) and 40 days (✕)

The bare  $\text{TiO}_2/\text{Ti}$  composite anode had the lowest degradation efficiency. With the growth of the biofilm on the  $\text{TiO}_2/\text{Ti}$  substrate, the degradation efficiency of phenol increased gradually. Apparently the electron transfer and cell density had an important effect on degradation of the phenol. After 6 days, the bacteria were slowly attaching to the microcrystalline foundation layer, creating a poor biofilm with a low electron transfer. As can be observed in Table 6.1, the current decreased with an increase in cell density. This may be due to the diminishment of the effective surface area of the electrodes as more initial cells covered a wider surface, which interfered with the photoelectrochemical reaction of the electrode. Eventually, when the biofilm was further formed, the current production was more rapid and the maximum current production levels were higher than those obtained after the first 6

days. Thus, the biofilm formed on the TiO<sub>2</sub>/Ti composite substrate after 12 and 20 days created a synergistic effect between the carrier and the electro-active microorganisms in the biofilm, increasing the electron transfer rate. However, PEC performed with biofilm of 40 days, showed low phenol degradation. This can be attributed to the low cell count in the biofilm (shown in Table 6.1), suggesting disintegration of the biofilm.

The stability of the photo-electrode was found to be stable from previous research and no deterioration of the biofilm was noticed up to six hours of experiment for all the thicknesses of the biofilms (Bennani, et al., 2014). However, measurements of the stability of the anode could be part of the further research since any long term estimation would be difficult to assume or predict.

Table 6.1. Current density and bacterial activity of electrodes with different growth times for biofilms

Development of biofilm/day	j/mAcm <sup>-2</sup>	Total cell count of the biofilm cells x10 <sup>8</sup> cm <sup>-2</sup>	Intact cells of the biofilm/%	Total cell count of the water phase cells x10 <sup>8</sup> cm <sup>-3</sup>	Intact cells of the water phase/%
0	0.0901453	/	/	/	/
6	0.0767330	3.08	72	1.81	82
12	0.0664798	5.06	44	1.62	76
20	0.0839511	5.33	40	2.27	54
40	0.0727993	0.79	3	0.37	50

### 6.3.4. Electrochemical monitoring

The growth of biofilm on the  $\text{TiO}_2/\text{Ti}$  composite electrode was monitored with an impedance spectroscopy. Figure 7 shows the impedance measurements presented as a Nyquist plot for different growth periods (0, 6, 12, 20 and 40 days) of the mixed culture on the  $\text{TiO}_2/\text{Ti}$  composite electrode when the electrode was polarized at 1 V vs Ag/AgCl during the impedance measurement.

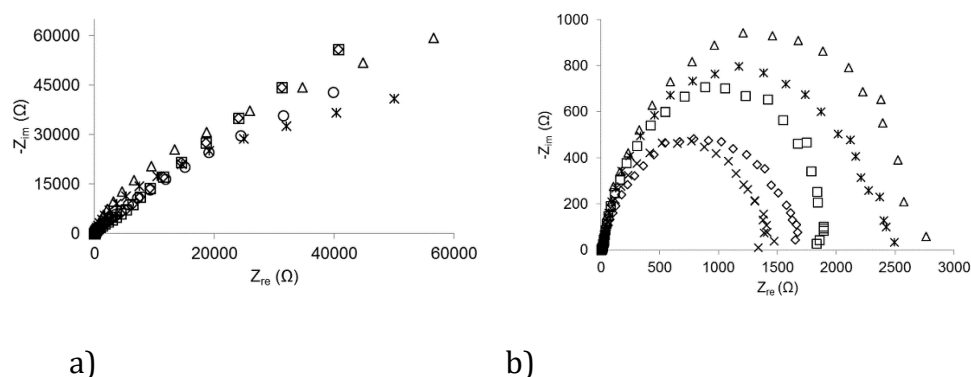


Figure 6.7. The EIS Nyquist plot of mixed-culture of electrochemically active biofilm developed for 0 (o); 6 (□); 12 (Δ); 20 (◇) and 40 (X) days the a) dark conditions and b) under solar ( $\text{UV}_{300-400}$ ) irradiation

Figure 6.7 b) exhibits the impedance measured under the simulated sunlight and compared to 6.7 a) the measured impedance in dark. The impedance measured under light conditions was sharply decreased compared to the impedance shown in the dark, indicating a decrease of charge transfer resistance; this suggests the enhancement of electro-kinetics under light due to photosynthesis. The justification for this can be the bending of the impedance arc in the low frequency ( $f$ ) region (the second arc) in the Nyquist

diagram, which indicates a process of charge transfer, while the linear relationship between the imaginary and real component of the impedance means a diffusion process controlled step. The arc radius of the measured electrodes in the Figure 6.7 a) didn't alter with the addition or growth of the biofilm.

On the other hand, from Figure 6.7 b) under the light irradiation, it can be observed that the growth and development of the biofilm reduced the charge transfer resistance. The calculated electron capacitance from Figure 6.7 was as follows:  $3.6 \times 10^{-7}$  F (6-day biofilm growth period),  $5.5 \times 10^{-7}$  F (12-day biofilm growth period),  $4 \times 10^{-7}$  F (40-day biofilm growth period),  $6.1 \times 10^{-7}$  F (no biofilm presence) and  $6.8 \times 10^{-7}$  F (20-day biofilm growth period). Lowered capacitance compared to the clean electrode after the growth period of 6 days could be attributed to partially-developed initial crystalline biofilm with poor activity. The increase in capacitance after the formation of the initial biofilm indicates adsorption of the cells on the surface of the  $\text{TiO}_2/\text{Ti}$  composite electrode.

The trend shows an increase in electron transfer with an increasing number of days for growth of electrochemically active biofilms. An increase with the increasing days of biofilm growth resulted in a higher concentration of attached bacterial cells, hence an increase in the density of the components connected in parallel, creating a higher capacity of biomaterial. It was found that higher conductive biofilms had a lower charge transfer resistance (Malvankar, et al., 2012). The oxidation of phenol by the electrochemically active biofilm generated an increasing number of electrons, which was then transferred extracellularly to the electrode. This observation can be supported by comparing Figure 6.6 and 6.7. A higher degradation efficiency of phenol can be found even with a higher electron transfer resistance and lower current density compared to the bare  $\text{TiO}_2/\text{Ti}$  electrode, especially for the anode with

the biofilm developed after 12 days, when the bacteria started to be present on the surface of the catalyst.

This observation was explained by R. Reguera by stating that microbial cells that were not in contact with the anode were present in the solution and contributed to the current production and degradation as much as the biofilm cells in direct contact with the anode (Reguera, et al., 2006). However, this statement seems unlikely due to the far-reaching aspects of the bacteria and the surface of the catalyst. A possible explanation could be that any energy barrier at the electrode surface, in this case the biofilm, is represented by charge transfer resistance. Higher degradation efficiency is proof of microbial cells performing as catalysts to oxidize organic matter. After 20 days, biofilm was fully developed on the surface of the anode and conductivity of the biofilm was high, additionally enhancing its efficiency.

#### **6.3.5. Self-cleaning and regeneration**

The result of the regeneration of the anode, which was based on the conclusions gained from the results of efficient life-time of the biofilm shown in Figures 6.6 and 6.7, led to the removal of adsorbed phenol molecules and biofilm in order to restore anode adsorptive capacity and to regenerate the current, which is illustrated in Figures 6.8 and 6.9.



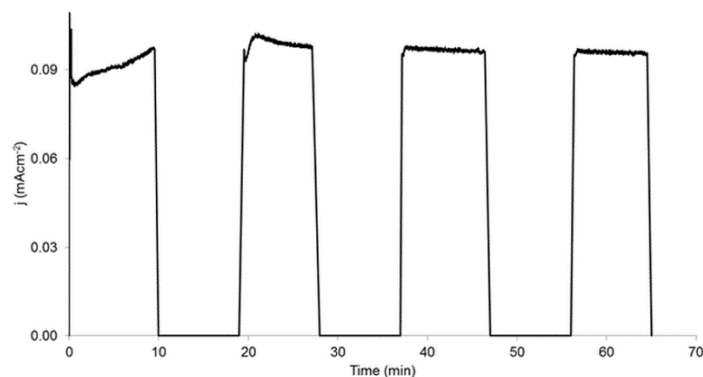


Figure 6.8. Effect of photoelectrocatalytic surface cleaning (electrode covered with biofilm grown 6 days) on the current and its regeneration using demineralized water

In the first two runs, the photoelectrocatalytic treatment was interrupted every 10 min. The surface of the  $\text{TiO}_2/\text{Ti}$  composite electrode was still covered with the biofilm which resulted in an unstable current. Unstable currents can result from uneven coverage of the initial biofilm containing little or no bacteria to transfer the electrons and enhance the process. This observation changed after 30 min of a cleaning process in demineralized water under solar light ( $\text{UV}_{300-400}$ ), where the current stabilized and the biofilm was removed.

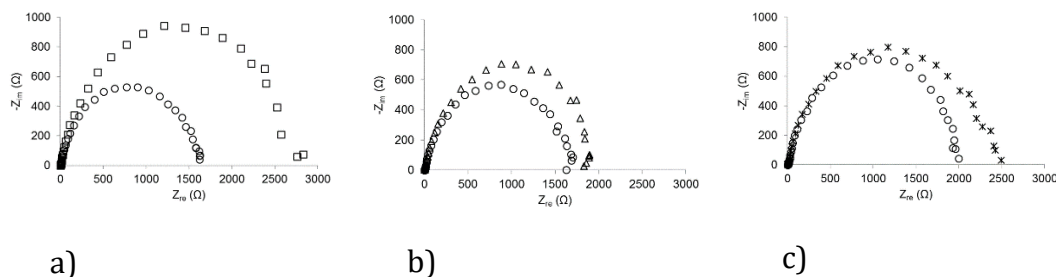


Figure 6.9. EIS Nyquist plot of  $\text{TiO}_2/\text{Ti}$  composite electrodes with mixed culture of electrochemically active biofilm developed after: a) 6 days ( $\square$ ); b) 12 days ( $\Delta$ ) and c) 40 days ( $\times$ ) and after exposure to the cleaning process ( $\circ$ ) in demineralized water under solar light ( $\text{UV}_{300-400}$ )

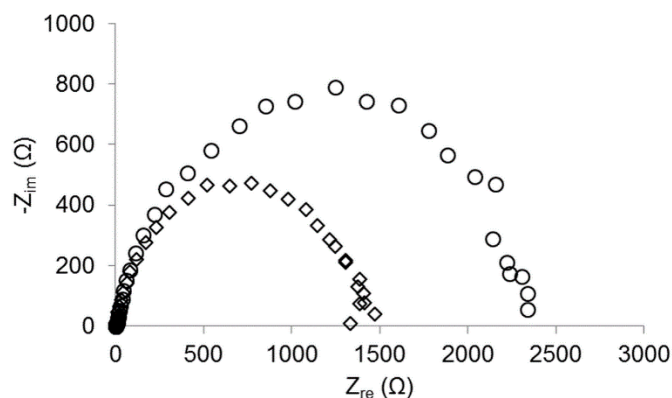


Figure 6.10. EIS Nyquist plot of  $\text{TiO}_2/\text{Ti}$  composite electrodes with mixed culture of electrochemically active biofilm developed for 20 days ( $\diamond$ ); and after exposure to the cleaning process ( $\circ$ ) in demineralized water under solar light ( $\text{UV}_{300-400}$ )

Figures 6.9 and 6.10 show the removal of attached cells and the effect of the cleaning process on the electron transfer resistance.

These figures show a comparison of the EIS response on the  $\text{TiO}_2/\text{Ti}$  composite electrode in the presence of the biofilm (6, 12, 20 and 40 days of biofilm growth) and after the cleaning process. The largest observed charge transfer resistance is a result of the biofilm developed on the electrode surface, which indicates the absence of electron transfer. However, the impedance-circle radius for biofilms grown after 6, 12 and 40 days (Figure 6.9) decreased rapidly after 1 hour of cleaning by illumination, indicating that the electrode was regenerated and no biofilm remained. A different observation can be made for the electrode that contained the biofilm with a growing period of 20 days (Figure 6.10). It is assumed that the biofilm consists of bacterial cells and the exopolysaccharide matrix with interwoven pores (Reguera, et al., 2006; Munoz-Berbel, et al., 2006; Ben-Yoav, et al., 2011). The biofilm resistance tends to decrease with an increasing growth period (Ben-Yoav, et al., 2011). When the biofilm was in a later stage, it resulted in a higher concentration of attached bacterial cells followed by an increase in biofilm density; its conductivity showed very low charge transfer resistance. By removing the biofilm, conductivity was lowered and the charge transfer resistance increased. However, at a certain point, in this case after 40 days, bacteria in the biofilm were dying, resulting in the loss of biofilm efficiency.

#### **6.4. Conclusions**

- An electrochemically active biofilm on the  $\text{TiO}_2/\text{Ti}$  composite electrode was found to increase the current density ( $8.4 \times 10^{-2} \text{ mAcm}^{-2}$ ) and charge transfer (lower impedance) and phenol degradation efficiency, confirming that electron transfer from bacteria to the electrode can be enhanced by biofilm formation on the electrode.

- A positive effect in phenol degradation efficiency (62 % after 4 hours) was observed by coupling photo(electro)catalysis and biofilm formation into one system.
- The degradation efficiency of phenol was far higher in the biofilm-electrode process than in the photocatalytic (23.2 %) and biological processes (2.3 %) within the same degradation time (four hours).
- Impedance related to biofilm was sensitive to the duration of biofilm growth (thickness) and it reached its lowest value at the optimal amount of bacteria coverage on the electrode (electrochemically active biofilm developed for 20 days).
- The performance of the electrode can be regenerated by reactivation of the  $\text{TiO}_2$  in demineralized water under solar light, making it reusable.

## References

- Balaji, K., Reddaiah, K., Reddy, T. M. & Reddy, S. R. J., 2011. Voltammetric reduction behaviour and electrode kinetics. *Port. Electrochim. Acta*, Volume 29, pp. 177-185.
- Balasubramanian, A. & Venkatesan, S., 2012. Removal of phenolic compounds from aqueous solutions by emulsion liquid membrane containing ionic liquid [BMIM]<sup>+</sup>[PF<sub>6</sub>]<sup>-</sup> in tributyl phosphate. *Desalination*, Volume 289, pp. 27-34.
- Barsoukov, E. & Macdonald, J. R., 2005. Impedance spectroscopy-theory, experiment, and applications. Hoboken: Wiley Interscience.
- Bartram, J. et al., 2003. Heterotrophic plate counts and drinking-water safety. London: World Health Organization; IWA Publishing.
- Benetton, X. D., Navarro-Ávila, S. G. & Carrera-Figueiras, C., 2010. Electrochemical evaluation of Ti/TiO<sub>2</sub>-polyaniline anodes for microbial fuel cells using hypersaline microbial consortia for synthetic-wastewater treatment. *J. New Mater. Electrochem. Syst.*, Volume 13, pp. 1-6.
- Bennani, Y., El-Kalliny, A. S., Appel, P. W. & Rietveld, L. C., 2014. Enhanced solar light photoelectrocatalytic activity in water by anatase-to-rutile TiO<sub>2</sub> transformation. *J. Adv. Oxid. Technol.*, Volume 17, pp. 285-296.
- Ben-Yoav, H., Freeman, A., Sternheim, M. & Shacham-Diamand, Y., 2011. An electrochemical impedance model for integrated bacterial biofilms. *Electrochim. Acta*, Volume 56, pp. 7780-7786.
- Bessegato, G. G., Guaraldo, T. T. & Zanoni, M. V. B., 2014. Enhancement of photoelectrocatalysis efficiency by using nanostructured electrodes, modern electrochemical methods in nano, surface and corrosion science. *InTech Open*, Volume 3, p. 271.
- Bond, D. R., Strycharz-Glaven, S. M., Tender, L. M. & Torres, C. I., 2012. On electron transport through *Geobacter* biofilms. *Chem. Sus. Chem.*, Volume 5, pp. 1099-1105.
- Broomfield, R. J., Morgan, S. D., Khan, A. & Stickler, D. J., 2009. Crystalline bacterial biofilm formation on urinary catheters by urease-producing urinary tract pathogens: a simple method of control. *J. Med. Microbiol.*, Volume 58, pp. 1367-1375.
- Chasib, K. F., 2013. Extraction of phenolic pollutants (phenol and p-Chlorophenol) from industrial wastewater. *J. Chem. Eng. Data*, Volume 58, pp. 1549-1564.

- Costerton, J. W. et al., 1995. Microbial biofilms. *Annu. Rev. Microbiol.* , Volume 49, pp. 711-745.
- Dumas, C., Basseguy, R. & Bergel, A., 2008. Electrochemical activity of *Geobacter sulfurreducens* biofilms on stainless steel anodes. *Electrochim. Acta*, Volume 53, pp. 5235-5241.
- Erable, B., Duțeanu, N. M., Ghangrekar, M. M., Dumas, C. & Scott, K., 2010. Application of electro-active biofilms. *Biofouling*, Volume 26, pp. 57-71.
- Exon, J. H., 1984. Review of Chlorinated phenols. *Vet. Hum. Toxicol.* , Volume 26, pp. 508-520.
- Fagerlind, M. G., Webb, J. S., Barraud, N., McDougald, D., Jansson, A., Nilsson, P., Harlén, M., Kjelleberg, S. & Rice, S. A., 2012. Dynamic modelling of cell death during biofilm development. *J. Theor. Biol.*, Volume 295, pp. 23-36.
- Fish, K. E., Collins, R., Green, N. H., Sharpe, R. L., Douterelo, I., Osborn, A. M. & Boxall, J. B., 2015. Characterization of the physical composition and microbial community structure of biofilms within a model full-scale drinking water distribution systems. *PLoS One*, Volume 10, p. 0115824.
- Gayán, E., Álvarez, I. & Condón, S., 2013. Inactivation of bacterial spores by UV-C light. *Innov. Food Sci. Technol.*, Volume 19, pp. 140-145.
- Kalathil, S., Khan, M. M., Ansari, S. A., Lee, J. & Cho, M. H., 2013. Band gap narrowing of titanium dioxide (TiO<sub>2</sub>) nanocrystals by electrochemically active biofilms and their visible light activity. *Nanoscale*, Volume 5, pp. 6323-6326.
- Kalathil, S., Khan, M. M., Benerjee, A. N., Lee, J. & Cho, M. H., 2012. A simple biogenic route to rapid synthesis of Au@TiO<sub>2</sub> nanocomposites by electrochemically active biofilms. *J. Nanopart. Res.*, Volume 14, pp. 1-9.
- Kalathil, S., Khan, M. M., Lee, J. & Choo, M. H., 2013. Production of bioelectricity, bio-hydrogen; high value chemicals and bioinspired nanomaterials by electrochemically active biofilms. *Biotechnol. Adv.*, Volume 31, pp. 915-924.
- Khan, M. M., Ansari, S. A., Lee, J. H., Lee, J. & Cho, M. H., 2014. Mixed culture electrochemically active biofilms and their microscopic and spectroelectrochemical studies. *ACS Sustain. Chem. Eng.*, Volume 2, pp. 423-432.
- Kougo, T., Kuroda, D., Wada, N., Ikegai, H. & Kanematsu, H., 2012. Biofouling of various metal oxides in marine environment. Aichi; Japan, s.n.

Kusic, H., Koprivanac, N. & Bozic, A. L., 2006. Minimization of organic pollutant content in aqueous solution by means of AOPs: UV- and ozone-based technologies. *Chem. Eng. J.*, Volume 123, pp. 127-137.

Liu, C., Zhao, H., Ma, Z., An, T., Liu, C., Zhao, L., Yong, D., Jia, J., Li, X. & Dong, S., 2014. Novel environmental analytical system based on combined biodegradation and photoelectrocatalytic detection principles for rapid determination of organic pollutants in wastewaters. *Environ. Sci. Technol.*, Volume 48, pp. 1762-1768.

Lovley, D. R., 2006. Bug juice: harvesting electricity with microorganisms. *Nat. Rev. Microbiol.*, Volume 4, pp. 497-508.

Malvankar, N. S., Tuominen, M. T. & Lovley, D. R., 2012. Biofilm conductivity is a decisive variable for high-current-density *Geobacter sulfurreducens* microbial fuel cells. *Energy Environ. Sci.*, Volume 5, pp. 5790-5797.

Marsolek, M. D., Kirisits, M. J. & Rottmann, B. E., 2007. Biodegradation of 2, 4, 5-trichlorophenol by anaerobic microbial communities: biorecalcitrance, inhibition, and adaptation. *Biodeg.*, Volume 18, p. 351.

Marsolek, M. D., Torres, C. I., Hausner, M. & Rittmann, B. E., 2007. Intimate coupling of photocatalysis and biodegradation in a photocatalytic circulating-bed biofilm reactor. *Biotechnol. Bioeng.*, Volume 101, pp. 83-92.

Moncayo-Lasso, A., Mora-Arismendi, L. E., Rengifo-Herrera, J. A., Sanabria, J., Benitez, N. & Pulgarin, C., 2012. The detrimental influence of bacteria (*E. coli*, *Shigella* and *Salmonella*) on the degradation of organic compounds (and vice versa) in  $\text{TiO}_2$  photocatalysis and near-neutral phot-Fenton processes under simulated solar light. *Photochem. Photobiol. Sci.*, Volume 11, pp. 821-827.

Morris, N. S., Stickler, D. J. & McLean, R. J. C., 1999. The development of bacterial biofilms on indwelling urethral catheters. *World J. Urol.*, Volume 17, pp. 345-350.

Munoz-Berbel, X., Munoz, V., Vignes, N. & Mas, J., 2006. On-chip impedance measurements to monitor biofilm formation in the drinking water distribution network. *Sens. Actuators B*, Volume 118, pp. 129-134.

Nickehslat, A., Amin, M. M., Izanloo, H., Fatehizadeh, A. & Mousavi, S. M., 2013. Phenol photocatalytic degradation by advanced oxidation process under ultraviolet radiation using titanium dioxide. *J. Environ. Public Health*, Volume 2013, p. 9.

- Nikel, P. I. & E. Martinez-Garcia, V. d. L., 2014. Biotechnological domestication of pseudomonads using synthetic biology. *Nat. Rev. Microbiol.*, Volume 12, pp. 368-379.
- NVON-Commission, 2004. Solubility of solid substances and liquids. Wolters-Noordhoff: BINAS.
- O'Toole, G., Kaplan, H. B. & Kolter, R., 2000. Biofilm formation as Microbial development. *Annu. Rev. Microbiol.*, Volume 54, pp. 49-79.
- Pant, D., Singh, A., v. Bogaert, G., Gallego, Y. A., Diels, L. & Vanbroekhoven, K., 2011. An introduction to the life cycle assessment (LCA) of bioelectrochemical systems (BES) for sustainable energy and product generation: Relevance and the key aspects. *Renew. Sust. Energ. Rev.*, Volume 15, pp. 1305-1313.
- Park, H. S., Kim, B. H., Kim, H. S., Kim, H. J., Kim, G. T., Chang, I. S., Park, Y. K. & Chang, H. I., 2001. A novel electrochemically active and Fe(III) reducing bacterium phylogenetically related to *Clostridium butyricum* isolated from microbial fuel cell. *Anaerobe*, Volume 7, pp. 297-306.
- Piciooreanu, C., Head, I. M., Katuri, K. P., v. Loosdrecht, M. & Scott, K., 2007. A computational model for biofilm-based microbial fuel cells. *Water Res.*, Volume 41, pp. 2921-2940.
- Prest, E. I., Hammes, F., Köttsch, S., v. Losdrecht, M. C. M. & Vrouwenvelder, J. S., 2013. Monitoring microbiological changes in drinking water systems using a fast and reproducible flow cytometric method. *Water Res.*, Volume 47, pp. 7131-7142.
- Rabaey, K., Boon, N., Siciliano, S. D., Verhaege, M. & Verstraete, W., 2004. Biofuel cells select for microbial consortia that self-mediate electron transfer. *Appl. Environ. Microbiol.*, Volume 70, pp. 5373-5382.
- Randviir, E. P. & Banks, C. E., 2013. Electrochemical impedance spectroscopy: an overview of bioanalytical applications. *Anal. Methods*, Volume 5, pp. 1098-1115.
- Ravichandran, A., Sugiyama, N., Tomita, M., Swarup, S. & Ishihama, Y., 2009. Ser/Thr/Tyr phosphoproteome analysis of pathogenic and non-pathogenic *Pseudomonas* species. *Proteomics*, Volume 9, pp. 2764-2775.
- Reddy, M. P., Srinivas, B., Kumari, V. D., Subrahmanyam, M. & Sharma, P. N., 2004. An integrated approach of solar photocatalytic and biological treatment of N-containing organic compounds in wastewater. *Toxicol. Environ. Chem.*, Volume 86, pp. 127-140.



- Reguera, G., Nevin, K. P., Nicoll, J. S., Covalla, S. F., Woodard, T. L. & Lovley, D. R., 2006. Biofilm and nanowire production leads to increased current in *Geobacter sulfurreducens* fuel cells. *Appl. Environ. Microbiol.*, Volume 72, pp. 7345-7348.
- Rijswick, M. v. & Havekes, H. J. M., 2012. European and Dutch Water Law. Groningen: Europa Law Publishing.
- Schloss, P. D., Gevers, D. & Westcott, S. L., 2011. Reducing the effects of PCR amplification and sequencing artifacts on 16S rRNA-based studies. *PLoS One*, Volume 6, p. 27310.
- Scott, J. P. & Ollis, D. F., 1995. Integration of chemical and biological oxidation process for water treatment; review and recommendations. *Environ. Progress.*, Volume 14, pp. 88-103.
- Shen, J., Xu, X., Jiang, X., Hua, C., Zhang, L., Sun, X., Li, J., Mu, Y. & Wang, L., 2014. Coupling of bioelectrochemical systems for p-nitrophenol removal in an upflow anaerobic sludge blanket reactor. *Water. Res.*, Volume 67, pp. 11-18.
- Song, T. S., Wu, X. Y. & Zhou, C. C., 2014. Effect of different acclimation methods on the performance of microbial fuel cells using phenol as a substrate. *Bioproc. Biosyst. Eng.*, Volume 37, pp. 133-138.
- Stickler, D. J. & Morgan, S. D., 2008. Observations on the development of the crystalline bacterial biofilms that encrust and block Foley catheters. *J. Hosp. Infect.*, Volume 69, pp. 350-360.
- Wang, Y., Claeys, L., v. d. Ha, H., Verstraete, W. & Boon, N., 2010. Effects of chemically and electrochemically dosed chlorine on *Escherichia coli* and *Legionella beliardensis* assessed by flow cytometry. *Appl. Microbiol. Biotechnol.*, Volume 87, pp. 331-341.
- Wataru, N. F. & Mitsumasa, O., 2003. Improvement of DOC removal by multi-stage AOP-biological treatment. *Chemosphere*, Volume 50, pp. 1043-1048.
- Yang, S., Lin, S., Kelen, G. D., Quinn, T. C., Dick, J. D. & Gaydos, C. A., 2002. Quantitative multiprobe PCR assay for simultaneous detection and identification to species level of bacterial pathogens. *J. Clin. Microbiol.*, Volume 40, pp. 3449-3454.
- Zhao, C. E., Wang, W. J., Sun, D., Wang, X., Zhang, J. R. & Zhu, J. J., 2014. Nanostructured graphene/TiO<sub>2</sub> hybrids as high-performance anodes for microbial fuel cells. *Chemistry*, Volume 20, pp. 7091-7097.



## PHOTOELECTROCATALYTIC OXIDATION OF PHENOL FOR WATER TREATMENT USING A $\text{BiVO}_4$ THIN-FILM PHOTOANODE

---

The removal of organics by photoelectrocatalytic oxidation offers a viable option to remove the contaminants at low concentrations. In this paper, we propose a  $\text{BiVO}_4$  thin films synthesized via spray pyrolysis for photoelectrocatalytic oxidation of phenol with solar light. We compare the properties of  $\text{BiVO}_4$  with those of the commonly used photocatalyst  $\text{TiO}_2$ . In addition,  $\text{BiVO}_4$  films with W gradient doping were fabricated and tested for improving the photocatalytic performance of  $\text{BiVO}_4$ . X-ray diffraction, atomic force microscopy, incident photon to current efficiency and spectrophotometry have been conducted for  $\text{BiVO}_4$  films of different thicknesses, as well as for  $\text{TiO}_2$ . The electrochemical impedance spectroscopy and dark conductivity measurements were conducted. Phenol removal has been measured for both the  $\text{TiO}_2$  and  $\text{BiVO}_4$  samples. The best performance was found to be for a 300 nm undoped  $\text{BiVO}_4$  film, being able to reduce the phenol concentration up to 30.0 % of the initial concentration in four hours.

### 7.1. Introduction

Access to clean water is, along with energy and food, one of the most important challenges that our society will face in the near and long term future. The degradation of many organic pollutants in water can be accomplished either by biological, physical or chemical means. The biological oxidation of pollutants is considered economically favorable, but many toxic compounds cannot be degraded by this method (Ranade & Bhandari, 2014). Physical methods such as filtration by membranes or adsorption are also widely used (Mixa & Staudt, 2008; Hameed & Rahman, 2008). However, in most cases these methods do not destroy the pollutants but only transfer them from one phase to another. Finally, chemical methods for water treatment offer a flexible and safe alternative to remove a wide variety of pollutants (Daghrir, et al., 2012). In particular, photocatalytic treatments are able to remove toxic organic compounds, including ecologically hazardous cyanides and other residual compounds, even at low concentrations, making this approach very suitable for the last stages of water purification (Pulkka, et al., 2014). In addition, sunlight is used to drive the chemical reaction has the potential to reduce the associated costs and make the process even more energy efficient.

In photocatalytic (PC) water treatment, the first step is the absorption of a photon in a photocatalyst or semiconductor, creating an electron-hole pair inside the material. Both charge carriers are then separated and migrate to the catalyst/water interface. Once the charge carrier arrives to the surface, the holes are trapped by  $\text{H}_2\text{O}$  or  $\text{OH}^-$  already adsorbed on the surface, which will produce reactive  $\cdot\text{OH}$  radicals (Lazar, et al., 2012). Due to the excellent oxidation ability of hydroxyl radicals, they will then react with the organic molecules. In some cases, the oxidation can be continued so that hydroxyl radicals mineralize organic pollutants to the final, less harmful products (Pasternak & Paz, 2013).

If the bond of the organic molecules with the surface is strong enough, they could even oxidize directly by the holes instead of the  $\cdot\text{OH}$  radicals (Kesselman, et al., 1997). However, PC faces the problem of rapid charge recombination and poor oxidation kinetics, since they are separated within the same particle or electrode, which leads to low quantum efficiency (Xiaoli, et al., 2003).

Compared to PC, in photoelectrocatalysis (PEC), photogenerated charges, once generated, they are separated to different electrode materials, where they perform the catalytic process. For example, electrons migrate towards the cathode and perform a reduction reaction, while holes remain at the surface of the anode and perform an oxidation reaction. This enhances the charge carrier separation mechanism and minimizes the recombination of electron-hole pairs, thus enhancing the degradation efficiency of the chosen pollutant (Liao, et al., 2012; Liang & Zhu, 2016; Selcuk, et al., 2003). In this method, the photoactivity strongly depends on the material properties and configuration of the electrode, as well as the presence of an applied potential (Bennani, et al., 2014; Liu & Chen, 2014).

PC and PEC treatment of organic compounds has been widely developed since the first experiments by Carey (Carey, et al., 1976). A wide variety of semiconductors have been studied for this purpose, such as  $\text{TiO}_2$ ,  $\text{ZnO}$  or  $\text{WO}_3$  (Wen, et al., 2015; Rao & Venkatarangaiah, 2014; Smith & Zhao, 2008; Smith & Zhao, 2010; Smith, et al., 2010). Although these semiconductors can be employed for water purification, they can only be excited under illumination of highly energetic light because of their large band gap energies. Therefore, UV light ( $\lambda \leq 400 \text{ nm}$ ) is commonly used in PC and PEC oxidation processes. Instead of using only UV light, utilizing the entire solar spectrum is more attractive, as it increases the amount of energy that can be converted. Using sunlight to drive the photo-oxidation of organic compounds in water makes the energy balance of this process much more favorable. Solar utilization in

PEC technologies may thus improve the process effectiveness without substantially increasing the costs of the water treatment.

Working toward this goal, much effort has been made to improve the optical absorption of catalysts for their photocatalytic activity, with metal, non-metal, or self-doping (Hameed & Rahman, 2008; Xiaoli, et al., 2003; Fakhouri, et al., 2014; Smith, et al., 2012; Smith, et al., 2012).

A simpler approach is to consider other photocatalysts based on metal oxides that are active under visible light.  $\text{BiVO}_4$ , which has previously been used for solar water splitting, is a suitable candidate due to its favorable optical and electronic properties (Li, et al., 2015; Li, et al., 2015). It has also been used for photocatalytic degradation of contaminants in a spindle-like structure modified by polyaniline ( $\text{PANI/BiVO}_4$ ), as a nanostructured electrode, and in a heterostructure as a photocatalyst for dye degradation (Abdi, et al., 2013; Shang, et al., 2009; Hou, et al., 2012). The advantage of  $\text{BiVO}_4$  over  $\text{TiO}_2$  is its lower bandgap energy (2.4 eV vs. 3.2 eV, respectively), allowing more absorption of the solar spectrum. In addition,  $\text{BiVO}_4$  thin films are relatively easy to manufacture and handle, since they can be simply deposited by spray pyrolysis (Abdi, et al., 2013). Furthermore,  $\text{BiVO}_4$  can be combined with light trapping structures such as surface texturing, already widely applied in solar cells, which are used to enhance the light absorption on thin films, reducing the need of thick absorber films (Yang, et al., 2015; Han, et al., 2014).

In this paper, we propose  $\text{BiVO}_4$  as a photoelectrode for the oxidation of phenol in water. Phenol has been chosen as a representative organic contaminant due to its toxicity at high concentrations, potential harm at low concentrations, and its easy detection using a UV/Vis spectrophotometer (Grabowska, et al., 2012). Due to the novelty associated with  $\text{BiVO}_4$  in the water treatment field, this study focuses on characterizing the  $\text{BiVO}_4$  film properties in order to explain the suitability of the material for PEC water treatment using solar illumination. The performance as a photoanode for water treatment is associated with the

optical, electrical and catalytic properties of  $\text{BiVO}_4$ . Absorption spectrophotometry characterizes the optical properties of the semiconductor. The electrical properties, which affect the charge separation process, were determined by EIS, dark conductivity and cyclic voltammetry measurements. Atomic force microscopy (AFM) was used to characterize the surface morphology of the photoelectrodes, which is also an important feature affecting the chemical activity. Furthermore, since the internal structure of the atoms can affect all of these properties, X-ray diffraction (XRD) measurements were conducted to determine the crystal phase composition of the films. Finally, the suitability of the films for water treatment was tested by determining the incident photon to current efficiency (IPCE) and the efficiency of this photocatalyst for phenol oxidation. The photoactive characteristics of  $\text{BiVO}_4$  were compared with  $\text{TiO}_2$ , one of the most widely used semiconductors for photocatalytic water treatment (Grabowska, et al., 2012; Wu, et al., 2009). In addition, a gradient doping of  $\text{BiVO}_4$  with tungsten (W) was studied to improve the charge separation in the material. This improvement can potentially promote the photocatalytic activity and degradation efficiency, as already shown for the case of solar water splitting (Abdi, et al., 2013; Abdi, et al., 2013).

## **7.2. Materials and methods**

### **7.2.1. Fabrication of the $\text{BiVO}_4/\text{FTO}$ and $\text{TiO}_2/\text{Ti}$ composite electrodes**

**$\text{BiVO}_4$  fabrication.** The  $\text{BiVO}_4$  thin films were synthesized via spray pyrolysis. The substrate was commercial Asahi UV-type (textured glass with an FTO coating), and it was cleaned using a sequence of acetone and isopropanol solutions. Prior to  $\text{BiVO}_4$  deposition, a thin layer of 5 nm  $\text{SnO}_2$  was deposited to avoid recombination in the FTO/semiconductor interface.

For the  $\text{BiVO}_4$  thin film spraying, a precursor solution was needed. The precursor solution was made by mixing a 19.4 g/L  $\text{Bi}(\text{NO}_3)_3 \cdot 5\text{H}_2\text{O}$  (98 % Alfa Aesar) solution in acetic acid (AcAc) (98 % Sigma Aldrich) with a 1.7 g/L  $\text{V}(\text{AcAc})_2$  (99 % Alfa Aesar) solution in absolute ethanol (Sigma Aldrich) in equimolar quantities.

This solution was then pumped through a nozzle and sprayed onto the substrate, which was 20 cm away from the nozzle and kept at a temperature of 450 °C. Each spray cycle consisted of 5 s of spraying at a rate of 0.2 mLs<sup>-1</sup> followed by a 55 s idle in order to allow the solvents to evaporate off the substrate, leaving behind  $\text{BiVO}_4$ . After deposition, the samples were annealed in a furnace with air. The temperature was raised to 450 °C at 5 °Cmin<sup>-1</sup> and then maintained for two hours. By modifying the spray time, different thicknesses were deposited (200 nm, 250 nm, 300 and 350 nm). The contacts were deposited as a 300 nm stripe of aluminium on the TCO by an electron beam physical vapor deposition (EBPVD). To fabricate tungsten (W)-doped  $\text{BiVO}_4$  with gradient doping from 1 % W in contact with the TCO to 0 % W at the surface, the precursor solution was made with a 1 % W content, and then V containing solution without W was added in steps. When depositing 1 % W-doped  $\text{BiVO}_4$ ,  $\text{W}(\text{C}_2\text{H}_5\text{O})_6$  was added to the  $\text{VO}(\text{AcAc})_2$  solution prior to the mixing with the  $\text{Bi}(\text{NO}_3)_3$  solution.

**TiO<sub>2</sub> fabrication.**  $\text{TiO}_2$  film electrodes were manufactured and prepared by Magneto special anodes B.V. (Schiedam, The Netherlands) according to the paint-thermal decomposition method (Beer, 1969). Electrodes coated with  $\text{TiO}_2$  film were prepared by applying a layer of a solution containing an organic, solvent-based titanium oxide precursor on a flat titanium substrate. After air drying for a several hours, the support with paint was transferred to an air-circulating oven for its first heat treatment at temperatures between 400 °C and 600 °C for two hours.



This heat treatment decomposed and oxidized the salt, giving an oxide layer. Up to six layers of paint were applied first, followed by drying and heat treatment for all the applied layers (Beer, 1969). The TiO<sub>2</sub> film electrodes were further modified by an annealing process, in order to gain the optimal ratio of anatase to rutile crystals in the TiO<sub>2</sub> structure (Bennani, et al., 2014).

The annealing treatment of the TiO<sub>2</sub> film was carried out in a furnace (NeyTech Vulcan Benchtop Muffle Furnace 3-550), according to the procedures already used in a previous study (Bennani, et al., 2014). The TiO<sub>2</sub> film was annealed for five hours at ambient pressure at 650 °C, and the temperature was ramped up at 8 °Cmin<sup>-1</sup> from room temperature. The final thickness of the TiO<sub>2</sub> was 2.04 µm and anatase to rutile ratio (A/R) was 82/18 (Bennani, et al., 2014).

### 7.2.2. Material Characterization

**X-ray diffraction (XRD).** For the BiVO<sub>4</sub> and TiO<sub>2</sub> films, quantification of the phase proportions was carried out by XRD (Bruker D8 Advanced diffractometer Bragg-Brentano with graphite monochromator and Vantec position sensitive detector) (Datye, et al., 1995). The analyses for the TiO<sub>2</sub> film were done using the method described by Spurr and Myers, which utilizes the ratio of the rutile (110) peak at 27.355  $\theta$ 2 to the anatase (101) peak at 25.176  $\theta$ 2. The X-ray film diffraction patterns were obtained using the Bruker D8 Discover with Eulerian cradle, goniometer radius 300 mm (Li, et al., 2002) The BiVO<sub>4</sub> measurements were coupled  $\theta$ - $\theta$ 2 scan 10°-110° with step size 0.034°  $\theta$ 2.

**Absorbance spectrophotometry.** The optical properties were determined by measuring the reflectance, transmittance and absorbance using the spectrophotometer PerkinElmer Lambda 950 UV/VIS. The optical bandgap of the material was determined using a Tauc plot (Tauc, et al., 1966).

In this method,  $(\alpha h\nu)^2$  is displayed against  $h\nu$ , in which  $\alpha$  is the absorption coefficient,  $h$  is Planck's constant and  $\nu$  is the frequency. Such plot shows a distinct linear regime that corresponds to the onset of the absorption. By extrapolating this linear trend to the abscissa, the energy of the optical bandgap is determined.

**Atomic force microscopy (AFM).** Surface roughness was measured by AFM (NTMDT Ntegra). Commercially available tips (Digital Instruments standard tips) were used and the surface was imaged in tapping mode.

The BiVO<sub>4</sub> films deposited on textured glass were investigated. The roughness of the film surface was quantified by means of a statistical data analysis of AFM images. The most used parameters in characterizing the surface topography are the average roughness ( $R_a$ ) and the root mean square roughness (RMS). The RMS roughness takes the mean squared absolute values of the surface roughness profile, making it more sensitive to peaks and valleys than the average roughness. RMS is particularly used to study temporal changes in the creation of a new surface as well as spatial differences when studying the surface feature using different scales (Saranya, et al., 2014).

### 7.2.3. Photoelectrochemical measurements and experiments

**Incident Photon-to-current Conversion Efficiency (IPCE).** In order to estimate the maximum possible conversion efficiency and gain more insight about the limiting factors in the photoelectrodes, IPCE was measured. The IPCE represents the fraction of incident photons that is converted to electrons (that are used to drive catalysis for PEC) and can be measured in the external circuit as a function of wavelength. An incident light beam from a Newport 6902 150 Watt Xe gas discharge lamp was modified to a single wavelength by a Oriel Cornerstone 130 monochromator and a Keithley 236 source. The measurement was done for a wavelength range from 300 nm to 600 nm with

a step size of 6 nm. The photocurrent was measured with respect to the wavelength of the incident light. The potential applied during this measurement is 1 V vs. Ag/AgCl. The photoelectrochemical cell used for the IPCE measurements consisted of a fused silica window through which the incident light entered. The working solution was contained in the central chamber into which the platinum counter electrode (CE) and the Ag/AgCl reference electrode were immersed via separate ports. A calibrated photodiode measured the intensity of the incident light.

An EG&G potentiostat controlled the potential of the photocathode and measured the current. From the obtained photocurrent the IPCE was calculated.

**Phenol degradation experiments.** Photoelectrochemical experiments for phenol degradation were carried out in a set-up consisting of a cylindrical quartz glass reactor with an effective vessel volume of 300 mL, an external solar light source Atlas solar simulator (SUNTEST XXL+), consisting of day filter, three Xenon lamps irradiating solar light (UV<sub>300-400</sub>) with intensity of 60 W/m<sup>2</sup> in the wavelength region between 300 and 400 nm and a three-electrode configuration (Liang & Zhu, 2016). The figure of the experimental setup can be found in the previous work (Liang & Zhu, 2016). The initial volume of the working solution was 250 mL phenol (≥99 %, Sigma Aldrich) with initial concentration of 20 mgL<sup>-1</sup>. Demineralized water (RiOs 5 Reverse Osmosis System) was used throughout the experiments for dilution. To eliminate the influence of solution resistance, 14.2 gL<sup>-1</sup> Na<sub>2</sub>SO<sub>4</sub> was chosen as the supporting electrolyte because it is an inert electrolyte which does not produce any reactive species during the photo(electro)lysis, except under special conditions where it may generate persulfate (Liu, et al., 2013; Qin, et al., 2016). It is possible that the presence of the inorganic ions in the reaction medium can modify the oxidation rate of the organic compounds as function of their nature and concentration (Segneanu, et al., 2013).

Inorganic anions can scavenge the  $\cdot\text{OH}$  radicals to form the corresponding anion radicals. Additionally, as function of the nature of the inorganic anions, at higher concentrations of  $0.1 \text{ molL}^{-1}$ , the inhibition order of oxidation rate is the following:  $\text{H}_2\text{PO}_4^- > \text{Cl}^- > \text{HCO}_3^- > \text{CO}_3^{2-} > \text{SO}_4^{2-}$  (Zhu, 2007; Zhu, et al., 2007). However, X. Zhu found that  $\cdot\text{OH}$  scavenging by  $\text{Cl}^-$ ,  $\text{SO}_4^{2-}$  or  $\text{HPO}_4^{2-}$  or direct oxidation of organics did not influence the reaction rate (Zhu, 2007). The 2 mL samples were collected from the reaction solution at regular time intervals (every 1 hour), added to a cuvette and measured with a UV/Vis spectrophotometer to determine the absorption/residual concentration of phenol.

The phenol concentration was monitored with a Hach Lange DR 5000 spectrophotometer by using Hach Lange cuvette tests (LCK 345 with a measuring range of  $0.05\text{-}5.00 \text{ mgL}^{-1}$ ,  $5\text{-}50 \text{ mgL}^{-1}$  and  $20\text{-}200 \text{ mgL}^{-1}$ , diazotized 4-nitroaniline method).

The photo(electro)catalytic degradation pathway for phenol under visible light irradiation in the presence of  $\text{BiVO}_4$  is presented in Figure 7.1, showing the complete mineralization process of phenol. Hydroxyl radicals produced on the photocatalyst surface react with phenol to produce hydroquinone. In addition phenol can also react with hydroxyl radicals to form resorcinol and catechol (Grabowska, et al., 2012). Hydroquinone can react with  $\text{OH}^-$  to form benzoquinone. Upon extended photo-oxidation, the benzene ring can open due to continuous oxidation, leading to the formation of aliphatic compounds, like formic acid, and ultimately mineralizing to form carbon dioxide ( $\text{CO}_2$ ) and water upon complete oxidation (Grabowska, et al., 2012).

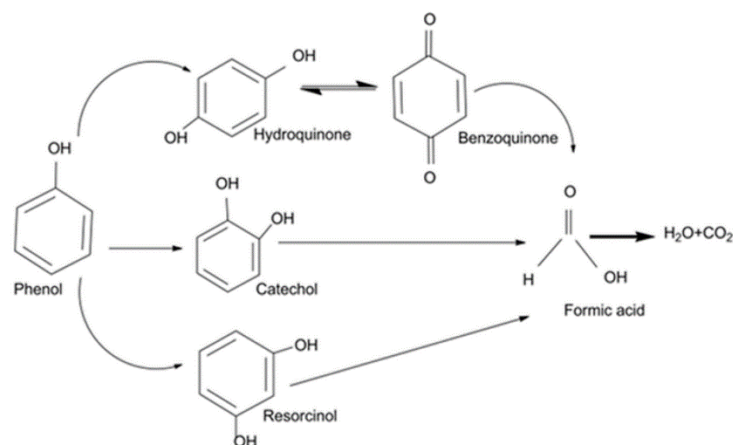


Figure 7.1. Photo(electro)catalytic degradation pathways of phenol under visible light irradiation in the presence of  $\text{BiVO}_4$

The photoanodes used in this experiment had an active surface area of  $16 \text{ cm}^2$ . At the start of each experiment, the  $\text{TiO}_2/\text{Ti}$  and  $\text{BiVO}_4$  electrodes were kept in the stirred phenol solution in the dark for one hour for adsorption to reach equilibrium. A graphite plate was used as a cathode and placed at a distance of 1 cm from the anode. The pH of the solution was kept constant at 7.2 and was measured before the experiment, using a Sentix 81 pH meter.

The temperature was maintained at  $25 \pm 1 \text{ }^\circ\text{C}$  by recirculating cooling water in a water bath equipped with a cooler (Julabo, FL300). During the experiments, the reactor was closed using a UV permeable quartz lid to prevent phenol from evaporating. The electrode potential and working current were controlled with a potentiostat-galvanostat system (Autolab PGSTAT128N with a BOOSTER10A). An  $\text{Ag}/\text{AgCl}$  (0.230 V vs. Standard Hydrogen Electrode (SHE)) electrode was used as the reference electrode. Nova Software provided the electrochemistry routine software, which included chronoamperometry (CA), cyclic voltammetry (CV) and EIS.

The phenol photodegradation experiments using  $\text{BiVO}_4$  were performed by applying different potentials, ranging from 0 to 1.2 V (vs Ag/AgCl, KCl saturated), to determine the optimum working point. The optimal potential for  $\text{TiO}_2/\text{Ti}$  composite electrode of 1 V (vs Ag/AgCl, KCl saturated) was taken from previous studies (Bennani, et al., 2014). Dark current and photocurrent were recorded, and the net current was then calculated by subtracting dark current from photocurrent in order to determine the photoactivity of the films.

**Electrochemical Impedance Spectroscopy (EIS).** The photoelectrochemical performance is largely dependent on charge transfer and the level of recombination of the photocatalyst (Balaji, et al., 2011). EIS was used to analyze the charge carrier transfer and recombination processes at the photocatalyst/electrolyte interface (Dumas, et al., 2008). Impedance is represented as a complex number, where the reactance is the imaginary part and the resistance is the real part. The real part is plotted on the x-axis and the imaginary part is plotted on the y-axis (Balaji, et al., 2011).

The EIS was conducted while maintaining a direct current voltage between the working electrode and the reference electrode. EIS was performed at a potential of 1 V versus Ag/AgCl, with a perturbation amplitude of 0.1 V and in the range of frequencies from  $10^5$  to 0.01 Hz. The values were measured in both dark and light periods. To interpret the EIS data, the electrochemical system was simplified to an equivalent electrical circuit model. This model uses a combination of resistance, capacitance and other electrical elements, which have a clear physical meaning, related with the response of the electrochemical system (Grabowska, et al., 2012). In this work the characteristic equivalent circuit model presented in Figure 7.2 was used. The simple circuit consists of a series resistor ( $R_s$ ) connected to a resistor ( $R_p$ ) and capacitor ( $C_p$ ) in parallel. This circuit model has been used to describe a similar EIS responses (Park, et al., 2001).

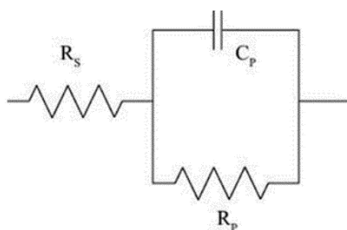


Figure 7.2. The equivalent circuit model representing the EIS response of the films

The impedance is expressed in a Nyquist plot. The left intersection with the x-axis is the solution resistance ( $R_s, \Omega$ ) and the diameter of the semicircle is the charge-transfer resistance ( $R_p, \Omega$ ).

The double-layer capacitance is equal to:

$$C_{dl} = \frac{1}{\omega \cdot R_{ct}}$$

where  $\omega=2\pi f$  is the angular frequency and  $f$  [Hz] is the frequency at the top of the semicircle (Park, et al., 2001).

### 7.3. Results and discussion

The performance of  $\text{BiVO}_4$  as a photoanode for water treatment depends partly on the optical properties of the material. The light absorption of the different photocatalysts studied is shown in Figure 7.3, as well as the reflectance and transmittance of each sample. Using a Tauc plot, it was determined that the optical bandgap of the undoped  $\text{BiVO}_4$  is  $2.47 \pm 0.02$  eV, while  $\text{TiO}_2$  has a bandgap of 3.30 eV. The band gap energy of the 1 % W gradient doped samples (2.53 eV) was found to be slightly bigger than the one for undoped  $\text{BiVO}_4$  (2.47 eV).

At longer wavelengths than those corresponding to the bandgap (lower energies), the observed absorption is attributed to the substrate, namely FTO coated textured glass for BiVO<sub>4</sub> and Ti plate for the TiO<sub>2</sub>/Ti composite. This would explain the much higher values in the case of the TiO<sub>2</sub>/Ti. Regarding the thickness of the BiVO<sub>4</sub> films, it could be expected that the thicker the film, the higher the light absorption. However, in this case the highest light absorption was obtained with a 250 nm BiVO<sub>4</sub> sample. The slightly lower absorption in the thicker 300 nm BiVO<sub>4</sub> could be explained by the reflection and transmittance measurements (Figure 7.3 b)). The reflection of the 300 nm BiVO<sub>4</sub> was higher with respect to the other two thicknesses, suggesting that at 300 nm the surface structure could have changed, as also can be seen for the 350 nm sample, leading to an increased reflectance and reduced light absorption. This effect was seen in all three samples made of undoped 300 nm BiVO<sub>4</sub> film and not in the samples made at other thicknesses. However, the phenomenon of higher reflectance at certain thicknesses was not observed in the case of tungsten (W) doped BiVO<sub>4</sub> samples (Figure 7.3 a)), in which the light absorption follows the trend of the increasing thickness of the film.



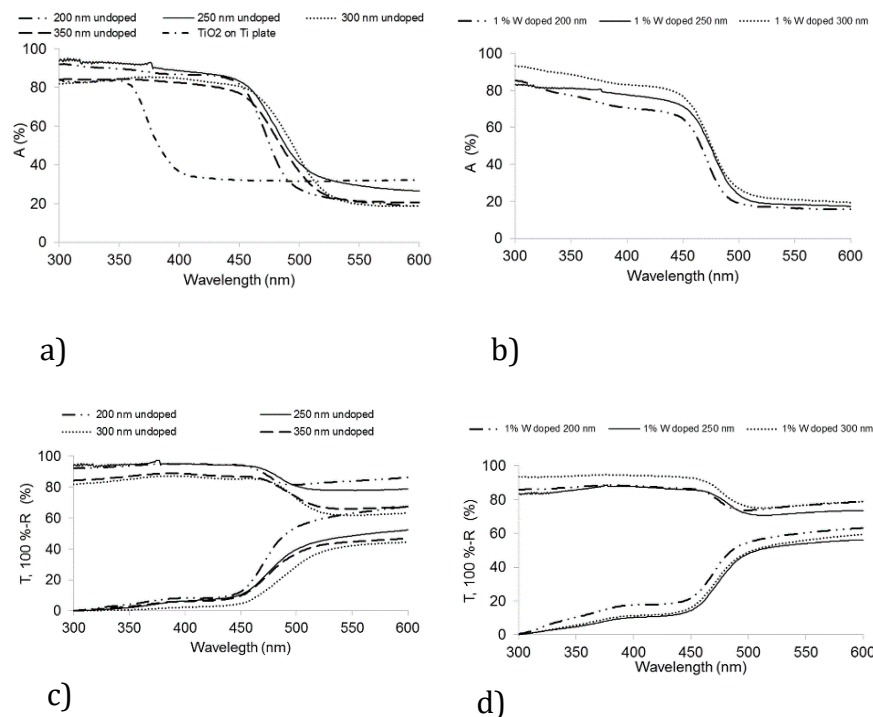


Figure 7.3. Absorption of light on a) both TiO<sub>2</sub>/Ti composite and undoped BiVO<sub>4</sub> films, b) and 1 % W gradient doped BiVO<sub>4</sub> films, and Reflectance and Transmittance of c) undoped and d) 1 % W gradient doped BiVO<sub>4</sub> at different wavelengths.

It is known from the photovoltaic field that the surface texture highly affects the optical properties of devices, especially of thin film devices (Dumas, et al., 2008; Yang, et al., 2015). Therefore, to assess the role of the surface roughness on the optical properties seen in the absorption measurements, AFM measurements were performed. In addition to the optical effects, the semiconductor surface area is also important for the electrode activity, since the area in contact with the electrolyte should be increased to enhance the number of catalytically active sites. Thus, a higher surface area will generally translate into higher reaction rates.

Figure 7.4 shows the AFM measurements of the different  $\text{BiVO}_4$  samples to determine how the surface characteristics change with thickness and doping. It can be seen that the surface roughness of undoped samples increases with thicknesses up to 300 nm and then decreases. These differences add to the hypothesis that varying surface texturing at different thicknesses affects the optical properties. The relatively flat roughness of the undoped 350 nm sample would correspond to the relatively high reflectance with respect to the other samples seen in Figure 7.3 c).

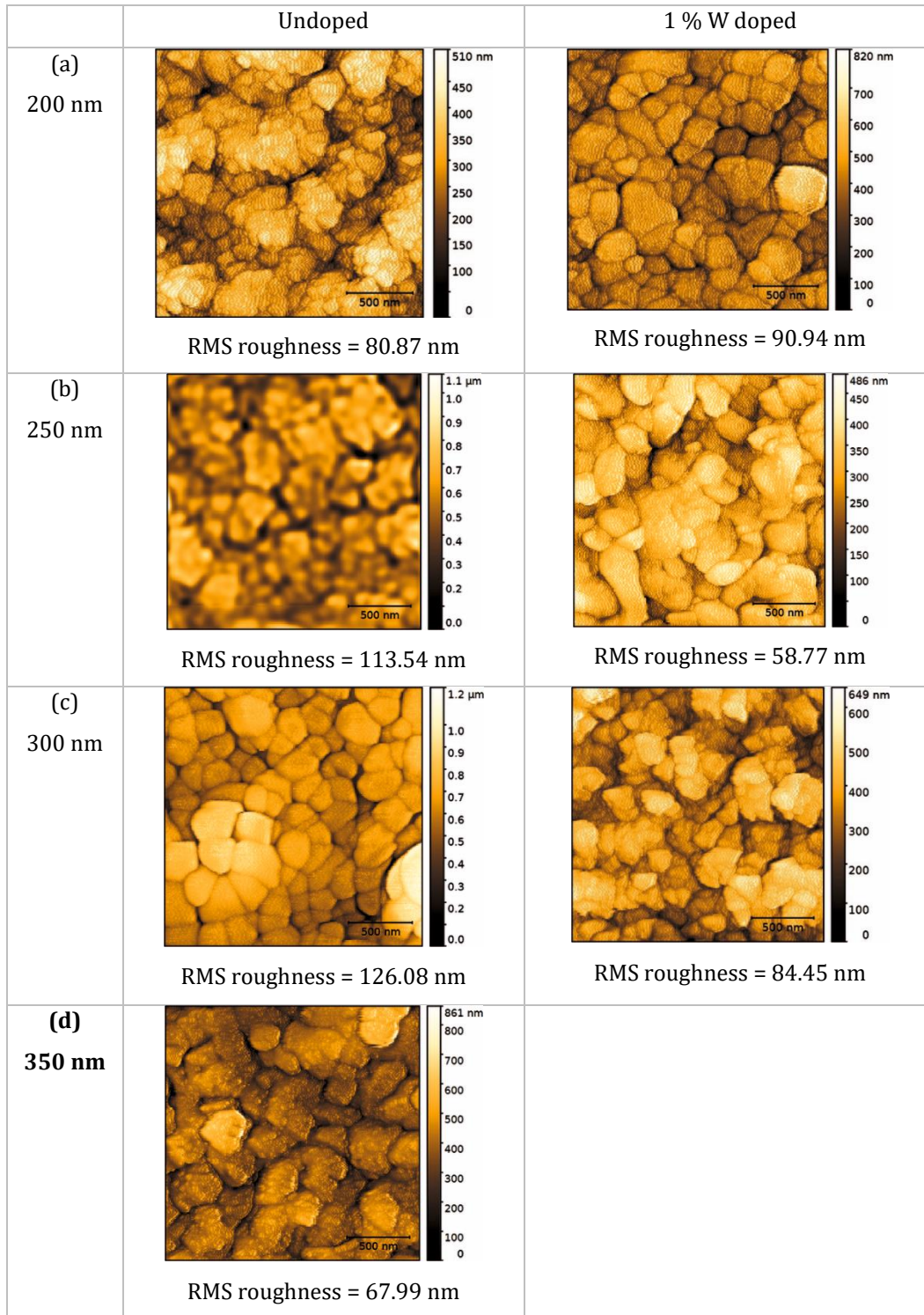


Figure 7.4. AFM scans from the different thicknesses a) 200 nm, b) 250 nm, c) 300 nm and d) 350 nm for 1 % gradient W doped and undoped BiVO<sub>4</sub>

The reasons for this surface change might be related to the phases present in the film. To determine that, the crystal structure was studied. The crystal properties of the films were determined using XRD. The two possible structures for the synthesized  $\text{BiVO}_4$  are tetragonal crystals or monoclinic scheelite (Yan, et al., 2015). Monoclinic scheelite has more local distortion, which is claimed to result in a higher photocatalytic activity due to an increase in local polarization (Tokunaga, et al., 2001). Figure 7.5 shows the XRD pattern of doped and undoped  $\text{BiVO}_4$  at different thicknesses, where the vertical lines represent the characteristic peaks of monoclinic scheelite and the dots represent the FTO peaks (Abdi, 2013). The interpretation of these samples suggests that the amount of monoclinic scheelite increased when the thickness of the sample increased up to 300 nm, being especially noticeable for the undoped samples. That could also explain the differences in reflection and transmission seen in Figure 7.3 b). The crystal structure depends on the heating process during fabrication and subsequent annealing (Mixa & Staudt, 2008). This phenomenon may thus be caused by the fact that thicker samples have a longer deposition time, and therefore they are exposed to high temperatures for a longer time. Additionally, inhomogeneities in the annealing process due to the possible temperature profiles could have an effect on the crystal structure.

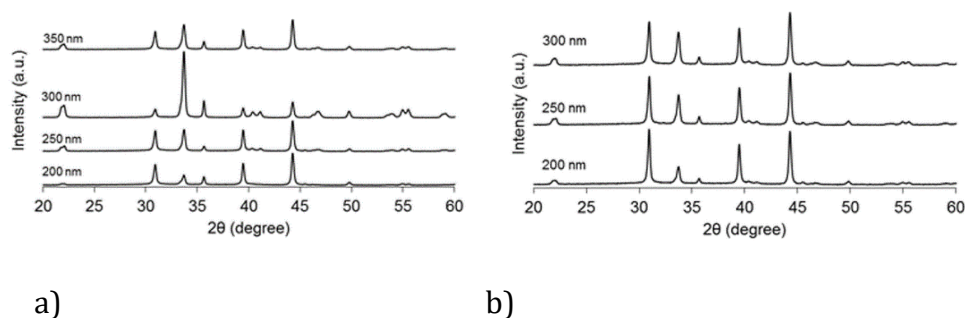


Figure 7.5. XRD pattern of samples of  $\text{BiVO}_4$  a) undoped and b) 1 % W gradient doped on FTO. The dotted peaks represent the FTO peaks and the vertical lines represent the monoclinic scheelite peaks. The intensity of the XRD signal has been adapted to fit in the graph, but it must be noted that the signal of all the FTO peaks is approximately the same in all cases since the substrate is the same, and thus they must be taken as a reference.

From these values, it can be seen what the 300 nm undoped  $\text{BiVO}_4$  presents a much higher monoclinic scheelite peak than the rest of the samples, suggesting that at 300 nm, a phase change occurred, showing a bigger amount of monoclinic scheelite in the film. Also, it is important to note that the 1 % W gradient doped samples have a lower peak height than the undoped samples, suggesting that the W doping affected the crystal properties of the material. In addition, a slight increase of the peak intensity of the 1 % W doped samples can be observed with increasing thicknesses.

Since  $\text{BiVO}_4$  is being used as a photoelectrode, the PEC oxidation process involves not only the optical and surface properties, but also the electrical properties. Figure 7.6 shows the Nyquist plot of the undoped and doped  $\text{BiVO}_4$  thin films.

The doped samples mostly showed a lower  $Z''$  for lower thicknesses compared to the undoped samples, which is related to the improved charge carrier separation by the electric field created inside the film with doping. However, the resistance in the 300 nm doped samples is the highest among all the samples. That is associated with the increase of defects by doping and the reduction of the diffusion length of the charge carriers. Regarding the thickness dependence of undoped samples, the resistance to charge transport reduced with increasing thickness, especially in the case of 300 nm. This might be related to a higher conductivity of the monoclinic scheelite. However, for doped samples the resistance to charge transfer increased with increasing thickness. When introducing doping, more defects were created in the film, reducing the diffusion length of the charge carriers inside the material which thereby increases the  $Z'$  impedance.

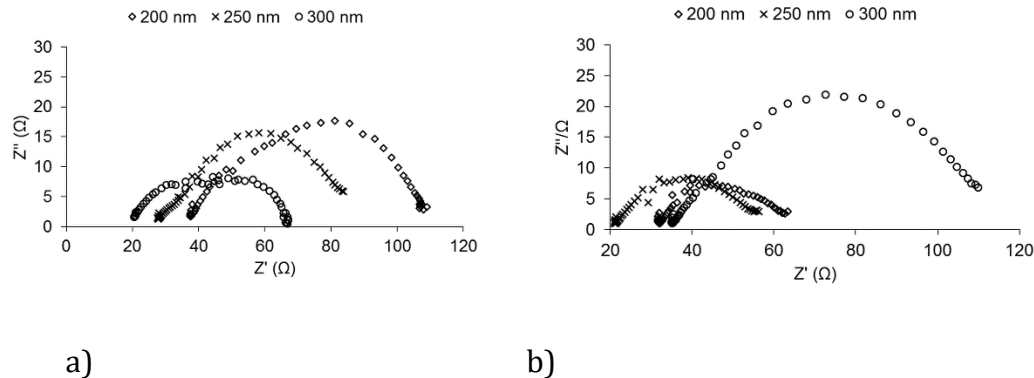


Figure 7.6. EIS measurements of a) undoped  $\text{BiVO}_4$  and b) 1 % W gradient doped  $\text{BiVO}_4$  samples in phenol solution under solar light

Another outcome from the EIS study is related to the solution resistance ( $R_s$ ). Despite the solution being the same in all cases, there is a shift in the origin of the curve (Figure 6 a) and b)) related to variations in  $R_s$ .

These changes are associated with variations in the surface because of structural changes in the material phase, as shown previously.

Finally, the photoresponse of  $\text{BiVO}_4$  is an important measure to determine how well the optical and electrical properties translate into the actual photoelectrochemical performance. Due to the electrical defect structure of the material, not all the energy of an absorbed photon was converted directly into current. The IPCE, shown in Figure 7.7, gives more information about the actual conversion efficiency from photons into current that is used in the chemical reaction. Due to the bandgap of each material,  $\text{TiO}_2$  produced a measurable current only at wavelengths lower than 400 nm, with a peak at a wavelength between 350 and 370 nm (Figure 7.7 a)). Undoped  $\text{BiVO}_4$  films showed a peak around 450 nm, due to its lower band gap energy compared to  $\text{TiO}_2$ . Increasing the thickness of the undoped  $\text{BiVO}_4$  film increased the IPCE response due to the higher light absorption of the material. The doped samples showed a better IPCE response for the 200 nm, mainly due to the enhancement of the charge carrier separation. However, when the thickness is increased, the IPCE decreased. This could be sign of electron transport loss occurring by enhanced electron generation at higher  $\text{BiVO}_4$  loading and doping. The mentioned phenomena reflect that there is an additional resistance between interconnected  $\text{BiVO}_4$  structures and doped elements which can be seen in Figure 7.6 b) as an increase in impedance with increase of the thickness layer, suggesting a higher recombination of the charge carriers (Son, et al., 2012).

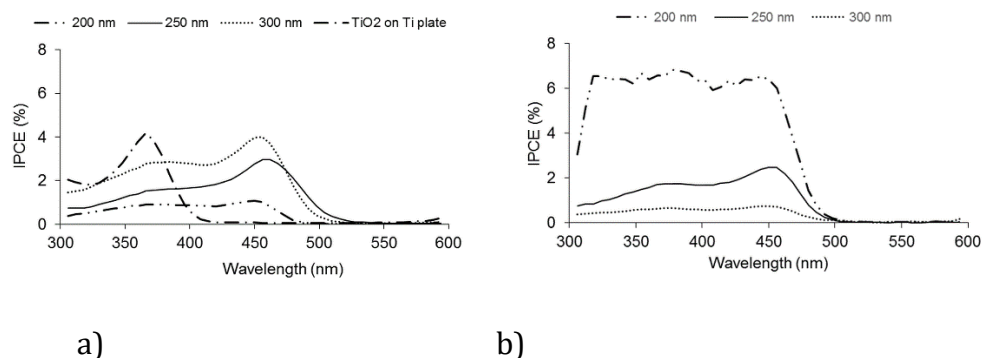


Figure 7.7. IPCE measurements for a)  $\text{TiO}_2$  and  $\text{BiVO}_4$  undoped and b)  $\text{BiVO}_4$  1 % W gradient doped electrodes using front illumination

The optical, structural and electrical properties have been summarized in Figure 7.8. The absorption and IPCE values shown in this graph are taken at a wavelength of 450 nm because, since it is slightly above the bandgap energy, it can be used as a comparison of the absorption for the different samples. To compare the different XRD measurements, the monoclinic scheelite peak at 35.68 degrees has been normalized with the FTO peak at 30.92 degrees. These peaks have been chosen as representative of the amount of monoclinic scheelite in  $\text{BiVO}_4$  because of their unlikely interaction with other peaks.

It can be seen in Figure 7.8 a) that the optical bandgap does not significantly change with thickness or doping. The absorption at a wavelength of 450 nm increased with thickness for the doped samples, but showed a maximum at 250 nm for the undoped samples. The peaks at 300 nm in the RMS roughness and XRD peak suggest that there was a change in the structure and surface morphology after 300 nm that translate in a reduction of absorption and increase in reflection.



The IPCE measurements showed an increase with thickness for undoped samples and a decrease for 1 % W gradient doped samples. This results are in agreement with the EIS measurements, which showed a decrease in electrical resistance in undoped samples with thickness, and an increase in 1 % W gradient doped films. This suggests that the doping profile introduced more defects in the material, creating new recombination centers, without enhancing the charge carrier separation.

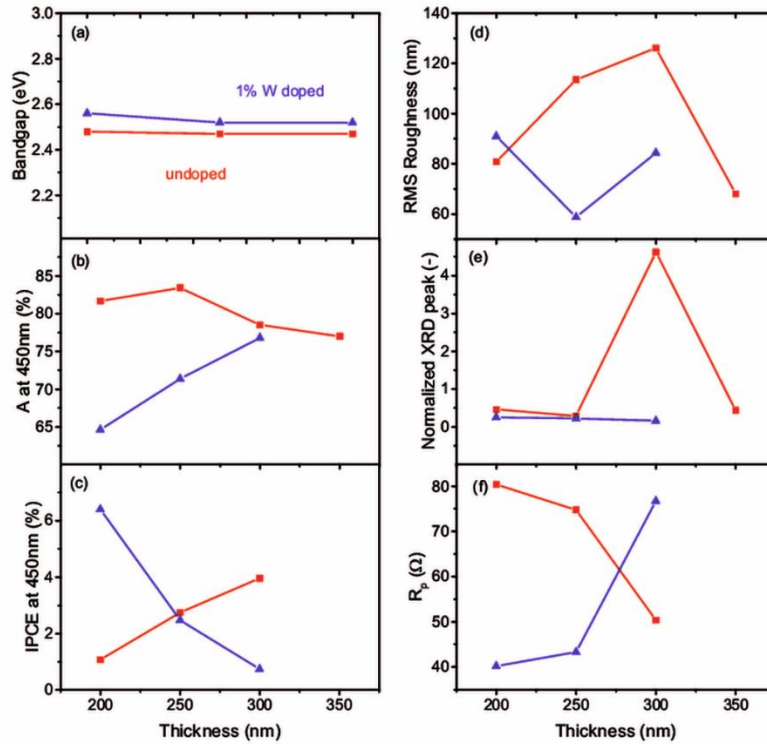


Figure 7.8. Summary and comparison of the measured properties for both 1 % W gradient doped (blue) and undoped BiVO<sub>4</sub> samples (red). a) Optical bandgap, b) Absorption taken at a wavelength of 450 nm, (c) IPCE taken at a wavelength of 450 nm, d) RMS roughness, e) XRD monoclinic scheelite peak normalized with the FTO peak, and f) R<sub>p</sub> electrical resistance calculated from EIS measurements

The current density vs. potential ( $JV$ ) plots of the photodegradation of phenol give more information on the optical, electrical and catalytic properties of the photoelectrodes. Figure 7.9 shows that the  $\text{BiVO}_4$  doped samples had the best  $JV$  characteristic, i.e. they demonstrate the lowest onset potential and highest current densities, followed by the  $\text{BiVO}_4$  undoped samples and finally the  $\text{TiO}_2$  samples. For undoped samples, the current corresponds with the fraction of monoclinic scheelite in the film, having 200 nm and 250 nm similar currents while the 300 nm shows a higher current. For the doped samples, the currents are higher due to the superior charge separation strategies. The current density increased from 200 nm to 250 nm due to the enhanced light absorption, and decreased after 250 nm due to the higher recombination caused by the doping, as seen in the EIS measurements. In this case, the crystalline structure does not play a big role because the fraction of monoclinic scheelite in all 1 % W gradient doped samples was similar, as shown by the XRD measurements.

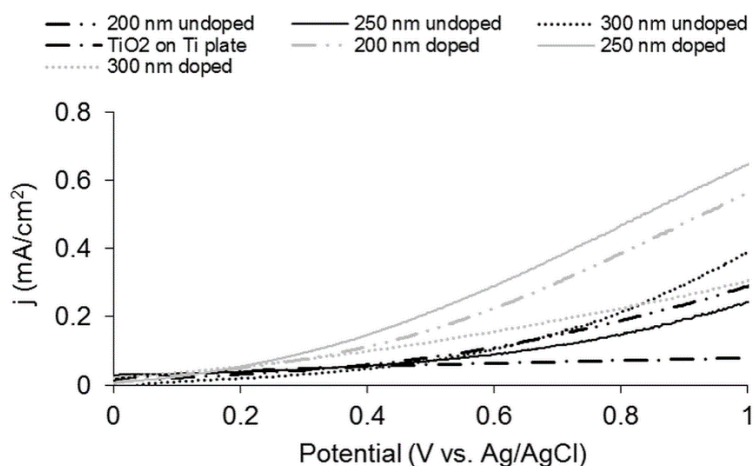


Figure 7.9.  $JV$  characteristics for the doped, undoped  $\text{BiVO}_4$  and  $\text{TiO}_2$  samples

However, a higher current density does not automatically translate in an improvement of the phenol degradation characteristics, and the actual degradation achieved must be measured. In order to perform degradation experiments, the optimum applied voltage was determined by using the undoped 300 nm BiVO<sub>4</sub> sample and by determining the highest kinetics of the phenol degradation reaction. Figure 7.10 shows the effect of the applied potential E on the first-order degradation rate constant k of phenol using the 300 nm BiVO<sub>4</sub> electrode after solar irradiation for four hours. The experiments were conducted by applying electrical biases of 0, 0.2, 0.4, 0.6, 0.8, 1 and 1.2 V (vs Ag/AgCl, KCl saturated). The applied potential causes an increase in the charge carrier separation. The rate constants of the phenol degradation with different constant potentials, k, were calculated through the linear relationship between  $\ln([C_6H_5O]/[C_6H_5O]_0)$  and time. Figure 7.10 b) shows that when the applied bias potential was low (<1.0 V vs Ag/AgCl), the degradation rate constant increased with the applied potential. A further increase in the applied potential beyond 1 V vs. Ag/AgCl led to a decrease in the first-order degradation rate constant, possibly due to competing reactions such as water splitting. The data showed that at the potential of 1 V vs. Ag/AgCl, the highest constant rate of phenol degradation was obtained. Therefore, this potential was used in further degradation experiments.

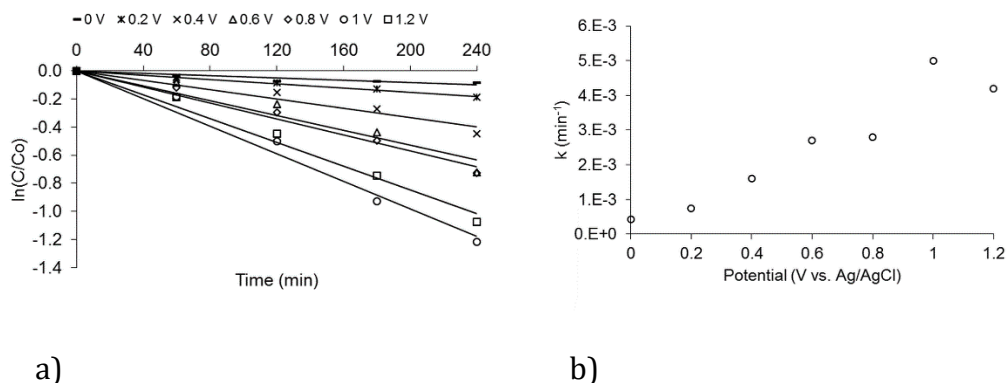


Figure 7.10. a) Corresponding kinetics plots for first-order reaction of phenol degradation rate constant for the undoped 300 nm  $\text{BiVO}_4$  photoanode at different applied potential; b) rate constant  $k$  achieved as a function of a potential

When the phenol degradation is measured at 1 V vs. Ag/AgCl at different thicknesses, undoped samples (Figure 7.11 a)) showed the maximum performance at 300 nm, after which the fraction of monoclinic scheelite decreased, affecting the phenol degradation. Increasing the thickness of the doped samples (Figure 7.11 b)) improved the performance, which is in agreement with IPCE. However, the differences between 250 nm and 300 nm were small, suggesting that there is a saturation point after which a thicker film does not improve the phenol degradation any more. The main reason for this improvement with thickness is the enhanced light absorption and conversion efficiency. EIS measurements showed a higher resistance for the thicker films in the 1 % W gradient doped case, which is not reflected in the phenol degradation characteristic, suggesting that the electrical properties are not the limiting factor in this case.

The observed optimal thickness was 300 nm, both for doped and undoped samples, which balances the trade-off between good optical properties with good electrical properties. The results suggest that the monoclinic scheelite crystal structure could be the preferred one for degradation, since it shows better optical, electrical and catalytic properties both on the surface and in the bulk of the material. For the photodegradation experiments pure photobleaching was excluded as previous work on photoluminescence (PL) and use of terephthalic acid (TA) has shown the qualitative determination of  $\cdot\text{OH}$  generated during the experiments at the surface of the catalyst.

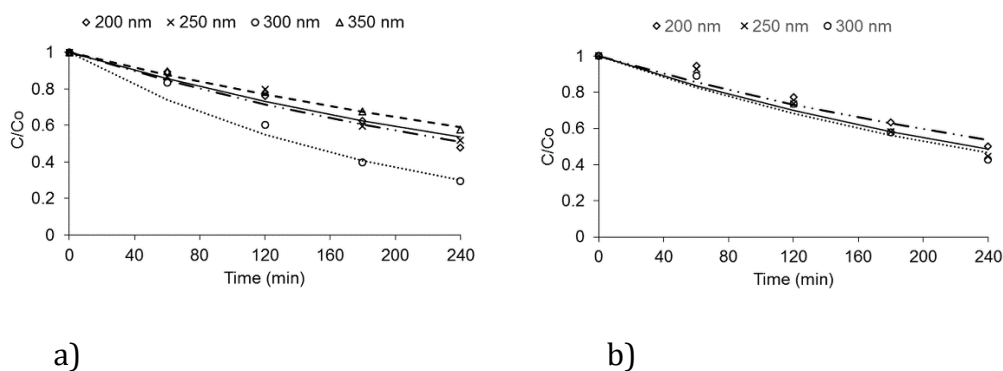


Figure 7.11. PEC degradation of phenol by using  $\text{BiVO}_4$  photoelectrodes with according 1<sup>st</sup> order kinetics for a) undoped  $\text{BiVO}_4$ , b) 1 % W gradient doped  $\text{BiVO}_4$  at different thicknesses

The suitability of  $\text{BiVO}_4$  as a photoanode for water treatment and the effect of doping in the material can be further determined by comparing the best thickness of 300 nm for both undoped and 1 % W gradient doped  $\text{BiVO}_4$ , and the performance of  $\text{TiO}_2/\text{Ti}$  composite. When comparing  $\text{BiVO}_4$  and  $\text{TiO}_2$ , Figure 7.12 confirms that  $\text{BiVO}_4$  was more suited for phenol removal from the solution by using solar light.

The optimal  $\text{BiVO}_4$ , 300 nm of undoped film, was able to reduce the phenol concentration, having 30 % of the initial concentration remaining after four hours, while the  $\text{TiO}_2/\text{Ti}$  composite electrode was only able to reduce the concentration up to 56 % of the original value during the same time span. The 1 % W gradient doping appeared not to improve the performance compared to undoped  $\text{BiVO}_4$ . The fitting for both 1 % W gradient doped and undoped  $\text{BiVO}_4$  was obtained with a first order reaction, with  $R^2$  values of 0.96 and 0.98, respectively. The reaction rate constants were  $0.0032 \text{ min}^{-1}$  for the 1 % W gradient doped samples,  $0.005 \text{ min}^{-1}$  for the undoped samples, and  $0.0024 \text{ min}^{-1}$  for the  $\text{Ti}/\text{TiO}_2$  composite, confirming that the 300 nm undoped  $\text{BiVO}_4$  gives the best reaction rates. The lower performance for the gradient doped samples could be due to two effects: the additional defects introduced in the structure by W atoms, which may lead to recombination centers and therefore poor electrical properties; and the surface and structural effects, as seen by the AFM scans and XRD spectra, which lead to less favorable catalysis at lower monoclinic scheelite fractions.

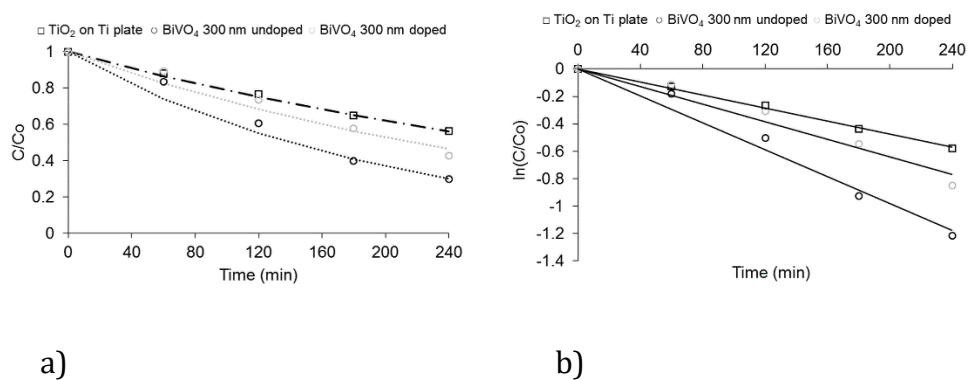


Figure 7.12. Comparison of the a) PEC degradation of phenol and b) corresponding kinetics plots for first order reaction of phenol degradation rate constant for the 300 nm thick 1 % W gradient doped and undoped  $\text{BiVO}_4$  with  $\text{TiO}_2/\text{Ti}$  composite

#### 7.4. Conclusions

BiVO<sub>4</sub> has been proposed as a viable option for photocatalytic oxidation using solar light, as opposed to the commonly used TiO<sub>2</sub>. The material studies have shown that BiVO<sub>4</sub>, with a bandgap of 2.5 eV, is a good absorber for solar light compared to TiO<sub>2</sub>. The BiVO<sub>4</sub> thickness had an effect on the optical properties due to enhanced absorption, but also suggested a phase change between 250 and 300 nm thick films. This change in phase and surface structure was confirmed by AFM and XRD measurements. BiVO<sub>4</sub> also showed a better phenol degradation performance compared to TiO<sub>2</sub>, confirming that the enhanced light absorption, surface properties and electrical properties translates in an increase in phenol degradation. Doping of the BiVO<sub>4</sub> with tungsten, however, did not improve the phenol degradation performance, suggesting that charge carrier separation is not a limiting factor in this system. The best performance was achieved by an undoped BiVO<sub>4</sub> film of 300 nm, reducing the phenol concentration in solution to 30.0 % of the initial concentration in four hours.

## References

- Abdi, F. F., 2013. Towards highly efficient bias-free solar water splitting, Delft: Delft University of Technology.
- Abdi, F. F., Firet, N. & Krol, R. v. d., 2013. Efficient BiVO<sub>4</sub> thin film photoanodes modified with cobalt phosphate catalyst and W-doping. *ChemCatChem*, Volume 5, pp. 490-496.
- Abdi, F. F., Han, L., Smets, A., Zeman, M., Dam, B. & and v. d. Krol, R., 2013. Efficient solar water splitting by enhanced charge separation in a bismuth vanadate-silicon tandem photoelectrode. *Nat. Commun.* , Volume 4, p. 2195.
- Balaji, K., Reddaiah, K., Reddy, T. M. & Reddy, S. R. J., 2011. Voltammetric reduction behaviour and electrode kinetics. *Port. Electrochim. Acta*, Volume 29, pp. 177-185.
- Beer, H., 1969. Improvements in or relating to electrodes for electrolysis. s.l. Patent No. GB1 Patent; 147; 442.
- Bennani, Y., Appel, P. & Rietveld, L. C., 2015. Optimisation of parameters in a solar light-induced photoelectrocatalytic process with a TiO<sub>2</sub>/Ti composite electrode prepared by paint-thermal decomposition. *J. Photochem. Photobiol. A*, Volume 305, pp. 83-92.
- Bennani, Y., El-Kalliny, A. S., Appel, P. W. & Rietveld, L. C., 2014. Enhanced solar light photoelectrocatalytic activity in water by anatase-to-rutile TiO<sub>2</sub> transformation. *J. Adv. Oxid. Technol.*, Volume 17, pp. 285-296.
- Carey, J., Lawrence, J. & Tosine, H., 1976. Photodechlorination of PCB's in the presence of titanium dioxide in aqueous suspensions. *Bull. Environ. Contam. Toxicol.* , Volume 16, pp. 697-701.
- Daghrir, R., Drogui, P. & Robert, D., 2012. Photoelectrocatalytic technologies for environmental applications. *J. Photochem. Photobiol. A*, Volume 238, pp. 41-52.
- Datye, A. K., Riegel, G., Bolton, J. R., Hunag, M. & Prairie, M. R., 1995. Microstructural characterization of a fumed titanium dioxide photocatalyst. *J. Solid State Chem.*, Volume 115, pp. 236-239.



Dumas, C., Basseguy, R. & Bergel, A., 2008. Electrochemical activity of *geobacter sulfurreducens* biofilms on stainless steel anodes. *Electrochim. Acta*, Volume 53, pp. 5235-5241.

Fakhouri, H., Smith, W., Pulpytel, J., Zolfaghari, A., Mortaheb, H., Meshikini, F., Jafari, R. & Arefi-Khonsari, F., 2014. Visible light water splitting and enhanced UV photocatalysis from nitrogen doped TiO<sub>2</sub> thin films. *Appl. Catal. B*, Volume 144, pp. 12-21.

Grabowska, E., Reszcyńska, J. & Zaleska, A., 2012. Mechanism of phenol photodegradation in the presence of pure and modified- TiO<sub>2</sub>: A review. *Water Res.*, Volume 46, pp. 5453-5471.

Hameed, B. H. & Rahman, A. A., 2008. Removal of phenol from aqueous solutions by adsorption onto activated carbon prepared from biomass material. *J. of Hazrd. Mater.*, Volume 160, pp. 576-581.

Han, L., Abdi, F. F., v. d. Krol, R., Liu, R., Huang, Z., Lewerenz, H. J., Dam, B., Zeman, M. & Smets, A. H., 2014. Efficient water splitting device based on bismuth vanadate photoanode and thin film silicon solar cells. *ChemSusChem*, Volume 7, pp. 2832-2838.

Hou, L., Yang, L., Li, J., Tan, J. & Yuan, C., 2012. Efficient sunlight-induced methylene blue removal over one-dimensional mesoporous monoclinic BiVO<sub>4</sub> nanorods. *J. Anal. Methods Chem.*, Volume 2012, p. 345247.

Kesselman, J. M., Weres, O., Lewis, N. S. & Hoffmann, M. R., 1997. Electrochemical production of hydroxyl radical at polycrystalline Nb-Doped TiO<sub>2</sub> electrodes and estimation of the partitioning between hydroxyl radical and direct hole oxidation pathways. *J. Phys. Chem. B*, Volume 101, pp. 2637-2643.

Lazar, M. A., Varghese, S. & Nair, S. S., 2012. Photocatalytic water treatment by titanium dioxide: recent updates. *Catalysts*, Volume 2, pp. 572-601.

Liang, F. & Zhu, Y., 2016. Enhancement of mineralization ability for phenol via synergetic effect of photoelectrocatalysis of g-C<sub>3</sub>N<sub>4</sub> film. *Appl. Catal. B*, Volume 180, pp. 324-329.

Liao, J., Lin, S., Zhang, L., Pan, N., Cao, X. & Li, J., 2012. Photocatalytic degradation of methyl orange using a TiO<sub>2</sub>/Ti mesh electrode with 3D nanotube arrays. *ACS Appl. Mater. Interfaces*, Volume 4, pp. 171-177.

- Li, T., He, J., Pena, B. & Berlinguette, C. P., 2015. Curing BiVO<sub>4</sub> photoanodes with ultraviolet light enhances photoelectrocatalysis. *Angew. Chem. Int. Ed.*, Volume 55, pp. 1769-1772.
- Liu, H., Cao, X., Liu, G., Wang, Y., Zhang, N., Li, T. & Tough, R., 2013. Photoelectrocatalytic degradation of triclosan on TiO<sub>2</sub> nanotube arrays and toxicity change. *Chemosphere*, Volume 93, pp. 160-165.
- Liu, L. & Chen, X., 2014. Titanium dioxide nanomaterials: self-structural modifications. *Chem. Rev.*, Volume 114, pp. 9890-9918.
- Li, X., Yu, J., Low, J., Fang, Y., Xiao, J. & Chen, X., 2015. Engineering heterogeneous semiconductors for solar water-splitting. *J. Mater. Chem. A*, Volume 3, pp. 2485-2534.
- Li, X. Z., Li, F. B., Fan, C. M. & Sun, Y. P., 2002. Photoelectrocatalytic degradation of humic acid in aqueous solution using a TiO<sub>2</sub>/Ti mesh photoelectrode. *Water Res.*, Volume 36, pp. 2215-2224.
- Mixa, A. & Staudt, C., 2008. Membrane-based separation of phenol/water mixtures using ionically and covalently cross-linked ethylene-methacrylic acid copolymers. *Int. J. Chem. Eng.*, Volume 2008, p. 12.
- Park, H. S., Kim, B. H., Kim, H. S., Kim, H. J., Kim, G. T., Chang, I. S., Park, Y. K. & Chang, H. I., 2001. A novel electrochemically active and Fe(III) reducing bacterium phylogenetically related to clostridium butyricum isolated from microbial fuel cell. *Anaerobe*, Volume 7, pp. 297-306.
- Pasternak, S. & Paz, Y., 2013. On the splitting and dissimilarity between photocatalytic water splitting and photocatalytic degradation of pollutants. *ChemPhysChem*, Volume 14, pp. 2059-2070.
- Pulkka, S., Martikainen, M., Bhatnagar, A. & Sillanpaa, M., 2014. Electrochemical methods for the removal of anionic contaminants from water- A review. *Sep. Puri. Technol.*, Volume 132, pp. 252-271.
- Qin, Y., Li, Y., Tian, Z., Wu, Y. & Cui, Y., 2016. Efficiently visible-light driven photoelectrocatalytic oxidation of As(III) at low positive biasing using Pt/TiO<sub>2</sub> nanotube electrode. *Nanoscale Res. Lett.*, Volume 11, p. 32.
- Ranade, V. V. & Bhandari, V. M., 2014. Industrial wastewater treatment, recycling and reuse. Oxford: Elsevier.
- Rao, A. N. S. & Venkatarangaiah, V. T., 2014. Metal-oxide coated anodes in wastewater treatment. *Environ. Sci. Pollut. Res.*, Volume 21, pp. 3197-3217.

Saranya, A., Pandiarajan, J., Jeyakumuran, N. & Prithivikumuran, N., 2014. Influence of annealing temperature and number of layers on the properties on nanocrystalline TiO<sub>2</sub> thin films: structural and optical investigation. *Int. J. ChemTech Res.*, Volume 6, p. 2237.

Segneanu, A. E. et al., 2013. <http://www.intechopen.com/books/water-treatment/wastewater-treatment-methods>. [Online]

[Accessed 19 November 2015].

Selcuk, H., Sene, J. J. & Anderson, M. A., 2003. Photoelectrocatalytic humic acid degradation kinetics and effect of pH, applied potential and inorganic ions. *J. Chem. Technol. Biotechnol.*, Volume 78, pp. 979-984.

Shang, M., Wang, W., Sun, S., Ren, J., Zhou, L. & Zhang, L., 2009. Efficient visible light-induced photocatalytic degradation of contaminant by sprindle-like PANI/BiVO<sub>4</sub>. *J. Phys. Chem.*, Volume 113, p. 20228.

Smith, W., Fakhouri, H., Mori, S., Pulpytel, J. & Arefi-Khansari, F., 2012. Oxidation kinetics of TiN films deposited by RF reacting sputtering at high and low pressure. *J. Phys. Chem. C*, Volume 116, p. 15855.

Smith, W., Fakhouri, H., Pulpytel, J. & Arefi-Khansari, F., 2012. Control of the optical and crystalline properties of TiO<sub>2</sub> in photoactive TiO<sub>2</sub>/TiN Bi-layer thin film stacks. *J. App. Phys.*, Volume 111, p. 024301.

Smith, W., Ingram, W. & Zhao, Y. P., 2010. The scaling of the photocatalytic decay rate with the length of aligned TiO<sub>2</sub> nanorod arrays. *Chem. Phys. Lett.*, Volume 479, pp. 270-273.

Smith, W. & Zhao, Y. P., 2008. Enhanced photocatalytic activity by aligned WO<sub>3</sub>/TiO<sub>2</sub> two-layer nanorod array. *J. Phys. Chem.*, Volume 112, pp. 19635-19641.

Smith, W. & Zhao, Y. P., 2010. Superior photocatalytic performance by vertically aligned core-shell TiO<sub>2</sub>/WO<sub>3</sub> nanorod arrays. *Catal. Commun.*, Volume 10, pp. 1117-1121.

Son, M. K., Seo, H., Kim, S. H., Hong, N. Y., Kim, B. M., Park, S., Prabakar, K. & Kim, H. J., 2012. Analysis on the light-scattering effect in dye-sensitized solar cell according to the TiO<sub>2</sub> structural differences. *Int. J. Photoenergy*, Volume 2012, p. 480929.

Tauc, J., Grigorovici, R. & Vancu, A., 1966. Optical properties and electronic structure of amorphous germanium. *Phys. Status Solidi b*, Volume 15, pp. 627-637.

Tokunaga, S., Kato, H. & Kudo, A., 2001. Selective preparation of monoclinic and tetragonal  $\text{BiVO}_4$  with Scheelite structure and their photocatalytic properties. *Chem. Mater.*, Volume 13, p. 4624–4628.

Wen, J., Li, X, Liu, W., Fang, Y., Xie, J. & Xu, Y., 2015. Photocatalysis fundamentals and surface modification of  $\text{TiO}_2$  nanomaterials. *Chinese journal of catalysis*, Volume 36, pp. 2049-2070.

Wu, X., Ling, Y., Liu, L. & Huang, Z., 2009. Enhanced photoelectrocatalytic degradation of methylene blue on smooth  $\text{TiO}_2$  nanotube array and its impedance analysis. *J. Electrochem. Soc.*, Volume 156, p. K65.

Xiaoli, Y., Huixiang, S. & Dahui, W., 2003. Photoelectrocatalytic degradation of phenol using a  $\text{TiO}_2/\text{Ni}$  thin-film electrode. *Korean J. Chem. Eng.*, Volume 20, pp. 679-684.

Yang, G., v. Swaaij, R., Tan, H., Isabella, O. & Zeman, M., 2015. Modulated surface textured glass as substrate for high efficiency microcrystalline silicon solar cells. *Sol. Energy Mater. Sol. Cells*, Volume 133, pp. 156-162.

Yan, X., Li, W., Aberle, A. & Venkataraj, S., 2015. Surface texturing studies of bilayer transparent conductive oxide (TCO) structures as front electrode for thin-film silicon solar cells. *J. Mater. Sci.: Mater. Electron*, Volume 26, pp. 7049-7058.

Zhu, X., 2007. Effects of pH; inorganic anions; and surfactants on the photocatalytic degradation of aqueous ammonia in gray water, Oklahoma: University of Oklahoma.

Zhu, X., Nanny, M. A. & Buttler, E. C., 2007. Effect of inorganic anions on the titanium dioxide-based photocatalytic oxidation of aqueous ammonia and nitrite. *J. Photochem. Photobiol. A*, Volume 185, pp. 289-294.



## TREATMENT OF ORGANIC POLLUTANTS USING A SOLAR ENERGY DRIVEN PHOTO-OXIDATION DEVICE

---

Two of the main problems of society in the near future are the access to clean water and energy, which are becoming increasingly limited, especially in remote and rural areas. In particular, organic pollutants can be a major health threat. Traditional methods for water treatment such as filtration or coagulation are not able to treat the organic pollutants in water up to the needed concentrations, where more advanced methods such as photochemical oxidation must be used. However, these advanced processes are energy intensive, which increases the costs and adds to the challenge of energy access. A trade-off is thus established between the pollutant treatment price and the final concentration that can be achieved. In this paper, a water treatment device is proposed in order to decouple these two variables. It uses advanced separation methods to reach low concentrations, and earth-abundant materials and solar light as the energy source for a low-cost solution. It consists of a  $\text{BiVO}_4$  photoanode combined with a thin film silicon solar cell.  $\text{BiVO}_4$  has a bandgap energy of 2.4 eV, and showed good catalytic properties for the degradation of phenol and chloroform. However, it needs an external bias voltage in order to reach the required potentials for pollutant degradation. To cover the voltage needs, an a-Si:H/nc-Si:H solar cell was coupled with the  $\text{BiVO}_4$ . This solar cell was specifically designed to work under the transmitted spectrum of the  $\text{BiVO}_4$ , with thicknesses of 300 nm and 2000 nm for the top and

bottom cell, respectively. This device has successfully been fabricated, and tested for removal of organic contaminants from an aqueous solution. The device with the solar cell performed better than the  $\text{BiVO}_4$  photoanode alone with a similar external bias voltage applied, suggesting that the solar cell does not only act as a voltage source, but also as a current source. To compare the performance of this device to the commercially available  $\text{TiO}_2$  photoanode illuminated by UV light, an energy balance for phenol removal was performed. The energy needed for phenol removal was reduced from 1.83 Wh/mg with the  $\text{TiO}_2$ /UV device to 0.79 Wh/mg with the  $\text{BiVO}_4$  with a solar cell, indicating the potential of the proposed device to improve the water treatment of organic pollutants by using earth-abundant materials and solar energy.

### 8.1. Introduction

The most pressing environmental problems associated with the growing world population are the lack of clean water, insufficient food production, and a sustainable generation and consumption of energy (IEA, 2011). Currently, 1.25 billion people have no access to electricity (The World Bank, 2015) and a similar number of people have no access to clean water (The World Bank, 2015). These problems cannot be tackled independently from each other, since poor electrification goes together with the lack of access to clean water. Hazardous effluents pollute many major water supplies, caused by heavy industrialization and urbanization. Among the most common contaminants are organic pollutants such as pesticides, pharmaceuticals, phenol compounds, chloroform or dyes (Martinez-Huitle, et al., 2008, Ribeiro, et al., 2015). Currently, these pollutants are hardly removed using traditional methods like filtration, chemical coagulation or aerobic and anaerobic treatment (Ribeiro, et al., 2015, Sarkka, et al., 2015). The main metrics used to evaluate the performance of these methods are cost-effectiveness and the minimum pollutant concentrations reached after purification. However, these two metrics are in competition. Costs are driven by the extent of the treatment, the energy consumption, and the usage of chemicals and other materials such as membranes. As a result, the more sophisticated treatment processes, that result in low pollutant concentrations, are typically more expensive. In this paper, we decouple these competitive metrics by proposing a solar powered photoelectrochemical solution. Low final concentrations of pollutants are expected to be obtained by using photoelectrochemical methods, and low cost-prices are obtained using free solar energy in combination with cheap, abundant materials.

In particular, photoelectrochemical oxidation is able to remove toxic organics, ecologically hazardous cyanides and other residual compounds even at low



concentrations, being therefore an ideal candidate for advanced water purification (Pasternak & Paz, 2013).

This method uses the light absorbed in a semiconductor to degrade the pollutants into less complex compounds that can be easier to remove by a post-treatment step. By either using a photoanode or a photocathode, oxidation or reduction of pollutants is possible, allowing different pollutants to be treated. In our work, the focus is on the photo-oxidation of organic pollutants using an n-type photoanode (Pulkka, et al., 2014, Daghrir, et al., 2012).

In photo-oxidation, an electron-hole pair is formed in an n-type semiconductor when light is absorbed. The hole would travel to the semiconductor/solution interface, while the electron would travel to the counter electrode through an external circuit. When the hole reaches the interface, it is able to react with water and create an  $\cdot\text{OH}$  radical, which is highly reactive and will degrade organic compounds into smaller and supposingly less harmful molecules, potentially reaching total decomposition into  $\text{CO}_2$  and  $\text{H}_2\text{O}$  (Daghrir, et al., 2012).

Among the candidates for photo-oxidation, metal oxides have been the most extensively used materials, with bismuth based compounds (Sun & Wang, 2014),  $\text{SnO}_2$  (Al-Hamdi, et al., 2016),  $\text{WO}_3$  (Smith & Zhao, 2010) and  $\text{TiO}_2$  (Ghaly, et al., 2011) as examples. In particular,  $\text{TiO}_2$  has been widely used as the semiconductor of choice for photo-oxidation of pollutants, since it is cheap and chemically stable (Chong, et al., 2010). However, its bandgap energy is rather high (3.2 eV) (Dette, et al., 2014), meaning that it can only be excited by UV light. Therefore, this material is very energy intensive, making the process less cost-effective.

To tackle the high energy consumption of traditional photoelectrochemical methods and decouple the low pollutant concentrations from low cost-effectiveness, alternative semiconductor materials to  $\text{TiO}_2$  that can work

effectively with the solar spectrum rather than light sources, must be considered. With the right choice of semiconductor, the reaction of water purification can be directly driven by sunlight. That way, not only the costs associated with energy can be reduced, but also the greenhouse gas emissions produced by these energy-intensive methods and the dependence on third parties for energy supply is minimized.

In this work,  $\text{BiVO}_4$  was used as a photoanode due to its bandgap energy of  $\sim 2.4\text{eV}$ , high stability and low price.  $\text{BiVO}_4$  is already used as a yellow pigment for paint and has been successfully demonstrated as a promising photoanode for solar water splitting (Abdi, et al., 2013).

However, a potential is needed inside the material so that the charge carriers are able to deliver enough energy to drive the reaction. Since these semiconductors are not able to produce these potentials by themselves, an external bias voltage is needed. Here, we propose to use a solar cell that utilizes the spectrum transmitted by the  $\text{BiVO}_4$  photoanode (Figure 1 b)) to create the voltage needed as extra bias. The options available include III-V technologies, perovskites, crystalline silicon (c-Si), thin-film amorphous and nanocrystalline silicon (a-Si & nc-Si) and CIGS (Huang, et al., 2016, Tyagi, et al., 2013) In order to choose the most suitable technology, it must be noted that the optimum external bias voltage is 1V (Bennani, et al., 2016). Therefore, multijunction solar cells, which consist of several cells monolithically stacked and series connected, may be required (Yang, et al., 2003, Siddiki, et al., 2010, Cotal, et al., 2009). Thin-film silicon was used due to the flexibility of its design, know-how on possible multijunction devices, stability of the devices and the low cost of materials. A thin-film silicon solar cell was specially designed to work in this device and was successfully integrated, demonstrating the viability of this device.

To tackle all challenges mentioned above, this paper proposes a new photoelectrochemical water purification system that operates spontaneously

using only solar irradiation and no external power supply. It consists of a photoanode combined with a solar cell and a conductive cathode counter electrode, as shown in Figure 8.1 a). This device has the potential to reduce the costs by using free solar energy and Earth-abundant materials, to achieve low final pollutant concentrations by using advanced photo-oxidation methods, and to have the additional advantage of being electrically autonomous from any external power source.

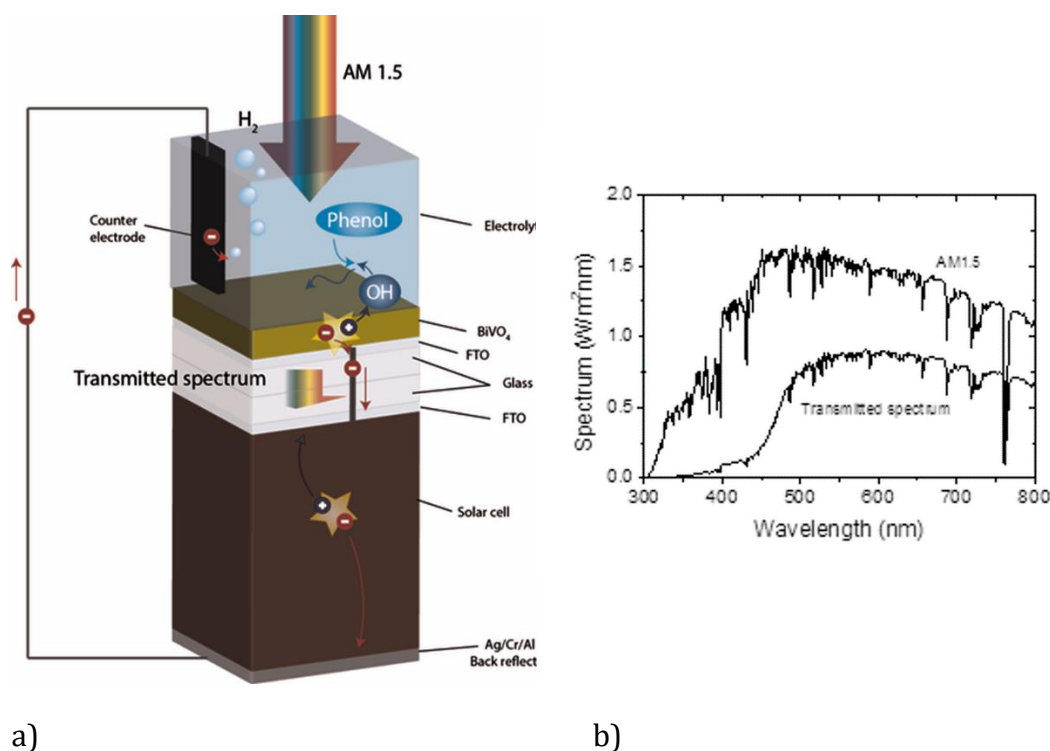


Figure 8.1. a) Schematic of a stand-alone device configuration combining a BiVO<sub>4</sub> photoanode and a solar cell and b) the AM1.5 spectrum compared to the transmitted spectrum after the BiVO<sub>4</sub> photoanode

Combining all these elements, a bias-free demonstrator based on Earth-abundant materials for organic pollutant removal was realized. This is the first time that a multijunction approach is used for better spectral utilization in a pollutant removal photo-oxidation process.

To determine the validity of this approach, an energy analysis was performed to determine how much energy is saved with this method compared to other advanced photo-oxidation technologies.

## 8.2. Material and methods

**BiVO<sub>4</sub> fabrication.** Asahi UV type textured glass was cleaned with a sequence of acetone and isopropanol, and used as a substrate for BiVO<sub>4</sub> thin film deposition. Prior to the BiVO<sub>4</sub>, a 5 nm SnO<sub>2</sub> layer was deposited by spray pyrolysis at 480°C to avoid recombination in the interface with the transparent conductive oxide (TCO). The precursor for BiVO<sub>4</sub> spraying was made by mixing equimolar quantities of Bi(NO<sub>3</sub>)<sub>3</sub>·5H<sub>2</sub>O (98 % Alfa Aesar) solution in acetic acid (98 % Sigma Aldrich) with V(AcAc)<sub>2</sub> (99 % Alfa Aesar) solution in absolute ethanol (Sigma Aldrich). This precursor solution was then deposited by spray pyrolysis at 450°C at a rate of 0.2 mL/s. Cycles consisting of 5 s of spraying plus 55 s of idle to evaporate the solvents were performed. An annealing step at 450°C for two hours followed, in order to achieve the desired crystal structure. The BiVO<sub>4</sub> thin films had a thickness of 300nm. The contacts consisted of a 300 nm Al stripe on the TCO deposited by electron beam physical vapour deposition (EBPVD). For the experiments involving only the BiVO<sub>4</sub>, an active area of 16 cm<sup>2</sup> was used, while for the combination of the solar cell, this was reduced to 1 cm<sup>2</sup> due to limitations in the TCO conductivity of the solar cell.

**Solar cell fabrication.** The solar cells were deposited by Plasma Enhanced Chemical Vapour Deposition (RF-PECVD) using a cluster tool from Electtrorava. The a-Si:H and a-Si:H/a-Si:H solar cells were deposited on Asahi UV substrates, while the a-Si:H/nc-Si:H solar cells were deposited in wet etched textured glass with Aluminium-doped Zinc Oxide (AZO) as a TCO. The texturing of the glass is described elsewhere (Yang, et al., 2014).

Nanocrystalline silicon oxide (nc-SiO<sub>x</sub>) has been used as p-layer (boron doped) and n-layer (phosphorous doped). The thickness of the absorber layers (intrinsic a-Si:H and nc-Si:H) has been varied by varying the deposition time. The deposition rates of a-Si:H and nc-Si:H were 0.16 and 0.71 nm/s, respectively.

The contacts have been deposited using Electron Beam Physical Vapour Deposition (EBPVD). A 300 nm aluminium stripe in contact with the TCO has been used as front contact. A stack of 200 nm silver, 30 nm chromium and 500 nm aluminium has been used as back reflector and back contact. The solar cell area was 1 cm<sup>2</sup>.

**Solar cell characterization.** External Quantum Efficiency (EQE) was measured in an in-house setup in TU Delft to obtain the amount of charge carriers generated per photon of a given wavelength incident on the solar cell. The JV curves of the solar cells have been measured using a two Xe lamp flash PASAN solar simulator (Class AAA) and corrected by the short-circuit current obtained from the integration of the EQE measurements. The BiVO<sub>4</sub> photoanode has been used as a filter to obtain the transmitted spectrum during both measurement.

#### **Photoelectrochemical measurements and sampling.**

Photoelectrochemical experiments for phenol and chloroform degradation were carried out with a set-up consisting of a cylindrical quartz glass reactor with an effective vessel volume of 300 mL, an Atlas solar simulator (SUNTEST XXL+) and a three-electrode configuration with an Ag/AgCl reference electrode. The initial volume of the working solution was 250 mL phenol (≥99 %, Sigma Aldrich) with initial concentration of 20 mg/L, and 250 mL chloroform solution (Baker analysed, containing 0.75 % ethanol as stabiliser) with initial concentration of 500 ppb. Demineralized water (RiOs 5 Reverse Osmosis System) was used throughout the experiments for dilution. To eliminate the influence of solution resistance, 0.1 M Na<sub>2</sub>SO<sub>4</sub> was chosen as

supporting electrolyte. The 2 mL samples of phenol solution and 25 mL of chloroform solution were collected from the reaction solution at regular time intervals (every 1 hour).

2 mL of phenol solution sample were added to a cuvette and measured with UV/Vis spectrophotometer (Hach Lange DR 5000, cuvette tests LCK 345 with a measuring range of 0.05-5.00 mg/L, 5-50 mg/L and 20-200 mg/L) to determine the residual concentration of phenol. Phenol reacts with 4-nitroaniline to form a yellow-coloured complex which is then measured by photometry. The possible measurement error of the Spectrophotometer is  $\pm 5\%$  (Hach Company, 2005).

At the start of each experiment, the  $\text{BiVO}_4$  electrodes were kept in the stirred phenol and chloroform solution in the dark for one hour for adsorption to reach equilibrium (Bennani, et al., 2015). In order to get an insight into the effect of the counter electrode on the PEC performance of the above described system, three counter electrodes were used. A graphite plate was used as a cathode in the experiments. To investigate the effect of the cathode on the PEC performance, carbon foam and a copper plate were additionally tested.

The pH of the solution was kept constant at 7.2 and was measured before the experiment, using a Sentix 81 pH meter. The temperature was controlled at  $25 \pm 1^\circ\text{C}$  by recirculating cooling water in a water bath equipped with cooler Julabo, FL300. During the experiments the reactor was closed by a UV permeable quartz lid to prevent evaporation of phenol. The electrode potential and working current were controlled with a potentiostat-galvanostat system (Autolab PGSTAT128N with a BOOSTER10A) by Nova Software.

The phenol and chloroform photo degradation experiments using only the  $\text{BiVO}_4$  photoanode were performed by applying the optimal potential of 1 V (vs. Ag/AgCl, KCl saturated) which was taken from previous studies (Bennani, et al., 2016, Lopes, et al.).

In the case of the combination with the solar cell, a voltage of 0V (vs. Ag/AgCl KCl saturated) was applied. The net current was determined by subtracting the dark current from the photocurrent.

### 8.3. Results and Discussion

In order to understand and improve the PEC performance of the proposed system, each of the active components (BiVO<sub>4</sub> photoanode, counter electrode and supporting solar cell) were studied separately. In addition, an energy balance of the newly proposed bias-free system was performed and compared with the more traditional systems based on a TiO<sub>2</sub> photoelectrode.

**BiVO<sub>4</sub> photoanode.** BiVO<sub>4</sub> has been previously successfully demonstrated as a photoanode for treatment of organic pollutants (Bennani, et al., 2016). However, when integrated in a working device, other variables such as scalability or stability are important. In addition, it is preferable that this device can treat different contaminants. Here, these features are considered to assess the suitability of BiVO<sub>4</sub> for this device.

Regarding the stability of the BiVO<sub>4</sub> photoanode, four consecutive degradation cycles were performed on the same sample. The results in Figure 8.3 show the constant rates of degradation ( $k$ ), obtained and normalized by dividing by the average  $k$  value (black line). The reaction rate constant remained within less than 10 % of the initial value for the 4 consecutive cycles tested. The possible measurement error of the Spectrophotometer is  $\pm 5$  % (Hach Company, 2005), and the maximum error of the fitting was  $\pm 2.5$  %. Therefore, the added possible error of these measurements is 7.5 %, represented in Figure 8.2 by the red dashed lines.

That shows that the variations observed in the reaction rate constant among the different measurements can be due to measurement inaccuracies, and the photoelectrode can be considered stable.

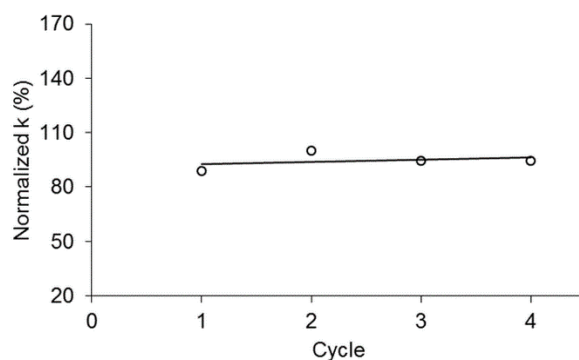
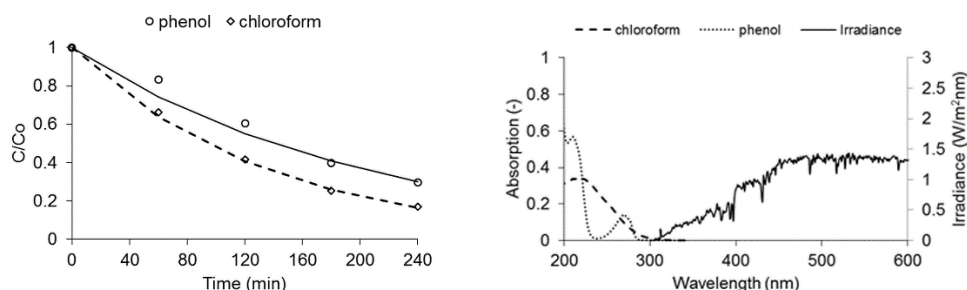


Figure 8.2. Reaction rate constant  $k$  normalized by the average reaction rate constant for several consecutive cycles on a  $\text{BiVO}_4$  photoanode with applied bias voltage of 1 V (vs. Ag/AgCl, KCl saturated). The percentage represents how much the reaction rate constant has change with respect to the average value (black line). The dotted lines represent the estimated possible error inherent to the measurement equipment and fitting procedures (7.5 %)

Finally, the flexibility of pollutants that can be treated with  $\text{BiVO}_4$  must be taken into consideration for a practical water treatment device.  $\text{BiVO}_4$  is a promising material for water treatment of organic pollutants, not only for phenol degradation but also for other organic compounds such as dyes (Lopes, et al., 2016). To further assess the flexibility of  $\text{BiVO}_4$  regarding pollutants, the degradation characteristics of phenol and chloroform were measured, and the results are shown in Figure 8.3 a). The reaction rate constants according to first order kinetics can be determined to be  $0.0053 \text{ min}^{-1}$  and  $0.0075 \text{ min}^{-1}$  for phenol and chloroform, respectively.



This shows that  $\text{BiVO}_4$  performed even better for chloroform removal than for phenol removal, with a higher reaction rate constant and reaching a final concentration of 17 % of the initial in 4 h. To determine if this effect might be due to the different light absorption of the two pollutants (Anachemia Chemicals, 2015, Brescia 2015), the absorption was measured, as shown in Figure 8.3 b). The absorption peak for phenol is at 200 nm, and the absorption peak for chloroform is found at 215 nm. Since the solar spectrum used for these experiments, showed in yellow in Figure 8.3 b), contains low amounts of light at wavelengths lower than 300 nm (Bird, et al., 1983), none of the solutions will absorb a significant part of the solar spectrum and thus the light absorption in the solution can be ruled out as a negligible factor. Therefore, the differences in degradation of pollutants observed in Figure 8.3 a) would mainly be caused due to enhanced adsorption and reaction rates on the photoanode surface for chloroform removal. In particular, some literature reports that  $\cdot\text{OH}$  radical addition can more easily target C-Cl bonds rather than C-H bonds (Demeestere, et al., 2007). Phenol was the used contaminant for further investigation as the “worst case” scenario in this study.



a)

b)

Figure 8.3. a) Degradation of phenol and chloroform solutions using a BiVO<sub>4</sub> photoanode with an applied bias voltage of 1 V (vs. Ag/AgCl, KCl saturated) and corresponding fitting considering first order kinetics. b) Light absorption of the phenol and chloroform solutions used, compared to the solar irradiance (right axis)

**Counter electrode.** The cathode material is where the hydrogen evolution reaction occurs, completing the circuit and redox reaction. It can affect the overall degradation reaction by electro-reduction of the dissolved oxygen into H<sub>2</sub>O<sub>2</sub>, electro-reduction of the organic pollutants or direct adsorption of these contaminants in porous cathodes (Rao & Venkatarangaiah, 2014).

In order to study the interaction between the electrochemical oxidation and reduction reactions, and to minimize the over-potential related to the counter electrode, different materials and configurations were tested. Ag, Al, Au, Cu, Ni, Pb, Pd, Pt, Ti, Zn, graphite, glassy carbon and activated carbon fiber (ACF) have been proposed in literature as cathode materials in the electrochemical treatment of water containing different organics pollutants (Shen, et al., 2001; Fan, et al., 2006).

In this paper, Cu and graphite were studied due to their relative low cost with respect to other more precious metals, and high removal efficiency (Martinez-Huitle & Brillas, 2008; Zeng, et al., 2012). The results are presented in Figure 8.4.

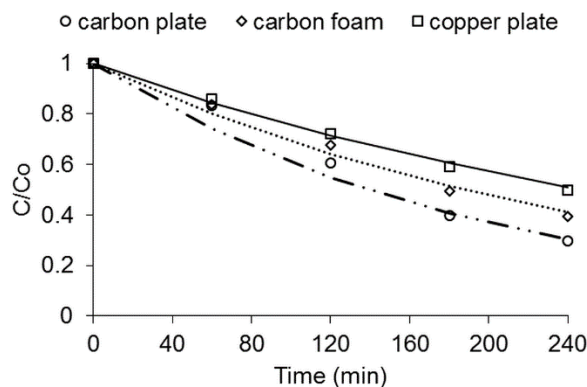


Figure 8.4. Phenol degradation related to the used counter electrode and corresponding fitting considering first order kinetics

The reaction rate constants obtained by fitting to a first order reaction are  $0.0053 \text{ min}^{-1}$  for the carbon plate counter electrode,  $0.0040 \text{ min}^{-1}$  for the carbon foam and  $0.0029 \text{ min}^{-1}$  for the copper plate. Therefore, carbon seems to be the best material to use as counter electrode. This might be due to the generation of  $\text{H}_2\text{O}_2$  on carbon electrodes, which helps the reaction by adding the possibility of homogeneous catalysis (Xie & Li, 2006). In addition, copper electrodes have a tendency to reduce the dissolved oxygen present in the aqueous phenol solution, negatively influencing phenol degradation (Sarala & Venkatesha, 2013). Dissolved oxygen acts as an effective electron acceptor to extend the hole's lifetime and to form the oxidizing species of hydroxyl radicals, affecting the photoactivity of the  $\text{BiVO}_4$  film (Dionysiou, et al., 2002).

Finally, despite the fact that carbon foam has a higher surface area, the carbon plate performs better, probably due to the easier mass transport to the surface.

**Solar cell.**  $\text{BiVO}_4$  needs a potential applied in order to work at its optimum, since the electrochemical potential of the reaction is higher than the one produced by the  $\text{BiVO}_4$  photoanode by itself. In previous studies, it was determined that the optimum external applied bias for phenol degradation was 1V vs. Ag/AgCl (Bennani, et al., 2016). In order to apply the needed potential, an additional solar cell can be added to the system. In this paper, thin-film silicon solar cells were used in combination with the  $\text{BiVO}_4$  photoanode due to its flexibility of design regarding the output voltage and current. Using this material, a multijunction approach can be used, allowing for higher operational voltages than single junctions and better spectral utilization. Using this approach, it is possible to have the Si solar cells produce the applied potential of 1 V at operational conditions, making the system autonomous and removed from an external power supply.

Three main options were explored to use as solar cell: an a-Si:H single junction, an a-Si:H/a-Si:H double junction and an a-Si:H/nc-Si:H double junction. Since the spectrum reaching the solar cells is not AM1.5 but the spectrum transmitted by the  $\text{BiVO}_4$  (Figure 8.1 b)), the absorber thicknesses were adjusted to optimize the output parameters, setting as boundary condition that the a-Si:H top absorber layers would not increase further than 300 nm to avoid strong light-induced degradation (Staebler & Wronski, 1977). For the a-Si:H/a-Si:H solar cell, the used top and bottom absorber thickness were 150 nm and 400 nm, respectively. The open-circuit voltage achieved with these cells was 1.59V and the short circuit current under the transmitted spectrum was 2.27 mA/cm<sup>2</sup>. Regarding the a-Si:H/nc-Si:H cell, the bottom cell absorber thickness was fixed at 2000 nm, and the top cell absorber thickness was optimized at 300 nm.

The short circuit current under the transmitted spectrum in that case was 3.86 mA/cm<sup>2</sup> and the open circuit voltage was 1.27 V. Finally, the single junction a-Si:H cell of 300 nm was chosen, which had a short circuit current under transmitted spectrum of 4.85 mA/cm<sup>2</sup> and an open circuit voltage of 0.83V. Figure 8.5 a) shows the different JV characteristics of the solar cells with optimum thicknesses, and Figure 8.5 b) shows the EQE measurements. It can be noticed from the EQE measurements that, even there is still room for improvement, there is good current matching of the tandem junction cells.

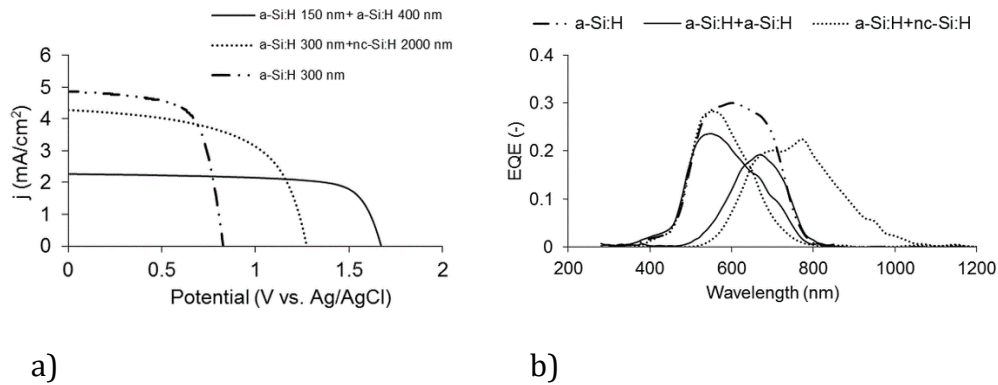


Figure 8.5. a) JV characteristics and b) EQE measured with the BiVO<sub>4</sub> transmitted spectrum of the a-Si:H/a-Si:H tandem solar cell (—), a-Si:H/nc-Si:H (····) solar cell and a-Si:H single junction cell (—·). The corresponding short circuit currents extracted from the EQE are shown in the graph in the corresponding color

The BiVO<sub>4</sub> photoanode was combined with the optimized solar cells of each technology presented, obtaining the phenol degradation curves displayed in Figure 6. All the curves were measured including an Ag/AgCl KCl saturated reference electrode for better comparison with the case at bias voltage of 1V vs. Ag/AgCl. Note that the cell area used was 1 cm<sup>2</sup>, maintaining the solution volume constant. The smaller area was chosen to avoid the conductivity limitations of the front TCO layer. The BiVO<sub>4</sub> active area was also 1 cm<sup>2</sup> to match that of the solar cell. However, it must be noted that because of the difference in volume to area ratio, the final degradation will be smaller.

These degradation characteristics could not be satisfactorily fitted to an order zero, first order or second order kinetics, suggesting that the interaction of all parameters is more complex than these relatively simple kinetics models. However, the general trends of degradation can be analyzed. It can be seen that with an a-Si:H single junction and a-Si:H/nc-Si:H double junction solar cells, combined with the BiVO<sub>4</sub> and no extra voltage applied, a better degradation was reached in comparison to the case of a BiVO<sub>4</sub> photoanode by itself with an applied bias voltage of 1 V vs. Ag/AgCl. The best cell, the a-Si:H/nc-Si:H double junction, which was able to degrade 15 % of the phenol present after 4 hours of degradation. Opposed to it, the BiVO<sub>4</sub> photoanode with 1 V vs. Ag/AgCl applied was only able to degrade 10 % of the phenol present. The improvement given by the solar cell could be because the solar cell acts a current source rather than a voltage source, providing more charge carriers to the solution, positively influencing phenol removal (Daskalakis, et al., 2013). The current will be adapted to the optimum current case, partly removing the limitation of charge carrier supply to the active surface and increasing the phenol degradation. The lower performance observed for the combination with an a-Si:H/a-Si:H double junction cell can be due to the fact that this cell provides a higher voltage, favoring the water splitting reaction and therefore lowering the performance regarding phenol degradation.

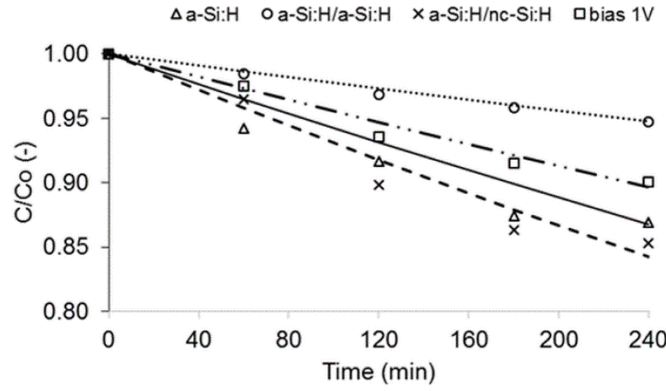


Figure 8.6. Phenol degradation of the  $\text{BiVO}_4$  photoanode with time when the optimum 1 V (vs Ag/AgCl, KCl saturated) potential is applied ( $\square$ ), and when it is combined with an a-Si:H ( $\Delta$ ), a-Si:H/a-Si:H ( $\circ$ ) and a-Si:H/nc-Si:H ( $\times$ ) solar cells without any extra bias is applied. Note that the  $C/C_0$  is plotted from 0.8 to 1 to ease the differentiation of the curves. The low absolute phenol removal of this case is caused by the big difference between photoanode area and solution volume

**Energy balance.** Once the best design for the device has been analyzed, an energy balance was performed to be able to compare it to different systems currently used or studied (Bennani, et al., 2016, Dixit, et al., 2010). This analysis takes into account all the energy inputs to the system, including light and electrical power. The energy necessary to remove 1 mg of phenol  $E$  is defined as

$$E = \frac{(P_{in} + V_{bias}J_{photo})A}{m_{removed}}$$

where  $P_{in}$  is the light power input in  $\text{W/m}^2$ ,  $V_{bias}$  is the applied bias voltage in V,  $J_{photo}$  is the photocurrent density produced in the material in  $\text{A/m}^2$ ,  $A$  is the

active area of the system in  $\text{m}^2$ , and  $m_{\text{removed}}$  is the total phenol mass removed from the solution in mg.

The conditions of each analyzed system, together with the energy needed per mg removed, are displayed in Table 8.1. The systems compared are the  $\text{BiVO}_4$  photoanode with and without the solar cell, a  $\text{TiO}_2/\text{Ti}$  composite illuminated by the solar spectrum, and a  $\text{TiO}_2$  based photoanode illuminated by UV light (Dixit, et al., 2010).

Table 8.1. Energy balance results for different configurations

Material	Light	Bias voltage (V)	E (Wh/mg)
$\text{TiO}_2$ (Dixit, et al., 2010)	UV( $125\text{W}/\text{m}^2$ )	0	1.83
$\text{TiO}_2$ (Bennani, et al., 2016)	AM1.5( $1000\text{W}/\text{m}^2$ )	1	4.21
$\text{BiVO}_4$	AM1.5( $1000\text{W}/\text{m}^2$ )	1	1.15
$\text{BiVO}_4$	AM1.5( $1000\text{W}/\text{m}^2$ )	Solar cell (0V)	0.79

The differences between the UV/ $\text{TiO}_2$  system (Dixit, et al., 2010) and the  $\text{TiO}_2/\text{Ti}$  plate system is mainly due to the different energies of the light sources, stressing the fact that if UV light is used, the  $\text{TiO}_2$  photoelectrode performance is better than with AM1.5.

The  $\text{BiVO}_4$  photoanode performed better than  $\text{TiO}_2$  in all cases, due to the improved phenol degradation characteristic. The use of  $\text{BiVO}_4$  alone instead of  $\text{TiO}_2$  with AM1.5 reduced the energy input needed per mg treated by more than 70 %. When the solar cell was introduced, the situation was further improved by reducing the energy needed to 0.79 Wh per mg of degraded phenol. It is important to note that most of the input energy in the AM1.5 cases would be coming directly from the Sun and not from an external source of energy, like it would be in the case for the  $\text{TiO}_2$  with UV light.



The reduction of the energy needed with the designed device would translate in a smaller, more compact equipment in a practical device, potentially reducing the costs of materials and installation. That makes the system more cost-effective. In addition, an autonomous system from external power sources would allow installation not only in main urban areas but also in remote rural places with no access to electricity.

#### **8.4. Conclusions**

A photo-oxidation device based on Earth-abundant materials and solar illumination was successfully demonstrated. It consists of a  $\text{BiVO}_4$  photoanode connected to a solar cell and a counter electrode to complete the reaction.  $\text{BiVO}_4$  was chosen as a suitable and stable material to use as a photoanode for photochemical degradation not only for phenol but also chloroform. The best material for the counter electrode was a flat carbon plate. A thin-film silicon solar cell was designed to operate under the transmitted spectrum of the photoanode, and to produce the best current and voltage at the operational point for water treatment. An a-Si:H/nc-Si:H tandem solar cell was found to give the best results, with a phenol removal of 15 % of the original concentration with a  $1 \text{ cm}^2$  photoanode treating 175 mL of solution. This solar cell is able to provide with the optimum voltage for phenol removal, as well as acting as a current source, facilitating the injection of charge carrier into the solution. The energy consumption of the system, defined as the energy needed to remove 1mg of pollutant, was used to compare different systems. In the case of the  $\text{BiVO}_4$  with an a-Si:H/nc-Si:H solar cell, it was only 0.79 Wh/mg for this device, compared to the 1.15 Wh/mg needed by a  $\text{BiVO}_4$  photoanode at 1 V vs. Ag/AgCl, KClbias .

In conclusion, this bias-free device can provide an efficient way to remove organic pollutants from water, reducing the costs and the greenhouse gas emissions. In addition, it could be applied as a stand-alone device, which could be independently installed even in remote areas without a stable electricity supply.

## References

- Abdi, F. F., Han, L., Smets, A. H., Zeman, M., Dam, B. & van de Krol, R., 2013. Efficient solar water splitting by enhanced charge separation in a bismuth vanadate-silicon tandem photoelectrode. *Nat. Commun.*
- Al-Hamdi, A. M., Sillanpaa, M., Bora, T. & Dutta, J., 2016. Efficient photocatalytic degradation of phenol in aqueous solution by SnO<sub>2</sub>: Sb nanoparticles. *Appl. Surf. Sci.*, pp. 229-236.
- Bennani, Y., Appel, P. & Rietveld, L., 2015. Optimisation of parameters in a solar light-induced photoelectrocatalytic process with a TiO<sub>2</sub>/Ti composite electrode prepared by paint-thermal decomposition. *J. Photochem. Photobiol., A*, Volume 305, pp. 83-92.
- Bennani, Y., Perez-Rodriguez, P., Alani, M. J., Smith, W. A., Rietveld, L. C., Zeman, M. & Smets, A. H., 2016. Photoelectrocatalytic oxidation of phenol for water treatment using a BiVO<sub>4</sub> thin-film photoanode. *J. Mater. Res.*, 31(17), pp. 2627-2639.
- Bird, R., Hulston, R. & Lewis, L., 1983. Terrestrial solar spectral data sets. *Sol. Energy*, 30(6), pp. 563-573.
- Chemicals, A., n.d. Anachemia. [Online] Available at: <http://www.anachemiachemicals.com/pdfs/split 34.pdf> [Accessed 20 November 2015].
- Chong, M. N., Jin, B., Chow, C. W. & Saint, C., 2010. Recent developments in photocatalytic water treatment technology: A review. *Water Res.*, Volume 44, pp. 2997-3027.
- Cotal, H., Fetzner, C., Boisvert, J., Kinsey, G., King, R., Hebert, P., Yoon, H. & Karam, N., 2009. III-V multijunction solar cells for concentrating photovoltaics. *Energy Environ. Sci.*, Volume 2, pp. 174-192.
- Daghrir, R., Droguia, P. & Robert, D., 2012. Photoelectrocatalytic technologies for environmental applications. *J. Photochem. Photobiol., A*, Volume 238, pp. 41-52.
- Daskalakis, V. M., Fulgione, I., Frontistisa, Z., Rizzob, L. & Mantzavinosa, D., 2013. Solar light-induced photoelectrocatalytic degradation of bisphenol-A on TiO<sub>2</sub>/ITO film anode and BDD cathode. *Catal. Today*, Volume 209, pp. 74-78.

- Demeestere, K., Dewulf, J. & Langenhove, H. V., 2007. Heterogeneous Photocatalysis as an Advanced Oxidation Process for the Abatement of Chlorinated, Monocyclic Aromatic and Sulfurous Volatile Organic Compounds in Air: State of the Art. *Crit. Rev. Environ. Sci. Technol.*, Volume 37, pp. 489-538.
- Dette, C., Pérez-Osorio, M. A., Kley, C. S., Punke, P., Patrick, C. E., Jacobson, P., Giustino, F., Jung, S. J. & Kern, K., 2014. TiO<sub>2</sub> Anatase with a Bandgap in the Visible Region. *Nano Lett.*, 14(11), pp. 6533-6538.
- Dionysiou, D. D., Burbano, A., Suidan, M. T., Baudin, I. & Laine, J. M., 2002. Effect of oxygen in a thin-film rotating disk photocatalytic reactor. *Environ. Sci. Technol.*, Volume 36, pp. 3834-3843.
- Fan, L., Zhou, Y., Yang, W., Chen, G. & Yang, F., 2006. Electrochemical degradation of Amaranth aqueous solution on ACF. *J. Hazard. Mater.*, 137(2), pp. 1182-1188.
- Ghaly, M. Y., Jamil, T. S., El-Seesy, I. E., Souaya, E. R. & Nasr, R. A., 2011. Treatment of highly polluted paper mill wastewater by solar photocatalytic oxidation with synthesized nano TiO. *Chem. Eng. J.*, Volume 168, pp. 446-454.
- Hach Company, 2005. DR5000 Spectrophotometer - Procedures Manual. s.l.:s.n.
- Han, L., Abdi, F. F., v. d. Krol, R., Liu, R., Huang, Z., Lewerenz, H. J., Dam, B., Zeman, M. & Smets, A. H., 2014. Efficient Water Splitting Device Based on Bismuth Vanadate Photoanode and Thin Film Silicon Solar Cells. *ChemSusChem*, Volume 7, pp. 2832-2938.
- Huang, H., He, Y., Li, X., Li, M., Zeng, C., Dong, F., Du, X., Zhang, T. & Zhang, Y., 2016. Bi<sub>2</sub>O<sub>2</sub>(OH)(NO<sub>3</sub>) as a desirable [Bi<sub>2</sub>O<sub>2</sub>]<sup>2+</sup> layered photocatalyst: strong intrinsic polarity, rational band structure and {001} active facets co-beneficial for robust photooxidation capability. *J. Mater. Chem. A*, Volume 3, pp. 24547-24556.
- Huang, J., Shao, Y. & Dong, Q., 2016. Organometal Trihalide Perovskite Single Crystals: A Next Wave of Materials for 25 % Efficiency Photovoltaics and Applications Beyond?. *J. Phys. Chem. Lett.*, Volume 6, pp. 3218-3227.
- IEA, 2011. Clean energy Progress Report, s.l.: IEA.

Lopes, O. F., Carvalho, K. T., Nogueira, A. E., Jr, W. A. & Ribeiro, C., 2016. Controlled synthesis of BiVO<sub>4</sub> photocatalyst: Evidence of the role of heterojunctions in their catalytic performance driven by visible light. *Appl. Catal., B*, Volume 188, pp. 87-97.

Martinez-Huitle, C. A. & Brillas, E., 2008. Decontamination of wastewaters containing synthetic organic dyes by electrochemical methods: A general review. *Appl. Catal., B*, Volume 87, pp. 105-145.

P. Brescia, 2012. BioTek. [Online] Available at: [http://www.biotek.com/assets/tech\\_resources/A260A280 Spectral Scanning App Note.pdf](http://www.biotek.com/assets/tech_resources/A260A280_Spectral_Scanning_App_Note.pdf) [Accessed 20 November 2015].

Pasternak, S. & Paz, Y., 2013. On the Splitting and Dissimilarity between Photocatalytic Water Splitting and Photocatalytic Degradation of Pollutants. *ChemSusChem*, Volume 14, pp. 2059-2070.

Pulkka, S., Martikainen, M., Bhatnagar, A. & Sillanpää, M., 2014. Electrochemical methods for the removal of anionic contaminants from water - A review. *Sep. Purif. Technol.*, Volume 132, pp. 252-271.

Rao, A. N. S. & Venkatarangaiah, V. T., 2014. The Effect of Cathode Materials on Indirect Electrochemical Oxidation of Methyl Orange, Malachite Green and Methylene Blue. *Port. Electrochim. Acta*, Volume 32, pp. 213-231.

Ribeiro, A. R., Nunes, O. C., Pereira, M. F. & Silva, A. M., 2015. An overview on the advanced oxidation processes applied for the treatment of water pollutants defined in the recently launched Directive 2013/39/EU. *Environ. Int.*, Volume 75, pp. 33-51.

Sarala, P. & Venkatesha, T., 2013. Effect of Cathode Materials on Electrochemical Degradation of Luganil Blue N and Acid Red I. *Port. Electrochim. Acta*, Volume 31, pp. 175-183.

Sarkka, H., Bhatnagar, A. & Sillanpää, M., 2015. Recent developments of electro-oxidation in water treatment - A review. *J. Electroanal. Chem.*, Volume 754, pp. 46-56.

Shen, Z., Wang, W., Jia, J., Ye, J., Feng, X. & Peng, A., 2001. Degradation of dye solution by an activated carbon fiber electrode electrolysis system. *J. Hazard. Mater.*, Volume 84, pp. 107-116.

Siddiki, M. K., Li, J., Galipeau, D. & Qiao, Q., 2010. A review of polymer multijunction solar cells. *Energy & Environ. Sci.*, Volume 3, pp. 867-883.

- Smith, W. & Zhao, Y.-P., 2010. Superior Photocatalytic Performance by Vertically Aligned Core-Shell  $\text{TiO}_2/\text{WO}_3$  nanorod Arrays. *Catal. Commun.*, Volume 10, p. 1117.
- Staebler, D. L. & Wronski, C. R., 1977. Reversible conductivity changes in discharge-produced amorphous Si. *Appl. Phys. Lett.*, Volume 31, pp. 292-294.
- Sun, S. & Wang, W., 2014. Advanced chemical compositions and nanoarchitectures of bismuth based complex oxides for solar photocatalytic application. *RSC Advances*, Volume 4, pp. 47136-47152.
- The World Bank, 2015. Access to electricity (% of population). [Online] Available at: <http://data.worldbank.org/indicator/EG.ELC.ACCS.ZS>
- The World Bank, 2015. Improved water source (% of population with access). [Online] Available at: <http://data.worldbank.org/indicator/SH.H2O.SAFE.ZS>
- Tyagi, V., Rahim, N. A., Rahim, N. & Selvaraj, J. A., 2013. Progress in solar PV technology: Research and achievement. *Renewable and Sustainable Energy Rev.*, Volume 20, pp. 443-461.
- Yang, G., van Swaaij, R. A. C. M. M., Isabella, O. & Zeman, M., 2014. A novel way of texturing glass for microcrystalline silicon thin film solar cells application. *Progress in Photovoltaics: Research and Application*.
- Yang, J., Banerjee, A. & Guha, S., 2003. Amorphous silicon based photovoltaics—from earth to the “final frontier”. *Sol. Energy Mater. Sol. Cells*, Volume 78, pp. 597-612.
- Zeng, X. L., Li, M. Y., Song, L. & He, B. Y., 2012. Photoelectrocatalytic Degradation of Benzoquinone Using Different Cathode Materials. *Adv. Mater. Res.*, Volume 610-613, pp. 86-89.



# 9

## CONCLUSIONS

---



In this final chapter the conclusions answering the research questions are presented. The objectives specified in chapter 1 are fulfilled. The summary of the main achievements in this research are described below. Some additional remarks on ongoing research and future developments are included too.

The presence of micro-pollutants in drinking water is of global concern, as these, often highly toxic, compounds are not removed by conventional water treatment and degrade slowly in nature. Consequently, there is an increasing need for finding solutions to the challenges of eliminating this weakness of conventional treatment processes. As it can be seen from the literature overview, presented in the chapter 1, titanium dioxide ( $\text{TiO}_2$ )-based photocatalysis has attracted extensive interest in environmental pollutants' treatment because it is chemically stable, non-toxic, inexpensive and has a wide band gap energy. However, to improve efficiencies, a photoelectrocatalytic (PEC) process for water treatment was proposed and developed, and various constraints were investigated, from the determination of a suitable crystalline structure of the catalyst to the simulation of PEC solar and low-pressure ultraviolet (LPUV) reactors for water treatment.

### **9.1. Overall conclusions**

An electrochemical cell was successfully assembled, scaled up and tested for PEC oxidation of organics. The PEC oxidation process was able to degrade the researched organic pollutants, being phenol and chloroform. Throughout the thesis a kinetic model was proposed for the photodegradation of organic compounds. A Langmuir-Hinshelwood (L-H) model was adopted in the kinetic modeling with both kinetic and adsorption constants being involved, and it

was found that the removal of organic compounds from the aqueous solution followed first-order kinetics. The rate constant of the reaction improved from 0.0028 up to 0.009 min<sup>-1</sup>, a total improvement of 3.2 times (Figure 9.1), by reducing the charge carriers' recombination (by changing the crystal structure and application of the bias) and optimizing the process conditions (optimal light intensity, agitation, surface/volume ratio, optimal potential). Figure 9.1 shows a view from all the possibilities and extend of the effects on enhancement of the rate of the reaction under different conditions.

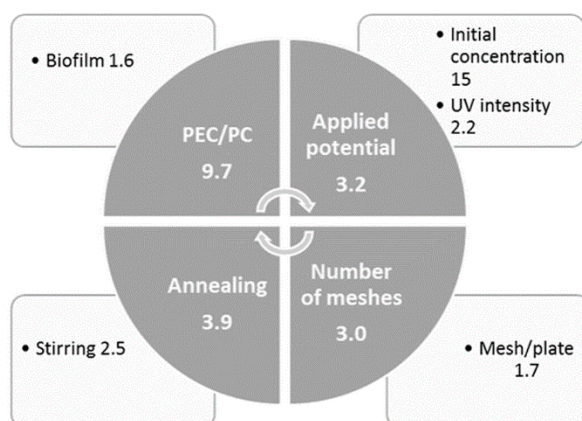


Figure 9.1. Optimization steps that promote increase in the rate of the reaction with the enhancement ratio

Such enhancements can be presented within the framework of conclusions, however the performance enhancement sum of all improvement steps should be done under the same conditions elsewhere.

Furthermore, PEC with TiO<sub>2</sub> under solar irradiation still required prolonged irradiation to achieve a degradation of the organics of 50 – 90 %, because of limitations in specific surface area. When sunlight as a semiconductor activation source was considered, a BiVO<sub>4</sub> – based photoanode was more favorable than TiO<sub>2</sub>, with respect to energy consumption and light absorption,

improving the overall process efficiency by two times. The three electrode cell using the BiVO<sub>4</sub> photoanode was successfully biased by a solar cell and, in that way, making it a stand-alone integrated water treatment system for remote areas.

## **9.2. Synthesis and structural changes of TiO<sub>2</sub> and BiVO<sub>4</sub> films**

A suitable catalyst immobilization method, which is non-complex and applicable for larger surface areas, was found prior to the research on PEC treatment of organics in water. A TiO<sub>2</sub> electrode was prepared by the paint thermal deposition method and it was observed that the TiO<sub>2</sub> layer was uniformly deposited on the titanium surface of the electrode showing good adhesion to the substrate. From literature it was known that temperature can modify the primary particle size and crystal composition. In chapter 2 it was concluded that six coating layers on a titanium plate or mesh, calcined at 650 °C for 5 h, were sufficient to obtain a reliable immobilized catalyst with a long durability, and an anatase to rutile ratio of 85/15. The PEC properties of the resultant TiO<sub>2</sub>/Ti composite photoanodes were systematically evaluated in both the bulk of the solution and on the coated layer of the photoelectrochemical cell, using water and model organic compounds such as terephthalic acid, phenol and chloroform. An electrochemically active biofilm on the TiO<sub>2</sub>/Ti composite electrode, discussed in chapter 6, was even found to increase the kinetics of the reaction by 1.6 times. This increase was assisted by an increase in charge transfer (by lowering impedance) and was also observed by a higher phenol degradation efficiency, confirming that electron transfer from bacteria to the electrode can be enhanced by biofilm formation on the electrode.

Using sunlight to drive the photo-oxidation of organic compounds in water makes the energy balance of this process more favorable than using  $\text{TiO}_2$  under UV light. However, the utilization of solar energy applied to PEC reactions for the degradation of organic pollutants requires an improvement of existing photoelectrochemical techniques, and an enhancement of functional materials in

PEC applications. Working towards this goal a pragmatic approach was considered in chapter 7.  $\text{BiVO}_4$ , which has previously been used for solar water splitting, was found to be a suitable candidate as alternative catalyst, due to its favorable optical and electronic properties. The advantage of  $\text{BiVO}_4$  over  $\text{TiO}_2$  is its lower bandgap energy (2.4 eV vs. 3.2 eV, respectively), allowing more absorption of the solar spectrum. The experimental work on material characterization, photocatalytic performances, with respect to the degradation of model organic pollutants, the stability and reusability of materials used in photocatalysis, and the relevant mechanisms of individual photosystems were discussed in chapter 7. The film thickness was found to be a key parameter in controlling the electron transfer as well as the light-harvesting efficiency with both the  $\text{TiO}_2$  and  $\text{BiVO}_4$  catalysts. The observations indicate that in case of  $\text{BiVO}_4$  300 nm film thickness assured the highest PEC achievement. The comparison of  $\text{BiVO}_4$  photocatalytic performances to  $\text{TiO}_2/\text{Ti}$  composite photocatalysts was presented. The material studies confirmed that  $\text{BiVO}_4$  is a better absorber for solar light compared to  $\text{TiO}_2$ .  $\text{BiVO}_4$  also showed a better phenol degradation performance compared to  $\text{TiO}_2$ , indicating that the enhanced light absorption, catalytic properties and electrical properties translates in an increase in phenol degradation. However, the actual energy conversion efficiency achieved with the  $\text{BiVO}_4$ -based materials was far below its theoretical value because  $\text{BiVO}_4$ -based materials suffer from some drawbacks. First, they have a poor electron-hole separation yield ( $\varphi$ ), leading to approximately 60–80 % of the electron-hole

pairs recombining before they reach the interfaces (Gan, et al., 2015). Secondly, one of the major limitations of BiVO<sub>4</sub> for further improving the solar energy conversion efficiency is its bandgap (~2.5 eV), which fundamentally limits photon absorption. Therefore there is a substantial number of photons in the 2.0–2.5 eV region of the solar spectrum, and a reduction in bandgap by even 0.1–0.3 eV can result in an efficiency increase (Murphy, et al., 2006; Vayssieres, 2009). Doping of the BiVO<sub>4</sub> was carried out in order to study the effect of tungsten (W) doping on the electronic structure, carrier dynamics, and photocurrent performance of the BiVO<sub>4</sub> photoanode. However, it did not improve the phenol degradation performance, suggesting that charge carrier separation is not a limiting factor in this system.

### **9.3. Optimization of the parameters in the solar light-induced PEC process**

The essential experimental parameters, such as light intensity, TiO<sub>2</sub> and BiVO<sub>4</sub> layer thickness, agitation and reactant initial concentration, were systematically investigated in chapters 3 and 7. The TiO<sub>2</sub> photocatalysis process was tested for the remediation of water polluted with chloroform and phenol. The use of the electrochemical approach to enhance the photocatalytic process demonstrated to improve the overall oxidation efficiency of such a light driven process by the enhancement ratio of the efficiency (PEC/PC) of 2.5. The application of an anodic bias may direct most of the photogenerated electrons away from the conduction band of TiO<sub>2</sub>, hence lowering electron–hole recombination events and promoting hole transfer to organic contaminants at the interface. Furthermore the results indicated that the different operating parameters influenced the rate and the extent of the degradation of the organic compounds. It was also observed that the

photocurrent, obtained from the PEC oxidation of the aqueous solution, increased with an increase in solar light intensity (UV<sub>300-400</sub>). Moreover, it was observed that the regenerated catalyst could be reused without losing its treatment properties.

In chapter 3 it was concluded that an increase in e.g. the phenol concentration led to a decrease in the degradation rate. Although an increase in the initial concentration of phenol increases the probability of phenol molecules to react with  $\cdot\text{OH}$ , it was calculated that at higher initial phenol concentrations, the available surface area for  $\cdot\text{OH}$  formation became the rate-limiting factor.

#### **9.4. Electrode configuration**

The development of an efficient electrode system for PEC, as described in chapter 4, remains a challenge. A practical electrode configuration must combine the maximal capture of photons throughout the reactor, minimal mass-transfer limitations to and from the electrodes, and minimal electrode resistance between the anode and cathode. By employing the mesh configuration approach, TiO<sub>2</sub> films with enhanced surface area to absorb light were obtained. Compared with the TiO<sub>2</sub>/Ti plate electrode, the mesh electrode therefore, had a higher efficiency in degrading e.g. chloroform. TiO<sub>2</sub> films were coated on a different number of meshes where TiO<sub>2</sub> coating on the four-mesh configuration yielded a 1.7 times faster constant removal rate of chloroform than the conventional plate configuration in PEC (Figure 9.1); and PEC (0.0078)/PC (0.0014), a 5.6 times faster constant removal rate than the plate configuration in photocatalysis. By introducing a four-mesh configuration into the PEC system, an incident photon to current efficiency (IPCE) of 7 % was achieved, meaning that more electrons were produced by incident photons than by the plate electrode at the same number of incident photons.

Correlation between electrochemical impedance spectroscopy and photo-degradation indicated that the adsorption and surface concentration of molecules on the catalyst were the limiting factors for the degradation of chloroform in this system.

### **9.5. PEC reactors and source of light**

In chapter 5, TiO<sub>2</sub>-based PEC reactor (solar and LPUV) designs were proposed for chloroform removal from water. The performance of the solar reactors was assessed on the optimum conditions that were previously determined in chapter 4 during the batch tests with a mesh electrode configuration and solar light. It was concluded that the performance of the PEC solar reactor improved proportionally to the increase in the surface area to volume ratio, meaning that adsorption of chloroform per volume was one of the rate determining steps of the reaction. Furthermore, light absorption and higher hydroxyl radicals production per volume could have influenced and the degradation of the organic compound. In addition, the removal efficiencies of chloroform in the LPUV reactor could be increased with increasing flow velocities (2.4 l/h to 14.4 l/h) up to a residence time of 5 min, which indicates possible mass transfer limitations. It was also found that the removal of the chloroform showed a dependence on distance between anode and cathode in the reactor. When the distance between anode and cathode was decreased, the degradation rate of the chloroform increased. This observation can be explained by the ohmic potential drop in relation to the anode and cathode distance increase. Decrease in electrolyte conductivity and current will appear together with increase in the resistance to mass transfer; leading to a slow-down of the kinetics of both charge transfer and chloroform oxidation.

### **9.6. Renewable energy and stand-alone system**

$\text{BiVO}_4$  was found to be a suitable material for use as a photoanode for photoelectrochemical degradation not only for phenol but also for chloroform. A stand-alone system for water treatment was designed based on this material and discussed in the chapter 8.

It consists of a  $\text{BiVO}_4$  photoanode connected to a solar cell and a counter electrode to complete the reaction. The material for the counter electrode was studied, finding that a flat carbon plate was the best option. The solar cell was designed to operate under the transmitted spectrum of the photoanode, and to produce the best current and voltage at the operational point for water treatment. An a-Si:H/nc-Si:H tandem solar cell was found to give the best results. This bias-free device would provide an efficient way to remove organic pollutants from water, reducing the costs and the greenhouse gas emissions. In addition, it could be applied as a stand-alone device, which could be independently installed even in remote areas without a stable electricity supply.

### **9.7. Recommendations and suggestions for the future work**

In this thesis, the use of PEC was demonstrated as a potential technology for water treatment, and, more specifically, organics removal. A systematic study of the properties, modification and selected applications of  $\text{TiO}_2$  was presented. Of the many different photocatalysts,  $\text{TiO}_2$  has been studied extensively and was also used in thesis. Due to the nonselective attack of hydroxyl radicals,  $\text{TiO}_2$  PEC can decompose virtually all organic contaminants and oxidize various inorganic anions. The quality of polished water depends on the properties of water and wastewater and the treatment parameters as discussed in the previous chapters.



### 9.7.1. Challenges and issues in TiO<sub>2</sub> PEC for water treatment

However, in this thesis it became clear that there are many factors that can exert considerable influence on PEC performance, including the electron-hole recombination, inability to use visible light efficiently, specific surface area, pore volume and structure, crystalline phase, and the exposed surface areas. Thus, in order to further develop and improve the performance improvements, the focus of PEC research remains on adjusting these factors. Some of the major problems associated with photocatalysis are rapid charge recombination and an inability to use visible light efficiently. Addition of electron donors can enhance photocatalytic activity by irreversibly reacting with valence band holes to prevent charge recombination. Doping of TiO<sub>2</sub> can inhibit charge recombination and expand its photoresponse to the visible region through the formation of impurity energy levels (Zhang, et al., 2016). Dye sensitization and coupling of semiconductors can also expand the light response of TiO<sub>2</sub> to the visible region (Grätzel, 2003). Excited dyes and small band gap semiconductors can inject electrons into the conduction of large band gap semiconductors, resulting in a more efficient charge separation and high photocatalytic efficiency (Grätzel, 2003; Mao, et al., 2016). Structural dimensionality was also a factor that affected the PEC performance and also had a considerable impact on the properties of TiO<sub>2</sub> materials. TiO<sub>2</sub> mesh sheets had an increased light absorption and organics adsorption compared to plates, but the PEC under solar irradiation still required prolonged irradiation times to reach high degradation percentages of organics. To overcome this problem in future studies there should be a focus on synthesis of nanorods, nanotubes and nanowires. These one-dimensional structures represent the smallest dimension for efficient transport of electrons and excitons. These non-carbon based materials have been demonstrated to exhibit superior electrical, optical, mechanical and thermal

properties, and can thus be used as fundamental building blocks (Wang, 2003). Three-dimensional TiO<sub>2</sub> hierarchical structures with pores potentially have larger surface to-volume ratios, which can provide an advantage in the form of efficient diffusion pathways for organic pollutants adsorption into the framework supporting more efficient purification at shorter residence times. Furthermore, immobilized-type TiO<sub>2</sub> reactors exhibit a low catalytic activity due to limitations in catalyst loading (surface area) on a support and catalyst activation at the near surface, partial loss of catalyst by attrition, and possible mass transfer limitations. The first two problems can be solved by novel preparation routes that aim at the precise fabrication of immobilized nanoporous TiO<sub>2</sub> catalyst with enhanced surface area and finely tuned nanoscale dimensions for better adhesion to the support. The third problem can be addressed by the development of innovative PEC reactors that reduce or eliminate the influence of mass transfer. Rotating Disk Photocatalytic Reactor (RDPC) has been particularly introduced in mixing studies, light intensity on the rotating disk, liquid carrying capacity of the rotating disk and degradation of organic compounds (Dionysiou, et al., 2000).

#### **9.7.2. Photoanode material for solar light utilization**

A wide variety of semiconductors have been studied for this purpose, such as TiO<sub>2</sub>, ZnO or WO<sub>3</sub>. Although these semiconductors can be employed for water purification, they can only be excited under illumination of highly energetic light because of their large band gap energies. Therefore, UV light ( $\lambda \leq 400$  nm) is commonly used in PC and PEC oxidation processes. Instead of using only UV light, utilizing the entire solar spectrum is more attractive, as it increases the amount of energy that can be converted. Using sunlight to drive the photo-oxidation of organic compounds in water makes the energy balance of this process much more favorable. Solar utilization in PEC technologies may thus

boost the process effectiveness without considerably increasing the costs of the water treatment.

Working toward this goal, much effort must be made to improve the optical absorption of catalysts for their photocatalytic activity, with metal, non-metal, or self-doping.

#### **9.7.3. By products of the PEC systems**

When utilizing the photooxidative decomposition properties,  $\text{TiO}_2$  has proven as a semiconductor for removal of organics, specifically phenol and chloroform. The conducted research in this thesis on the PEC reactions of organics however have not identified by-products. PEC oxidation of chloroform has somewhat distrusted as there have been concerns about the formation of possible mutagenic chlorinated by-products due to parallel electrochemical oxidation. Therefore, it would seem valuable to investigate the effect of ions on both the photoelectrochemical oxidation process as well as the chlorination procedure with focus on to the generation of by-products.

#### **9.7.4. Fouling of the photoelectrodes**

Over time, adsorption of (natural) organic matter to the  $\text{TiO}_2$  coated surface may drastically increase fouling, and reduce efficiency. There have been few studies on the removal of natural organic matter by photocatalysis, most of which has focused on the effect of treatment parameters, such as pH,  $\text{TiO}_2$  concentration, airflow, irradiation intensity, catalyst loading, catalyst species and initial humic acids concentration on removal efficiency (Rizzo, et al., 2007; Dong, et al., 2006). However, these parameters cannot elucidate the adsorption of humic substances on the electrode surface, which could lead to loss of current density and a further decrease of operational efficiency.

#### **9.7.5. Degradation of mixture of pollutants in water using PEC**

To optimize the efficiency of the process and the anode selectivity of these processes, it is important to study and understand the complex reactions of the organic compounds within PEC. The majority of studies so far have involved simplified models of water containing a single organic pollutant (Zhong, et al., 2016; Fang, et al., 2012; M. E. Osugi, et al., 2008). From such investigations it was recognized that, besides the effects due to the experimental conditions and to the type of the voltage applied to produce the bias, there is also a dependence of the process efficiency on the chemical nature of the target organic compound and on its initial concentration. In a step towards more realistic models, the investigation of binary mixtures of two or more different organic pollutants should be undertaken to identify possible competition and entrainment effects in the treatment of water. The aim of this work would be to develop a systematic methodology for degrading mixtures of pollutants, starting from a rather manageable system to more complex aggregates. Based on this, a complete reaction layout for the mixture can be proposed that is suitable for mathematical modeling based on reaction kinetics of the mixture, being able to predict degradation under changing conditions.

## References

- Dionysiou, D. D., Balasubramanian, G., Suidan, M. T., Khodadoust, A. P., Baudin, I. & L  n  , J. M., 2000. Rotating disk photocatalytic reactor: development, characterization; and evaluation for the destruction of organic pollutants in water. *Water Res.*, Volume 34, pp. 2927-2940.
- Dong, Y., Li, J., Li, X., Bai, J. & Zhou, B., 2006. The promotion effect and mechanism of methanoic acid on the photoelectrocatalytic degradation of fulvic acid. *J. Chem.*, Volume 2006, p. 7.
- Fang, T., Yang, C. & Liao, L., 2012. Photoelectrocatalytic degradation of high COD dipterex pesticide by using TiO<sub>2</sub>/Ni photo electrode. *J. Environ. Sci.*, Volume 24, pp. 1149-1156.
- Gan, J., Lu, X., Rajeeva, B. B., Menz, R., Tong, Y. & Zheng, Y., 2015. Efficient photoelectrochemical oxidation over hydrogen-reduced nanoporous BiVO<sub>4</sub> with Ni-Bi electrocatalyst. *ChemElectroChem*, Volume 2, pp. 1385-1395.
- Gr  tzel, M., 2003. Dye-sensitized solar cells. *J. Photochem. Photobiol., C*, Volume 4, pp. 145-153.
- Osugi, M. E., Zandoni, M. V. B., Chenthamarakshan, C. R., de Tacconi, N. R., Woldemariam, G. A., Mandal, S. S. & Rajeshwar, K., 2008. Toxicity assesment and degradation of disperse azo dyes by photoelectrocatalytic oxidation on Ti/TiO<sub>2</sub> nanotubular array electrodes. *J. Adv. Oxid. Technol.*, Volume 11, pp. 425-434.
- Mao, X., Zhou, R., Zhang, S., Ding, L., Wan, L., Qin, S., Chen, Z., Xu, J. & Miao, S., 2016. High efficiency dye-sensitized solar cells constructed with composites of TiO<sub>2</sub> and the hot-bubbling synthesized ultra-small SnO<sub>2</sub> nanocrystals. *Sci. Rep.*, Volume 6, p. 19390.
- Murphy, B., Barnes, P. R. F., Randeniya, L. K., Plumb, I. C., Grey, I. E., Horne, M. D. & Glasscock, J. A., 2006. Efficiency of solar water splitting using semiconductor electrodes. *Int. J. Hydrogen Energy*, Volume 31, pp. 1999-2017.
- Rizzo, L., Uyguner, C. S., Selcuk, H., Bekbolet, M. & Anderson, M., 2007. Activation of solgel titanium nanofilm by UV illumination for NOM removal. *Water Sci. Technol.*, Volume 55, pp. 113-118.

Vayssieres, L., 2009. On solar hydrogen and nanotechnology. s.l.: John Wiley & Sons (Asian).

Wang, Z. L., 2003. Nanowires and nanobelts. Materials, properties and devices. Metal and semiconductor nanowires. s.l.: Kluwer Academic Publishing.

Zhang, N., Chen, D., Niu, F., Wang, S., Qin, L. & Huang, Y., 2016. Enhanced visible light photocatalytic activity of Gd-doped BiFeO<sub>3</sub> nanoparticles and mechanism insight. Sci. Rep., Volume 6, p. 26467.

Zhong, J. S., Wang, Q. Y., Zhou, J., Chen, D. Q. & Ji, Z. G., 2016. Highly efficient photoelectrocatalytic removal of RhB and Cr(VI) by Cu nanoparticles sensitized TiO<sub>2</sub> nanotube arrays. Appl. Surf. Sci., Volume 367, pp. 342-346.



## LIST OF PUBLICATIONS

---

Bennani, Y., Košutić, K., Dražević, E. & Rožić, M., Wastewater from wood and pulp industry treated by combination of coagulation, adsorption on modified clinoptilolite tuff and membrane processes, *Environ. Technol.*, Vol. 33, pp. 1159-1166, 2012.

Bennani, Y., El-Kalliny, A., Appel, P. & Rietveld, L., Enhanced solar light photoelectrocatalytic activity in water by anatase-rutile TiO<sub>2</sub> transformation, *J. Adv. Oxid. Technol.* Vol. 17, No. 2, 285-296, 2014.

Bennani, Y., Appel, P. & Rietveld, L. C., Optimisation of parameters in a solar-light induced photoelectrocatalytic process with a TiO<sub>2</sub>/Ti composite electrode prepared by paint-thermal decomposition method, *J. Photochem. Photobiol., A*, Vol. 305, pp. 83-92, 2015.

Bennani, Y., Peters, M. C. F., Appel, P. & Rietveld, L. C., Electrochemically active biofilm and photoelectrocatalytic regeneration of the titanium dioxide composite electrode for advanced oxidation in water treatment, *Electrochim. Acta*, Vol. 182, pp. 604-612, 2015.

Bennani, Y., Perez-Rodriguez, P., Alani, M. J., Smith, W. A., Rietveld, L. C., Zeman, M. & Smets, A. H. M., Photoelectrocatalytic Oxidation of Phenol for Water Treatment Using a BiVO<sub>4</sub> Thin-film Photoanode, *J. Mater. Res.*, Vol. 31, pp. 2627-2639, 2016.





# CURRICULUM VITAE

---

Yasmina Bennani was born in Osijek, Croatia in 1986. She finished bachelor and master study at the Faculty of Chemical Engineering and Technology in Zagreb, Croatia (September 2005 – July 2010). Both, bachelor and master final work researches were related and dealing with membrane processes and water treatment technologies. After the studies, she moved to Netherlands to pursue her carrier in Water Treatment Technology. She got an opportunity to work as a researcher at UNESCO-IHE, Netherlands till September 2011. In October 2011 she began PhD research on photoelectrocatalysis at TU Delft, under supervision of prof. L. C. Rietveld and P. Appel. During the past 4 years, she explored the potential of applying photo(electro)catalysis for water treatment, studying the fundamentals of reaction mechanisms, optimizing sustainable degradation and focusing on use of the photoelectrochemical devices based on Earth-abundant materials for water treatment.

After the PhD research she joined Proton Ventures as a research engineer at the business development department at Schiedam, the Netherlands. Her research interests center on sustainable energy, water electrolysis and concept power to ammonia, mainly through the technical and economic feasibility studies, process performance evaluation and aiming towards the demonstration.

